

# Removal of ammonia from drinking water by biological nitrification in a fixed film reactor

Ben van den Akker  
B.EnvHlth, B.Sc (Hons)

Submitted in fulfillment of the requirements for the Degree of  
Doctor of Philosophy



Department of Environmental Health, School of Medicine

(14<sup>th</sup> January 2008)

## Table of contents

<b>SUMMARY</b> .....	<b>12</b>
<b>DECLARATION</b> .....	<b>14</b>
<b>ACKNOWLEDGMENTS</b> .....	<b>15</b>
<b>1 INTRODUCTION</b> .....	<b>17</b>
1.1 GENERAL INTRODUCTION.....	17
1.2 CHLORINE DISINFECTION.....	18
1.3 BUARAN WATER TREATMENT PLANT, EAST JAKARTA, INDONESIA.....	20
1.3.1 Background.....	20
1.3.2 Raw water quality.....	20
1.4 PROCESS SELECTION.....	21
1.5 NITRIFYING TRICKLING FILTERS.....	23
1.6 BIOFILMS.....	29
1.6.1 Definition.....	29
1.6.2 Mass transport.....	29
1.6.3 Extracellular polysaccharides.....	30
1.7 MICROBIOLOGICAL PROCESSES SPECIFIC TO NTFs.....	34
1.7.1 Autotrophic nitrification.....	34
1.7.2 Denitrification.....	35
1.7.3 Carbon oxidation.....	35
1.7.4 Nitrogen assimilation.....	36
1.7.5 Anaerobic ammonia oxidation (anammox).....	36
1.8 FACTORS INFLUENCING NITRIFICATION.....	37
1.8.1 Mass transport.....	37
1.8.2 Interspecies competition.....	38
1.8.3 Environmental parameters.....	39
1.8.4 Operational and design parameters.....	40
1.8.5 In situ analysis of biofilm population structure.....	42
1.9 PROJECT AIMS.....	44
<b>2 REVIEW OF THE RAW WATER QUALITY AT BUARAN AND IMPACT ON WATER TREATMENT</b> .....	<b>45</b>
2.1 INTRODUCTION.....	45
2.2 METHODS.....	52
2.2.1 Water quality data.....	52
2.2.2 Technical visit.....	52
2.3 RESULTS .....	53
2.3.1 Inorganic nitrogen.....	53
2.3.2 Organic carbon.....	55
2.3.3 C:N ratio.....	58
2.3.4 Dissolved oxygen.....	58
2.3.5 Turbidity and suspended solids.....	58
2.3.6 Microbial load.....	62
2.4 DISCUSSION.....	63

<b>3</b>	<b>GENERAL METHODOLOGY .....</b>	<b>68</b>
3.1	INTRODUCTION.....	68
3.2	LARGE PILOT-SCALE NITRIFYING TRICKLING FILTER .....	68
3.2.1	NTF column.....	68
3.2.2	Trickling Filter support stand.....	70
3.2.3	Media support stand and frames.....	70
3.2.4	Biofilm support media.....	75
3.2.5	Primary pump.....	76
3.2.6	PVC manifold.....	78
3.2.7	Rotating distribution arm.....	81
3.2.8	Hydraulic flow.....	81
3.2.9	Ventilation ports and effluent drains.....	83
3.2.10	Filtrate and biofilm sample sites.....	83
3.2.11	Aqueous phase sampling.....	83
3.3	DOSING.....	86
3.3.1	Ammonia dosing.....	86
3.3.2	External organic carbon source dosing.....	86
3.3.3	Suspended solids dosing.....	86
3.3.4	Electrical wiring.....	90
3.3.5	Pilot plant troubleshooting.....	90
3.4	SMALL PILOT-SCALE NTFs.....	93
3.5	WATER ANALYSIS.....	95
3.5.1	Total alkalinity.....	95
3.5.2	Ammonia-nitrogen.....	95
3.5.3	Oxidised nitrogen (nitrite-N and nitrate-N).....	95
3.5.4	Total organic carbon.....	95
3.5.5	Five-day soluble biological oxygen demand.....	96
3.5.6	pH.....	96
3.5.7	Total suspended solids.....	96
3.5.8	Turbidity.....	96
3.6	ONLINE INSTRUMENTATION .....	97
3.6.1	Turbidity analyser.....	97
3.6.2	Dissolved Oxygen.....	97
3.6.3	Temperature.....	97
3.7	BIOFILM ANALYSIS.....	98
3.7.1	Biofilm sampling and extraction for protein and carbohydrate analysis.....	98
3.7.2	Protein analysis.....	98
3.7.3	Carbohydrate analysis.....	98
3.7.4	Heterotrophic plate count.....	99
3.7.5	Fluorescent in situ hybridisation.....	99
3.7.6	Scanning electron microscopy.....	103
3.8	HYDRAULIC TRACER ANALYSIS.....	104
3.9	STATISTICAL ANALYSIS.....	105
<b>4</b>	<b>APPLICATION OF TRICKLING FILTERS TO REMOVE LOW CONCENTRATIONS OF AMMONIA ....</b>	<b>106</b>

4.1	INTRODUCTION.....	106
4.2	METHODS.....	109
4.2.1	Large pilot-scale NTF.....	109
4.2.2	Small pilot-scale NTFs.....	109
4.2.3	NTF start-up.....	110
4.2.4	Ammonia loading.....	110
4.2.5	Effect of hydraulic load on nitrification performance.....	111
4.2.6	Effect of suspended solids on nitrification performance.....	112
4.2.7	Large pilot-scale NTF—sampling and chemical analysis.....	112
4.2.8	Small pilot-scale NTFs—sampling and chemical analysis.....	113
4.2.9	Hydraulic tracer analysis.....	113
4.2.10	Total protein and total carbohydrate.....	113
4.2.11	Weighing of the support media.....	113
4.3	RESULTS.....	115
4.3.1	Large pilot-scale NTF start-up.....	115
4.3.2	Performance comparison of the old and newly reconstructed pilot NTFs.....	120
4.3.3	Inorganic nitrogen depth profile.....	123
4.3.4	Nitrification rate profile.....	125
4.3.5	Nitrification rates as a function of ammonia-N surface load.....	128
4.3.6	Nitrification rate as a function of hydraulic surface load.....	130
4.3.7	Percentage nitrification as a function of hydraulic surface load and ammonia surface load.....	132
4.3.8	Distribution of biomass through the large pilot-scale NTF.....	135
4.3.9	Impact of seasonal variation on nitrification performance.....	137
4.3.10	Impact of inert solids on NTF performance.....	142
4.3.11	Hydraulic characterisation of the large pilot-scale NTF.....	146
4.4	DISCUSSION.....	148
<b>5</b>	<b>INFLUENCE OF ORGANIC CARBON LOADING ON NITRIFYING TRICKLING FILTER PERFORMANCE</b>	
	<b>162</b>	
5.1	INTRODUCTION.....	162
5.2	METHODS.....	165
5.2.1	Experimental design.....	165
5.2.2	Large pilot-scale NTF—sampling and chemical analysis.....	166
5.2.3	Small pilot-scale NTF—sampling and chemical analysis.....	166
5.2.4	Organic carbon biodegradability test.....	166
5.2.5	Pearce's nitrification model.....	167
5.3	RESULTS.....	169
5.3.1	Comparing organic carbon biodegradability of Buaran raw water with selected carbon sources.....	169
5.3.2	Comparison of nitrification performance between experiments.....	171
5.3.3	Percentage nitrification as a function of organic load.....	173
5.3.4	Nitrification rate as a function of organic load.....	173
5.3.5	Nitrification as a function of C:N ratio.....	174
5.3.6	Effect of carbon loading and operation time on nitrification: low ammonia-N loaded NTF.....	178

5.3.7	Nitrification depth profile and nitrogen budget: low ammonia-N loaded NTF.....	180
5.3.8	Effect of carbon loading and operation time on nitrification: high ammonia-N loaded NTF.....	190
5.3.9	Nitrification depth profile and nitrogen budget: High ammonia-N loaded NTF....	194
5.3.10	Organic carbon removal.....	201
5.3.11	Environmental parameters.....	204
5.3.12	Nitrification model.....	207
5.4	DISCUSSION.....	210
<b>6</b>	<b>EFFECT OF CARBON TO NITROGEN RATIO ON BIOFILM PROTEIN AND CARBOHYDRATE COMPOSITION .....</b>	<b>223</b>
6.1	INTRODUCTION.....	223
6.2	METHODS.....	225
6.2.1	Experimental design.....	225
6.2.2	Total Protein and total Carbohydrate.....	225
6.2.3	Heterotrophic plate counts.....	226
6.2.4	Hydraulic tracer analysis.....	226
6.3	RESULTS .....	228
6.3.1	Biofilm carbohydrate composition.....	228
6.3.2	Biofilm protein composition.....	234
6.3.3	Protein:carbohydrate ratio.....	236
6.3.4	Biofilm heterotrophic composition.....	237
6.3.5	Hydraulic characterisation.....	239
6.4	DISCUSSION.....	242
<b>7</b>	<b>MICROBIAL ECOLOGY OF A NITRIFYING TRICKLING FILTER TREATING POTABLE WATER .....</b>	<b>250</b>
7.1	INTRODUCTION.....	250
7.2	METHODS.....	253
7.2.1	Experimental design.....	253
7.2.2	Biofilm sampling.....	253
7.2.3	FISH and SEM.....	253
7.2.4	Large pilot-scale NTF—sampling and chemical analysis.....	253
7.2.5	Small pilot-scale NTFs—sampling and chemical analysis.....	254
7.3	RESULTS .....	256
7.3.1	Nitrification performance.....	256
7.3.2	Distribution of AOB and NOB during low organic carbon loads: Experiment A.....	259
7.3.3	Vertical distribution of AOB, NOB and heterotrophs during high organic carbon loads	265
7.3.4	Experiment I: comparing the in situ structure of organic fertiliser-fed and sucrose-fed biofilms.....	279
7.3.5	Biofilm thickness.....	281
7.4	DISCUSSION.....	283
<b>8</b>	<b>GENERAL DISCUSSION.....</b>	<b>288</b>
	<b>REFERENCES .....</b>	<b>298</b>
	<b>APPENDIX.....</b>	<b>313</b>

PUBLICATIONS RELEVANT TO THIS THESIS .....313

## List of figures

### Chapter 1

<b>Figure 1.1.</b> Theoretical breakpoint curve.....	19
<b>Figure 1.2.</b> Illustration of a trickling filter.....	25
<b>Figure 1.3.</b> Schematic representation of a biofilm cross-section.....	33

### Chapter 2

<b>Figure 2.1.</b> Summary of schematic water treatment process at Buaran WTP.....	47
<b>Figure 2.2.</b> General layout of the Citarum and Ciliwung catchments and location of pollution discharge points.....	48
<b>Figure 2.3.</b> Seasonal variation in raw water ammonia-N concentrations at Buaran WTP during 2001.....	54
<b>Figure 2.4.</b> Seasonal variation in raw water organic matter and COD concentrations at Buaran WTP during 1999.....	56
<b>Figure 2.5.</b> Seasonal variation in raw water BOD <sub>5</sub> concentrations at Buaran WTP during 2004.....	57
<b>Figure 2.6.</b> One through to five day BOD and sBOD test.....	57
<b>Figure 2.7.</b> Seasonal variation in raw water organic matter and turbidity concentrations at Buaran WTP during 2003.....	59
<b>Figure 2.8.</b> Relationship between raw water turbidity and SS during 2004.....	60
<b>Figure 2.9.</b> Profile of SS and turbidity, measured along the Tarum canal during September 2000, and corresponding photographs taken on the technical visit during March 2004.....	61
<b>Figure 2.10.</b> Seasonal variation in raw water total coliforms at Buaran WTP during 2003.....	62

### Chapter 3

<b>Figure 3.1.</b> Schematic representation of the small pilot-scale NTFs.....	94
--	----

### Chapter 4

<b>Figure 4.1.</b> Progression of nitrification during start-up after supplementing the influent with low concentrations of ammonia on day 0.....	117
<b>Figure 4.2.</b> Concentration profiles of inorganic nitrogen species measured throughout the depth of the large pilot-scale NTF during start-up.....	118
<b>Figure 4.3.</b> Comparison of nitrate-N generation rates between the old large pilot-scale NTF and the newly reconstructed large pilot-scale NTF, for various ammonia-N concentration loads of: (a) 0.5 mg/L; (b) 2.0 mg/L; and (d) 5.0 mg/L.....	122
<b>Figure 4.4.</b> Steady-state concentration profiles of inorganic nitrogen species measured with the large pilot-scale NTF for various ammonia-N concentration loads of: (a) 0.5 mg/L; (b) 1.0 mg/L; (c) 2.0 mg/L; (d) 3.0 mg/L; and (e) 5.0 mg/L.....	124
<b>Figure 4.5.</b> Nitrification rates measured throughout the depth of the large pilot-scale NTF, represented as: mg NH <sub>4</sub> -N per unit of surface area (m <sup>2</sup> ); and per kg of biomass; for various influent ammonia-N concentrations.....	126
<b>Figure 4.6.</b> Nitrification rates as a function of influent ammonia-N concentration for four filter bed depths when operated under a constant hydraulic surface loading of 173 L m <sup>-2</sup> d <sup>-1</sup> .....	127
<b>Figure 4.7.</b> Relationship between ammonia-N surface load and apparent nitrification rate for: large pilot-scale NTF; and small pilot-scale NTF.....	129
<b>Figure 4.8.</b> Relationship between ammonia-N surface load and apparent nitrification rate when operated under various hydraulic surface loads, at relatively constant ammonia-N concentration loads of 4.1 ± 2.2 mg/L.....	131
<b>Figure 4.9.</b> Percentage nitrification as a function of hydraulic load for various ammonia concentration loads.....	133

<b>Figure 4.10.</b> Percentage nitrification and corresponding nitrification rate as a function of the ammonia surface load. ....	134
<b>Figure 4.11.</b> Distribution of biomass measured down the large pilot-scale NTF and corresponding ammonia-N and TOC concentration profiles. ....	136
<b>Figure 4.12.</b> Seasonal variation of influent temperature during the year 2004. ....	140
<b>Figure 4.13.</b> Relationship between ammonia-N removal and total alkalinity consumption. ....	141
<b>Figure 4.14.</b> Relationship between ammonia-N removal and magnitude pH reduction. ....	141
<b>Figure 4.15.</b> Impact of high inert solids on the apparent nitrification rate of the large pilot-scale NTF. ....	143
<b>Figure 4.16.</b> Impact of high inert solids on nitrification rates measured through the depth of the large pilot-scale NTF. ....	144
<b>Figure 4.17.</b> Residence time distribution curves resulting from a pulse injection of the tracer rhodamine WT, observed: one week into start-up; on completion of start-up; under steady-state conditions when operating under high ammonia loads; and corresponding fluorescent micrographic representations of biomass abundance. ....	147

## Chapter 5

<b>Figure 5.1.</b> Comparison of BOD <sub>1</sub> to BOD <sub>5</sub> of selected carbon sources and of Buaran raw water. ....	170
<b>Figure 5.2.</b> Effect of influent sBOD <sub>5</sub> concentration and external carbon source on NTF performance. ....	172
<b>Figure 5.3.</b> Steady-state relationship between percentage nitrification and organic load, obtained from experimental data where ammonia-N was loaded between $94 \pm 10$ to $815 \pm 130$ mg NH <sub>4</sub> -N m <sup>-2</sup> d <sup>-1</sup> . ....	175
<b>Figure 5.4.</b> Apparent nitrification rate as a function sBOD <sub>5</sub> surface load, observed under: (i) low ammonia-N loads of $94 \pm 10$ mg NH <sub>4</sub> -N m <sup>-2</sup> d <sup>-1</sup> ; and (ii) high ammonia-N loads $815 \pm 130$ mg NH <sub>4</sub> -N m <sup>-2</sup> d <sup>-1</sup> . ....	176
<b>Figure 5.5.</b> Nitrification performance of the NTF, as a function of time, following an increase in influent sBOD <sub>5</sub> concentration from 1.3 to $5.8 \pm 27$ mg/L (on day 0). ....	179
<b>Figure 5.6.</b> Concentration profiles of inorganic nitrogen species measured throughout the depth of the NTF. ....	184
<b>Figure 5.7.</b> Nitrogen mass-balance showing effluent nitrogen species composition as percentage of total inorganic nitrogen. ....	186
<b>Figure 5.8.</b> Comparison of nitrification rates measured through the depth of the large pilot-scale NTF during operational periods of high and low influent sBOD <sub>5</sub> concentrations. Low influent ammonia-N concentrations fixed at $0.5 \pm 0.2$ mg NH <sub>4</sub> -N m <sup>-2</sup> d <sup>-1</sup> . ....	189
<b>Figure 5.9.</b> NTF nitrification performance as a function of time, once influent sBOD <sub>5</sub> concentration was increased on day 1 by the addition of sucrose. ....	192
<b>Figure 5.10.</b> Concentration profiles of inorganic nitrogen species measured throughout the depth of the NTF. ....	196
<b>Figure 5.11.</b> Inorganic nitrogen mass-balance showing effluent nitrogen species composition as percentage of total inorganic nitrogen. ....	198
<b>Figure 5.12.</b> Comparison of nitrification rates measured down the large pilot-scale NTF during operational periods of high and low influent sBOD <sub>5</sub> concentrations. High influent ammonia-N concentrations fixed at $5.0 \pm 0.7$ mg NH <sub>4</sub> -N m <sup>-2</sup> d <sup>-1</sup> . ....	200
<b>Figure 5.13.</b> Relationship between sBOD <sub>5</sub> surface load and removal rate. ....	202
<b>Figure 5.14.</b> Relationship between TOC surface load and removal rate. ....	202
<b>Figure 5.15.</b> Concentration profiles of TOC and sBOD <sub>5</sub> measured throughout the NTF. ....	203
<b>Figure 5.16.</b> Steady-state relationship between influent sBOD <sub>5</sub> concentration and effluent DO. ....	205
<b>Figure 5.17.</b> Steady-state relationship between effluent DO, % nitrification and carbon removal. ....	206

<b>Figure 5.18.</b> Observed and predicted effluent ammonia-N concentration as a function of organic surface load.....	209
--	-----

**Chapter 6**

<b>Figure 6.1.</b> NTF depth profile of biofilm carbohydrate ( $\mu\text{g}/\text{cm}^2$ ) and corresponding influent ammonia-N and sBOD <sub>5</sub> concentrations.....	230
<b>Figure 6.2.</b> Relationship between biofilm carbohydrate ( $\mu\text{g}/\text{cm}^2$ ) and apparent nitrification rate in response to an increase in organic carbon loading on.....	233
<b>Figure 6.3.</b> NTF depth profile of biofilm protein ( $\mu\text{g}/\text{cm}^2$ ) for each experiment and corresponding influent ammonia and sBOD <sub>5</sub> concentrations.....	235
<b>Figure 6.4.</b> Large pilot-scale NTF: depth profile of biofilm heterotrophic concentration (CFU/cm <sup>2</sup> ) for each experiment and the corresponding sucrose induced influent sBOD <sub>5</sub> concentrations.....	238
<b>Figure 6.5.</b> RTD curves after a trace pulse injection of rhodamine WT and corresponding table of biomass concentrations represented as total carbohydrate and total protein.....	240
<b>Figure 6.6.</b> Steady-state relationship between HRT and NTF nutrient surface load measured as the sum of ammonia-N + sBOD <sub>5</sub> mg m <sup>-2</sup> d <sup>-1</sup> .....	241

**Chapter 7**

<b>Figure 7.1.</b> Concentration profile of: ammonia-N; nitrite-N; and nitrate-N observed through the depth of the large pilot-scale NTF during time of biofilm harvest.....	257
<b>Figure 7.2.</b> Mean percentage nitrification values measured for all experiments.....	258
<b>Figure 7.3.</b> Profile of biofilm thickness throughout the depths of the trickling filter during high sBOD <sub>5</sub> loads (8.8 mg/L) at NH <sub>4</sub> -N load of 4.7 mg/L (Experiment F).....	282

**Chapter 8**

<b>Figure 8.1.</b> Comparison of nitrification rate profile obtained in this study when operated under low ammonia-N concentrations (<5.0 mg NH <sub>4</sub> -N/L), to that obtained from wastewater investigations by Parker et al. (1989), when operated under higher influent ammonia concentrations (>5.0 NH <sub>4</sub> -N/L).....	291
<b>Figure 8.2.</b> Comparison of ammonia-N depth profiles obtained from this study to that obtained from wastewater investigations by Pearce (2004), when operated under high organic loads of 0.32 and 0.29 kg BOD <sub>5</sub> m <sup>-3</sup> d <sup>-1</sup> respectively.....	293

**List of tables**

**Chapter 1**

<b>Table 1.1.</b> Typical trickling filter classifications and corresponding design characteristics: Comparison between conventional wastewater filters with the potable NTF designed for this study.....	26
<b>Table 1.2.</b> Optimum values of environmental factors for nitrification.....	40

**Chapter 2**

<b>Table 2.1.</b> Pearson r correlation coefficient for raw water data collected during the year 2003 at Buaran water treatment plant.....	54
<b>Table 2.2.</b> Summary of organic carbon concentrations represented as BOD <sub>5</sub> , COD and organic matter for the years 1999 – 2004.....	56

### **Chapter 3**

<b>Table 3.1.</b> Hybridisation solutions used for FISH.....	101
<b>Table 3.2.</b> Wash buffers used for FISH.....	101
<b>Table 3.3.</b> 16S rRNA-targeted oligonucleotide probes used in this study.....	102

### **Chapter 4**

<b>Table 4.1.</b> Summary of pilot NTFs used in the study and their operating conditions.....	111
<b>Table 4.2.</b> Summary of the physicochemical analysis of the large pilot-scale NTFs Influent and effluent.....	139

### **Chapter 5**

<b>Table 5.1.</b> Experimental conditions used to determine the effect of carbon loadings on the performance of the nitrifying trickling filters: influent ammonia-N and sBOD <sub>5</sub> concentrations and corresponding C/N ratio and loading rates.....	168
<b>Table 5.2.</b> Spearman's correlation coefficient highlighting relationships between NTF performance and physicochemical water quality parameters.....	177

### **Chapter 6**

<b>Table 6.1.</b> Influent ammonia-N and sBOD <sub>5</sub> concentrations and corresponding loading rates that the NTF was operated under.....	227
<b>Table 6.2.</b> Spearman's correlation coefficients highlighting relationships between nitrification, organic (sBOD <sub>5</sub> ) loading and C:N ratio with biofilm carbohydrate, protein and heterotrophic composition.....	231

### **Chapter 7**

<b>Table 7.1.</b> Trickling filter influent ammonia-N and sBOD <sub>5</sub> concentrations and corresponding loadings rate.....	255
---	-----

## **List of plates**

### **Chapter 1**

<b>Plate 1.1.</b> Scanning electron micrographs showing the diversity of microorganisms found in nitrifying biofilms.....	32
---	----

### **Chapter 2**

<b>Plate 2.1.</b> Illustration of bank side residents located within the Ciliwung and Citarum basin, who have direct water use for life activities.....	49
<b>Plate 2.2.</b> Floating toilet: Discharge of excreta into the water supply.....	49
<b>Plate 2.3.</b> Pre-chlorination dosing point at Buaran WTP.....	51

### **Chapter 3**

<b>Plate 3.1.</b> Large pilot-scale NTF, located at Hope Valley WTP, Adelaide.....	69
<b>Plate 3.2.</b> NTF support stand.....	71
<b>Plate 3.3.</b> Media support stand.....	72
<b>Plate 3.4.</b> External media support frame.....	73
<b>Plate 3.5.</b> Birds eye view: 1 of 2 internal media support frames.....	74

<b>Plate 3.6.</b> Close up photograph of the polypropylene media highlighting the steep channels and corrugated foils.....	75
<b>Plate 3.7.</b> Installation of the primary pump situated on the weir above the Hope Valley reservoir. .....	77
<b>Plate 3.8.</b> Influent PVC pipe manifold.....	79
<b>Plate 3.9.</b> Influent PVC manifold continued, depicting SS and organic carbon dosing points.....	80
<b>Plate 3.10.</b> Rotating distribution arm.....	82
<b>Plate 3.11.</b> NTF effluent drains and ventilation parts.....	84
<b>Plate 3.12.</b> Location of biofilm and filtrate sample sites.....	85
<b>Plate 3.13.</b> Clay mixing tank.....	88
<b>Plate 3.14.</b> Set-up of clay dosing pump(s).....	89
<b>Plate 3.15.</b> Earlier version of the large pilot-scale NTF.....	91
<b>Plate 3.16.</b> NTF support stand.....	91
<b>Plate 3.17.</b> 1 of 3 biofilm sample sites (draws).....	92
<b>Plate 3.18.</b> The original NTF: Squashed biofilm sample draw.....	92

## Chapter 4

<b>Plate 4.1.</b> In situ examination of biofilm harvested at 0.3 m during start-up using FISH and SEM..	119
<b>Plate 4.2.</b> SEM depicting the in situ ultra structure of the NTF biofilm during high SS loads.....	145

## Chapter 5

<b>Plate 5.1.</b> Impact of high carbon loads on NTF support media.....	187
---	-----

## Chapter 7

<b>Plate 7.1.</b> Fluorescent micrographs showing in situ structure of the nitrifying biofilm sampled from the surface (0 m) of the trickling filter, at low organic carbon loads ( $1.3 \pm 0.5$ mg sBOD <sub>5</sub> /L) during Experiment A.....	261
<b>Plate 7.2.</b> In situ structure of the nitrifying biofilm sampled from trickling filter bed depth of 0.3 meters during Experiment A, at low organic loads ( $1.3 \pm 0.5$ mg sBOD <sub>5</sub> /L).....	262
<b>Plate 7.3.</b> In situ structure of the biofilm at various filter bed depths during Experiment A, at low organic loads ( $1.3 \pm 0.5$ mg sBOD <sub>5</sub> /L).....	263
<b>Plate 7.4.</b> In situ structure of the biofilm at various filter bed depths during: Experiment C– high sBOD <sub>5</sub> ( $5.4 \pm 0.15$ mg/L) loading using sucrose.....	268
<b>Plate 7.5.</b> In situ structure of the biofilm sampled from the top (0.3 m) of the trickling filter during Experiment F – high sBOD <sub>5</sub> ( $8.8 \pm 2.9$ mg/L) loading using sucrose.....	271
<b>Plate 7.6.</b> In situ structure of the biofilm sampled from the middle (1.5 m) of the trickling filter during Experiment F– high sBOD <sub>5</sub> ( $8.8 \pm 2.9$ mg/L) loading using sucrose.....	273
<b>Plate 7.7.</b> In situ structure of the biofilm sampled from the bottom (2.7 m) of the trickling filter obtained during Experiment F – high sBOD <sub>5</sub> ( $8.8 \pm 2.9$ mg/L) loading using sucrose.....	275
<b>Plate 7.8.</b> In situ structure of the biofilm sampled from the top of the trickling filter (0.3 m) during Experiment G – Fed intermittent organic spikes ( $9.4 \pm 0.9$ mg sBOD <sub>5</sub> /L) using sucrose.....	278
<b>Plate 7.9.</b> In situ structure of the biofilm samples from the trickling filter bed depth of 0.3 m during Experiment F (fed sucrose equivalent to $8.8 \pm 2.9$ mg sBOD <sub>5</sub> /L) and 1 fed organic fertilizer equivalent to ( $11.5 \pm 3.4$ mg sBOD <sub>5</sub> /L).....	280

## SUMMARY

The absence of water catchment protection often results in contamination of drinking water supplies. Waters in South East Asia have been exploited to support extensive agriculture, industry, power generation, public water supply, fisheries and recreation use. Ammonia has been identified as a significant contaminant of drinking water because of its ability to affect the disinfection efficiency of chlorine. The interference of ammonia with chlorination is a prevalent and expensive problem faced by many water treatment plants (WTPs) located throughout South East Asia. The conventional approach for ammonia removal was to pre-chlorinate using high concentrations of chlorine, which has a number of disadvantages including the formation of disinfection by-products and high chlorine consumption.

This thesis investigated the application of high rate nitrifying trickling filters (NTFs) as a means of ammonia removal from a polluted lowland water source as an alternative to pre-chlorination. NTFs are widely used for the biological remediation of ammonia rich *wastewater*, however their performance when required to operate under low ammonia concentrations for *potable water* applications was unknown.

A NTF pilot facility consisting of one large-scale, and three small-scale NTFs were constructed at Hope Valley WTP in South Australia. The NTFs were operated to simulate the raw water quality of a polluted catchment identified in Indonesia (Buaran WTP), including variations in ammonia, biological oxygen demand (BOD<sub>5</sub>), and turbidity. Results confirmed that plastic-packed NTFs were able to operate equally successfully under low ammonia-N concentrations, some 10- to 50-fold lower than that of conventional wastewater applications, where complete conversion of ammonia to nitrate was consistently observed under these markedly reduced loadings. Results also showed that when operated under mass loads equivalent to typical ammonia loading criteria for wastewater NTFs, by increasing hydraulic flow, comparable apparent nitrification rates were achieved. These results confirmed that mass transport limitations posed by low ammonia-N concentrations on overall filter performance were insignificant.

This thesis also investigated the impact of organic carbon quantity and biodegradability on the nitrification behaviour of the pilot NTF. Results demonstrated that organic carbon loading, rather than the C:N ratio, was an important regulator of filter nitrification capacity, where a linear decline in nitrification performance correlated well with sucrose and methanol augmented

carbon loads. Extensive monitoring of inorganic nitrogen species down the NTF, to profile nitrification behaviour, showed sucrose-induced carbon loads greater than  $870 \text{ mg sBOD}_5 \text{ m}^{-2} \text{ d}^{-1}$  severely suppressed nitrification throughout the entire filter bed. This study also confirmed that critical carbon loads for nitrification varied among carbon sources. In contrast to sucrose, when a more native-like carbon source was dosed (organic fertiliser), no significant decline in nitrification capacity was observed. This could be attributed to differences in carbon biodegradability.

This research has provided new insights into the microbial ecology of a potable water NTF. The combination of fluorescent *in situ* hybridisation (FISH) and scanning electron microscopy (SEM) for *in situ* analysis of biofilms was successful in identifying the spatial distribution of ammonia oxidising bacteria (AOB), nitrite oxidising bacteria (NOB) and heterotrophs. When the NTF was operated under low organic loads, clusters of AOB and NOB were abundant, and were located in close proximity to each other. Uniquely, the study identified not only *Nitrospira* spp but also the less common *Nitrobacter* spp within the NTF biofilm. Biofilm analysis showed that the type of carbon source also strongly influenced the biofilms characteristics in terms of biomass ecology, morphology, and polysaccharide composition, which was correlated with NTF performance. Results showed that an increase in  $\text{sBOD}_5$  via the addition of sucrose promoted the rapid growth of filamentous heterotrophic bacteria and production of large amounts of polysaccharide. Stratification of nitrifiers and heterotrophs, and high biofilm polysaccharide concentrations were observed at all filter bed depths, which coincided with the impediment of nitrification throughout the entire filter column. High biofilm polysaccharide concentrations also coincided with a significant increase (40 %) in filter hydraulic retention time, as determined by hydraulic tracer experiments. In contrast to sucrose-fed biofilms, organic fertiliser-fed biofilms had a more uniform and dense ultra-structure dominated by many rod shaped bacteria, and was significantly lower in polysaccharide composition. This observation was coupled with superior nitrification performance.

This study confirmed that a well functioning NTF is a viable, low cost alternative for ammonia removal from source water abstracted from poorly protected catchments found in many developing countries. Pre-treatment using NTFs has the potential to reduce the chlorine dose required for pre-chlorination. Thereby improving water quality by minimising the formation of disinfection by-products, and improving the control of chlorination. NTFs could also find ready application in other situations where ammonia interferes with chlorine disinfection.

# **DECLARATION**

I certify that this thesis does not incorporate without acknowledgement any material previously submitted for any degree or diploma in any university; and that to the best of my knowledge and belief it does not contain any material previously published or written by another person except where due reference is made in the text.

Ben van den Akker

14/01/2008

# ACKNOWLEDGMENTS

First and foremost, I would like to thank my supervisors Howard Fallowfield, Nancy Cromar and Mike Holmes for their vast knowledge, support, guidance and enthusiasm.

I would like to thank all United Water staff from Hope Valley Water Treatment Plant, and their Research and Development group for their support and hospitality.

I would also like to thank all those people who have provided significant technical expertise and project support including (in no particular order) Pete Pearce, Alana Hansen, Kerry Gascoigne, Michelle Lewis, Flinders Biomedical Engineering, Richard Evans, Guy Abell, Michael Short, Trish Ameer and Cheryl Caldwell. Each of you have provided something that was essential to this thesis and as such I am extremely grateful.

Thank you to all staff and students from the department of Environmental Health, who have provided feedback and support over the course of my studies there, and who have most importantly provided support, friendship and encouragement. A special thanks to Michael, Akio, Sharyn, Emily, Richard, Lewis, Katarina and Linda for your friendship and fun times in the lab.

I am grateful to my close friends Sam, Akio, Michael, Vince, and Pete for their huge support, words of encouragement and motivation. Sam, thanks for all the coffees and words of inspiration.

I would like to extend a very special thanks to Kate Biedrzycki and my family for their huge support, understanding, encouragement and for always been there during the good and bad times.

***This research project was proudly funded by Thames Water and supported by United Water International as part of their commitment to innovation and responsible water management.***

## Abbreviations

Ammonia-N- ammonia-nitrogen  
AOB- ammonia oxidising bacteria  
BAF- biological aerated filter  
BNR- biological nutrient removal  
BOD<sub>5</sub>- total 5 day biological oxygen demand  
CFU- colony forming units  
COD- chemical oxygen demand  
DAPI- 4',6-diamidino-2-phenylindole  
DO- dissolved oxygen  
DOC- dissolved organic carbon  
EDTA- ethylenediamine tetra-acetate dihydrate  
EPS- extracellular polysaccharide  
FISH- fluorescent *in situ* hybridisation  
HPC- heterotrophic plate count  
HRT- hydraulic retention time  
Nitrate-N- nitrate-nitrogen  
Nitrite-N- nitrite-nitrogen  
NOB- nitrite oxidising bacteria  
NO<sub>x</sub>- oxidized nitrogen (nitrite-N + nitrate-N)  
NTF- nitrifying trickling filter  
NTU- Nephelometric turbidity units  
PAC- powdered activated carbon  
PBS- phosphate-buffered saline  
PVC- polyvinylchloride  
RFL- relative fluorescence  
RNA- ribonucleic acid  
rRNA- ribosomal ribonucleic acid  
 $r_s$ - Spearman's correlation coefficient  
RTD- residence distribution curve  
sBOD<sub>5</sub>- soluble 5 day biological oxygen demand  
SD- standard deviation  
SEM- scanning electron microscopy or scanning electron micrograph  
SS- suspended solids  
TOC- total organic carbon  
WTP- water treatment plant  
WWTP- wastewater treatment plant

# 1 INTRODUCTION

## 1.1 General Introduction

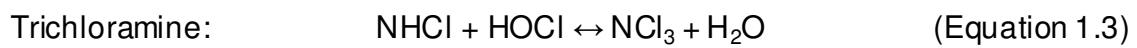
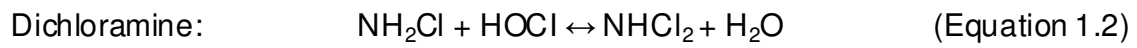
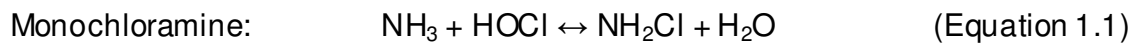
It is generally recognised that water quality is the single biggest factor affecting the future prosperity of many countries. Human activity has affected the quantity and quality of many water bodies around the world (Henry and Heinke 1996). Intensification of populations into major city zones, coupled with poor water catchment protection has led to the deterioration in water quality. This necessitates enhancements in water treatment and water resource management practices (McIntosh 2003). Fortunately, developed nations have the financial and technical support to maintain potable water of high standards for their consumers despite the deterioration in water quality (Henry and Heinke 1996). However, developing countries often do not have this advantage, especially at times of population growth when water needs are most crucial. Water treatment technologies in developing countries are limited, where capital resources for their installation and maintenance are a major challenge (Henry and Heinke 1996). The pollution of raw water supplies in these countries intensifies the financial burden, where contaminants adversely affect treatment processes and increase treatment costs. Developing countries require new technological advances in order to meet the demand for safe drinking water by an exponentially growing population (Henry and Heinke 1996). This is especially the case in Jakarta, Indonesia where the quality of surface waters is threatened by over-development and other human-related factors. Pollution of catchment water has resulted from a failure to invest in wastewater collection and treatment, consequently much of the raw sewage is discharged directly into receiving water bodies. Water availability has also encouraged industries to establish nearby, which incidentally, contributes significantly to the pollution load due to the failure of many to conform to legislation (Palupi *et al.* 1995). These problems are wide spread throughout Asia's developing countries (McIntosh 2003). The high pollution load results in raw water which is difficult to treat, and subsequently incurs higher costs when trying

to reach drinking water guidelines. In particular, ammonia has been identified as a significant contaminant in polluted drinking water catchments, because of its ability to adversely affect the disinfection efficiency of chlorine.

## **1.2 Chlorine disinfection**

The addition of chlorine in water and wastewater is the most practical and widely adopted disinfection process. The presence of ammonia greatly reduces the disinfection efficiency of chlorine. The chemistry is based upon the reaction of chlorine with ammonia, which forms chloramines (White 1999; Metcalf and Eddy 2003). The reactions of chlorine with ammonia are represented in Equations 1.1, 1.2, and 1.3. The chlorine in chloramine compounds is called "combined available chlorine", which has lower oxidation potential than free available chlorine and therefore is less effective as an oxidant (Davis and Cornwell 1991). In order to maintain adequate disinfection, breakpoint chlorination is desirable (Figure 1.1). Breakpoint chlorination involves the addition of chlorine until a point where enough free residual chlorine is available (zone 3), after the formation of chloramines (zone 1 and 2), to destroy bacteria and other harmful pathogens. The interference of ammonia requires a chlorine to ammonia ratio of 10:1 for the reaction to be complete. The presence of ammonia therefore requires higher dosage of chlorine to achieve breakpoint chlorination, which increases operational costs and can impact on public health due to the production of disinfection by-products (Davis and Cornwell 1991). Similarly, 1 mg/L of nitrite-N requires the application of 7.5 mg/L of chlorine (Davis and Cornwell 1991).

Chlorine disinfection problems arising from the presence of ammonia are prevalent and expensive problems faced by many WTPs located throughout South East Asia, which receive polluted water from unprotected drinking water catchments. However, for the purpose of this thesis, Jakarta City, in particular Buaran WTP and its neighbouring catchments were selected as a case study, due to the availability of water quality and WTP operations data.



(Davis and Cornwell 1991)

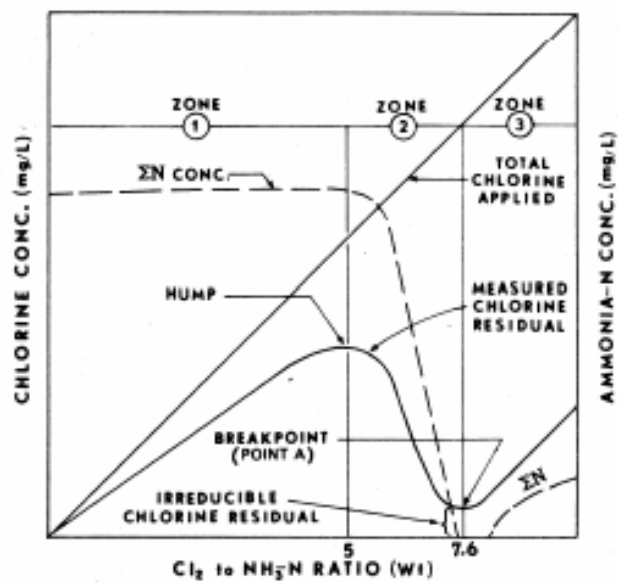


**Figure 1.1.** Theoretical breakpoint curve, obtained from White (1999).

## **1.3 Buaran Water Treatment Plant, East Jakarta, Indonesia**

### **1.3.1 Background**

Buaran WTP supplies water to approximately two million consumers in East Jakarta, Indonesia (Cammarota, 2001). Buaran WTP is capable of treating 432 ML/d of water supplied by the West Tarum Canal. The Tarum Canal plays a vital role in the economic, social and environmental life of Jakarta (Bukit 1995; Palupi *et al.* 1995). Water quality is a major issue within the canal and neighbouring catchments because of the importance of the water for potable, industrial, agricultural and public amenity uses, life style activities and also as an aquatic ecosystem. The sub-optimal condition of waterways within the catchments can be largely attributed to elevated concentrations of nutrients owing to the discharge of waste from industries and bank-side residents without adequate pre-treatment (Bukit 1995; Palupi *et al.* 1995). Erosion within these systems during rainstorm events and the effects of high suspended solids are an additional concern with respect to the water quality. Currently, due to the poor quality of the raw water, Buaran WTP can only achieve Indonesian clean water standards (Ministry of Health Decree No. 416/Menkes/Per/IX/90; Mustika Sari 2004). In order to meet tightening regulatory standards, Buaran WTP requires the implementation of more innovative, cost-effective, yet simple approaches to supply safe municipal drinking water which complies with new regulations set by the Ministry of Health (Decree No. 907/Menkes/SK/VII/2002; Mustika Sari 2004).

### **1.3.2 Raw water quality**

The pollution of West Tarum Canal (Buaran's source water) was the result of poor water catchment protection within the Ciliwung and Citarum Basins. The raw water was subject to intermittent changes in water quality, particularly ammonia, organic material, DO and turbidity. The raw water quality was characterised by intermittent high turbidity with peaks up to 10,000 NTU during rainstorm events. The total BOD<sub>5</sub> varied between 7 to 10 mg/L with occasional short-lived peaks of up to 20 mg/L. Ammonia-N concentrations fluctuated daily. Mean ammonia-N concentration was 0.8 mg/L with frequent peaks up to 2.5 mg/L, which adversely impacts on chlorination (Cammarota

2001). A more thorough discussion characterising pollution sources, water quality analysis and the subsequent impact on water treatment is discussed in Chapter 2.

Preliminary treatment for ammonia removal ahead of pre-chlorination is needed to reduce the chlorine demand of raw water so that the risk of chlorine by-product formation is reduced and the application of chlorine will be better controlled, and more cost-effective (see Section 2.3; Mustika Sari 2004). Currently, the effective control of chlorine dosing requires intensive monitoring of the raw water quality (Mustika Sari 2004). A process to peak-lop ammonia-N concentrations below 0.1 mg/L is desired to improve disinfection and may be accomplished using biological filtration (Holmes *et al.* 2001; Cammarota 2001). Any adopted process would need to be easily retrofitted at the front-end of existing WTPs and must not impact on down-stream treatment process (e.g. coagulation and flocculation). The process needs to be robust and capable of consistently producing highly nitrified effluent, even during periods of high suspended solids and organic loads.

#### **1.4 Process selection**

Biofilms consist of a range of microorganisms which are capable of degrading inorganic and organic nutrients (Wuertz *et al.* 2003). Therefore, any process which artificially enhances active biofilm density can provide sufficient nutrient removal and stabilisation of nutrient rich water. Thus biofiltration was seen as having potential for the pre-treatment of polluted potable water supplies. Of interest to the current study is the biological oxidation of ammonia, via the process termed nitrification, where nitrifying bacteria readily oxidise ammonia to potentially less chlorine consuming forms of nitrogen. A number of biological treatment processes, which include BAFs, fluidized beds, or moving bed reactors have the potential to biologically oxidise ammonia. However, an earlier study on Buaran WTP by Cammarota (2001), identified plastic media NTFs as the best option for ammonia removal for a number of reasons which are outlined below. Traditionally, they have been used for biological nitrification of ammonia-

rich *wastewater*, however their design and performance when required to operate under low ammonia concentrations (i.e., for *potable water* applications) is unknown.

Any biological process adopted that requires effluent clarification / biomass separation would incur excessive costs, due to the need to construct clarifiers or settlement tanks. Suspended growth systems such as the activated sludge process were therefore not considered. Fixed film processes considered were BAFs, fluidised beds and NTFs.

BAFs are process variants of granular media filters with the addition of a mechanical aeration capability. Many types of BAFs have been developed, the common factor being that they are filled with solid supports (or media) of high specific surface area, selected to provide attachments sites for biofilms and particle removal by depth filtration. When biomass / particulates accumulate in the filter bed leading to increased loss of head, intermittent backwashing is necessary, which is usually achieved by a combination of air scouring and water backwashing. In comparison to NTFs, BAFs have a higher capital cost. They require a water retaining filter shell, aeration and backwashing components. They produce a waste stream that must be treated and disposed. BAFs also exhibit poor oxygen-transfer efficiency and are mechanically complex and therefore expensive to operate. They are however, much more compact than NTFs and so require a much smaller footprint.

Fluidised beds are similar to BAFs in that biomass is grown on a medium, usually sand, however they operate in an up-flow mode and the velocity of the influent is sufficient to expand the bed (Cammarota 2001; Pearce 2003). They have a very high surface area to volume ratio provided by the small sand media and are mechanically simple and high rate. However the main disadvantage is the high pumping costs to provide the required fluidisation velocities and oxygen transfer to sustain nitrification (Cammarota 2001; Pearce 2003).

Plastic media NTFs were favoured for several reasons. Any adopted process needs to be relatively low technology and capable of operating with minimal and unskilled

maintenance. NTFs, as well as meeting this requirement, also have a low power requirement due to the efficient oxygen transfer. Power is only required for pumping to the top of the filter and so overall power consumption is dependent upon the aspect ratio adopted for the design (Pearce 2004). The disadvantage of NTFs is that they are relatively low rate processes compared to BAFs and fluidised beds.

## 1.5 Nitrifying trickling filters

Trickling filters have been in use for nearly 100 years for the biological remediation of high strength municipal and industrial wastewater (Daigger *et al.* 1994; Liu and Liptak 1997). They were traditionally used for the oxidation of biodegradable organic matter, but interest in their ability to achieve nitrification has increased in the past 20 years (Daigger *et al.* 1994). Figure 1.2 illustrates the major components of a typical NTF. The operational principle of NTFs is simple. They are a fixed biofilm process that involves infiltrating water flowing over a vertical gradient of highly permeable support media, high in surface area. A hydraulically-driven rotating distribution arm, evenly distributes water to the filter body, with very low maintenance requirements and self-cleaning operation under high-flow conditions. Many different types of physical biofilm support media can also be used e.g. natural gravels, wood or artificial plastic media. The more recently developed 'high specific surface area' plastic media, which promotes a highly aerobic environment, has become popular for the more intensive treatment applications.

NTFs are classified as an attached-growth biological process because water percolates through the inert support media on which a naturally produced biological layer or biofilm is growing in a highly aerobic environment (see Section 1.6). This active biofilm biologically transforms or physically entraps contaminants within the inflowing water such as inorganic and organic nutrients and suspended solids. In particular the nitrifying population within the biofilm readily oxidises ammonia to potentially less bio-available forms of nitrogen (i.e., nitrite and nitrate) via the process termed nitrification (see Section 1.7.1). In addition to biological ammonia oxidation, NTFs improve the water quality in other ways. Through normal operation, NTFs also develop a heterotrophic

microbial population within the active microbial biofilm which assists in reducing the BOD<sub>5</sub> of the water via the oxidation of organic carbon, especially DOC (see Section 1.7.3)

NTFs have been successfully applied to a number of treatment scenarios, including the treatment of concentrated municipal and industrial wastewaters. To achieve a desired outcome, trickling filters can be operated in many different configurations as discussed by Metcalf and Eddy (2003). Types of trickling filters are classified by their hydraulic or organic loading rates (Metcalf and Eddy 2003). Typical wastewater trickling filter classifications and loadings are summarised in Table 1.1. This table also compares the design characteristics of wastewater NTFs with the NTF designed for this study. Wastewater NTFs are mostly classified as low- or high-rate filters. In contrast to wastewater applications, the NTF employed in this study was classified as *super* high-rate because it was designed to operate under hydraulic loads (irrigation velocity) some 30 to 100 times greater than most standard low-rate wastewater NTFs. Conventionally, super high-rate filters were not designed for nitrification, instead they have been used to treat organic loads substantially higher than that of low-rate filters (Metcalf and Eddy 2003). However, due to the uniquely low ammonia feed concentrations the filter in this study was expected to operate under, high hydraulic loads were required to achieve ammonia mass loads closer to that of conventional low-rate wastewater NTFs.

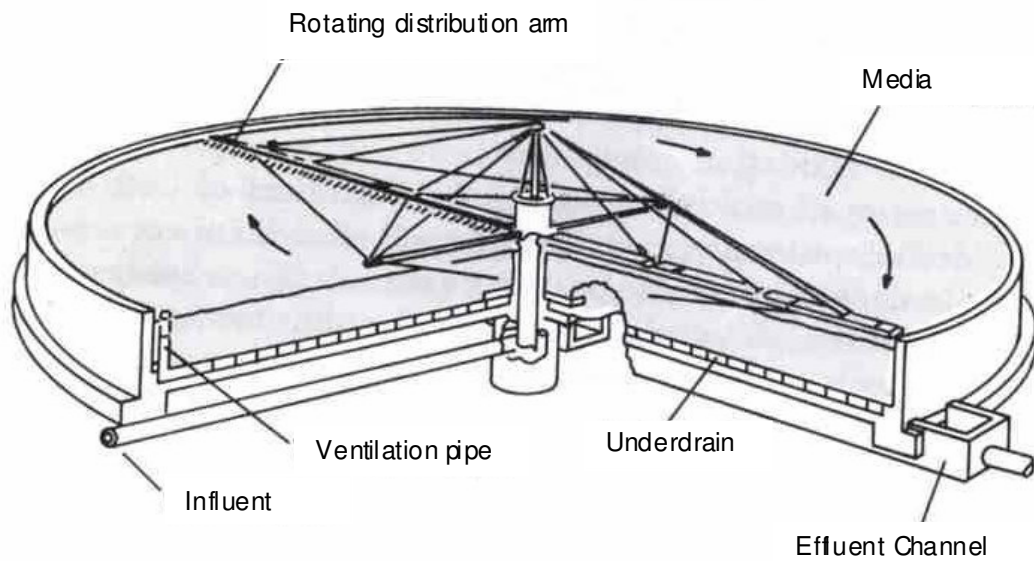


**Figure 1.2.** Illustration of a trickling filter from Liu and Liptak (1997).

**Table 1.1.** Typical trickling filter classifications and corresponding design characteristics: Comparison between conventional wastewater filters with the potable NTF designed for this study (Gullicks and Cleasby 1986; Parker *et al.* 1989; Andersson *et al.* 1994; Parker *et al.* 1997; Pearce, 1999; Pearce and Foster, 1999; Metcalf and Eddy 2003; Pearce, 2004).

Design characteristics	Wastewater trickling filters			*Potable water trickling filter
	Low rate	High rate	Super high rate	Super high rate
**Irrigation velocity ( $\text{m}^3 \text{ m}^{-2} \text{ d}^{-1}$ )	1 – 4	10 – 75	40 – 200	>125
Organic loading ( $\text{kg BOD}_5 \text{ m}^3 \text{ d}^{-1}$ )	0.07 – 0.3	0.6 – 3.2	>1.5	0.01 – 0.55
ammonia-N loading ( $\text{g NH}_4\text{-N m}^{-2} \text{ d}^{-1}$ )	0.7 – 3.2	>2.5	n/a	0.04 – 1.0
Influent ammonia-N (mg/L)	10 – 30	10 – 30	10 – 30	0.5 – 5.0
Recirculation ratio	0	1 – 2	0 – 2	0
Designed effluent quality	Well nitrified	Low in organic carbon / some nitrification	Low in organic carbon / no nitrification	Unknown

\*Large pilot-scale NTF employed in this study.

\*\*Unit flow volume per unit of cross-sectional surface area (plan area) of trickling filter per day.

In the past years, there has been increasing interest in the use of so-called 'innovative' and 'alternative' biofilm technologies for the treatment of different types of wastewaters (Odegaard *et al.* 1994). This increased interest in NTFs is likely due to the inherent advantages of these systems such as:

- Aerobic stabilisation of labile sources of oxidisable materials (i.e. ammonia and DOC), thereby reducing oxygen demand and increasing dissolved oxygen concentrations;
- Owing to their simple design and operational requirements, NTFs are less capital and labour-intensive than other more highly engineered treatment technologies;
- They operate at an insignificant internal head-loss, and an associated elimination of the need for filter backwashing or active internal recycling of biomass as 'return-sludge' (Odegaard *et al.* 1994); and
- Low power requirement due to the efficient oxygen transfer.

These advantages make NTFs an attractive proposition for water treatment scenarios such as at Buaran WTP, where capital input, operational costs, and skilled maintenance need to be minimised. The nitrification performance of NTFs is strongly influenced by many environmental and operational conditions, many of which have been extensively explored at the pilot- and full-scale level for *wastewater* treatment. However, their application as a pre-treatment step to remove low concentrations of ammonia, ahead of a conventional *water treatment* process, was a novel concept that was assessed in this study. It was anticipated that this research would demonstrate that NTFs could offer real potential for affordable and sustainable management of the ammonia related problems at Buaran WTP, and therefore worthy of investigation. It was further envisaged that they would serve to reduce the ammonia and nitrite related chlorine demand, thereby improving disinfection and the control of disinfection, which may have other beneficial 'knock-on' effects for the water treatment process (see Chapter 2).

As reviewed above, NTFs are an attached biological growth process. Therefore, filter performance is dependant on biofilm processes which are influenced by gaseous and solute mass transfer, and the microbial community structure.

## **1.6 Biofilms**

### **1.6.1 Definition**

Biofilms consist of complex, interrelated, mixed populations of micro-organisms embedded in a matrix of extracellular polymeric substances (Characklis and Marshall 1990; Wuertz *et al.* 2003). Biofilms, attached to the media of trickling filters, contain aerobic, anaerobic, and facultative bacteria, fungi, algae and protozoans (Liu and Liptak 1997; Plate 1.1). The predominance of microorganisms within biofilms is influenced by many environmental conditions as well as interactions with other groups of microorganisms, which either have positive or negative effects on filter performance (Parker *et al.* 1997).

### **1.6.2 Mass transport**

A cross-section schematic representation of a biofilm attached to support media is illustrated in Figure 1.3. Solutes such as inorganic and organic nutrients are transported from the bulk liquid into the biofilm, which are then utilised by the relevant microbial community. Biological processes of interest to trickling filters included nitrification, carbon oxidation, and denitrification (see Section 1.7). The transportation of solutes into the biofilm is termed "mass flux" or "mass transport" and is driven by a number of processes including diffusion, convection and dispersion (Characklis and Wilderer 1989; Wuertz *et al.* 2003). Diffusion is considered to be the most significant mechanism responsible for mass transport where solutes move down the concentration gradient at a rate determined by the gradient's magnitude, towards a point of uniform distribution (Harremoës 1982). Furthermore, by existing in biofilms attached to surfaces, the immobilised microorganisms increase the relative flow velocity between themselves and the bulk liquid, and therefore can benefit from convective transportation of solutes (Wuertz *et al.* 2003). The rate at which solutes are replenished, whether it is by diffusion or convection, is a key determinant for the growth of microorganisms, because it determines the availability of essential nutrients (Wuertz *et al.* 2003).

Mass transfer resistance increases with an increase in biofilm depth (Zhang *et al.* 1994). As a biofilm increases in thickness, the inner depths encounter diffusion limitations, whereby organic material and nutrients become metabolised before they can reach the microorganisms closest to the media surface. The inner depths become starved of nutrients and enter into an endogenous phase (Metcalf and Eddy 2003). The biofilm then becomes susceptible to detachment and can be washed away in the filtrate, allowing development of a new biofilm. Detachment (or the erosion of biomass from engineered systems) can also be mechanically induced by changes in hydrodynamic conditions (e.g. increased hydraulic surface loading or backwashing) and by the presence of toxic loads (Characklis and Marshall 1990; Boller *et al.* 1997). Biofilms are continually renewed, and the process of detachment is commonly termed “sloughing”. Biofilms generally exist in a stationary state where mass gained from growth is balanced by the mass lost via detachment (Alpkvist and Klapper 2007).

### **1.6.3 Extracellular polysaccharides**

The main constituents of extracellular polymeric substances are polysaccharides, proteins, humic compounds, and nucleic acids, with polysaccharides considered a major component (Wuertz *et al.* 2003; Jefferson 2004). Extracellular polysaccharides (EPS) are considered a pre-requisite for the formation of biofilms where they are responsible for: (i) adhesion of cells to surfaces; and (ii) bioflocculation of bacterial cells in suspension. As well as playing a significant role in forming aggregated communities, EPS represents an important survival advantage for the immobilised microbial community (Wuertz *et al.* 2003; Jefferson 2004). Some of these survival functions include provision of a protective barrier, offering mechanical stability, retention of water, sorption and accumulation of nutrients, and a source of available carbon (Wuertz *et al.* 2003).

Polysaccharide composition of biofilms is of significant interest because the diffusive properties of biofilms may be strongly influenced by the concentration and properties of extracellular polysaccharides (Wuertz *et al.* 2003). Variation in biofilm extracellular polysaccharide composition and yield occurs in response to both chemical and physical

environmental conditions. In particular, polysaccharide production is generally governed by the availability and concentration of nutrients. For suspended growth BNR processes, the C:N:P ratio has been shown to influence the EPS composition of microbial flocs (Bengtsson 1991; Veiga *et al.* 1997; Wuertz *et al.* 2003). Many studies have shown carbon utilisation to shift towards EPS synthesis during periods of high C:N ratio, and/or when nitrogen concentrations are limiting (Stover 1980; Punal *et al.* 2000; Liao *et al.* 2001). Despite the importance of EPS in forming microbial aggregates or biofilms, excessive amounts have been shown to negatively influence the performance of BNR processes. For attached growth systems, EPS may form a diffusive barrier, and limit the mass transfer of oxygen and nutrients within biofilms (Characklis and Marshall 1990; Wuertz *et al.* 2003). Therefore, for a potable water NTF operating under low nitrogen concentrations, which are some 10- to 50-fold lower than traditional wastewater application, the impact of nitrogen limitation on EPS production and the adverse impact it may pose on NTF performance requires further consideration.

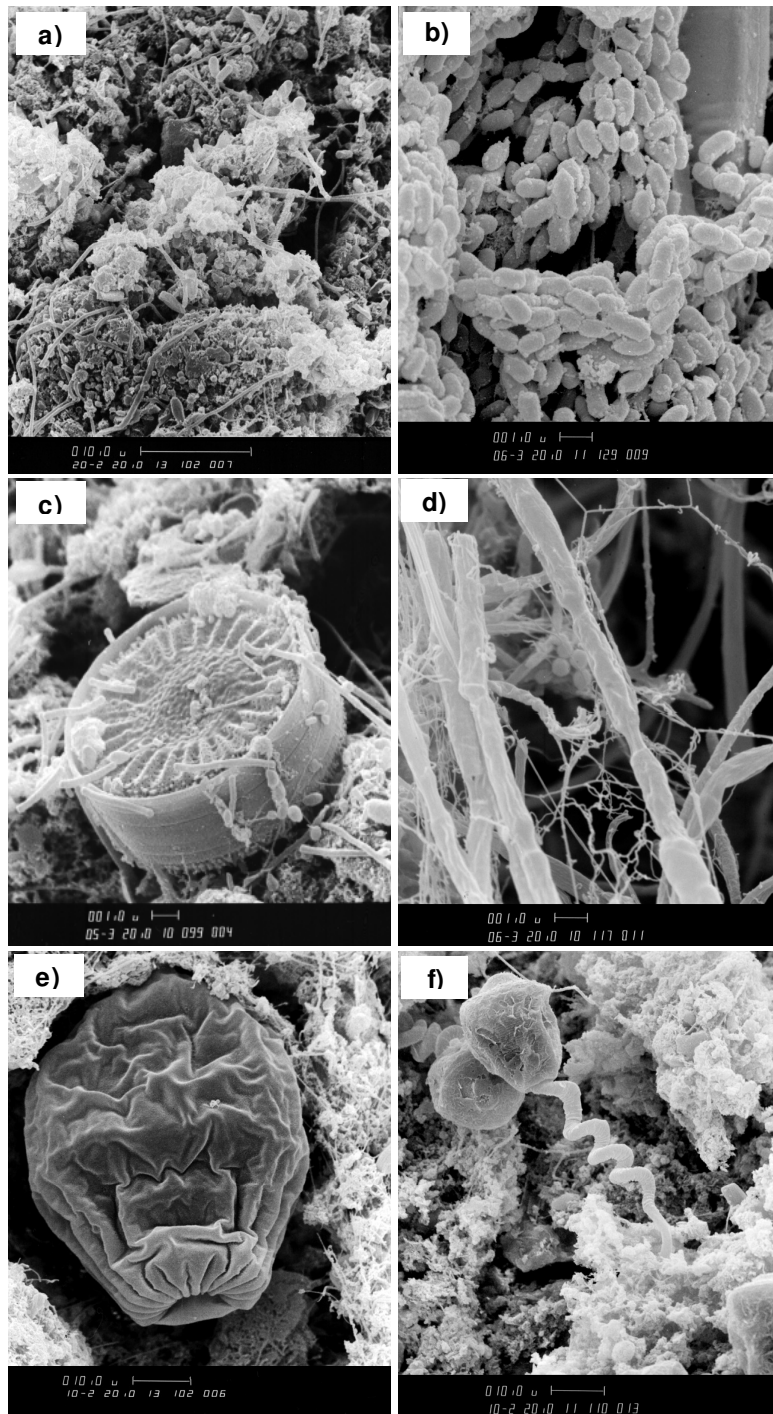


**Plate 1.1.** Scanning electron micrographs showing the diversity of microorganisms found in nitrifying biofilms: (a) ultra structure of biofilm; (b) bacterial cells; (c) centric algal diatom frustule; (d) filamentous bacteria; (e) Testate amoeba; and (f) ciliated stalked protozoa. Taken by the author.

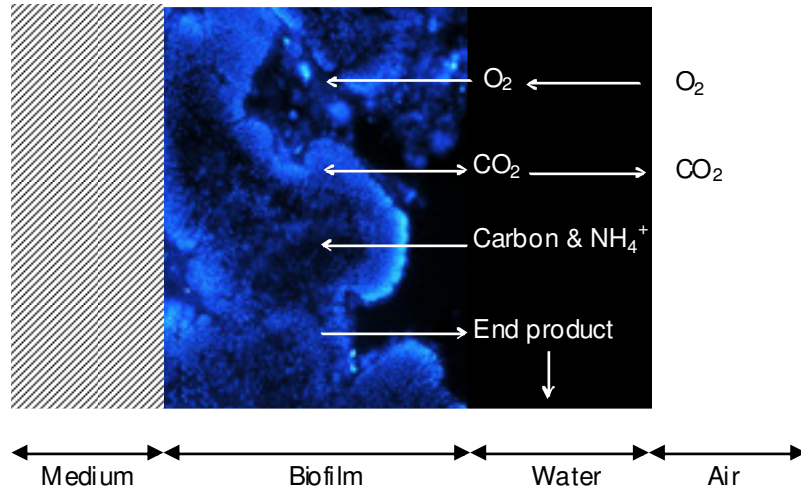


**Figure 1.3.** Schematic representation of a biofilm cross-section.

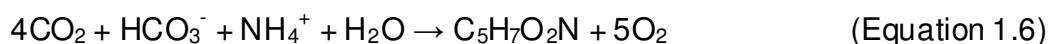
## 1.7 Microbiological processes specific to NTFs

### 1.7.1 Autotrophic nitrification

Biological nitrification is a fast energy-yielding reaction, which involves a two-step successive process, performed by aerobic nitrifying bacteria. The first step is the oxidation of ammonia to nitrite by AOB (Metcalf and Eddy 2003; Noda *et al.* 2003; Equation 1.4). In the second step, nitrite is oxidised to nitrate by NOB (Noda *et al.* 2003; Equation 1.5). From the equations, it can be seen that molecular oxygen must be present as the terminal electron acceptor for oxidation to proceed. Oxygen is therefore the limiting factor for both nitrification activity and abundance of nitrifying bacteria in biofilms (Schramm *et al.* 1996).



Species belonging to AOB and NOB are principally Gram negative chemolithoautotrophic bacteria, meaning they fix inorganic carbon to fulfil their carbon requirements for the synthesis of cellular material (Metcalf and Eddy 2003; Noda *et al.* 2003). The reaction for cellular synthesis is represented in Equation 1.6.



The energy production of nitrifying bacteria is primarily devoted to fixing carbon dioxide (Metcalf and Eddy 2003). It is for this reason that nitrifiers have a slow growth rate: approximately  $0.08 \text{ h}^{-1}$  at  $30^\circ\text{C}$  (Wiesmann 1994; vanBenthum *et al.* 1997). This is extremely long when considering the growth rate of aerobic heterotrophic organisms (approximately  $0.3$  to  $0.5 \text{ h}^{-1}$  at  $30^\circ\text{C}$ ), which are discussed further in Sections 1.7.3 and 1.8.2 (Wiesmann 1994; vanBenthum *et al.* 1997).

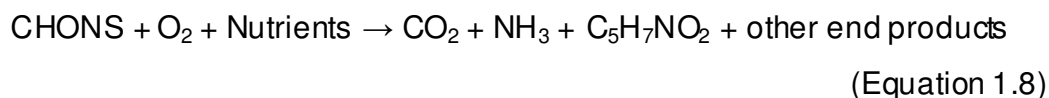
### 1.7.2 Denitrification

NTF biofilms are mostly aerobic, but under conditions which promote oxygen transfer limitations, anoxic micro-habitats can develop, which can facilitate denitrification. Denitrification is the process where nitrate is reduced biologically under anoxic conditions to nitrogen gas (Equation 1.7). Denitrification can be accomplished by several genera of heterotrophic bacteria which include *Achromobacter*, *Aerobacter*, *Alcaligenes*, *Bacillus*, *Brevibacterium*, *Flavobacterium*, *Lactobacillus*, *Micrococcus*, *Proteus* and *Pseudomonas* (Metcalf and Eddy, 2003). The conversion of nitrate to di-nitrogen gas provides these bacteria with energy for growth, However, they require a source of organic carbon for cell synthesis (Metcalf and Eddy 2003; Waki *et al.* 2007).



### 1.7.3 Carbon oxidation

In contrast to autotrophic nitrifying bacteria, heterotrophic bacteria utilise organic carbon for the formation of cell tissue (Metcalf and Eddy 2003; Pearce 2004). The oxidation and synthesis of organic carbon by heterotrophic bacteria is shown in Equation 1.8 (Metcalf and Eddy 2003). The ability to utilise organic carbon means heterotrophs have much higher growth rates than autotrophic nitrifying bacteria (vanBenthum *et al.* 1997; Metcalf and Eddy 2003).



where,

CHONS = Organic material

C<sub>5</sub>H<sub>7</sub>NO<sub>2</sub> = New bacterial cells

#### **1.7.4 Nitrogen assimilation**

In addition to NTFs achieving nitrification, significant amounts of nitrogen can be removed via nitrogen assimilation (uptake) into the active heterotrophic biomass. Research conducted on mineral media trickling filters by Pearce (2004) has shown assimilative demands for nitrogen to increase with BOD<sub>5</sub> loading and removal, which can account for up to 55 % of total nitrogen removal. Heterotrophic assimilative demands for nitrogen equate to approximately 0.0325 mg N/L for every 1 mg/L of BOD<sub>5</sub> removed through biofiltration (Pearce 2004).

#### **1.7.5 Anaerobic ammonia oxidation (anammox)**

Anammox is a relatively new microbial process employed for nitrogen removal from wastewater, where ammonia is biologically oxidised under strict anaerobic conditions to nitrogen gas (Jetten *et al.* 2002; Waki *et al.* 2007; see Equation 1.9). Anammox can be achieved by several genera of autotrophic bacteria (*Brocadia anammoxidans*, *Kuenenia stuttgartiensis* and *Scalindua sorokinii*), which belong to the phylum planctomycetes (Jetten *et al.*, 2002).



From Equation 1.9, it can be seen that nitrite must be present as the preferred electron acceptor for oxidation to proceed. In practice, to fulfil the nitrite requirements, nitrogen is partly oxidized to nitrite via nitrification before the anammox process, or the compound is added (Jetten *et al.*, 2002; Waki *et al.* 2007). To the author's knowledge, research on the anammox process has been limited to suspended growth systems such as the sequencing batch reactor and fluidised bed reactor. The contributory role of anammox to nitrogen removal within NTFs is considered to be minimal, because of the highly aerobic environment the plastic media promotes. Research conducted by Lydmark *et al.*, (2006) on a full-scale plastic media NTF, found that anammox bacteria represented only 2 % of all *Bacteria* present, which were thought to be confined to anaerobic microenvironments scattered deep within the biofilm.

## 1.8 Factors influencing nitrification

Although many attributes of nitrification have been intensively studied, nitrification is still difficult to maintain in biologically engineered processes (Noda *et al.* 2003). Achieving optimal process performance with NTFs is dependent upon the ability to maintain high nitrification rates. In achieving these rates, the requirements of nitrifying biofilms need to be recognised. The following section focuses on environmental and operational parameters and how they influence the nitrifying capacity of NTFs, focusing on conditions which impose mass transfer limitations and thus reduce the efficiency of nitrification.

### 1.8.1 *Mass transport*

Trickling filters are biofilm processes therefore the rate of microbial transformations, and hence their performance, is strongly regulated by the mass transport of nutrients and oxygen into the biofilm. Nitrification rates of fixed film processes, for example NTFs, are mostly limited by the mass transport of DO and/or ammonia from the bulk liquid into the biofilm (Boller *et al.* 1994; Boller *et al.* 1997; Metcalf and Eddy 2003). Oxygen-limited nitrification occurs in the presence of high ammonia and/or organic loads, such as those encountered by wastewater NTFs, where nitrification rates are regulated by the flux of oxygen into the biofilm. For wastewater NTFs treating concentrated wastewater, ammonia removal generally exhibits linear or zero-order behaviour down the filter bed and therefore the design of many wastewater NTFs can be based on zero-order kinetics (Gullicks and Cleasby 1986). In contrast, ammonia-limited nitrification is encountered in environments where the biofilm becomes exposed to low concentrations of ammonia (<5.0 mg NH<sub>4</sub>-N/L), such as those commonly detected at Buaran WTP and throughout many other polluted surface water catchments (see Chapter 2). Here, nitrification rates may become limited by the rate at which ammonia diffuses into the biofilm, as determined by the concentration gradient. For wastewater NTFs, ammonia-limited nitrification is only apparent at the lower depths of a well-functioning filter where ammonia concentrations are lowest (Boller *et al.* 1994). Designing a potable water NTF to remove low concentrations of ammonia based on wastewater design criteria that has

been developed from zero-order kinetics with respect to ammonia removal, would therefore be insufficient. Investigating the impact of diffusion limitations posed by low concentrations of ammonia on NTF performance was therefore an essential component of this study.

### **1.8.2 Interspecies competition**

When two or more species in a community rely on similar limited resources, they become subject to inter-species competition. For mixed population biofilms such as those found in NTFs, competition for oxygen, nutrients, and aerobic space between different microbial groups will affect the performance of NTFs (Villaverde *et al.* 2000). It is widely documented that in such biofilm systems, competitive interactions between heterotrophic bacteria and nitrifying bacteria, usually leads to a decrease in nitrifying capacity; an important factor to consider when designing a NTF for the pre-treatment of polluted source water (Fdz-Polanco *et al.* 2000; Satoh *et al.* 2000; van Loosdrecht *et al.* 2000; Villaverde *et al.* 2000).

A study by Kindaichi *et al.* (2004) explored the microbial composition of autotrophic biofilms under conditions (i.e., low organic loads) which favoured the growth of nitrifiers, and found that the ratio of nitrifiers (AOB plus NOB) to heterotrophs was close to 1:1. Due to the large difference in biomass yield between heterotrophs and nitrifiers, high organic carbon loads (of soluble or particulate nature) can cause this ratio to decrease where nitrifiers become diluted by the fast growing heterotrophic community (vanBenthum *et al.* 1997). The survival of the nitrifiers is therefore limited by the density of competing heterotrophic bacteria, which is determined by the C:N ratio (Okabe *et al.* 1996). On a long-term basis, high carbon loads can eventually cause a “washout” of the residential nitrifying community from biological reactors (Boller *et al.* 1997).

In addition to dilution of nitrifiers, heterotrophs increase oxygen transfer resistance through the biofilm depth. Due to the difference in biomass formation rates between heterotrophs and autotrophs, stratification through the biofilm depths can occur (Okabe *et al.* 1995; vanBenthum *et al.* 1997). This results in an outer heterotrophic layer that

restricts nitrifiers deep within the biofilm. The over growth of nitrifiers by heterotrophs is disadvantageous because nitrifiers experience additional oxygen transfer limitations when an organic substrate is present (vanBenthum *et al.* 1997). This was confirmed by Zhang *et al.* (1994) using microelectrodes, showing that an increase in organic carbon (glucose) decreased ammonia oxidation because the heterotrophs out-competed the nitrifiers for DO. Many studies have shown that the magnitude of nitrification inhibition and degree of stratification can be regulated by the C:N ratio, where a high carbon loads generally increases inter-species competition for oxygen and aerobic space (Okabe *et al.* 1995; Okabe *et al.* 1997). High C:N ratio also promotes inter-species competition for available nitrogen (i.e. ammonia). This may be the case in aquatic systems, such as Buaran's, where relative to wastewater, they present low ammonia concentrations. Here heterotrophic bacteria may become subject to nitrogen limitation and out-compete with nitrifiers for available nitrogen to satisfy assimilative requirements. This phenomenon was observed in nitrogen limited fresh water systems by Verhagen and Laanbroek (1991) and Strauss and Lamberti (2002). It is also important to note that the critical C:N ratio has been shown to vary between systems, since oxygen availability and transfer is the primary controller of nitrification, which can be manipulated by reactor design and operation variables (Boller *et al.* 1994; Zhang *et al.* 1994). Given that polluted source water can present high organic carbon concentrations, for the current study it was necessary to consider the possibility of nitrification suppression caused by heterotrophs competing for DO and/or nitrogen, and to determine the critical C:N ratio.

### **1.8.3 Environmental parameters**

The nitrifying capacity of a biological system is a function of biological growth kinetics, i.e., characteristics of the environment needed for their growth. Effective environmental control in biological treatment systems is based on understanding the basic principles governing microbial growth. Environmental parameters including temperature, pH, DO, alkalinity, and toxic substances all have an important effect on the survival, growth and activity of nitrifiers. Desired values for nitrification for each environmental factor are presented in Table 1.2. In general, nitrification is most efficient at pH levels ranging from about 7.5 to 8.5, and can decline significantly at levels outside this range (Metcalf and Eddy 2003). Temperature also directly affects growth and nitrification rates of nitrifying

bacteria as well as DO saturation constants. Nitrification rates are slower at lower temperatures (2°C) and increase linearly through the range of temperatures outlined below. Although warm waters increase the metabolic activity and growth rates of nitrifiers, Gebert and Wilderer (2000) reported that a NTF artificially heated to 32°C could not sustain optimal nitrifying capacity. It was concluded that reduced oxygen solubility, and mass transfer limitations owing to increased biofilm thickness, were the primary causative factors, when operated under these high temperatures. Alkalinity, may also be a rate limiting factor, given that 7.14 mg/L of alkalinity (CaCO<sub>3</sub>) is consumed for every 1 mg/L of ammonia-N oxidised via nitrification (Liu and Liptak 1997).

**Table 1.2.** Optimum values of environmental factors for nitrification. (Bardolet 1997; Yoo *et al.* 1999; Metcalf and Eddy 2003).

<b>Environmental factor</b>	<b>Range</b>
pH	7.5 – 8.5
Dissolved oxygen	> 1 mg/L
Temperature	2 – 30°C
Salinity	0 – 44 ppt
Alkalinity (CaCO <sub>3</sub> )	*Sufficient

\*For every 1 mg/L ammonia-N oxidised, 7.14 mg/L of CaCO<sub>3</sub> is consumed.

#### **1.8.4 Operational and design parameters**

Much of the available literature has demonstrated that nitrification performance of biological reactors has a strong dependency on the mass transfer of DO and ammonia into the biofilm. Therefore, it is expected that any measures taken to improve the diffusion of DO and ammonia into the biofilm would improve NTF performance. In addition, research obtained from many experimental studies on improving the design and operation of fixed film processes has shown that the distribution of biomass is also integral to reactor nitrification performance (Boller *et al.* 1994).

Oxygen transfer can be influenced by operation parameters such as hydraulic load (Boller *et al.* 1994). Andersson *et al.* (1994) and Boller *et al.* (1994) showed that an increase in flow and velocity can increase oxygen transfer by turbulence, which in turn enhances nitrification rates. Oxygen transfer can also be enhanced through media selection and positive ventilation (Parker *et al.* 1989). In recent years many traditional rock bed filters have been retrofitted using various configurations of 'high specific surface area' plastic packing. The uniquely high void space of this media promotes an aerobic environment due to excellent passive aeration of infiltrating water. Maximising oxygen concentrations within the bulk solution is of key importance since the higher the DO concentration, the deeper oxygen can penetrate into the biofilm (Zhang *et al.* 1994).

Nitrification rates can also be improved through biofilm control (Parker *et al.* 1997). Since mass transfer resistance increases with biofilm depth, a thick biofilm does not necessarily result in high nitrification rates (Boller *et al.* 1994). Changing the hydraulic characteristics (e.g. by increasing hydraulic flow and back-washing) of attached growth systems can induce detachment which helps maintain a thin biofilm with enhanced mass transport properties (Boller *et al.* 1994).

More uniform nitrification rates can also be achieved by improving the distribution of biomass through the depths of a NTF (Boller *et al.* 1994). Patchy biofilm development has been shown to negatively impact nitrification rates within NTFs, and is generally caused by conditions which promote biofilm predation, and at bed depths which are ammonia limited (Gujer 1984; Parker *et al.* 1989; Biesterfeld *et al.* 2003). Biofilm predation can be overcome by flooding the filter or increasing the wetting rate (Parker *et al.* 1989; Parker *et al.* 1997). Boller *et al.* (1994) confirmed that heterogeneous distribution of nitrifier activity and biomass caused by ammonia limitation was significantly improved by operating two NTFs in series, where the order of the two filters was inverted weekly. This configuration led to more uniform nitrification rates throughout the filters.

Finally, the operation of NTFs can be manipulated to achieve other desired out-comes. For example, Pearce (2004) showed that recirculation of wastewater effluent improved total nitrogen removal via denitrification and nitrogen assimilation. Recirculation introduces nitrate into the top of the filter where organic carbon, heterotrophic activity and denitrification potential is highest. Significant carbon removal was also observed with the recycled nitrate during denitrification (Pearce 2004).

From the literature reviewed above, biofilm behaviour and control are important regulators of NTF performance. Therefore, improved understanding of the microbial ecology and biofilm processes that occur within, are necessary for optimising process design and control.

#### **1.8.5 *In situ analysis of biofilm population structure***

It is widely accepted that for the successful application of biological reactors, microorganisms with the desired metabolic activity have to establish and be maintained within the systems (Wuertz *et al.* 2003). From the review above, it is also clear that the performance of biofilm reactors depend on the biofilm structure, in particular the distribution and activity of microbial species, which can be significantly affected by environmental, design and operational parameters. Therefore, information about the population structure of biofilms can be used to optimise the design and operation of engineered biofilm reactors and can be used to explain and predict reactor performance (Wuertz *et al.* 2003).

The composition of microbial communities can be investigated using many techniques (Wimpenny *et al.* 2000; Wuertz *et al.* 2003), however, in most recent years, FISH has become the most popular tool for identifying the taxonomic structure of biofilms (Wuertz *et al.* 2003). FISH uses fluorescently labelled phylogenetic markers (16S and 23S rRNA oligonucleotide probes) to detect intact cells of microorganisms on the basis of a sequence of RNA within their natural microhabitat (Wimpenny *et al.* 2000; Wuertz *et al.* 2003). Visualisation and quantification of target microorganisms can then be achieved using fluorescent microscopy (epifluorescence or confocal laser scanning microscopy).

FISH has provided a better understanding of microbial diversity and structure of biofilms within biological wastewater reactors, which in the past have been regarded as a “black-box”. In particular, FISH has been widely adopted to identify competitive and ecophysiological interactions between species within biofilms, sampled from various types of biological reactors (Okabe *et al.* 2002; Kindaichi *et al.* 2004), and was employed within this project.

## 1.9 Project aims

This study provided a unique opportunity to investigate the application of NTFs for pre-treatment of polluted raw water supplies using Buaran WTP as the case study. The rationale for this work as reviewed above is that NTFs are widely used for the biological stabilisation of nutrient rich wastewater, however little is known about their performance when operated under lower ammonia concentrations some 10- to 50-fold lower than conventional applications. The thesis project presented here describes a series of pilot-plant investigations, with a focus on assessing the suitability of NTFs for the pre-treatment of potable water. In particular, this project investigated application of NTFs to remove low concentrations of ammonia from polluted water supplies as an alternative to pre-chlorination.

Several factors need to be considered, and the research of this thesis seeks to address these. Factors include: mass transfer limitation presented by low ammonia concentrations and high organic loads; impact of hydraulic surface load; and the understanding of biofilm microbial ecology and biofilm characteristics in response to changes in filter conditions.

The specific aims were therefore to:

1. Determine the impact of low ammonia concentrations and hydraulic surface load on NTF performance.
2. Determine the influence of various organic carbon loads and C:N ratios on the NTFs nitrifying capacity.
3. Determine the effect of C:N ratio on the protein and polysaccharide composition of biofilms, and to correlate changes in biofilm composition with NTF performance.
4. Survey the microbial ecology within the pilot-NTF and correlate changes in microbial composition and architecture with NTF performance.

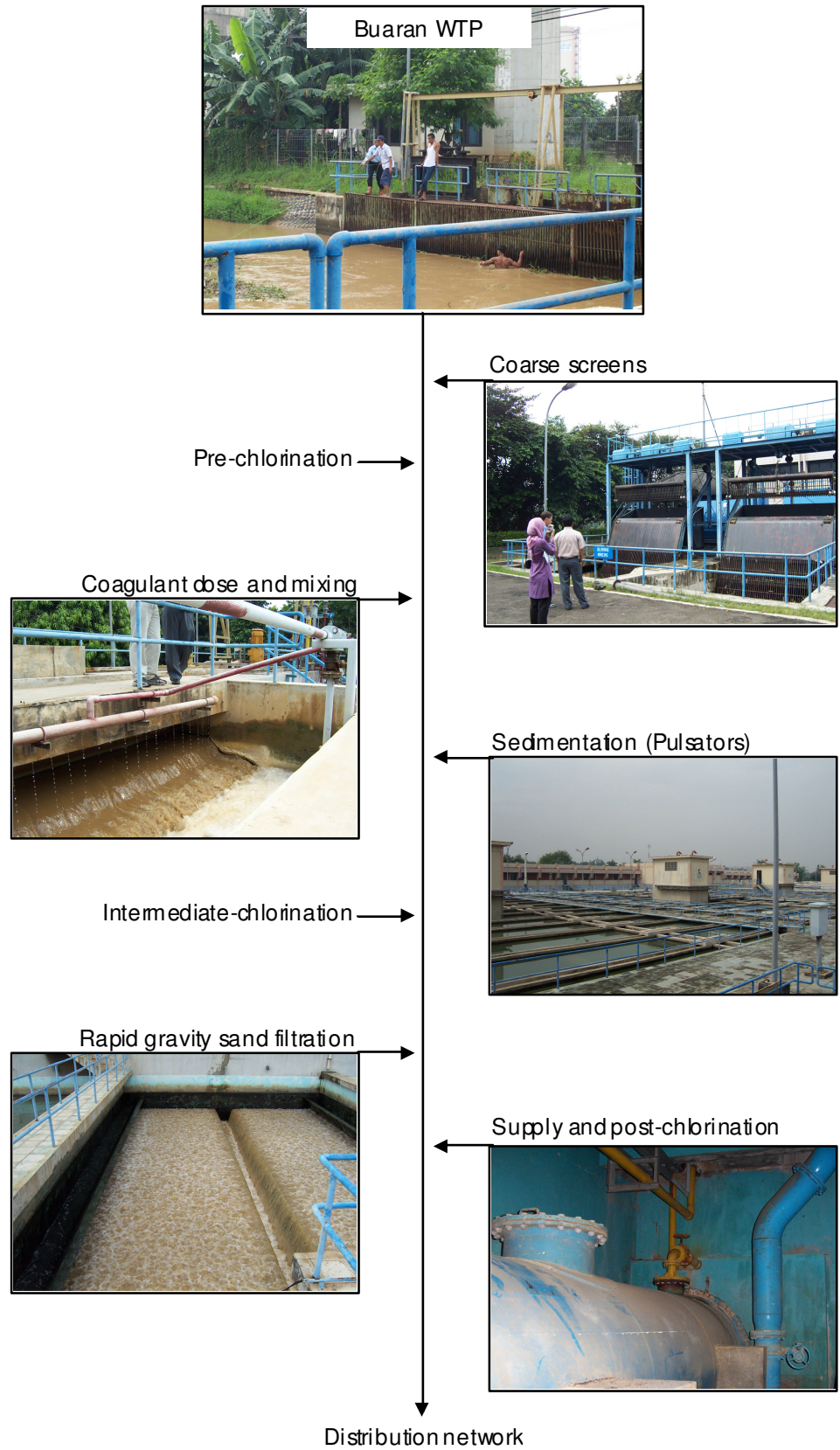
## 2 REVIEW OF THE RAW WATER QUALITY AT BUARAN AND IMPACT ON WATER TREATMENT

### 2.1 Introduction

Buaran WTP is a conventional plant, consisting of screens, coagulation, flocculation, sedimentation, and rapid gravity sand filtration. A summary of the physical and chemical treatment processes used is presented in Figure 2.1. The WTP is situated within the Ciliwung Basin and supplies water to approximately two million consumers in East Jakarta, Indonesia (Cammarota 2001). The raw water is extracted from the West and East Tarum Canal, which is supplied mainly by the Jatiluhur Reservoir, located in the Citarum Basins. A schematic layout of the Ciliwung and Citarum basins is presented in Figure 2.2. The distance between Jatiluhur and Buaran WTP is approximately 70 km, which provides many opportunities for the water to become contaminated. Due to the absence of water catchment protection, the East and West Tarum Canal are intercepted by many rivers, which support many industries and local residents who contribute significantly to the pollution of the raw water (Bukit 1995; Palupi *et al.* 1995; Cammarota 2001). Waters within the catchments have also been exploited to support extensive agriculture, hydroelectric power, public water supply, fisheries and recreation (Bukit 1995). Several studies have characterised the water quality within the catchments, in terms of microbiological, physical and chemical parameters, and have attributed the deteriorating quality and high pollution load to many of these activities (Bukit 1995; Palupi *et al.* 1995; Cammarota 2001; Hart *et al.* 2002). In particular, contamination was caused by the discharge of effluent from bank-side residents and industries (Bukit 1995; Palupi *et al.* 1995). 2500 industries located within the Citarum catchment have been identified as the major pollution sources of the Citarum River (Bukit 1995). These industries include textiles, clothing and footwear, electronics, aviation, mineral extraction, metals and building materials (Palupi *et al.* 1995; Cammarota 2001; Figure 2.2). Many of these adjacent industries discharge their effluent into the rivers without adequate pre-treatment despite the presence of regulations to control effluent discharge (Palupi *et al.* 1995; Cammarota 2001). Bank side residents situated around the Ciliwung

and Citarum catchments, use the rivers as their excreta and solid waste disposal sites (see Plate 2.1 and Plate 2.2; Bukit 1995 and Palupi *et al.* 1995). Five million residents are said to be located within the Citarum catchment, whereby 5 to 15 % of the population have direct water use from the river for their life activities, and more than 50 % discharge domestic waste directly into surface waters (Bukit 1995).

**Figure 2.1.**  
Summary of  
schematic water  
treatment process  
at Buaran WTP.  
Photographs  
taken by the  
author.



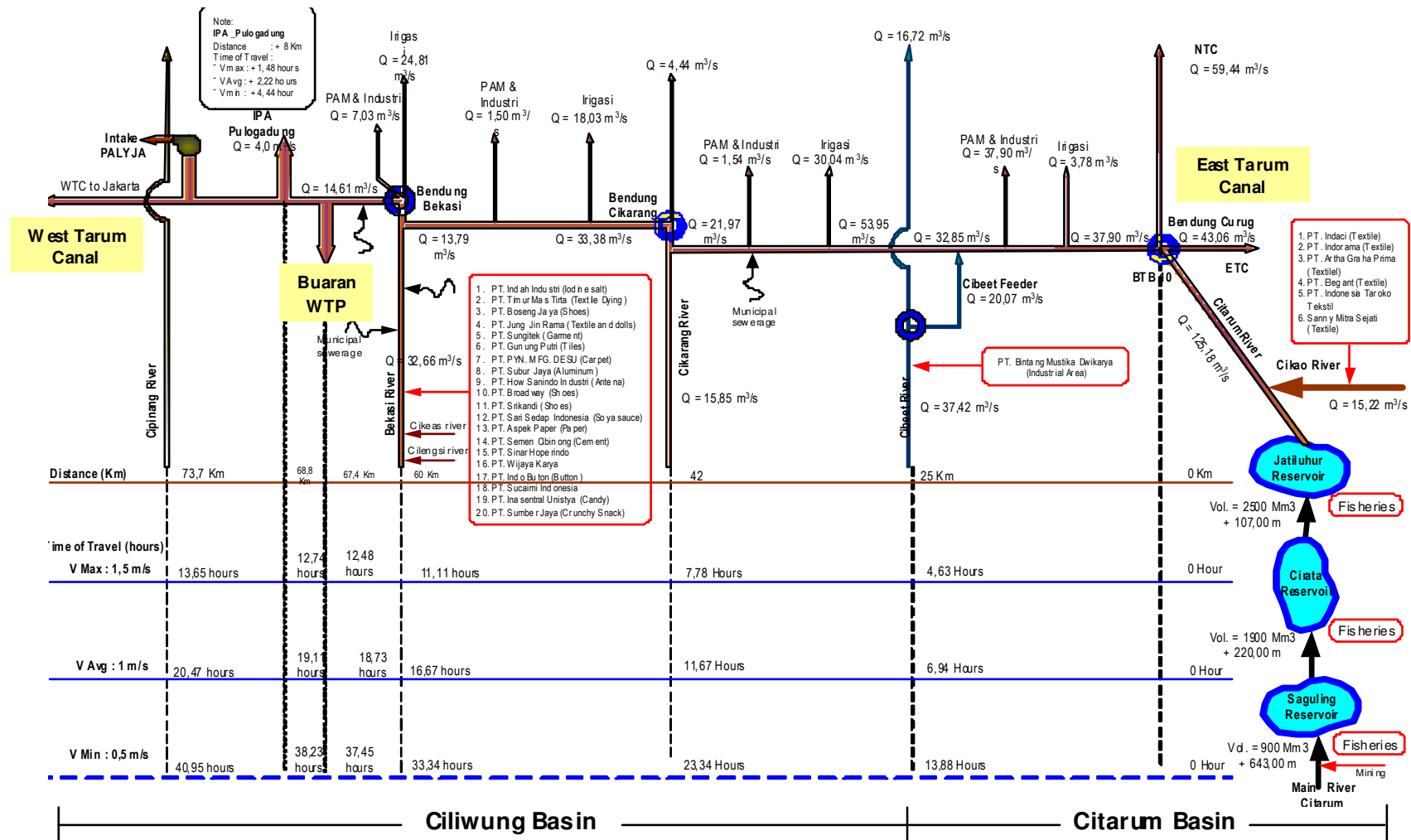
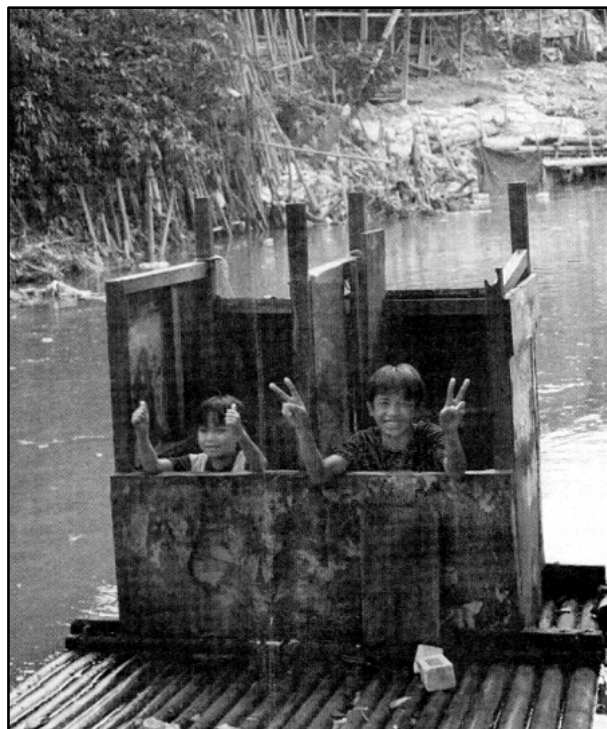


Figure 22. General layout of the Citarum and Ciliwung catchments and location of pollution discharge points (Modified and provided by Thames Pam Jaya).



**Plate 2.1.** Illustration of bank-side residents located within the Ciliwung and Citarum basin, who have direct water use for life activities (Holmes 1999).



**Plate 2.2.** Floating toilet: Discharge of excreta into the water supply (Holmes 1999).

The climate of the Citarum basin can be characterised as tropical, with distinct wet and dry seasons. The wet season extends between the months of November and April, while the dry season extends between May and October (Hart *et al.* 2002). The average annual rainfall is 2322 mm, with 80 % falling during the wet season (Hart *et al.* 2002). The differences in rainfall between seasons reflect flows within the catchments, which are expected to impact on water quality.

Previous investigations have characterised the raw water at Buaran WTP to be of poor quality, containing high concentrations of SS, organic carbon, nitrogen, faecal coliforms, manganese and iron (Cammarota 2001; Mustika Sari 2004). Many of these contaminants adversely affect treatment processes, which in turn increases treatment costs. In particular, ammonia has been considered a major pollutant, owing to the discharge of waste into the catchment, and is of key importance because of its ability to affect the disinfection efficiency of chlorine. The conventional practice for ammonia removal at Buaran WTP was to pre-chlorinate by dosing high concentrations of chlorine ahead of the water treatment process (Plate 2.3). This has a number of disadvantages including the formation of disinfection by-products, including trihalomethanes and high chlorine consumption. An earlier study on Buaran WTP highlighted these problems and considered plastic-media trickling filters as the best option for ammonia removal (Cammarota 2001). The wider focus of this thesis was therefore to investigate the application of NTFs to remove ammonia as an alternative to pre-chlorination.

The proposed NTFs need to be integrated within the existing WTP while the plant remains in operation (Cammarota 2001). A football field close to the coarse and medium screens has been identified as a suitable location to install several NTFs. If NTFs were to be put in operation, they would be situated after the coarse and medium screens, ahead of pre-chlorination. It should be noted that a pre-treatment step for SS removal may be required upstream of the NTFs to peak-lop SS during periods of extremely high concentrations, greater than 100 mg SS/L. If successful, NTFs could be a substitute for current ammonia removal method of pre-chlorination, which would reduce operational costs, improve disinfection and minimise the formation of disinfection

by-products. Furthermore, reducing the mass of chlorine needed can minimise the occupational health and safety issues associated with storing large quantities of chlorine on site.

It is important to emphasise that ammonia was not the only pollutant identified but is the focus of this study, and other relevant contaminants that influence the stability of NTF performance such as organic carbon and SS needed to be characterised in more detail. By examining historical water quality data and conducting a technical visit to Buaran WTP and the surrounding catchments, the aim of this chapter is to characterise the raw water quality. In particular, patterns in ammonia, organic carbon, and SS concentrations are examined. This information was subsequently used to design the operational conditions for well controlled pilot experiments, detailed in Chapters 4, 5, 6 and 7.



**Plate 2.3.** Pre-chlorination dosing point (white arrow) at Buaran WTP. Taken by the author.

## **2.2 Methods**

### ***2.2.1 Water quality data***

Water quality data for years 1999 to 2004 was provided by staff from Buaran WTP. Analysis of raw water quality parameters were conducted onsite either daily (ammonia-N, turbidity, organic matter as permanganate ( $\text{KMnO}_4$ ), total coliforms, total iron, total manganese) or weekly ( $\text{BOD}_5$ , COD, nitrite-N, nitrate-N, SS) by laboratory staff. Analysis was conducted using methods described by Mustika Sari (2004). DO, organic matter, SS and turbidity data measured along the Tarum canal was obtained from the appendices of Cammarota (2001).

### ***2.2.2 Technical visit***

A field visit to Buaran WTP and its surrounding catchments (Ciliwung and Citarum basins) was conducted in May 2004.

## 2.3 Results

### 2.3.1 Inorganic nitrogen

Analysis of ammonia-N data obtained between the period 1999 to 2004 showed mean ammonia-N concentration of Buaran raw water was close to 0.5 mg/L, with frequent spikes within the range of 1.0 to 2.5 mg NH<sub>4</sub>-N/L commonly detected. Figure 2.3 gives an example of seasonal variations in ammonia-N concentrations for the year 2001. No distinct seasonal pattern in ammonia concentration between wet and dry season can be seen. The variation in ammonia-N concentrations is often very short term. The influent ammonia-N can increase from below 0.5 mg/L to over 1.5 mg/L and then return to below 0.5 mg/L on consecutive daily samples. In some instances, there is a progressive increase and decrease over a few days, but many of the peaks are of less than 24 h duration. Ammonia-N correlated well with organic matter, turbidity, total iron and total manganese (Table 2.1), however, it was independent of BOD<sub>5</sub> (Pearson  $r = 0.04$ ;  $p > 0.05$ ). Statistical analysis confirmed a significant correlation between raw water ammonia-N concentration and total chlorine dosed at Buaran WTP (Table 2.1). The relationship confirmed that 9.75 mg/L of free chlorine were dosed for every 1 mg/L of ammonia-N, which was close to the theoretical value of 10 mg Cl<sub>2</sub>/L. Furthermore, from Table 2.1, it can be seen that other chlorine demanding contaminants such as organic matter, and total manganese, positively correlated with total chlorine dose.

For the years 2000 to 2004, total oxidised nitrogen (NO<sub>x</sub>) of Buaran WTP raw water fluctuated between 0.8 to 6.05 mg/L, and existed mostly in the form of nitrate-N. The mean NO<sub>x</sub> concentration was 1.72 mg/L.

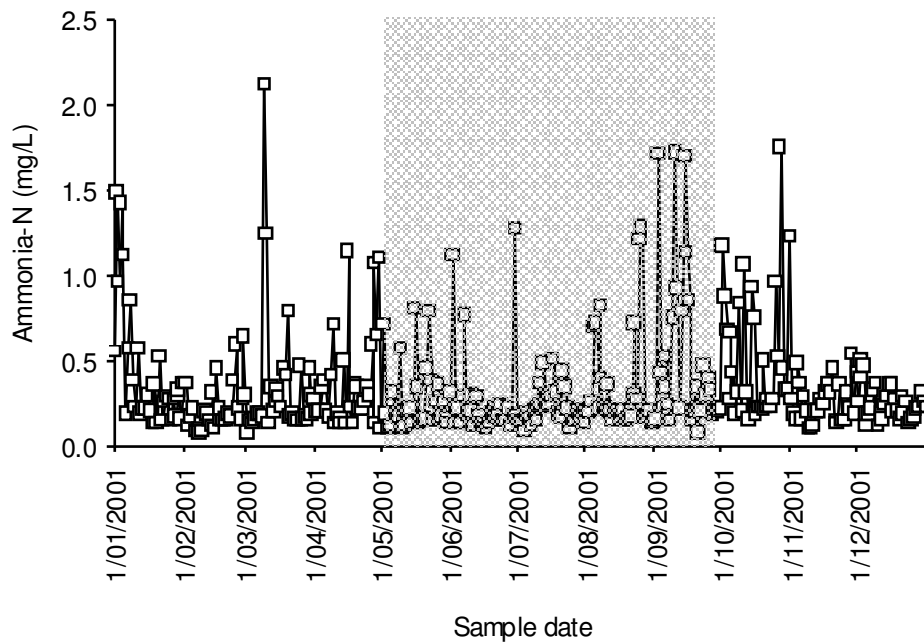


**Figure 2.3.** Seasonal variation in raw water ammonia-N concentrations at Buaran WTP during 2001. Shaded region represents the dry season.

**Table 2.1.** Pearson *r* correlation coefficient for raw water data collected during the year 2003 at Buaran water treatment plant.

	Total Cl <sub>2</sub> dosed (mg/L)	Ammonia-N (mg/L)	Organic Matter (mg/L)	Turbidity (NTU)	Total manganese (mg/L)
Ammonia-N (mg/L)	0.43**				
<i>n</i>	358				
Organic Matter (mg/L)	0.13*	0.15**			
<i>n</i>	358	359			
Turbidity (NTU)	0.34**	0.45**	0.57**		
<i>n</i>	358	359	359		
Total manganese (mg/L)	0.26**	0.27**	0.53**	0.76**	
<i>n</i>	358	359	359	359	
Total Iron (mg/L)	-0.13*	0.28**	0.44**	0.49**	0.45**
<i>n</i>	358	359	359	359	359

\*Correlation is significant at  $p < 0.05$  level (2-tailed); \*\*Correlation is significant at  $p < 0.01$  level (2-tailed).

### **2.3.2 Organic carbon**

Organic matter, BOD<sub>5</sub> and COD was used to characterise the organic content of the raw water, which was of key interest since high concentrations have been shown to adversely affect the nitrifying capacity of BNR processes (Pearce and Foster 1999; Pearce and Williams 1999). Descriptive analysis (min, max, mean, median) for each parameter obtained over the past five years are presented in Table 2.2. By analysing the seasonal data, it can be seen that variations in COD agreed well with organic matter concentrations, where a significant correlation was established (Pearson  $r = 0.64$ ;  $p < 0.01$ ; Figure 2.4). Furthermore, distinct differences in COD and organic matter between wet and dry seasons were clearly evident, whereby these parameters were typically highest during the wet season. In contrast, BOD<sub>5</sub> data obtained for 2004, showed concentrations to be mostly stable throughout the year, deviating only slightly from the mean of 9.2 mg/L by  $\pm 1.9$  mg/L (Figure 2.5). BOD<sub>5</sub> was independent of COD and organic matter (respective Pearson  $r = 0.17, -0.21$ ;  $p > 0.05$ ). Soluble BOD<sub>5</sub> (sBOD<sub>5</sub>) was not monitored, however based on a limited data set ( $n = 4$ ), the soluble fraction can represent anywhere between 62 % and 85 % of the total BOD<sub>5</sub> concentration. Furthermore, to characterise carbon biodegradability, a 1– through to 5–day BOD<sub>5</sub> and sBOD<sub>5</sub> test was used to monitor oxygen consumption at 24 h intervals over five days, and was of vital interest because the severity of nitrification suppression within aquatic systems has been shown to vary depending on the biodegradability of the native carbon source (Strauss and Lamberti 2002). From Figure 2.6 it can be seen that high biodegradation occurred within the first 24 h of the five day period, where  $70 \pm 13$  % and  $73 \pm 7$  % of the total oxygen consumption had occurred within the first 24 h for BOD<sub>5</sub> and sBOD<sub>5</sub> respectively. These results suggest that Buaran's raw water contained readily available organic carbon.

**Table 2.2.** Summary of organic carbon concentrations represented as BOD<sub>5</sub>, COD and organic matter for the years 1999 – 2004.

	BOD <sub>5</sub> (mg/L)	COD (mg/L)	Organic matter (mg/L KMnO <sub>4</sub> )
<b>Min</b>	3.0	0.2	0.48
<b>Mean (± 1 SD)</b>	9.6 (±3.3)	14.2 (±16.7)	14.7 (±25.5)
<b>Maximum</b>	28.0	135.0	575.8
<b>Median</b>	9.0	9.8	9.4
<b>n</b>	113	212	1786

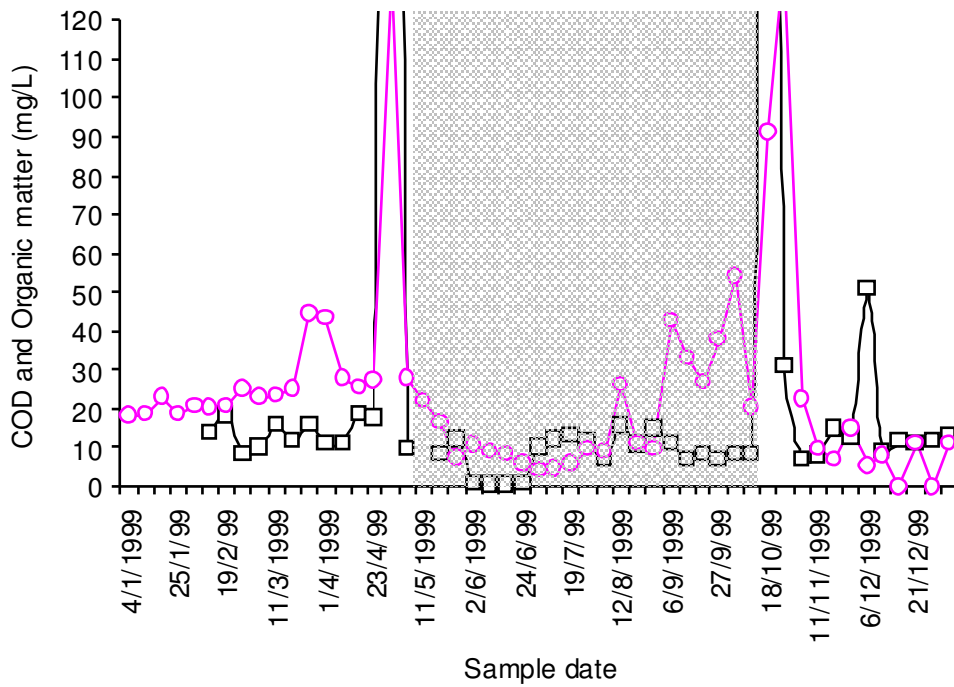


**Figure 2.4.** Seasonal variation in raw water organic matter (○) and COD (□) concentrations at Buaran WTP during 1999. Shaded region represents the dry season. y-axis scale was modified to depict baseline concentrations.

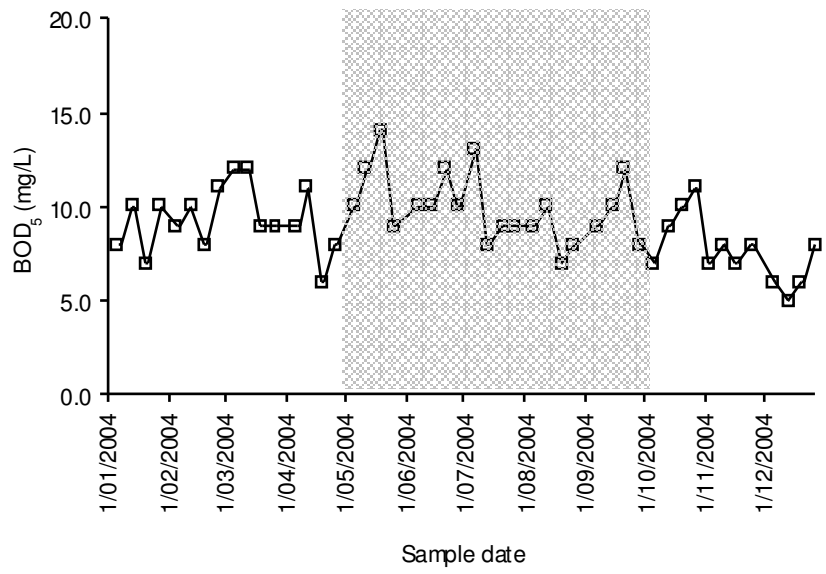


**Figure 2.5.** Seasonal variation in raw water BOD<sub>5</sub> concentrations at Buaran WTP during 2004. Shaded region represents the dry season.

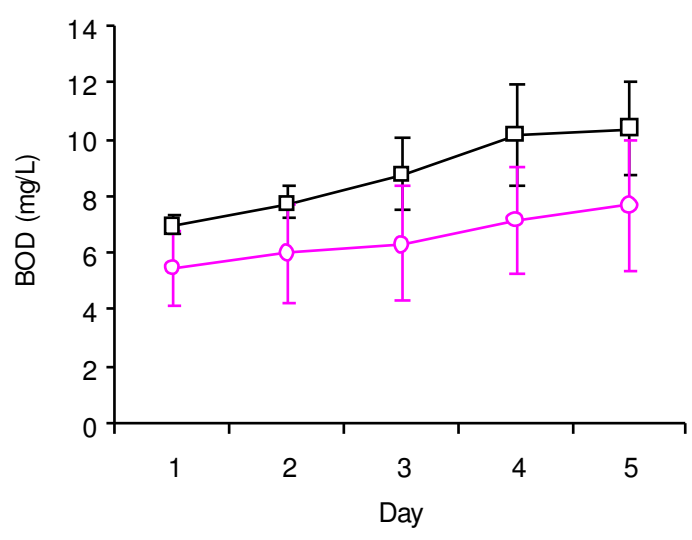


**Figure 2.6.** One through to five day BOD (□) and sBOD (○) test. Data points show parameter means ± 1 SD of four determinations.

### **2.3.3 C:N ratio**

The C:N is ratio was defined in this study as  $BOD_5$  / total inorganic nitrogen. For the year 2004, the C:N ratio fluctuated between 1.6 (min) and 9.1 (max). The mean C:N ratio was  $5.1 \pm 1.7$ .

### **2.3.4 Dissolved oxygen**

DO concentrations within the raw water at Buaran can vary between 2.2 and 5.0 mg/L. Using data provided by Cammarota (2001) from the year 2000, it was identified that the DO concentration increased along the Tarum canal, where concentrations were typically highest at the WTP intake. The increase in DO correlated well with a decline in organic matter ( $r_s = -0.30$ ;  $p < 0.0001$ ).

### **2.3.5 Turbidity and suspended solids**

Daily monitoring of Buaran WTP raw water demonstrated that the baseline turbidity ranged between 30 to 50 NTU, with short intermittent spikes as high as 1000 to 10,000 NTU. Turbidity spikes were typically short lived, lasting between 48 to 72 h. Distinct differences in turbidity between wet and dry seasons were clearly evident, where turbidity was highest during the wet season due to soil erosion within the catchment (Figure 2.7). Turbidity data correlate well with SS, where the turbidity : SS ratio was close to 1 (Pearson  $r = 0.8$ ;  $p < 0.0001$ ; Figure 2.8). Turbidity also correlated with ammonia, iron, manganese and organic matter (Table 2.1). From Figure 2.7, it can be seen that turbidity spikes coincided with spikes in organic matter. Similarly, SS correlated well with organic matter and COD (Respective Pearson  $r = 0.57, 0.47$ ;  $p < 0.01$ ), however, was independent of  $BOD_5$  ( $r = -0.10$ ;  $p > 0.05$ ).

When analysing data provided by Cammarota (2001), it was also observed that turbidity and SS obtained during 2000 increased significantly along the Tarum canal (Figure 2.9). Photographs taken after a rainstorm event highlighted the deterioration in turbidity along the canal (Figure 2.9).

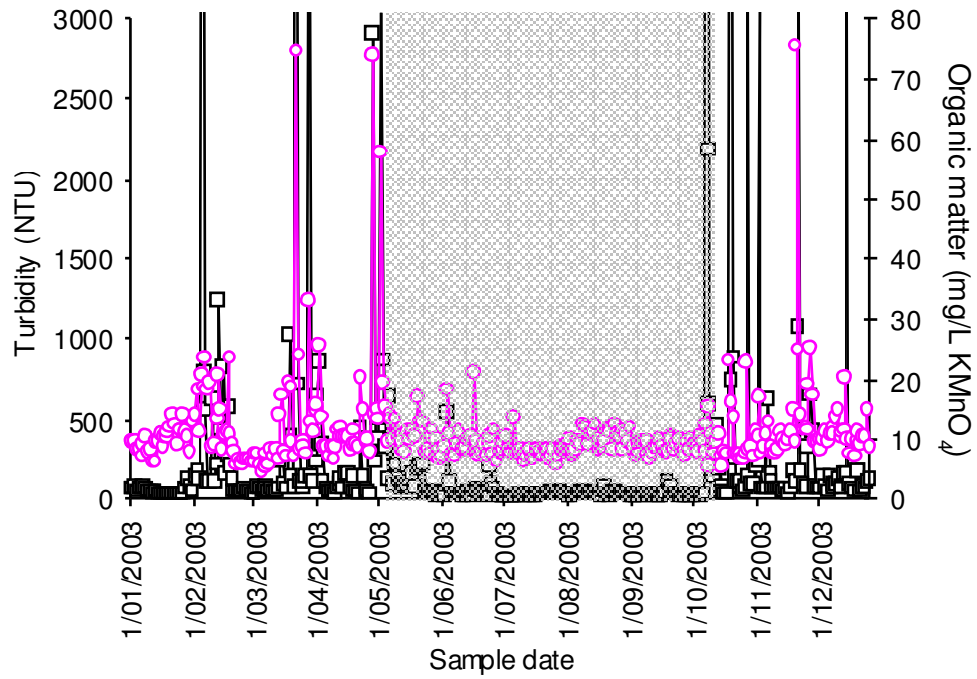


**Figure 2.7.** Seasonal variation in raw water organic matter (○) and turbidity (□) concentrations at Buaran WTP during 2003. Shaded region represents the dry season. y-axis scale was modified to depict baseline concentrations.

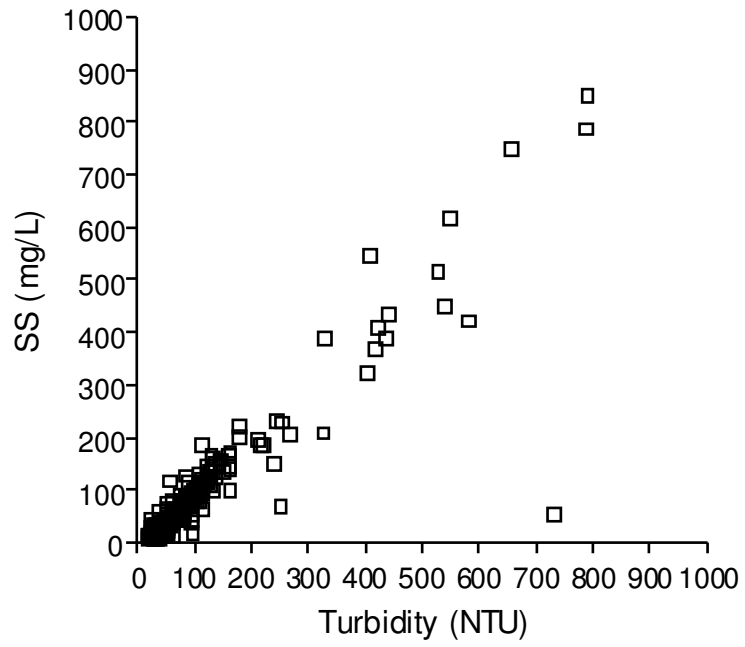
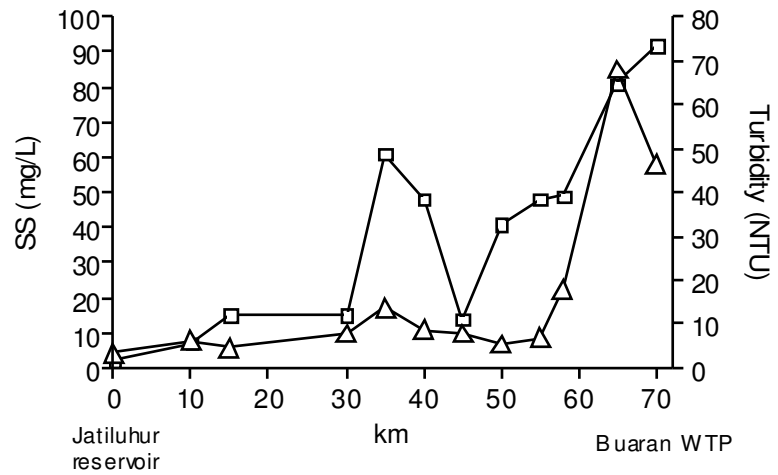


**Figure 2.8.** Relationship between raw water turbidity and SS during 2004.



0 km: Jatiluhur reservoir outlet



10 km



70 km: Buaran WTP inlet

**Figure 2.9.** Profile of: (□) SS; and (△) turbidity, measured along the Tarum canal during September 2000, and corresponding photographs taken on the technical visit during March 2004. Data was obtained from Cammarota (2001). Photographs taken by the author.

### 2.3.6 Microbial load

Daily monitoring of total coliforms within the raw water at Buaran WTP during 2003 is presented in Figure 2.10. Concentrations greater than  $100 \times 10^3$  CFU/100 ml were commonly detected. Distinct differences in concentrations between the wet and dry season can be seen, where spikes above  $50 \times 10^3$  CFU/100 ml were most common during the wet season. On average, total coliforms measured during the wet season were almost double that recorded during the dry season, measuring  $57.3 \times 10^3$  CFU/100 ml and  $30.5 \times 10^3$  CFU/100 ml, respectively. Statistical analysis confirmed a significant correlation between total coliforms and turbidity, where peaks in total coliform concentrations coincided with turbidity peaks, after rainstorm events ( $r_s = 0.56$ ;  $p < 0.0001$ ).

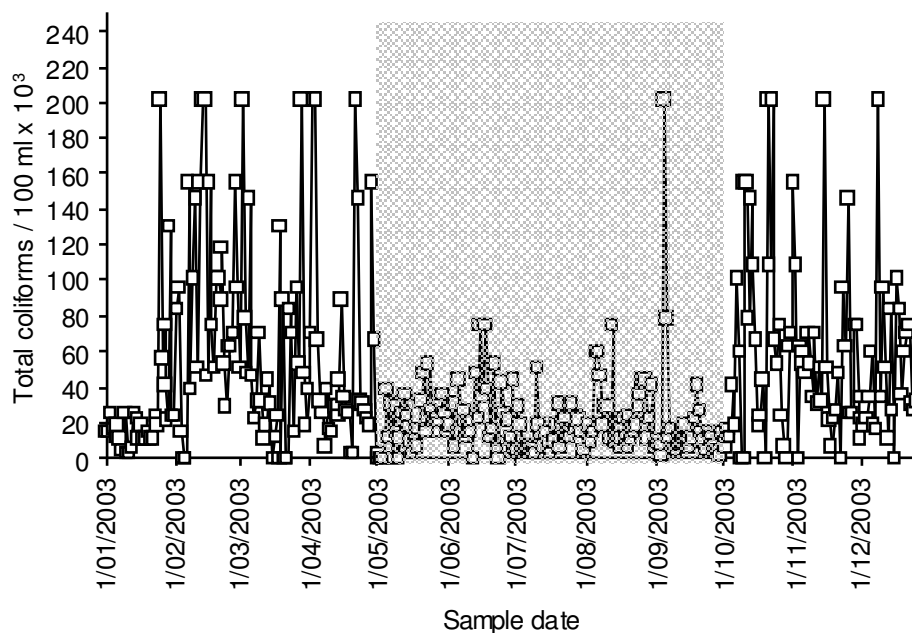


**Figure 2.10.** Seasonal variation in raw water total coliforms at Buaran WTP during 2003. Shaded region represents the dry season.

## 2.4 Discussion

The main focus of this chapter was to characterise the raw water quality at Buaran WTP, which was later used to design well controlled pilot experiments, which investigated the competency of NTFs for potable water treatment.

Raw water quality data obtained from Buaran WTP showed ammonia-N concentrations varied between 0.5 and 2.5 mg/L. Previous investigations have confirmed concentrations as high as 10 mg NH<sub>4</sub>-N/L within the lower basin of Citarum river (Bukit 1995). The main sources of nitrogen pollution identified are chemical industries, animal and food processing wastes, overflowing septic tanks and domestic waste from bank-side residents (Palupi *et al.* 1995; Cammarota 2001). An earlier report by Holmes (1999) suggested that ammonia present in the raw water had a significant impact on chlorine dose rates at Buaran WTP. It is widely accepted that ammonia greatly reduces the disinfection efficiency of chlorine, whereby the presence of ammonia demands the application of more chlorine to achieve breakpoint chlorination (Davis and Cornwell 1991). Statistical analysis from the current study confirmed this relationship for Buaran WTP, where a positive linear relationship between the total amount of free chlorine dosed and ammonia-N concentration was observed. Results indicate that 9.75 mg/L of chlorine were dosed for every 1 mg/L of ammonia-N, which was close to the theoretical value of 10 mg Cl<sub>2</sub>/L (Davis and Cornwell 1991). Breakpoint chlorine doses greater than 20 mg/L at Buaran WTP were therefore common practice. Unlike many other water quality parameters that were measured, no distinct seasonal trends in ammonia-N concentration were identified. Ammonia concentrations were seen to fluctuate daily, or even hourly as reported in earlier studies by Pearce *et al.* (2003) and Cammarota, (2001). Since chlorine dose was strongly related to ammonia concentration, rapid fluctuation in ammonia-N makes the dosage of chlorine difficult to control, which increases the risk of over- or under-dosing. Findings from Mustika Sari, (2004) confirmed episodes where free ammonia-N was present in the product water— a sign of insufficient control of chlorination. Control of residual chlorine at Buaran WTP is important for a number of reasons:

Low chlorine-to-ammonia dose ratio (under dosing) can result in the following:

1. Formation of taste and odour compounds, including di- and tri-chloramines can form, which may lead to customer complaints.
2. Failures in microbiological compliance, with a potential risk to public health.
3. Chlorine residual is required for the oxidation of soluble manganese.
4. Free chlorine residual within the distribution network is desired to minimise microbiological regrowth, biofilm formation, and achieve microbiological compliance.

High chlorine-to-ammonia dose ratio (over dosing) can result in the following:

1. Expensive practice, increasing the cost of treatment.
2. Increase formation of trihalomethanes, some of which are considered to be carcinogens (Davis and Cornwell, 1991).
3. Taste and odour complaints.
4. High free chlorine residual can cause severe corrosion to plant infrastructure e.g. electrical control systems.

(Holmes, 1999 and Mustika Sari, 2004)

Historical data has confirmed a significant increase in raw water ammonia-N concentration and frequency in spikes, which is expected to place a greater burden on pre-chlorination, and disinfection control within the near future (TPJ 2003). Currently, the pre-chlorination capacity at Buaran WTP is 5400 kg per day, which may not be sufficient to cope with the projected deterioration in water quality (Holmes 1999). Pre-treatment using NTFs have the potential to remove the ammonia and nitrite related chlorine demand, thereby improving the control of disinfection, which can prevent many of the problems outlined above. Results show that one of the key challenges for applying NTFs to potable water treatment was the low ammonia concentration, relative to conventional wastewater applications. For a NTF operating under low ammonia

concentrations, nitrification may become rate-limited by the diffusion of ammonia into the biofilm, which requires further investigation.

Results confirmed that the raw water quality in terms of turbidity, SS, total coliforms, COD and organic matter was generally worse during the wet season, where maximum values were most evident after rainstorm events. Raw water turbidity was significantly higher during the wet season, most likely due to the erosion of the canal banks and intercepting rivers. Once water was discharged from the Jatiluhur reservoir, a profile of solids taken along the canal confirmed a significant deterioration in SS and turbidity. The SS appeared colloidal, with minimal settling occurring over a 24 h period. Since the NTF was proposed to be a front-end process, the design needs to accommodate high solid loads, and the impact of inert SS on NTF performance needs to be considered. The impact of high levels of inert suspended solids on the nitrification performance of NTFs is not well known, with little previous experience published (Camarota 2001; Pearce 2003). At Buaran WTP, raw water turbidity spikes, some as high as 10 000 NTU, coincided with spikes in organic matter, COD, manganese, iron and total coliforms. The high microbial load of the raw water was parallel to findings from Palupi *et al.* (1995) who identified high faecal coliforms within the Ciliwung catchment, which implied that waters were heavily polluted by human excreta, since many residents defecate directly into the rivers. Palupi *et al.* (1995) also attributed the high microbial load to overflowing household drains and septic tanks which discharge into rivers. The higher microbial load observed at Buaran WTP during the wet season may result from: (i) an increase in run-off; (ii) increase in seepage from septic tanks; (iii) re-suspension from sediments caused by more turbulent flows; and (iv) higher flows into the Tarum canal from neighbouring rivers, which support high density housing and industries. Due to the unpredictable nature of ammonia concentrations, and large spikes in total coliforms, which coincide with other chlorine demanding contaminants, disinfection during the wet season is more difficult to control, and is therefore more vulnerable to failures in microbiological compliance.

Characterising BOD<sub>5</sub> and nitrogen concentrations is of key interest, since the C:N ratio is widely considered to be critical factor which influences the spatial distribution of heterotrophs and nitrifiers within biofilm processes, and therefore is an important regulator of nitrification (Zhang *et al.* 1994; Okabe *et al.* 1996). Data collected from Buaran WTP indicate that influent BOD<sub>5</sub> concentrations varied from 3 to 28 mg/L but was most frequently between 7 and 10 mg/L. Unlike COD, organic matter, and turbidity data, no distinct seasonal pattern in BOD<sub>5</sub> between wet and dry season was identified. Results confirmed that despite fluctuations in organic carbon represented as COD and organic matter, no significant change in the available fraction of carbon—measured as total BOD<sub>5</sub> was observed—where BOD<sub>5</sub> was independent of both COD and organic matter. BOD<sub>5</sub> was also independent of turbidity and SS, where turbidity spikes did not accompany high BOD<sub>5</sub> concentrations. These results may suggest that the SS and organic matter was of inert or recalcitrant nature. Based on limited data, the soluble fraction (sBOD<sub>5</sub>) represented 62 to 85 % of total BOD<sub>5</sub>, suggesting a large fraction was immediately available to the heterotrophic community, who may be responsible for suppressing nitrification in BNR processes. To maintain a stable ammonia removal process, it was therefore necessary to consider the impact of BOD<sub>5</sub> and C:N ratio observed at Buaran WTP on NTF performance. Furthermore, the biodegradable nature of the organic carbon was of interest because the severity of nitrification inhibition can vary depending on the biodegradability of the carbon source (Strauss and Lamberti 2000). To characterise the biodegradability of the organic carbon substrate, a 1–through to 5–day sBOD<sub>5</sub> test was used to monitor oxygen consumption at 24 h intervals over a five day period. Results confirmed that the carbon substrate was of readily degradable nature, where the majority of oxygen consumed (70 %) during microbial degradation had occurred within the first 24 h of incubation. This observation may be indicative of nearby or 'fresh' pollutant sources, such as municipal sewage and food industries, which are in close proximity to the WTP (Figure 2.2). Characterising the biodegradable nature of the carbon at Buaran also provided valuable information for selecting a suitable surrogate carbon source for the controlled pilot-scale investigations (see Chapter 5).

According to the BOD<sub>5</sub> data, much of the waste discharged into the Tarum canal contained oxygen demanding substances, which was responsible for the low DO concentrations recorded. The negative correlation observed between organic matter and DO measured along the canal, confirmed the impact of organic content on de-oxygenation of the raw water. Factors identified by Palupi *et al.* (1995) that were responsible for low DO were human faeces, waste from food processing industries and solid wastes. Cammarota (2001) also confirmed that DO concentrations generally increased along the Tarum canal, where highest concentrations were recorded at the WTP intake, which was most likely attributed to physical mixing. Despite significant oxygenation of the raw water, DO as low as 2 mg/L was reported, which needed to be considered in the design of the NTF. For example, oxygenation of the inflowing water can be enhanced through media selection (see Chapter 3, Section 3.2.4).

## 3 GENERAL METHODOLOGY

### 3.1 Introduction

This chapter outlines the general methodology used throughout the study. Methods for pilot-plant construction, *in situ* biofilm analysis, water analysis, and statistical analysis are described below.

### 3.2 Large pilot-scale nitrifying trickling filter

A large, super high rate, pilot-scale NTF was constructed at Hope Valley WTP, Adelaide, Australia. A summary of the pilot-plant's key components are presented in Plate 3.1.

#### 3.2.1 NTF column

The NTF column was constructed using two 2700 L corrugated polypropylene water tanks (Team Polly, Adelaide, Australia). Both water tanks were plastic-welded together, attached from top to bottom to create one large column, 3.4 m high, 1.44 m in diameter, with a total volume of 5.54 m<sup>3</sup> (Plate 3.1). A collar to reduce overspray, 0.5 m high, was added to the top of the column, which housed the rotating distribution arm making the total height 3.9 m. The polypropylene column did not provide any structural support, rather existed to prevent water loss and wind chill. Access to the top of the filter was provided using a 3 m high scaffold (Maxi-Scaff), with a platform surface area of 1.5 m<sup>2</sup>.

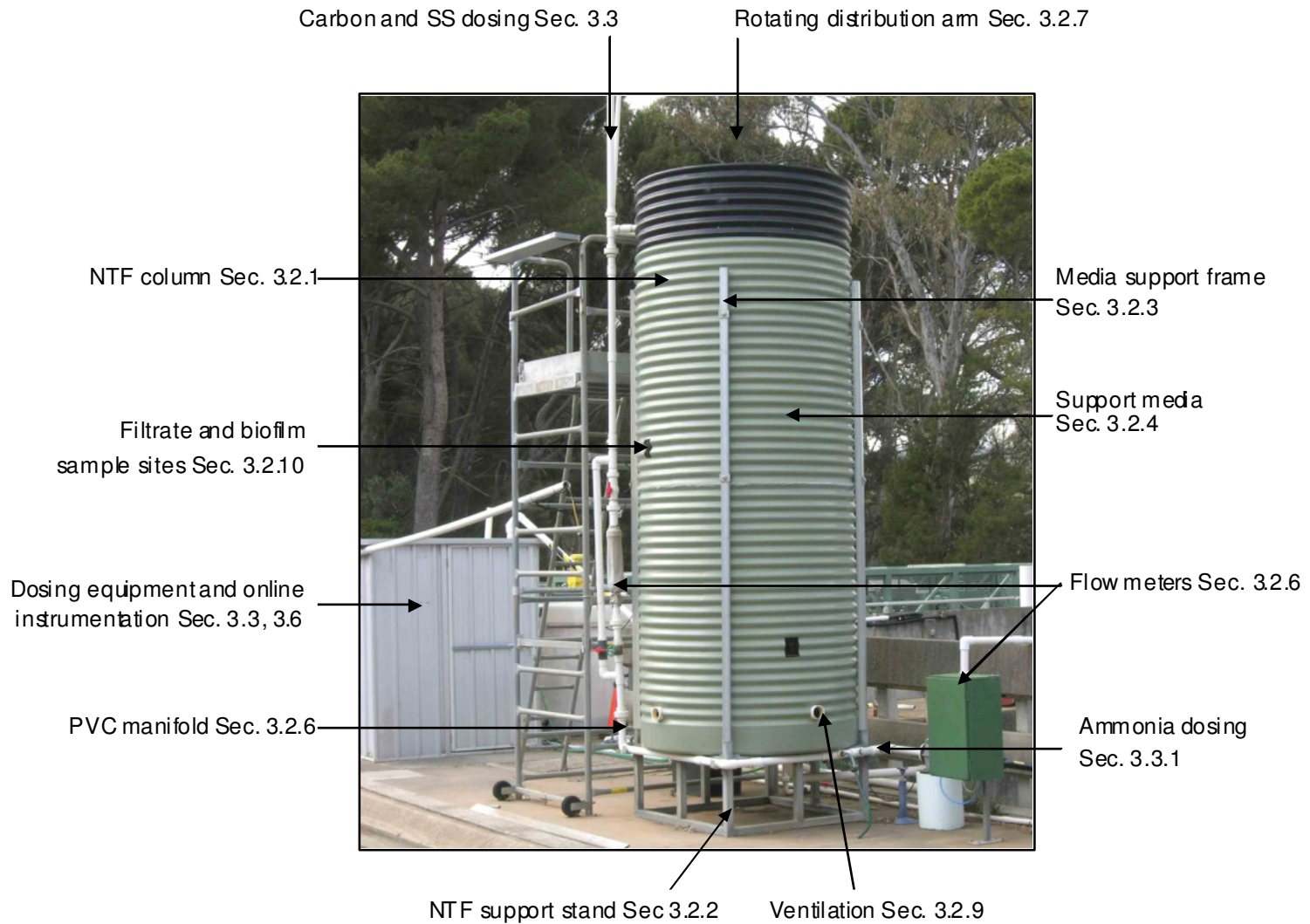


**Plate 3.1.** Large pilot-scale NTF, located at Hope Valley WTP, Adelaide.

### **3.2.2    *Trickling Filter support stand***

A galvanised steel stand was fabricated by Biomedical Engineering Department, Flinders Medical Centre. The stand was designed to support the NTF 0.5 m from the floor to facilitate effluent drainage via gravity feed (Plate 3.2). Support struts extended across the top to prevent the polypropylene base of the NTF column from sagging. Steel cylindrical pegs were positioned on each corner of the stand which supported the external galvanised posts (see Section 3.2.3; Plate 3.4). The NTF support stand was designed to support a load greater than two tonne.

### **3.2.3    *Media support stand and frames***

The internal media support stand and frames were fabricated using marine grade stainless steel by the Biomedical Engineering Department, Flinders Medical Centre.

#### *Media support stand*

The media support stand consisted of parallel struts 100 mm apart and was inserted inside the NTF column to support the synthetic media 0.3 m from the base of the filter (see Plate 3.3). Each strut extended the entire width of the NTF column to maximise media support. The media support stand allowed the filtrate to drain free from the media, enabling air to circulate through the bed.

#### *Media support frames*

For additional media support, two frames were positioned within the NTF column, at heights of 1.76 m and 2.80 m from the base. The internal frames were fastened to four external galvanised posts using brackets (Plate 3.4 and Plate 3.5). The external posts were positioned over each of the cylindrical pegs, which were situated on all corners of the NTF support stand. Each post extended vertically along the external wall of the NTF column. A detailed description of the internal frames, mounting brackets, and external posts is depicted in Plates 3.4 and 3.5.



**Plate 3.2.** NTF support stand.



**Plate 3.3.** (a) Media support stand; and (b) birds-eye view of the stand once positioned inside the NTF column.



**Plate 3.4.** External media support frame: (a) external posts which support internal media support frames; (b) external mounting bracket; and (c) 1 of 4 external posts positioned over a cylindrical peg.

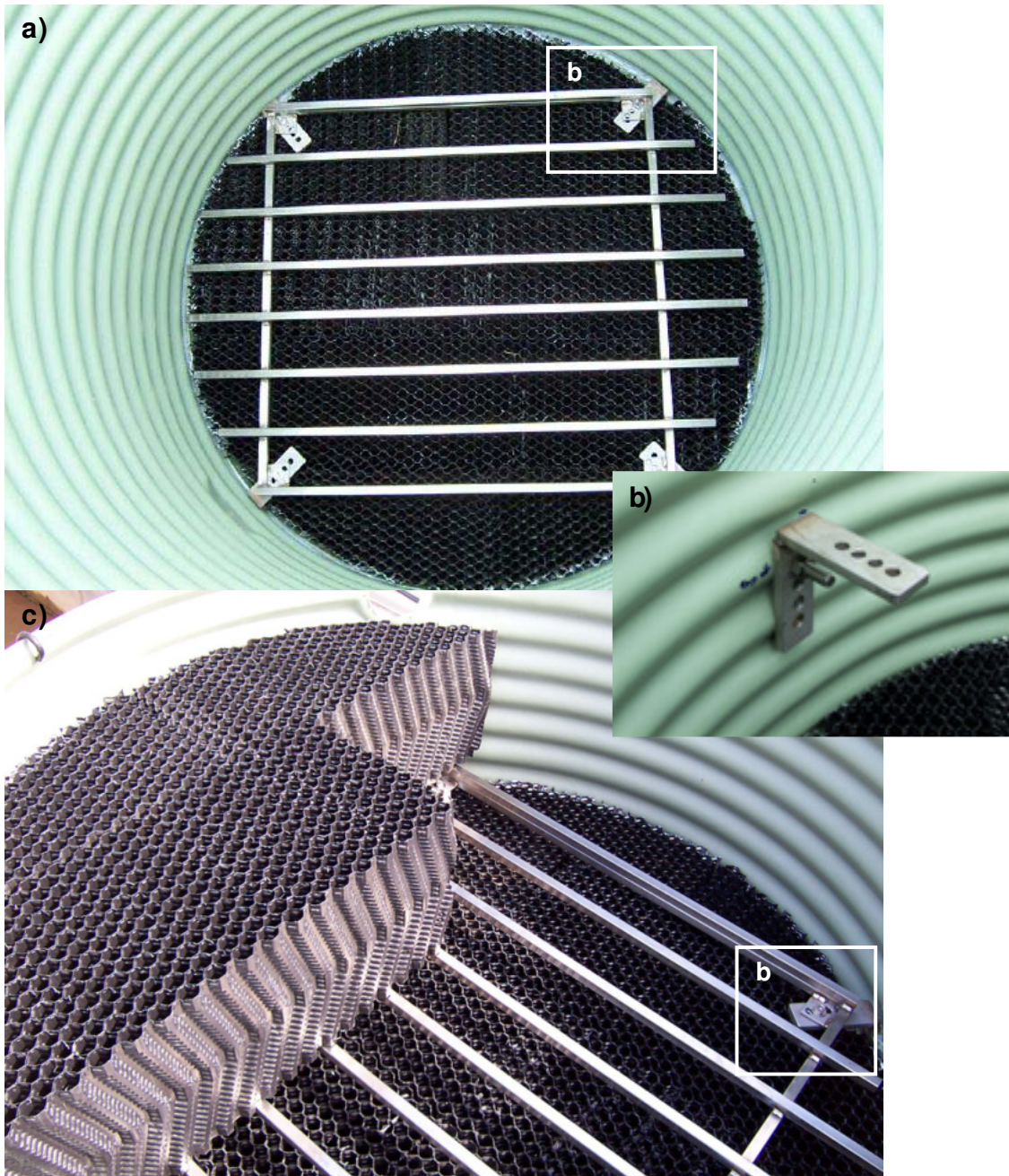


**Plate 3.5.** (a) Birds eye view: 1 of 2 internal media support frames; (b) internal bracket fastened to the external support post; and (c) internal media support frame stacked with media.

### 3.2.4 *Biofilm support media*

The media support stands accommodated a 3 m bed (10 layers) of TKP 312 polypropylene fill media (2H Plastics, Victoria Australia) which had an area to volume ratio of  $240 \text{ m}^{-2} \text{ m}^{-3}$ . The total surface area of the entire bed was  $1108.4 \text{ m}^2$ . The media was manufactured from corrugated polypropylene foils 0.3 mm thick, welded together to form a labyrinth of surfaces with channels at  $60^\circ$  to the vertical (Plate 3.6). The media blocks were lightweight, rigid, and self-supporting, which eliminated the need for heavy duty external housing. To minimise power requirements, a high void space (95 %) was necessary to maximise passive aeration of infiltrating water, without the need for forced ventilation. High void space, steep channels, and the uniform configuration of the media allowed water to percolate without clogging, which minimises head-loss, and eliminates the need for a backwash function. These were key requirements as the influent at Buaran WTP can be low in DO, and present high solid loadings during frequent high turbidity episodes. The media blocks interlocked with one another to form a tight fit and were tightly packed against the inner wall of the NTF to prevent the short-circuiting of filtrate. In order to increase contact time, each layer of media was stacked at  $90^\circ$  to the layer laid previously, which ensured the filtrate pursued a tortuous and indirect route through the filter.

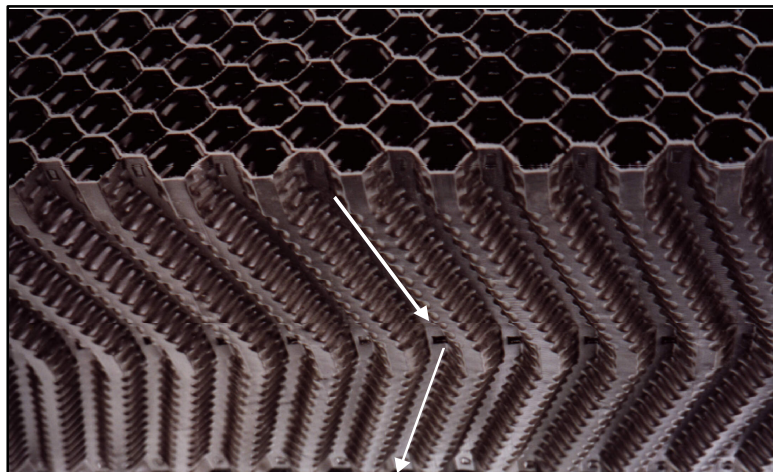


**Plate 3.6.** Close up photograph of the polypropylene media highlighting the steep channels and corrugated foils.

### **3.2.5 Primary pump**

Raw water was abstracted from Hope Valley reservoir using a single stage centrifugal pump (Grundfos, model NP50, Australia), which was located on a weir, above the source water. Raw water was drawn up a 7 m length of 50 mm rigid PVC pipe, which contained a non-return valve (foot valve) on the end to prevent the backflow of water into the reservoir (Plate 3.7). The pump was installed inline using a 32 mm PVC flange for the inlet and a 50 mm PVC flange for the outlet (Plate 3.7). Each flange was connected to 50 mm class 12 PVC pipe. The outlet PVC line of the pump was connected to two sections of 50 mm (OD) polypropylene pipe, each containing two alloy ball valves. Via the aid of a pressure gauge, the ball valves were adjusted to allow the pump to operate at its optimum pressure of 230 kpa. Raw water was pumped from the reservoir to the rigid PVC manifold (attached to the NTF) along 80 m of 50 mm (OD) class 12.5 polypropylene pipe.



**Plate 3.7.** Installation of the primary pump situated on the weir above the Hope Valley reservoir.

### **3.2.6 PVC manifold**

Water was pumped from the reservoir to a PVC manifold which was attached to the NTF. The manifold was constructed using class 12 rigid 40 mm PVC pipe, with the objective of controlling hydraulic flow and to provide dosing points for ammonia, organic carbon and SS, before the rotating distribution arm. From Plate 3.8, it can be seen that the flow rate was controlled by adjusting a brass gate valve, which diverted a portion of the flow to waste. An electromagnetic flow meter (ABB Kent-Taylor) was installed, which provided a continuous digital reading of the flow. Immediately after the flow meter, two dosing points were installed for the ammonia, and tracer solutions. Each dosing point was fitted with a non-return valve to prevent the backflow of water into the dosing lines. Due to frequent blockages of the non-return valve, and subsequent un-even dosing pattern, the SS and organic carbon dosing points were installed at the top of manifold, where the clay and sucrose solution was dosed into an open pipe, ahead of the rotating distribution arm (Plate 3.9). An inline variable-area flow meter (rotameter) was installed at eye level, to provide an accurate visual flow rate reading. A flow-bypass was constructed around the rotameter to maintain uninterrupted flow of water to the distribution system during cleaning. An influent sample point was inserted above the rotameter, for the online measurement of temperature, turbidity and DO.

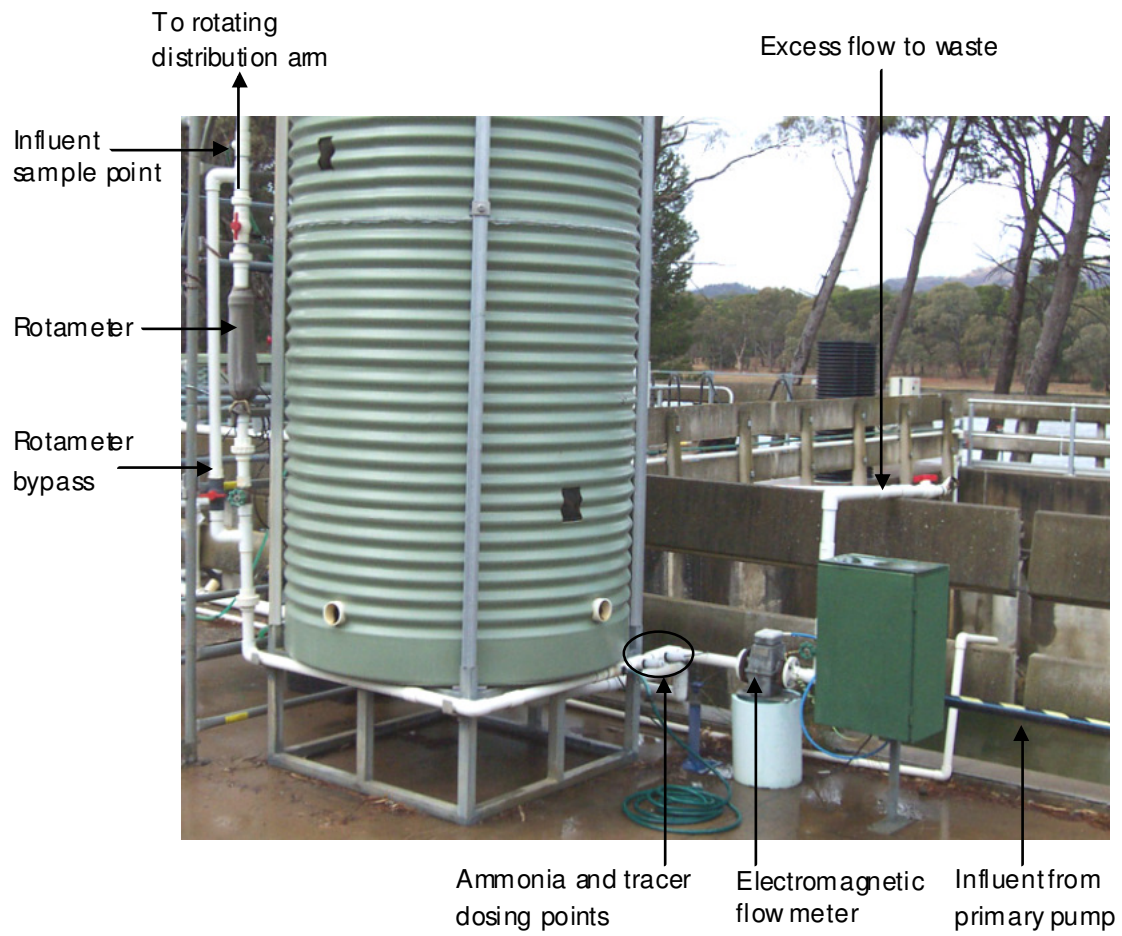


**Plate 3.8.** Influent PVC pipe manifold.

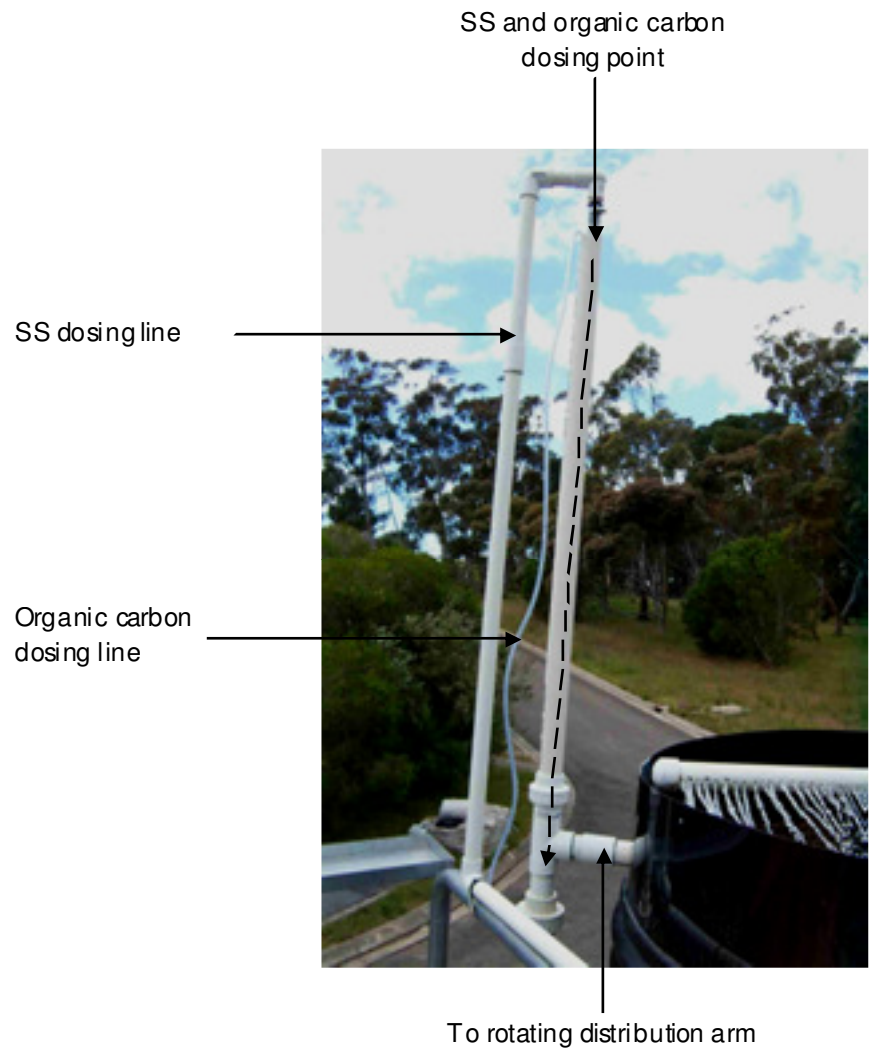


**Plate 3.9.** Influent PVC manifold continued, depicting SS and organic carbon dosing points.

### **3.2.7 Rotating distribution arm**

Water was applied using a PVC rotating distribution arm. The arm was mounted on a pivot in the centre of the filter and rotated on a horizontal plane, hydraulically driven by the discharge of water from the nozzles. Plate 3.10 demonstrates in detail how the distributor was constructed. A nylon bush was inserted in between the pivot and the rotating arm to prevent wearing of the join. The nozzles on the arm consisted of holes ranging from 4 mm to 10 mm in diameter. To maintain a uniform distribution of water, the larger nozzles were positioned closest to the end of the arm so a greater flow per unit of length was achieved near the periphery than at the centre (see Plate 3.10.a). The size and location of the nozzles were arranged so that the wetting rate of any selected surface area did not vary by more than 10 %. The rotation speed was altered by twisting each arm to change the trajectory of the spray, and was fixed at 35 rpm for all experiments.

### **3.2.8 Hydraulic flow**

The influent hydraulic flow rate was constant for all experiments and was calibrated using an inline variable-area flow meter (rotameter), and the electromagnetic flow meter. The influent hydraulic flow rate was 8 m<sup>3</sup>/h, resulting in a hydraulic surface load (per unit of media surface area) of 173.3 L m<sup>-2</sup> d<sup>-1</sup>. The irrigation velocity (total influent flow rate per unit of cross-sectional surface area per day) was 124.6 m<sup>3</sup> m<sup>-2</sup> d<sup>-1</sup>. The corresponding filtration rate was a rapid 5.2 m/h. The filter only operated under single pass and therefore was not configured to recirculate a portion of the treated effluent.

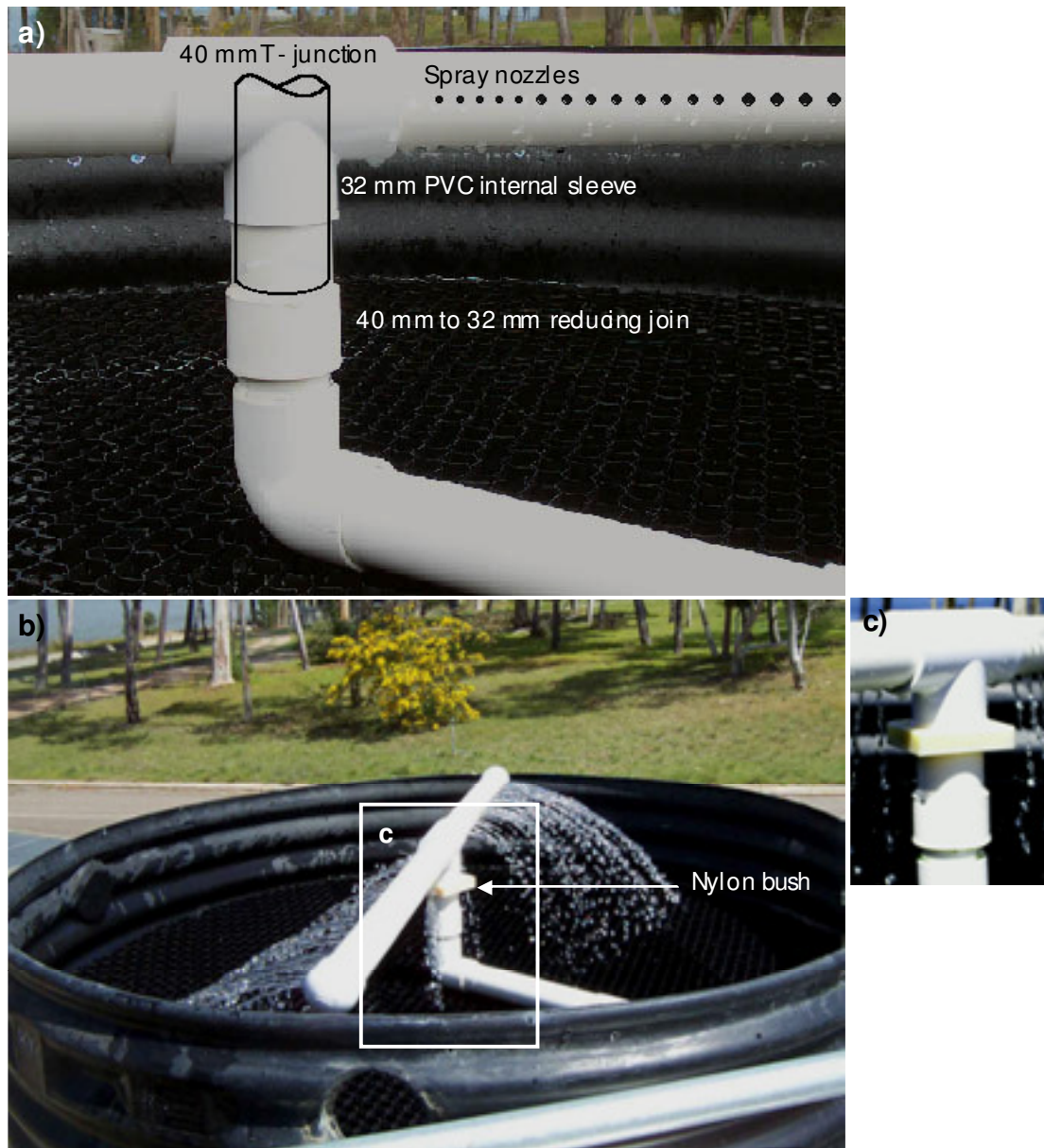


**Plate 3.10.** Rotating distribution arm: (a) description of key components; (b) functioning distribution arm; and (c) nylon bush inserted in between the joint to prevent wearing.

### **3.2.9 Ventilation ports and effluent drains**

Four ventilation ports 900 mm in diameter were evenly distributed around the trickling filter 210 mm from the base to facilitate natural draft (Plate 3.11). PVC sleeves were inserted to minimise water loss caused by splashing.

Two PVC drainage pipes (50 mm in diameters) were installed to ensure rapid drainage of the effluent from the base of the NTF (Plate 3.11). Effluent was transported via gravity feed back into Hope Valley reservoir. An additional effluent sampling point was installed at the base of the NTF for the online measurement of turbidity, DO and the hydraulic tracer.

### **3.2.10 Filtrate and biofilm sample sites.**

Filtrate and biofilm sample sites were positioned down the vertical axis of the NTF at bed depths of 0.3, 1.5 and 2.7 m to allow for *in situ* monitoring of water chemistry and biofilm analysis (Plate 3.12.a). Biofilm sample trays consisted of small lengths of the TKP 312 polypropylene fill media (80 x 80 x 720 mm), which were embedded within blocks of media, and extended horizontally into the centre of the bed (Plate 3.12.b and c). Each of the three biofilm sample sites was staggered at 90° to the horizontal of one another to prevent them from overlapping through the depth of the filter bed.

### **3.2.11 Aqueous phase sampling**

Influent grab samples (0.5 L) were taken directly underneath the rotating distribution arm. Filtrate grab samples (0.5 L) were taken down the vertical axis of the NTF, at bed depths of 0.3, 1.5, 2.7 and 3.0 m. Filtrate samples were collected by inserting a polypropylene collection trough (2.5 cm diameter) horizontally through the biofilm sample port, which extended half way across the NTF (Plate 3.12). Filtrate captured by the trough was collected into a sample bottle. Depth profiles were collected sequentially from bottom (effluent) to top (influent) within a period of approximately 5 minutes.

Samples were stored on ice during transport to the laboratory for immediate analysis. Additional influent and effluent sample points were inserted to feed online DO and turbidity analysers (Section 3.6).

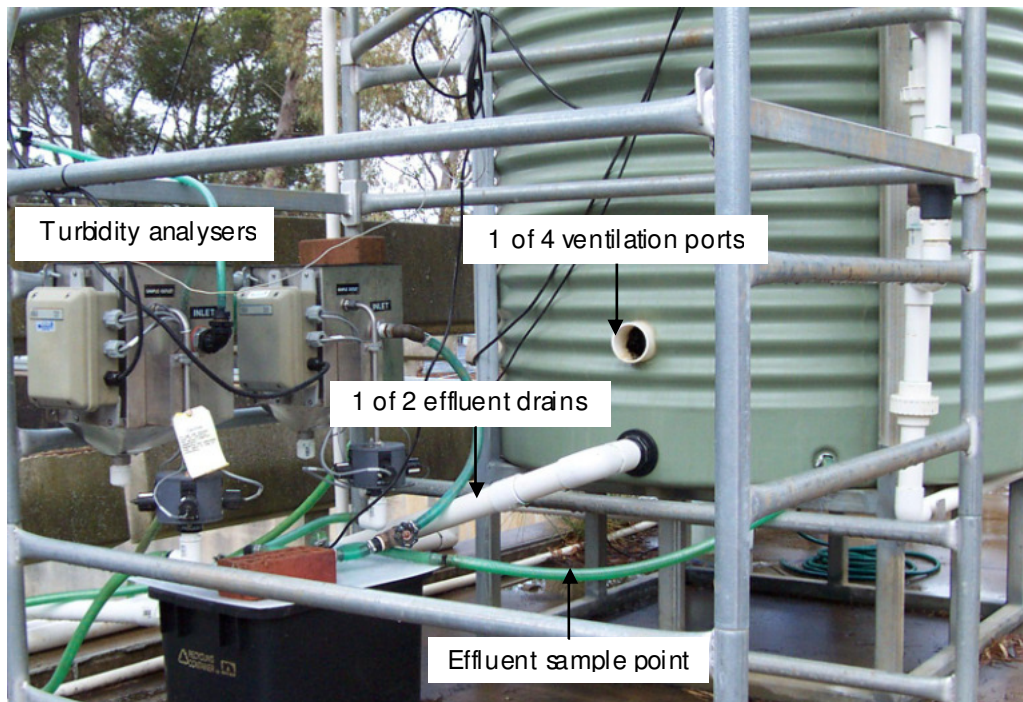


**Plate 3.11.** NTF effluent drains and ventilation ports.

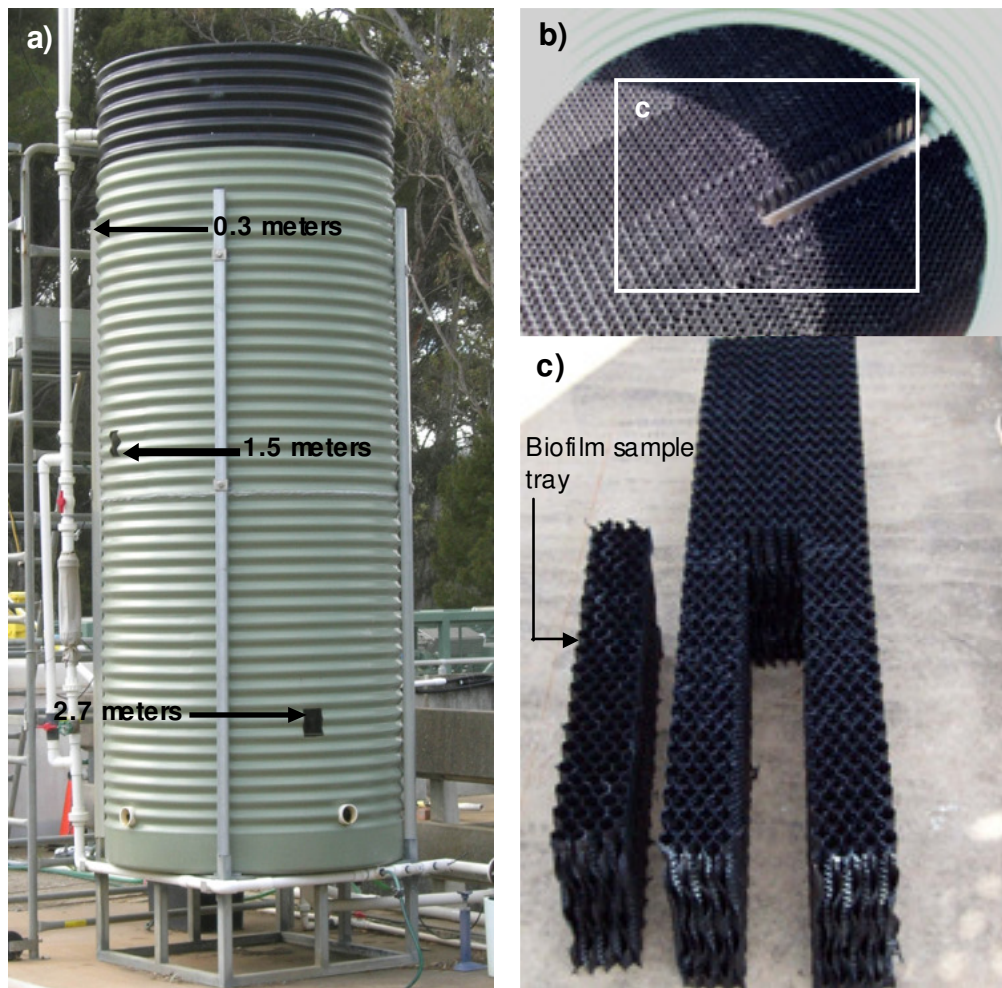


**Plate 3.12.** (a) Location of biofilm and filtrate sample sites; and (b and c) 1 of 3 biofilm sample sites. The filtrate sampling trough was inserted into these biofilm sample sites.

### **3.3 Dosing**

#### **3.3.1 Ammonia dosing**

Ammonium sulphate in the form of fertilizer (Pivot, Australia) was used to supplement the NTF's influent with ammonia-N. An ammonium stock solution was prepared by dissolving a desired quantity of ammonium sulphate into 60 L of water. A digital dosing pump (Grundfos, model DME) was used to dose the ammonia stock into the PVC line using a 5 mm polypropylene dosing line. The dosing pump was set at a fixed dose rate of 500 ml/h. Influent ammonia-N concentrations were typically between 0.5 to 5.0 mg/L ammonia-N.

#### **3.3.2 External organic carbon source dosing**

A sucrose stock solution was prepared every 48 h, which ranged from 1.5 to 5 % wt/vol, depending on the desired influent sBOD<sub>5</sub> concentration. A digital dosing pump (Grundfos, model DME) was used to dose the sucrose solution into the top of PVC manifold, via a 5 mm dosing line (Plate 3.9). The dosing rate was maintained at 1.0 L/h. Influent sBOD<sub>5</sub> concentrations could be varied between 2.0 and 10.0 mg/L. Where specified, sucrose was substituted with 100 % methanol or soluble organic fertiliser.

#### **3.3.3 Suspended solids dosing**

To simulate raw water quality at Buaran water treatment plant, a SS dosing unit was constructed. Pottery clay was chosen as the best material to increase raw water SS loads and turbidity. A mixing tank (1000 L) was employed to mix the clay into an homogenous slurry, ready for dosing (Plate 3.13). 1000 L of water was constantly maintained within the tank by the use of a float valve, which regulate the inflow of water into the mixing tank (Plate 3.13.b). A three day stock was prepared by loading the mixing tank with approximately 60 kg of clay. Continual mixing produced a saturated clay slurry. An outlet pipe (30 mm PVC) extended from the base of the mixing tank to a clay dosing mono pump (Plate 3.14.b). The dosing rate was controlled using a variable speed drive (Zener, model MSC-3; Plate 3.14.a), and was varied to obtain the desired

influent turbidity and SS concentration. A back-up metering pump (ProMinent® Sigma, model SIBa) was installed to provide uninterrupted SS dosing during maintenance and cleaning. The dosing line (30 mm rigid PVC pipe) extended from the clay dosing pump to a dosing point located at the top of the NTF (See Plate 3.14 and Plate 3.9). Here, the 30 mm PVC line was reduced to 12 mm flexible hose prior to being dosed into the main influent stream.

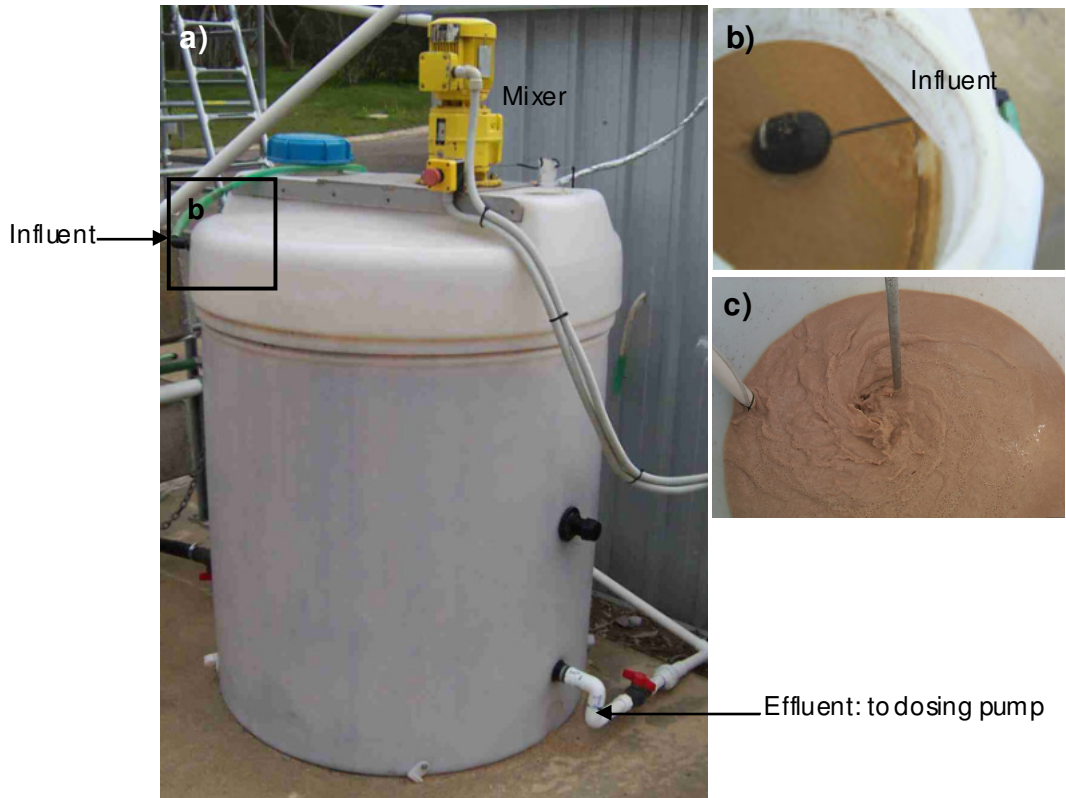


**Plate 3.13.** (a) Clay mixing tank; (b) float valve, used to maintain a 1000 L stock of water within the tank; and (c) mixing of clayslurry.

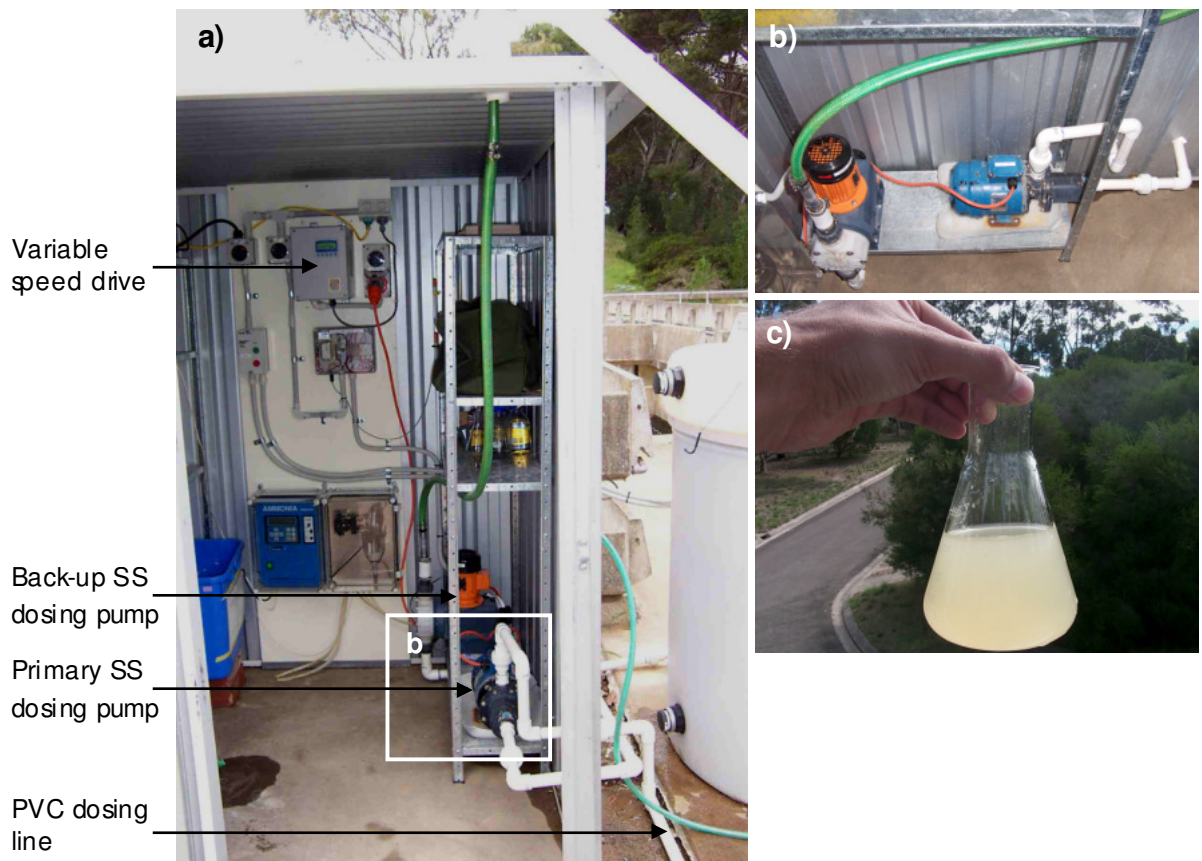


**Plate 3.14.** (a and b) set-up of clay dosing pump(s); and (c) final product—sample taken from the NTF's influent after dosing.

### **3.3.4      *Electrical wiring***

A licensed electrician prepared all hard wiring of electrical appliances. A shed, which housed all online instrumentation and other electrical appliances was fitted with a 10, 15 and 32 amp power supply.

### **3.3.5      *Pilot plant troubleshooting***

Throughout the course of the study, several modifications were made to large pilot-scale NTF. For reason discussed in Chapter 5, Section 5.3.7, the NTF needed to be decommissioned, and reconstructed. Both the old and newly reconstructed NTF were identical in terms of size, and operated under the same conditions, however several alterations were made to: (i) provide additional filter and media support; and (ii) to each biofilm sample site. Up until this point, the methods have referred to the newly reconstructed NTF. This section describes the modifications made to the old-NTF (Plate 3.15), which gave rise to the reconstructed NTF.

#### *NTF support stand*

As described in Section 3.2.2, additional horizontal steel struts were positioned across the NTF support stand to provide additional support and prevent the base of the NTF column from sagging during times of excessive biomass accumulation as seen in Plate 3.16.

#### *Media support frames*

As described in Section 3.2.3, additional media support frames were inserted within NTF to evenly distribute the weight of the media throughout the NTF. The additional support frames prevented the bottom layer of media and biofilm sample sites from becoming compressed as observed during times of excessive biomass accumulation.

#### *Biofilm sample sites*

As seen in Plate 3.17, the earlier biofilm sample sites consisted of drawers, which extended horizontally across the entire NTF bed. Due to inadequate media support and

their large size, these drawers were susceptible to becoming squashed (Plate 3.18). As described in Section 3.2.10, the biofilm sample drawers were substituted with smaller biofilm sample trays embedded within media blocks, which extended only half way across the media bed.



**Plate 3.15.** Earlier version of the large pilot-scale NTF.



**Plate 3.16.** NTF support stand: Base of NTF column sagging due to excessive accumulation of biomass and the absence of horizontal steel struts. Carjacks were used to help support the base. Car-jacks were later substituted with horizontal support struts (see Section 3.2.2).

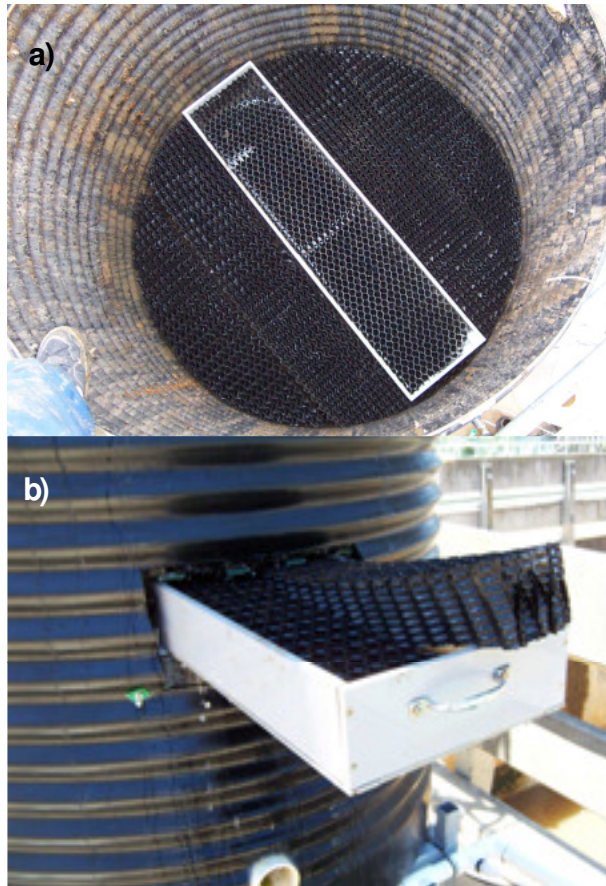


**Plate 3.17.** 1 of 3 biofilm sample sites (drawers): (a) birds eye view; and (b) open drawer ready for biofilm sampling within the original NTF before modification.



**Plate 3.18.** The original NTF: Squashed biofilm sample drawer.

### 3.4 Small pilot-scale NTFs

Three small-scale NTFs were employed to investigate the influence of hydraulic surface load on nitrification performance. The main components of the small-scale NTFs are illustrated in Figure 3.1. The filter columns were 0.225 m in diameter, 2 m high, and contained a 1.5 m bed of polypropylene media (specific surface area of  $240 \text{ m}^{-2} \text{ m}^{-3}$ ), identical to that used in the large pilot-scale NTF, described in Section 3.2.4. Similar to the large pilot-scale NTF, the feed water was extracted from Hope Valley reservoir, and supplemented with ammonia by dosing ammonium sulphate. Each of the NTFs operated in parallel, and therefore received identical ammonia-N concentration loads. The water distribution system was fixed, consisting of four small plastic irrigation nozzles. Each of the three small NTF operated under fixed hydraulic surface loading rates of: 174 to 202 (Filter 1); 274 (Filter 2); and 402 (Filter 3)  $\text{L m}^{-2} \text{ d}^{-1}$ . Where specified, the  $\text{sBOD}_5$  loading of Filter 1 was augmented using soluble organic fertiliser (Chicken manure, Rooster Booster). The stock was prepared by mixing 2 kg of dry fertiliser into 40 L of water, and allowed to settle. The supernatant was dosed using a peristaltic pump (Watson Marlow), set at a flow rate of 0.5 L/h.

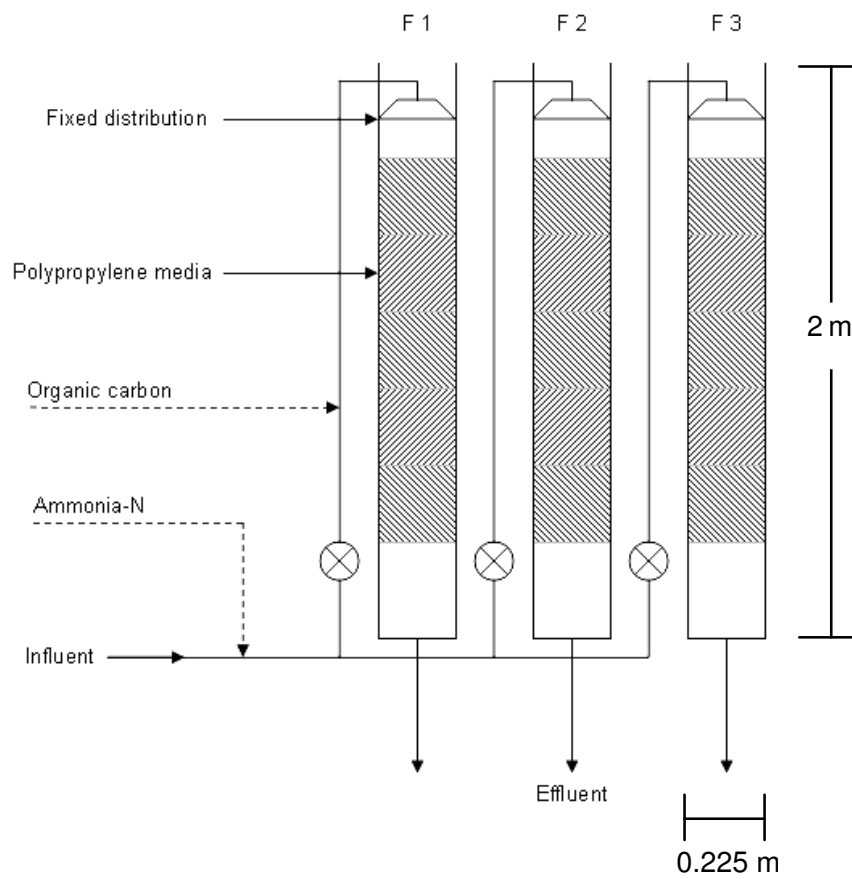


**Figure 3.1.** Schematic representation of the small pilot-scale NTFs.

## **3.5 Water analysis**

### **3.5.1 Total alkalinity**

Alkalinity was performed onsite using the titrimetric method (APHA Method 2320). Samples were pre-treated with 2 drops of 0.1 N sodium thiosulphate. After the addition of methyl orange indicator, total alkalinity was determined by titrating the samples against 0.02 N sulphuric acid until a colour change from colourless to pink. The volume of titrant was recorded and total alkalinity quantified as mg CaCO<sub>3</sub>/L.

### **3.5.2 Ammonia-nitrogen**

Ammonia-N (NH<sub>4</sub>-N) was determined using the Nesslerization method (APHA Method 4500-NH<sub>3</sub>). To improve colour development, EDTA was substituted with 1 drop of mineral stabiliser (Biolab, cat. 23766-26) and 1 drop of Polyvinyl alcohol dispersing agent (Biolab, cat. 23765-26). For quality assurance, analysis was performed in triplicate, together with a validation standard.

### **3.5.3 Oxidised nitrogen (nitrite-N and nitrate-N)**

Nitrite-N (NO<sub>2</sub>-N), and nitrate-N (NO<sub>3</sub>-N) was determined using the colorimetric method (APHA Method 4500-NO<sub>2</sub><sup>-</sup> B) and hydrazine reduction methods (APHA Method 4500-NO<sub>3</sub><sup>-</sup> G) respectively. Analysis was performed in triplicate. For quality assurance, analysis was performed in triplicate, together with a validation standard.

### **3.5.4 Total organic carbon**

Total organic carbon was determined using a 5000A TOC analyser (Shimadzu, New South Wales, Australia).

### **3.5.5 Five-day soluble biological oxygen demand**

Samples were filtered using through glass fibre papers (GFC, 0.45 µm effective pore size, Whatman<sup>®</sup>, UK). 100 µl of nitrification inhibitor (1000 mg/L allylthiourea solution) was added to all samples. The soluble 5-day biological oxygen demand was determined using WTW OxiTop<sup>®</sup>-C equipped with WTW OxiTop<sup>®</sup>-OC100 controller.

### **3.5.6 pH**

pH was measured using a hand held WTW Weinheim pH 320 meter.

### **3.5.7 Total suspended solids**

Triplicate, 100 ml aliquots of well mixed samples were filtered through pre-dried (105°C 24 hours) and weighed glass fibre papers (GFC, 0.45 µm effective pore size, Whatman<sup>®</sup>, UK). Papers and residue were then dried at 105°C for 24 h and weighed and quantified for total SS in mg/L.

### **3.5.8 Turbidity**

Turbidity was quantified using a HACH Ratio/XR turbidimeter.

## **3.6 Online Instrumentation**

### **3.6.1 *Turbidity analyser***

Influent and effluent turbidity was measured online using turbidimeters (Great Lakes International, model 95T/8220). Data was recorded at 10 minute intervals using a data logger (Data taker™, model DT400). Installation was achieved in accordance with the manufacturer's instruction manual.

### **3.6.2 *Dissolved Oxygen***

DO was measured online using a dissolved oxygen sensor (Danfoss Evita Oxy Sensor). Data was recorded at 10 minute intervals using a data logger (Data taker™, model DT400).

### **3.6.3 *Temperature***

Influent temperature was recorded at 30 minute intervals using a T-Tec, type 6 data logger (Temperature Technologies, Adelaide, Australia).

## **3.7 Biofilm analysis**

### **3.7.1 *Biofilm sampling and extraction for protein and carbohydrate analysis***

Media surface samples (1 cm<sup>2</sup>) were taken with cotton swabs from each of the 3 biofilm samples sites, and transported back to the laboratory in 1 ml of distilled water. Sampling was performed in triplicate. Biomass was extracted from the cotton swabs by sonication (10 minutes, 700 W, 35 kHz; Cooper Vision Model 895, Irvine, CA, USA) followed by vigorous vortex mixing for 2 minutes. Samples were centrifuged (Phoenix Orbital, Model 100) at 5000 rpm for 10 minutes, and supernatant was decanted. The extracted biomass pellet was quantified for total carbohydrate and protein.

### **3.7.2 *Protein analysis***

The protein content of biofilm swabs was determined using the Bradford method (Bradford 1976). Extracted biomass was resuspended in 0.1 ml of 0.2 M sodium hydroxide (total volume 0.1 ml) and incubated at room temperature for 1 h for cell lysis. Bradford protein reagent (100 mg/L coomassie brilliant blue G-250, 5 % v/v ethanol, 10 % v/v phosphoric acid; 5 ml) was added to the samples and vortexed. Absorption at 595 nm was measured after 20 minutes (Shimadzu, model UV-1700 spectrophotometer) and protein quantified using bovine serum albumin as standards. Results are presented as mass of total protein (µg) per cm<sup>2</sup> of media surface area.

### **3.7.3 *Carbohydrate analysis***

The total carbohydrate content of biofilm swabs was determined using the phenol reaction method (Hanson and Phillips 1981). Extracted biomass was resuspended in 1.0 ml of distilled water. 1.0 ml of phenol reagent (5.0 g of reagent grade phenol, 100 ml of distilled water) was added to the samples and vortexed. Samples were then digested in 5 ml of reagent grade concentrated sulphuric acid, vortexed and incubated at room temperature for 15 minutes. Absorption at 488 nm was measured (HACH, model 2000 spectrophotometer) and total carbohydrates quantified using glucose as standards.

Results are presented as mass of total carbohydrate ( $\mu\text{g}$ ) per  $\text{cm}^2$  of media surface area.

### **3.7.4 Heterotrophic plate count**

Heterotrophic bacteria were enumerated from each of the three biofilms samples sites positioned down the vertical axis of the NTF bed using the spread plate technique (APHA Method 9215 A). Media surface samples ( $1 \text{ cm}^2$ ) were taken with sterile cotton swabs in triplicate, and transported back to the laboratory in 1.0 ml of sterile peptone dilution water (0.1 % peptone, Oxoid Ltd). Aqueous suspension of biomass were extracted from the swabs by vortex mixing for 5 minutes, and serially diluted to  $10^{-2}$  and  $10^{-3}$  in sterile peptone water. 100  $\mu\text{l}$  aliquots of the two dilutions were plated in triplicate on R2A agar plates and incubated aerobically at  $30^\circ\text{C}$  for 48 h. Results were enumerated by visually counting individual colonies and are reported in colony forming units (CFU) per  $\text{cm}^2$  of media surface area.

### **3.7.5 Fluorescent in situ hybridisation**

#### *Biofilm sampling and fixation*

Biofilm sampling was carried out once steady state nitrification performance was reached. Pieces of polypropylene cross-flow media (approximately  $1.0 \times 2.0 \text{ cm}^2$ ) were cut from each of the biofilm samples sites positioned through the NTF bed, and immediately fixed in 4 % paraformaldehyde in PBS (130 mM NaCl, 7 mM  $\text{Na}_2\text{HPO}_4$ , 3 mM  $\text{NaH}_2\text{PO}_4$ ; pH 7.2) at  $4^\circ\text{C}$  for 1–2 h.

#### *Embedding and sectioning*

Embedding and sectioning of biofilm samples for FISH analysis was adopted from Hamsen *et al.* (1996) and Lanthier *et al.* (2002). Biofilm samples were dehydrated in a graded series of ethanol solutions (70, 80, 90 and 100 %) for 10 minutes, incubated in chloroform for 12 h, followed by incubating twice in pure paraplast wax at  $60^\circ\text{C}$  for 2 h, and twice in pure paraplast under heated vacuum at -25 kpa for 2 h. The biofilm was

carefully removed from support media, and embedded into paraplast blocks and sectioned (5 – 8  $\mu\text{m}$ ) using a rotary microtome. Sections were placed onto glass slides ready for FISH.

### *Hybridisation*

FISH procedure was adopted from Abell and Bowman (2005) using hybridisation and wash buffers shown in Table 3.1 and Table 3.2. Widely published oligonucleotide probes specific for AOB, NOB and members of the domain *Bacteria*, were synthesised and fluorescently labelled with Cy3 at the 5' end by Geneworks Australia and SIGMA Genosys. NON-EUB338 was used as a negative control in all FISH experiments, to test for non-specific binding. All probe sequences, and hybridisation conditions are given in Table 3.3. Hybridisation and wash stringencies were obtained from probeBase: <http://www.microbial-ecology.de/probebase/> (Loy *et al.* 2003). For hybridisation, 16  $\mu\text{l}$  of appropriate hybridisation buffer and 2  $\mu\text{l}$  of fluorescently labelled probe (concentration of 50 ng/ $\mu\text{l}$ ) were added onto the glass slide containing biofilm cross-sections. Different formamide concentrations were used for each probe (Table 3.3). Where applicable, an unlabelled competitor probe (concentration of 50 ng/ $\mu\text{l}$ ) was added to the mixture (Table 3.3). A hybridisation chamber (CoverWell™ chamber 20 mm X 0.5 mm, catalogue no. H570, ProSciTech, Queensland, Australia) was placed on top of the slide. Slides were inserted into a pre-warmed dark humidified chamber, and incubated at 46°C for 1.5 h.

### *Wash*

Following hybridisation, a stringent wash step was performed in the dark for 15 minutes at 48°C in a pre-warmed wash buffer containing appropriate NaCl concentrations (Table 3.3) and 2  $\mu\text{g}/\text{ml}$  of 4', 6-diamidino-2-phenylindole (DAPI). A cover slip containing a drop of immersion oil was placed onto the slides once dry.

### *Microscopy and image analysis*

Slides were examined using an Olympus BX50 epifluorescent microscope fitted with specific filter for DAPI and Cy3 fluorophores (Cy3; 515 to 550 nm excitation, DAPI; 360 to 370 nm excitation). Black and white photomicrographs were taken with a

Photometrics Cool-Snap *fx* digital camera. Biofilm thickness was measured using ImageJ version 1.34s software, and calibrated using a slide- and eyepiece-micrometer.

**Table 3.1.** Hybridisation solutions used for FISH (Abell and Bowman 2004).

Hybridisation solution	NSO190	EUB338& Non-EUB338	NSO1225	NT3 & CNIT3	NTSPA662 & CNTSPA662
NaCl	1.04 g (0.889M)	1.04g (0.889M)	1.04g (0.889M)	1.04g (0.889M)	1.04g (0.889M)
Tris HCl (0.04M, pH 7.4)	8.8ml (0.02M)	10ml (0.02M)	10ml (0.02M)	10ml (0.02M)	10ml (0.02M)
10% (w gt/vol.) SDS	200µl (0.01%)	200µl (0.01%)	200µl (0.01%)	200µl (0.01%)	200µl (0.01%)
Deionised formamide	11ml	4ml	7ml	8ml	7ml
Milli-Q w ater	0ml (55%)	5.8ml (20%)	2.8ml (35%)	1.8ml (40%)	2.8ml (35%)

**Table 3.2.** Wash buffers used for FISH (Abell and Bowman 2004).

Wash solution	NSO190	EUB338& Non-EUB338	NSO1225	NIT3 & CNIT3	NTSPA662 & CNTSPA662
NaCl	0.1169g (20mM)	1.314g (225mM)	0.467g (80mM)	0.327g (56mM)	0.467g (80mM)
Tris HCl (1M, pH7.4)	2ml (0.02M)	2ml (0.02M)	2ml (0.02M)	2ml (0.02M)	2ml (0.02M)
EDTA (0.5M pH8.0)	1ml (0.005M)	1ml (0.005M)	1ml (0.005M)	1ml (0.005M)	1ml (0.005M)
1% SDS	1ml (0.01%)	1ml (0.01%)	1ml (0.01%)	1ml (0.01%)	1ml (0.01%)
Milli-Q w ater	96 ml	96 ml	96 ml	96 ml	96 ml

**Table 3.3.** 16S rRNA-targeted oligonucleotide probes used in this study.

Probe	Sequence	Specificity	Formamide <sup>†</sup> (%)	NaCl <sup>††</sup> (mM)	Reference
EUB338	5'- GCT GCC TCC CGT AGG AGT -3'	Most Bacteria	20	225	(Amann <i>et al.</i> 1990)
Non EUB338	5'- ACT CCT ACG GGA GGC AGC -3'	Non specific label	20	225	
NIT3	5'- CCT GTG CTC CAT GCT CCG -3'	<i>Nitrobacter</i> spp.	40	56	(Wagner <i>et al.</i> 1996)
Comp NIT3	5'- CCT GTG CTC CAG GCT CCG -3'	Unlabelled competitor to NIT3			
Ntspa662	5'- GGA ATT CCG CGCTCC TCT -3'	Genus <i>Nitrospira</i>	35	80	(Daims <i>et al.</i> 2001)
Comp Ntspa662	5'- GGA ATT CCG CTCTCC TCT -3'	Unlabelled competitor to Ntspa662			
Nso1225	5'- CGC CAT TGT ATT ACG TGT GA -3'	Beta-proteobacterial AOB	35	80	(Mobary <i>et al.</i> 1996)
Nso190	5'- CGA TCC CCT GCT TTT CTC C -3'	Beta-proteobacterial AOB	55	20	(Mobary <i>et al.</i> 1996)

### **3.7.6 Scanning electron microscopy**

Pieces of polypropylene cross-flow media were cut (approximately 0.5 cm<sup>2</sup>) from each biofilm sample site. Samples were immediately fixed in 4 % paraformaldehyde and incubated at 4°C between 2 to 24 h. After fixation, samples were stored in PBS solution (130 mM NaCl, 7 mM Na<sub>2</sub>HPO<sub>4</sub>, 3 mM NaH<sub>2</sub>PO<sub>4</sub>; pH 7.0) at 4°C prior to analysis. Samples were further fixed in 1 % osmium tetroxide for 30 minutes. Samples were washed twice for 10 minutes in distilled water, and dehydrated in serial ethanol baths (50, 75, 85, 95 and 100 %) for 5 minutes, followed by critical control point drying. Samples were mounted on a stub, contacted with carbon dag, coated in gold (E5200 SEM auto-coating unit; Polaron, West Sussex, UK) and examined for surface structure using a Scanning Electron Microscope (Seimens, New South Wales, Australia).

### 3.8 Hydraulic tracer analysis

Hydraulic tracer experiments were performed to characterise the patterns of flow within the large pilot-scale NTF. These tracer studies were done using a fluorescent dye (rhodamine WT) in conjunction with a SCUFA<sup>®</sup> submersible fluorometer/data logger (Turner Designs, Inc., Sunnyvale, CA). Rhodamine dye is well suited to hydraulic tracer studies (Smart and Laidlaw, 1977). Initial rhodamine injection dosage was calculated so as to allow for sufficient fluorescence peak height in the effluent according to Kilpatrick (1970). A pulse of the rhodamine ( $10^{-2}$  dilution; 5 ml) was injected to the large pilot-scale NTF's influent prior to distribution using a 10 ml syringe (Plate 3.8). Over a period of 20 minutes rhodamine fluorescence was measured every 5 seconds in the filters effluent using the SCUFA<sup>®</sup> submersible fluorometer with internal data logging capabilities, and was expressed as relative fluorescence. Hydraulic flow rates were also recorded at the commencement and cessation of each tracer experiment. RTD curves were compiled using PRISM 4.03 (GraphPad Software, San Diego, CA, USA). The HRT was calculated from the measured fluorescence, using Equation 3.1 (Levenspiel 1999). From the equation,  $t_i$  represents the elapsed time (seconds) since tracer addition and  $C_i$  represents the effluent tracer concentration at each logged time interval.

$$\bar{t} = \frac{\sum t_i C_i}{\sum C_i}$$

Equation 3.1

### **3.9 Statistical analysis**

All mean values were calculated as arithmetic means  $\pm$  1 SD except where otherwise indicated. Where  $n \geq 12$  and data sets possessed significantly normal distributions, statistical analysis was performed using parametric methods. Where  $n < 12$  and/or data sets possessed non-normal distributions, statistical analysis was assessed by way of non-parametric methods. Statistical significance was accepted at the  $p < 0.05$  level. All statistical analyses were compiled using Graphpad PRISM (Version 4.0, Graphpad software, California, USA) and SPSS (Version 10.0, SPSS, Illinois, USA). Graphical data was created using Graphpad PRISM and Excel XP (Microsoft Corporation, USA).

## 4 APPLICATION OF TRICKLING FILTERS TO REMOVE LOW CONCENTRATIONS OF AMMONIA

### 4.1 Introduction

As part of the current research, investigations into the removal of low concentrations of ammonia by *high* hydraulic rate NTFs were carried out in order to assess NTF process efficacy as a potentially viable alternative to pre-chlorination for *potable water* treatment. More commonly, *low* hydraulic rate NTFs are widely used for the remediation of nitrogen-rich *wastewater*, and as such, the vast majority of research to date has been derived from studies based on research at the wastewater treatment level.

Much of the available literature has considered mass transport of solutes through the biofilm integral to the stability and performance of NTFs, because it strongly influences the rates of microbial transformations (Gullicks and Cleasby 1986; Parker *et al.* 1989; Boller *et al.* 1994). The mass flux of solutes into a biofilm occurs by a combination of diffusion, advection and dispersion (Characklis and Wilderer 1989; Wuertz *et al.* 2003), with molecular diffusion considered to be the most important mechanism (Wuertz *et al.* 2003).

Nitrification rates in fixed-film wastewater biological reactors are widely believed to be rate-limited by the diffusion of oxygen and/or substrate ammonia through the biofilm depth (Boller *et al.* 1990; Boller *et al.* 1994; Metcalf and Eddy 2003). According to the literature, oxygen transfer limitations have been considered a major concern in the process design of wastewater NTFs, especially under high organic and nitrogen surface loading (Metcalf and Eddy 2003 and Boller *et al.* 1994). The substrate surface loading rate is therefore an important operational variable, as it represents the mass of substrate applied per unit of media surface area, per unit time; with variation in surface

loading rate achieved either by changing the hydraulic loading rate and/or the influent substrate concentration.

In contrast to conventional wastewater applications, one of the key challenges for applying NTFs to potable water treatment is the low influent ammonia concentrations. Ammonia-N data obtained from Buaran WTP showed that mean concentrations were 0.5 mg/L, although peaks as high as 2.5 mg/L were commonly detected. For a NTF operating under such low ammonia concentrations, nitrification was hypothesised to become rate-limited by the diffusion of ammonia through the biofilm depth. This initial hypothesis was indeed supported by previous reports from Gullicks and Cleasby (1986), Parker and Richards (1986), Parker *et al.* (1989) and Boller *et al.* (1994) on wastewater NTFs, which have indicated that ammonia-limited nitrification occurs at concentrations below 5.0 mg NH<sub>4</sub>-N/L, and is generally most evident at the lower bed depths (Boller *et al.* 1994).

This chapter presents the findings from a series of pilot experiments which were designed to investigate the impact of low ammonia concentrations on NTF performance. The aims were to firstly determine whether a nitrifying population could be established under low feed ammonia-N concentrations, secondly, whether it would then be capable of achieving complete nitrification, and finally to investigate the effect of specific operating conditions—namely low ammonia feed concentrations and variations in hydraulic surface load—on overall NTF nitrifying capacity. The nitrification behaviour within the NTF was also characterised by measuring the distribution of inorganic nitrogen species (ammonia, nitrite and nitrate) vertically through the entire NTF bed. Much of the earlier research into the application of NTFs to potable water treatment by van den Akker (2003) was achieved by analysing influent and effluent inorganic nitrogen concentrations to determine “apparent” rates, with no consideration given to internal nitrification performance. This initial approach assumed that nitrification rates were uniform with depth, and as such, basing future NTF design criteria on this preliminary data was deemed inadequate. To date, most of the available literature characterising internal nitrification behaviour in response to various environmental and operation

conditions has been obtained from wastewater NTFs operating under much higher, *non-ammonia-limited* feed concentrations (Gulicks and Cleasby 1986; Boller *et al.* 1994; Biesterfeld *et al.* 2003). Available data shows that for a large portion of a wastewater NTF column, ammonia-N concentrations are generally high enough such that internal nitrification rates are 'zero-order' and are therefore mostly uniform throughout the bed depth (Parker *et al.* 1989; Metcalf and Eddy 2003). To the author's knowledge, no studies have been reported which have characterised microbial nitrification throughout a potable-water NTF designed to operate under very low or ammonia-limiting concentrations. In addition to process chemistry, the impact of substrate nitrogen profiles on the distribution of attached biomass—measured as total protein and total carbohydrate throughout the NTF bed depth—was also investigated. Results from this study will provide insight into both the distribution of biomass, as well as nitrification rates throughout a potable water NTF in response to operating under ammonia-limiting concentrations.

Furthermore, findings from Chapter 2 showed that the raw water at Buaran WTP experienced intermittent changes in turbidity and SS, which needed to be considered in the design of the NTF. High SS have been shown to have a negative impact on nitrification due to the organic component promoting heterotrophic competition for available oxygen (Parker *et al.* 1995), however, little is known regarding the impact of biologically inert SS on the nitrification capacity of NTFs. Since the NTF was designed to be a front-end water treatment process (i.e., ahead of pre-chlorination), the impact of high concentrations of inert SS on the nitrification capacity of a NTF was also investigated.

## 4.2 Methods

Experiments were conducted on pilot scale NTFs which were operated under specially controlled conditions aimed at mimicking the quality of Buaran WTP raw water supply; namely low influent ammonia concentration and high turbidity. A descriptive summary of each pilot NTF, showing details of: bed size; hydraulic load; and ammonia load; is given in Table 4.1. A more detailed description of each pilot NTF can be found in Chapter 3.

### 4.2.1 *Large pilot-scale NTF*

Long-term experiments were mostly conducted on a large-scale pilot NTF, therefore experimental data in the current chapter was obtained from this filter unless otherwise stated. As discussed in Chapter 3, the large pilot-scale NTF needed to be decommissioned and reconstructed. Both the old and the newly reconstructed NTFs were identical in terms of physical dimensions, and were operated under identical conditions. Having said this however, several small design modifications were implemented pertaining to the additional media support stands, and also alterations to biofilm and filtrate sample collection sites. Nitrification rates and nitrate generation rates measured throughout the NTF bed were used to compare nitrification performance between the old and newly reconstructed NTFs to ensure consistent nitrifying behaviour. Differences between nitrification performances were examined by *t*-test. Statistical significance was set at the  $p < 0.05$  level.

### 4.2.2 *Small pilot-scale NTFs*

The large pilot-scale NTF was limited to operating under influent ammonia concentrations of 5.5 mg/L (or an  $\text{NH}_4\text{-N}$  loading of  $\approx 966 \text{ mg m}^{-2} \text{ d}^{-1}$ ). This was due to the fact that under such high flow rates ( $192,000 \text{ L d}^{-1}$ ), it was neither practical, nor feasible, to dose and maintain higher ammonia loads for lengthy periods of time. Furthermore, due to the high head loss experienced during pump operation, the

maximum achievable hydraulic surface load that the large pilot-scale NTF could operate under was  $173 \text{ L m}^{-2} \text{ d}^{-1}$ . Three smaller pilot-scale NTFs (see Chapter 3, Section 3.4) were therefore employed to investigate the influence of higher hydraulic surface loads ( $>173 \text{ L m}^{-2} \text{ d}^{-1}$ ) and high ammonia-N influent loads ( $> 5.0 \text{ mg/L}$ ) on nitrification capacity.

#### **4.2.3 NTF start-up**

Re-construction of the large pilot-scale NTF provided an opportunity to monitor nitrification during the commissioning or 'start-up' phase. Ammonia-N was maintained at low concentrations of  $1.1 \pm 0.3 \text{ mg/L}$ , which was representative of raw water concentrations observed at Buaran WTP. Influent, effluent, and profile data was collected two to three times per week over a two month monitoring period. To monitor biofilm development, media samples with attached biomass were harvested from a bed depth of 0.3 m on days 8, 16, and 80 following initial start-up, and examined using SEM and FISH according to the procedures described in Chapter 3, Section 3.7.

#### **4.2.4 Ammonia loading**

In successive experiments, surface ammonia loads were increased in small increments by dosing additional ammonium sulphate into the inflow. The measurement of nitrification rates under non-ammonia-limiting conditions was undertaken in order to provide valuable information with respect to maximum achievable nitrification rates. Experiments were conducted on both the large and small (Filter 1) pilot-scale NTFs. For both NTFs, the *hydraulic* surface loading was maintained relatively constant at  $173\text{--}174 \text{ L m}^{-2} \text{ d}^{-1}$ . Therefore, in order to achieve high ammonia-N *surface* loads ( $\text{mg NH}_4\text{-N m}^{-2} \text{ d}^{-1}$ ), the influent ammonia-N concentration ( $\text{mg/L}$ ) was increased. The large pilot-scale NTF operated under a range of ammonia-N surface loads; increasing from 40 to a maximum of  $966 \text{ mg NH}_4\text{-N m}^{-2} \text{ d}^{-1}$  (Table 4.1). Experiments were conducted on both the old and newly reconstructed NTFs. The small pilot-scale NTF (Filter 1), was employed to examine the impact of higher ammonia surface loads, beyond 966 to  $1998 \text{ mg NH}_4\text{-N m}^{-2} \text{ d}^{-1}$  (Table 4.1). All NTFs were operated under each discrete ammonia

load until steady-state nitrification performance was reached. Steady-state nitrification was assumed to have been attained once the daily coefficient of variation in percentage nitrification was  $\leq 5\%$ .

#### 4.2.5 Effect of hydraulic load on nitrification performance

The influence of hydraulic loading on NTF performance was investigated over a five month period using the three small pilot-scale NTFs operating under ammonia-N loads described in Table 4.1. Each of the three small-scale NTFs operated in parallel under three discrete but fixed hydraulic surface loading rates: 202; 274; and 402 L m<sup>-2</sup> d<sup>-1</sup>; and therefore received identical ammonia-N *concentration* loads (mg NH<sub>4</sub>-N/L) at any given time, but each received different ammonia-N *surface* loads (mg NH<sub>4</sub>-N m<sup>-2</sup> d<sup>-1</sup>) due to the differences in hydraulic throughput. Higher ammonia-N surface loads were therefore achieved by increasing the hydraulic load.

**Table 4.1.** Summary of pilot NTFs used in the study and their operating conditions.

Pilot NTF	Media volume	**Hydraulic surface load (L m <sup>-2</sup> d <sup>-1</sup> )	Ammonia conc. loading range (NH <sub>4</sub> -N mg/L)	*** Ammonia surface loading range (NH <sub>4</sub> -N mg m <sup>-2</sup> d <sup>-1</sup> )	Duration of operation (months)
*Large F	4.6 m <sup>3</sup>	173	0.5–5.5	40–966	24
Small F1	0.6 m <sup>3</sup>	174–202	0.7–9.9	138–1998	5
Small F2	0.6 m <sup>3</sup>	274	0.7–9.9	189–2725	5
Small F3	0.6 m <sup>3</sup>	402	0.7–9.9	277–3997	5

\*Combination of old and newly reconstructed NTF. \*\*Hydraulic surface load represented as volume (L) applied per m<sup>2</sup> of media surface area per day. \*\*\*Ammonia surface load represented as mass ammonia-N (mg) applied per m<sup>2</sup> of media surface area per day.

#### **4.2.6 Effect of suspended solids on nitrification performance**

To investigate the impact of high inert solid loading on NTF nitrification performance, a clay slurry was dosed into the inflow of the large pilot-scale NTF, resulting in an increased turbidity from background concentrations of 2–17 NTU, to a mean concentration of  $42 \pm 32$  NTU (equating to  $51 \pm 25$  mg SS/L). High SS loads were maintained for 30 consecutive days. During this time, influent, effluent, and profile grab samples were collected regularly. A more detailed description of the clay dosing unit can be found in Chapter 3, Section 3.3.3.

#### **4.2.7 Large pilot-scale NTF—sampling and chemical analysis**

Influent, effluent, and depth profile 0.5 L grab sampling was performed on average between two and three times per week, with samples collected at 10:00 am ( $\pm 2$  h). Samples were stored on ice during transport to the laboratory, and were analysed within two hours of sampling for ammonia-N, nitrite-N, nitrate-N, TOC, and sBOD<sub>5</sub> using procedures described in Chapter 3, Section 3.5. Profile samples were taken from the NTF, at bed depths of 0.3, 1.5 and 2.7 m from the surface, in accordance with the procedure described in Chapter 3, Section 3.2.11. Ammonia-N and nitrate-N profile data was used to calculate nitrification rates and nitrate-N generation rates for the NTF at the time of sampling. Influent and effluent samples were analysed regularly for total alkalinity, pH, DO, turbidity, and SS using methods described in Chapter 3, Section 3.5. Influent temperature was recorded online at 30 minute intervals (as per Chapter 3, Section 3.6.3). Long-term monitoring of influent temperature, total alkalinity, pH, DO, turbidity, TOC and sBOD<sub>5</sub> from the large pilot-scale NTF was performed to evaluate the impact of seasonal variation of these parameters on nitrification performance. Statistical analysis using Spearman's correlation coefficient ( $r_s$ ) was used to identify relationships between these parameters and percentage nitrification. Statistical significance was set at the  $p < 0.05$  level.

#### **4.2.8 Small pilot-scale NTFs—sampling and chemical analysis**

Influent and effluent grab samples were taken on average once or twice weekly, at 10:00 am ( $\pm 2$  h). Samples were stored on ice during transport and analysed within two hours of sampling for ammonia-N, nitrite-N and nitrate-N. TOC and sBOD<sub>5</sub> were measured within the influent on average once weekly.

#### **4.2.9 Hydraulic tracer analysis**

Hydraulic tracer experiments were conducted on the large pilot-scale NTF to monitor shifts in HRT in response to biofilm development and changes in ammonia loads. Tracer analysis was performed using procedures described in Chapter 3, Section 3.8 under three varying conditions: (i) relatively clean media, seven days into filter start-up; (ii) on completion of filter start-up; and (iii) at steady state performance once ammonia-N substrate loading had been increased from 1.0 to 5.0 mg/L. Hydraulic flow was maintained at 8 m<sup>3</sup>/h (5.2 m/h) for all experiments. The HRT of the NTF was then calculated from the recorded tracer time–concentration data as described in Chapter 3, Section 3.8.

#### **4.2.10 Total protein and total carbohydrate**

The distribution of biomass throughout the large NTF was determined by quantifying total protein and total carbohydrate concentrations per cm<sup>2</sup> of media surface area. Biomass was harvested from biofilm sample sites located at bed depths of 0.3, 1.5 and 2.7 m from the surface and analysed for total protein and total carbohydrates in accordance with procedures described in Chapter 3, Section 3.7.

#### **4.2.11 Weighing of the support media**

The distribution of biomass throughout the large pilot-scale NTF was also determined by weighing the support media with the biomass attached. Modifications made to the old large pilot-scale NTF provided a unique opportunity during disassembly to weigh each of the 10 layers of support media; with individual media blocks being weighed

immediately after each layer was removed from the NTF column. The media was not allowed to dry out during this process, therefore results are presented as wet-weight (kg) of media (and attached biomass) per unit of depth.

## 4.3 Results

### 4.3.1 Large pilot-scale NTF start-up

During start-up, the NTF's influent (Hope Valley Reservoir) water was amended with low concentrations of ammonia-N ( $1.1 \pm 0.3$  mg/L), chosen to mirror those concentrations previously recorded in the abstracted water at Buaran WTP. At the time, native organic carbon concentrations of the influent were low, measuring  $6.5 \pm 1.6$  mg TOC/L and  $2.3 \pm 1.2$  mg BOD<sub>5</sub>/L. Mean values of influent pH, total alkalinity, and DO remained steady, measuring 7.9, 105.7 mg CaCO<sub>3</sub>/L and 6.4 mg DO/L respectively. Influent temperature varied from 15.5 to 22.3°C. Changes in inorganic nitrogen species composition within the NTF's influent and effluent (Figure 4.1), and *in situ* analysis of the biofilm (Plate 4.1) monitored over a two month period, was used to characterise NTF start-up. In addition, profiles of inorganic nitrogen species were regularly measured throughout the NTF to profile the development of internal nitrification performance (Figure 4.2).

From Plates 4.1.a and 4.1.b, it can be seen that FISH analysis of biofilms harvested from a bed depth of 0.3 m on day 8 revealed the early and equal development of AOB and NOB, despite no evidence of nitrification (Figure 4.1). Positive signals were obtained from oligonucleotide probes NSO1225 and NIT3, which confirmed the presence of both *Nitrosomonas* and *Nitrobacter* species. Despite the early development of AOB and NOB, the first sign of nitrification was not observed until day 14; characterised by a small decrease in effluent ammonia, which coincided with the generation of both effluent nitrite and nitrate (Figure 4.1). A depth profile of inorganic nitrogen species measured throughout the NTF bed on day 15, confirmed the small and equal generation of both nitrite and nitrate with depth (Figure 4.2). By day 19, results showed that the generation of nitrite and nitrate measured throughout the NTF bed and within the final effluent had increased, in conjunction with improved ammonia removal (Figures 4.1 and 4.2) Effluent nitrite-N continued to increase, reaching a maximum concentration of 0.42 mg/L on day 19, before subsiding to concentrations below 0.2 mg/L by day 35 (Figure 4.1). The marked decrease in nitrite coincided with a further

increase in effluent nitrate concentrations. When comparing profiles of inorganic nitrogen species measured throughout the NTF between days 19 and 34, it can also be seen that nitrite concentrations measured through the NTF had decreased (Figure 4.2). This observation was coupled with an increase in nitrate production with depth. From Figure 4.1, it can be seen that the steady-state for percentage nitrification was initially achieved within 40 d, characterised by negligible concentrations of effluent ammonia-N and nitrite-N and high concentrations of effluent nitrate-N. Further analysis of nitrification behaviour throughout the NTF showed that steady-state performance within the NTF was maintained between days 55 and 84 (Figure 4.2). Corresponding fluorescence and electron microscopic visualisation of biofilm abundance, measured on day 80, confirmed considerable improvement in biofilm development (Plate 4.1).

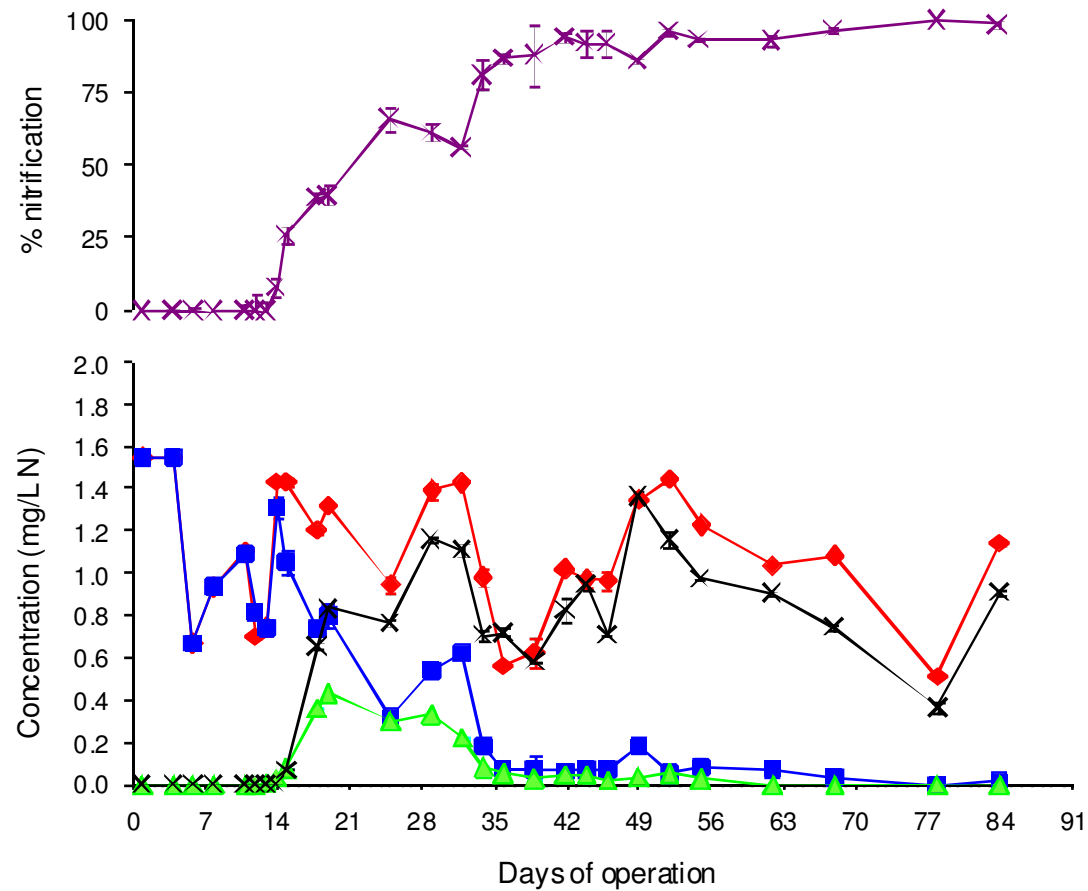


**Figure 4.1.** Progression of nitrification during start-up after supplementing the influent with low concentrations of ammonia on day 0. Data points show average influent ammonia-N (♦), effluent ammonia-N (■), effluent nitrite-N (▲), and effluent nitrate-N (X) concentrations  $\pm 1$  SD.

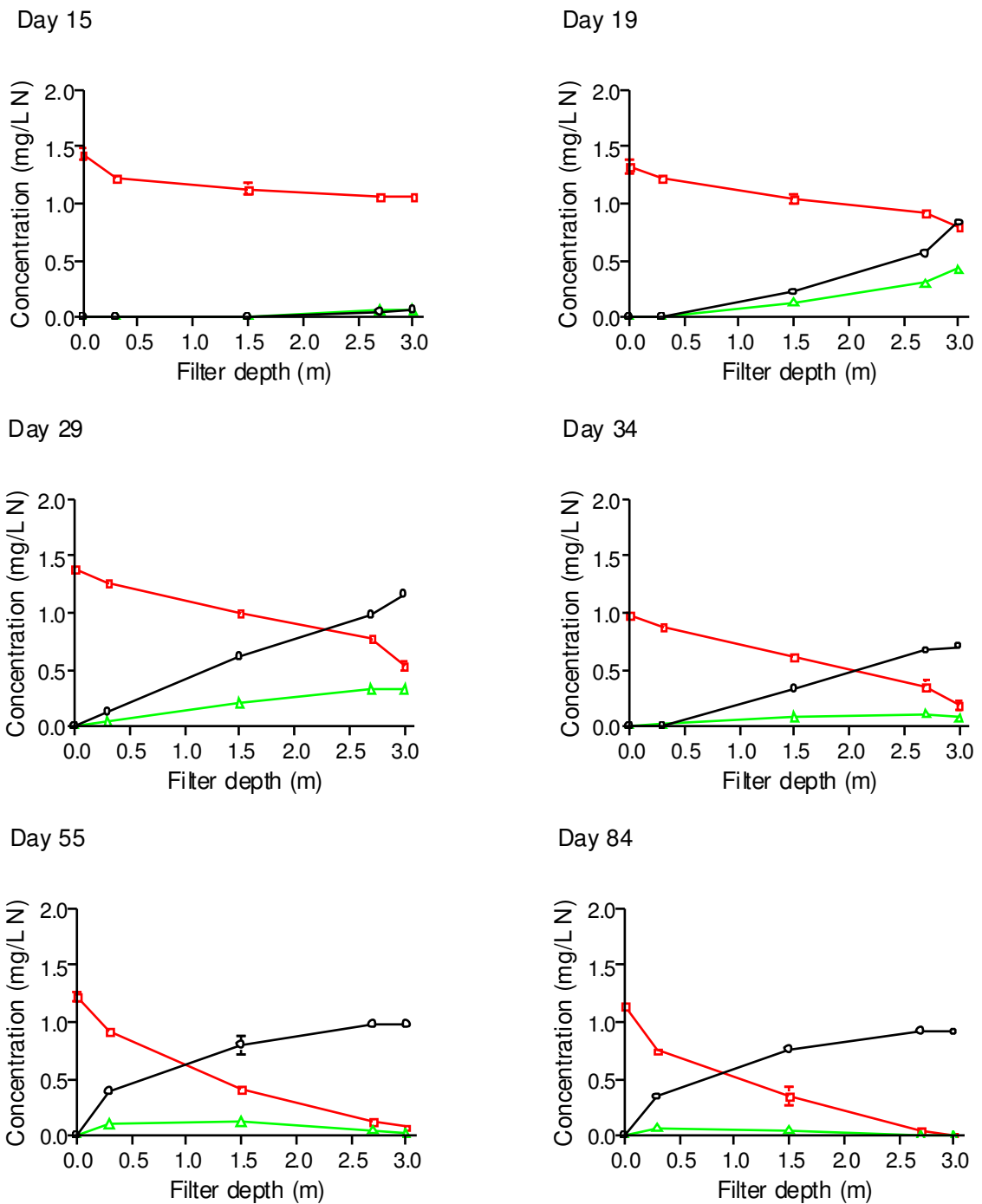
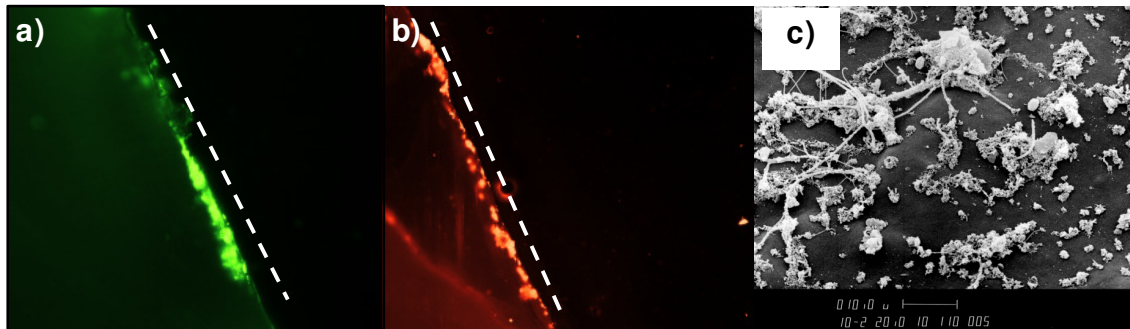
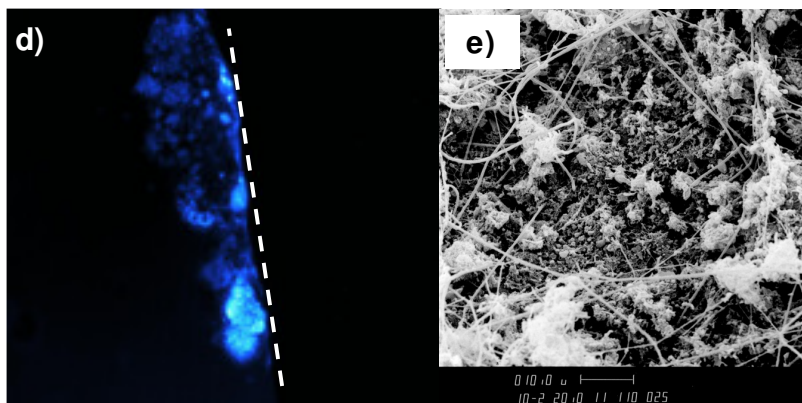


**Figure 42.** Concentration profiles of inorganic nitrogen species measured throughout the depth of the large pilot-scale NTF during start-up. Data points represent average ammonia-N (□), nitrite-N (△), and nitrate-N (○) concentrations ± 1 SD.

Biofilm aged 8 days



Biofilm aged 16 days



Biofilm aged 80 days

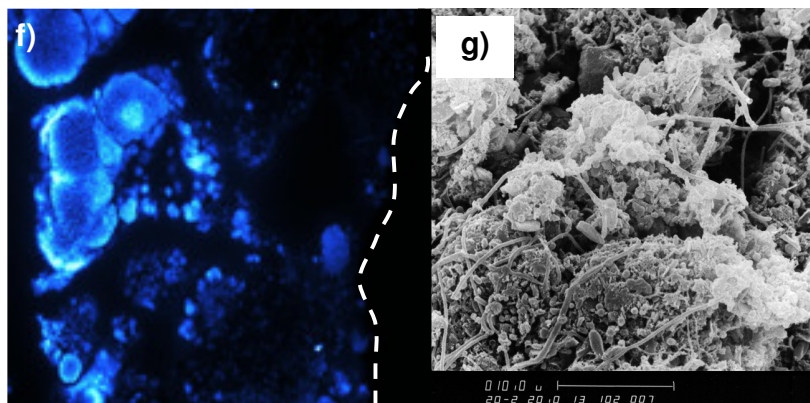


**Plate 4.1.** *In situ* examination of biofilm harvested at 0.3 m during start-up using FISH and SEM: (a) fluorescent micrograph showing AOB targeted with probe NSO1225 after FISH; (b) fluorescent micrograph depicting NOB targeted with probe NIT3 after FISH; (c, e, g) SEM of media surface; and (d and f) fluorescent micrograph depicting total biomass stained with DAPI. Dashed line represents filter media. (Fluorescent micrographs taken at 400x Magnification).

### **4.3.2 Performance comparison of the old and newly reconstructed pilot NTFs**

As explained in Chapter 3, Section 3.3.5, the large pilot-scale NTF was decommissioned and reconstructed, during which time some small alterations were made to the biofilm and filtrate sample sites, and also to the media support structure. Once the newly reconstructed NTF had been commissioned, the filter was operated under a range of ammonia-N concentrations and surface loads, identical to those under which the decommissioned NTF had previously operated. Apparent steady-state and internal nitrification performance between the old and newly reconstructed NTF was compared.

Overall percentage nitrification measured from both the old and newly reconstructed NTFs for a range of ammonia-N concentration loads (0.5–5.0 mg/L) were the same ( $t$ -test;  $p > 0.05$ ). Similarly, when comparing apparent nitrification rate as a function of ammonia-N load, regression analysis also confirmed that differences between the two slopes were not significant (ANCOVA;  $p > 0.05$ ). Further investigation of the distribution of nitrification performance vertically through each NTF was also required to ensure that internal nitrification behaviour between the two NTFs was the same. Differences in performance were based on comparing nitrate generation rates throughout the NTF, as a measure of nitrification activity, and were evaluated by  $t$ -test. Nitrate generation rates were used as a measure of true nitrification activity due to it disregarding any other ammonia removal process (e.g. ammonia air stripping, volatilisation or assimilation) which may bias the implied nitrification performance. Long term nitrate-N profile data collected from the old and newly reconstructed NTFs were used to determine nitrate generation rates through the NTF bed depth. The operational data set was divided into periods of uniform ammonia concentration loads ( $\pm 0.2$  mg/L) for each NTF. Three different ammonia concentration loads were selected to represent low, medium and high concentrations for each of the NTFs to operate under during the course of the study. Nitrate generation rates were calculated for bed depths 0.3, 1.5, 2.7 and 3.0 m by measuring the difference in nitrate concentrations between these adjacent sample depths, and were calculated as a function of media surface area measured between each depth. The mean was calculated from eight individual sampling events obtained

from both NTFs. Results are presented in Figure 4.3 and clearly show, for each ammonia-N concentration load, that the nitrification performance measured down the old and newly reconstructed pilot NTF bed were very similar ( $t$ -test;  $p > 0.05$ ). Due to the excellent reproducibility in nitrification performance between the old and newly reconstructed large pilot-scale NTFs, all data from this point onward is derived from both NTFs and was subsequently combined prior to analysis and presentation.

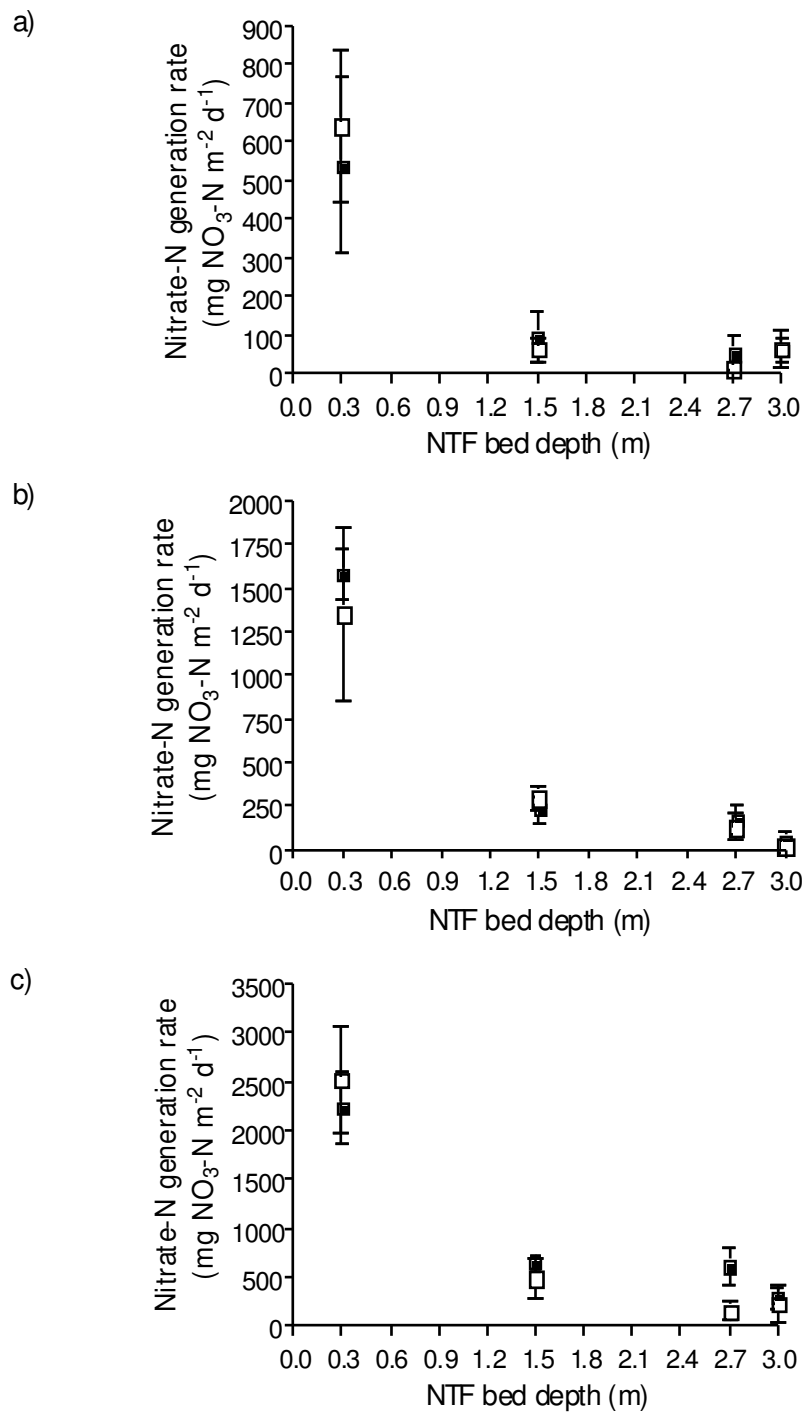


**Figure 4.3.** Comparison of nitrate-N generation rates between the old large pilot-scale NTF (■) and the newly reconstructed large pilot-scale NTF (□), for various ammonia-N concentration loads of: (a) 0.5 mg/L; (b) 2.0 mg/L; and (d) 5.0 mg/L. Data points show parameter means  $\pm$  1 SD of eight individual sampling events.

### **4.3.3 Inorganic nitrogen depth profile**

Figure 4.4 shows the steady-state distribution of inorganic nitrogen concentrations through the large pilot-scale NTF bed depth for varying ammonia concentration loads. The mean of four to six sampling events obtained from both the old and newly reconstructed NTF is presented. For all profiles, significant oxidation of ammonia can be seen at a bed depth of just 0.3 m, after which it reduces with depth. The generation of nitrate complemented the decline in ammonia throughout the bed depth. Depth profiles showed that nitrite did not accumulate appreciably within the NTFs. Only small accumulation of nitrite can be seen at bed depth of 0.3 m when operated under high ammonia concentrations of 5.0 mg NH<sub>4</sub>-N/L. Regardless of influent ammonia-N concentrations, the final effluent contained negligible concentrations of ammonia-N (<0.1 mg/L), no nitrite-N, and was characteristic of complete nitrification whereby a high conversion of ammonia to nitrate had occurred. A nitrogen budget demonstrated that 85 to 100 % of ammonia-N removed was recovered in the form of nitrite-N and nitrate-N throughout the entire NTF bed. The narrow error bars are also an indication of excellent reproducibility between sampling events and between the old and newly reconstructed NTFs.

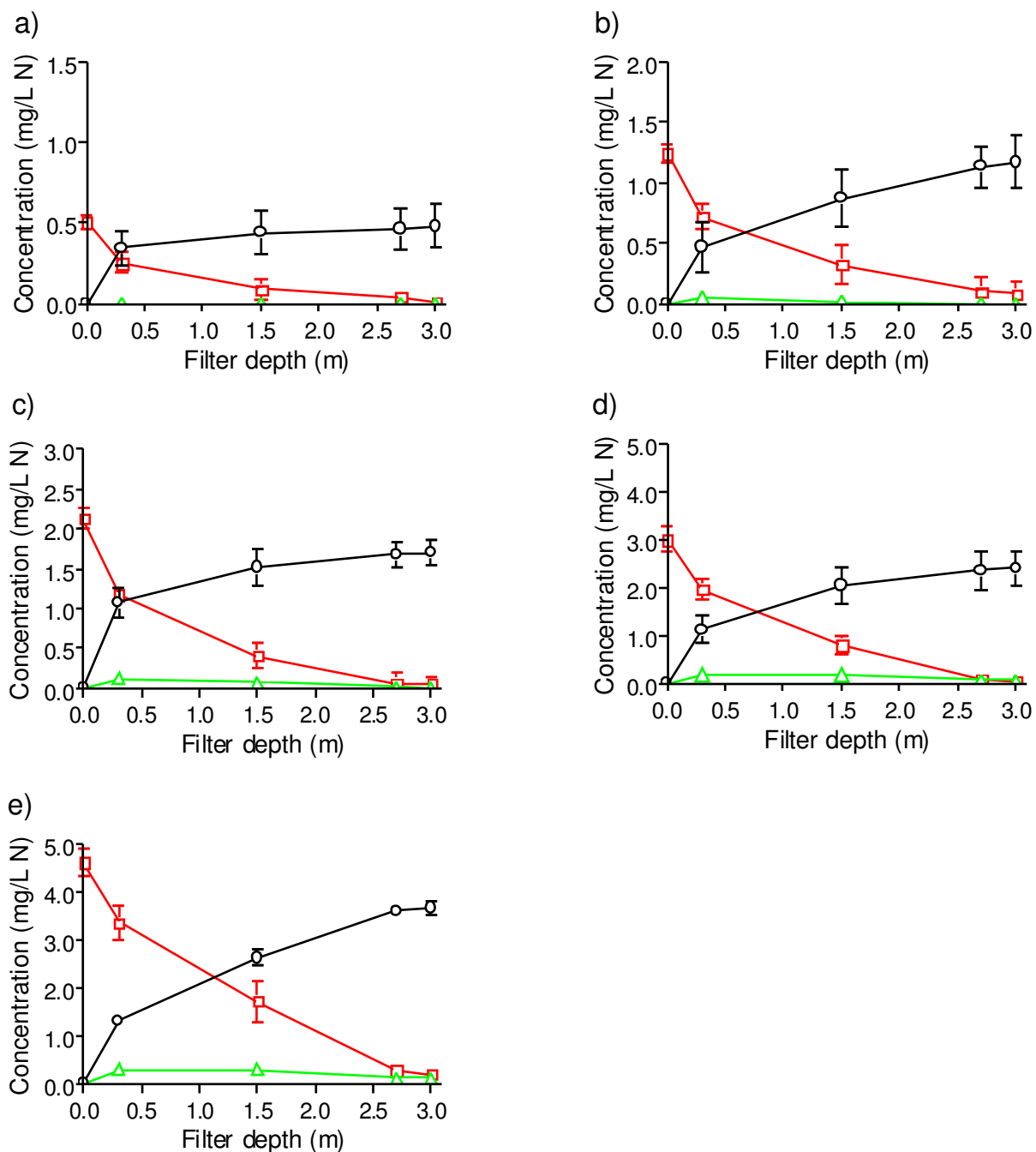


**Figure 4.4.** Steady-state concentration profiles of inorganic nitrogen species measured within the large pilot-scale NTF for various ammonia-N concentration loads of: (a) 0.5 mg/L; (b) 1.0 mg/L; (c) 2.0 mg/L; (d) 3.0 mg/L; and (e) 5.0 mg/L. Individual data points show mean ammonia-N ( $\square$ ), nitrite-N ( $\triangle$ ) and nitrate-N (O) concentrations  $\pm 1$  SD of 4–6 individual sampling events.

#### **4.3.4 Nitrification rate profile**

Long-term ammonia profile data collected during operation of the old and newly reconstructed NTFs, provided a basis for calculating nitrification rates throughout the NTF. The operational data set was divided into periods of uniform ammonia concentration loads ( $\pm 0.2$  mg/L) obtained from both the old and newly reconstructed NTFs. Nitrification rates were calculated at bed depths 0.3, 1.5, 2.7 and 3.0 m by using the difference in ammonia-N concentrations between these adjacent sample depths, and were determined as a function of media surface area and as a function of biomass weight. Profiles of nitrification activity measured down the large pilot-scale NTF bed are shown in Figure 4.5. For each concentration load, the data presented represents the mean of five to nine individual sampling events, obtained from both the old and newly reconstructed pilot NTFs. The narrow error bars are again an indication of excellent reproducibility between sampling events for both the old and newly reconstructed NTFs. From Figure 4.5.a, it can be seen that the nitrification rates measured per unit of surface area decreased considerably with depth. In successive experiments, ammonia loading was increased in small increments in an attempt to reduce ammonia limitation throughout the lower depths of the NTF. As the ammonia-N concentration loading was increased from 0.5 to 5.0 mg/L, a considerable increase of nitrification rates throughout the lower depths of the filter was observed. Furthermore, the nitrification rates complemented the nitrate generation rates presented in Figure 4.3. Similarly, when nitrification activity was normalised to the biomass data obtained from Figure 4.11, results clearly showed a decrease in nitrification activity per weight (kg) of biomass with an increase in bed depth (Figure 4.5.b).

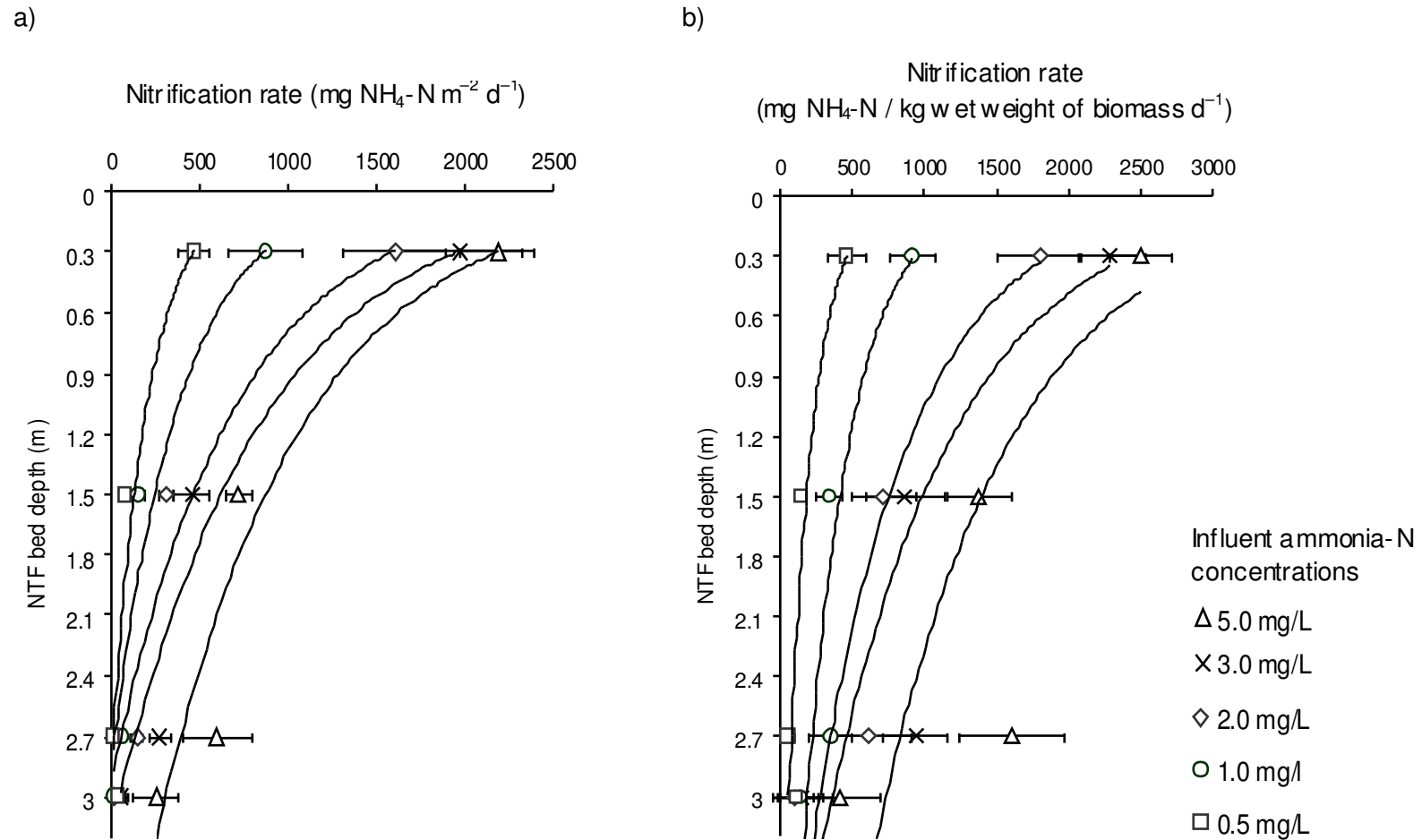


**Figure 4.5.** Nitrification rates measured throughout the depth of the large pilot-scale NTF, represented as: (a)  $\text{mg NH}_4\text{-N}$  per unit of surface area ( $\text{m}^2$ ); and (b) per kg of biomass; for various influent ammonia-N concentrations. Nitrification rate data was obtained under a constant hydraulic surface loading of  $173 \text{ L m}^{-2} \text{ d}^{-1}$ . Solid lines represent trend lines (Data points represent parameter means  $\pm 1$  SD).

Figure 4.6 shows the nitrification rates at different filter bed depths as a function of influent ammonia concentration. Similar to Figure 4.5, nitrification rates declined significantly with filter bed depth. The plateau or zero-order region seen on the 0 – 0.3 meter curve, represents the maximum nitrification rates reached during the study ( $\approx 2180 \text{ mg NH}_4\text{-N m}^{-2} \text{ d}^{-1}$ ), which occurred when influent ammonia-N concentrations were maintained above 4.0 mg/L. Here, nitrification rates were independent of the influent ammonia concentration. In contrast, the remaining lower depths of the NTF exerted a first-order linear relationship between nitrification rate and influent ammonia-N concentration. This linear or first-order region for each nitrification rate curve demonstrates the rate-limiting effects of a low ammonia concentration.

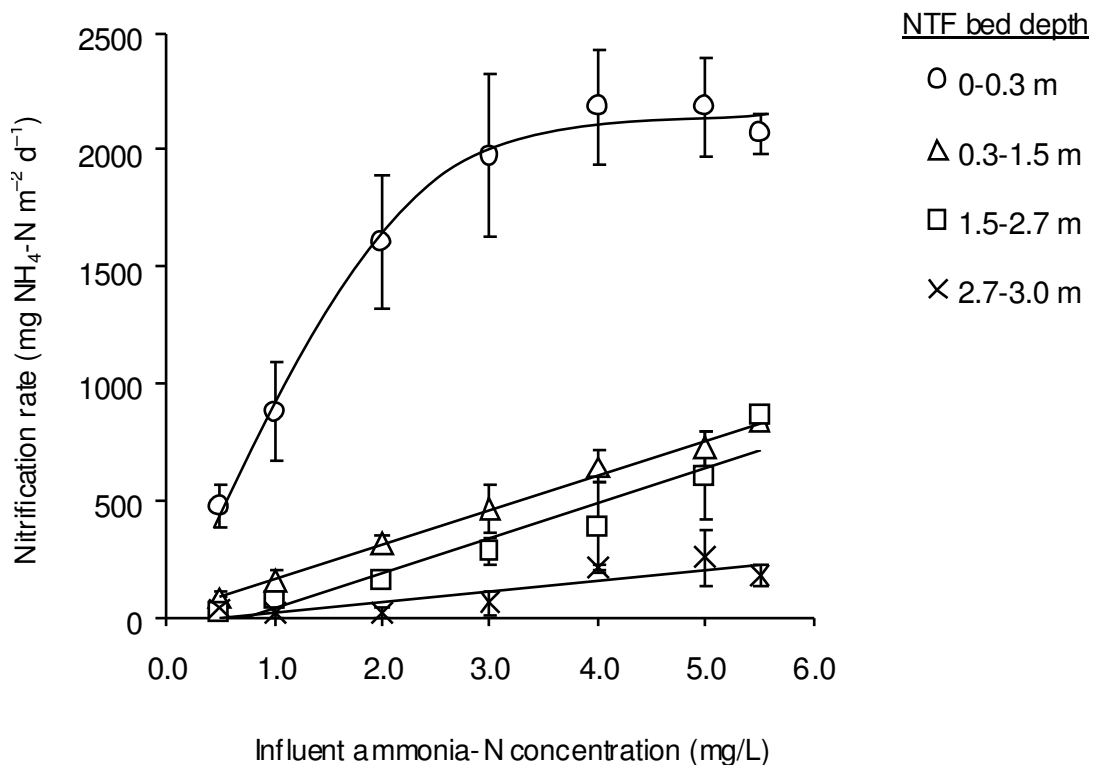


**Figure 4.6.** Nitrification rates as a function of influent ammonia-N concentration for four filter bed depths when operated under a constant hydraulic surface loading of  $173 \text{ L m}^{-2} \text{ d}^{-1}$ . (Data points represent parameter means  $\pm 1 \text{ SD}$ ).

#### **4.3.5 Nitrification rates as a function of ammonia-N surface load**

Once a mature nitrifying biofilm was established, ammonia loads were increased in small increments to determine the maximum achievable nitrification rate. Figure 4.7 shows the relationship between ammonia-N surface loads and apparent nitrification rate. Combined data from the small and large pilot-scale NTFs are presented. Hydraulic surface loading was kept within a narrow range of 170–175 L m<sup>-2</sup> d<sup>-1</sup>, with variations in ammonia-N surface loading achieved by changing influent ammonia-N concentrations. Ammonia-N loading was increased in small increments from 40 to 966 (large pilot-scale NTF) and 138–2100 mg NH<sub>4</sub>-N m<sup>-2</sup> d<sup>-1</sup> (small pilot-scale NTF). The nitrifying performance of both the small- and large-pilot NTFs behaved similarly (*t*-test; *p*>0.05), with a similarly high percentage of nitrification (>90 %) achieved when ammonia-N surface loads were maintained within the range of 138 to 966 mg NH<sub>4</sub>-N m<sup>-2</sup> d<sup>-1</sup>. The first-order region of the curve demonstrates that the apparent nitrification rates increased with an increase in ammonia load. This observation was most likely the result of spare capacity at the lower filter depths, and/or improved mass transport caused by higher ammonia concentrations. Nitrification rates in the zero-order region remained relatively constant between 800 and 1000 mg NH<sub>4</sub>-N m<sup>-2</sup> d<sup>-1</sup>, which indicated that the maximum nitrification rate was achieved, and suggested that the NTF was likely to be substrate-saturated at ammonia-N loads exceeding 1000 mg NH<sub>4</sub>-N m<sup>-2</sup> d<sup>-1</sup>. Based on the data presented here, the impact of ammonia diffusion limitation on apparent nitrification performance appeared to be insignificant.

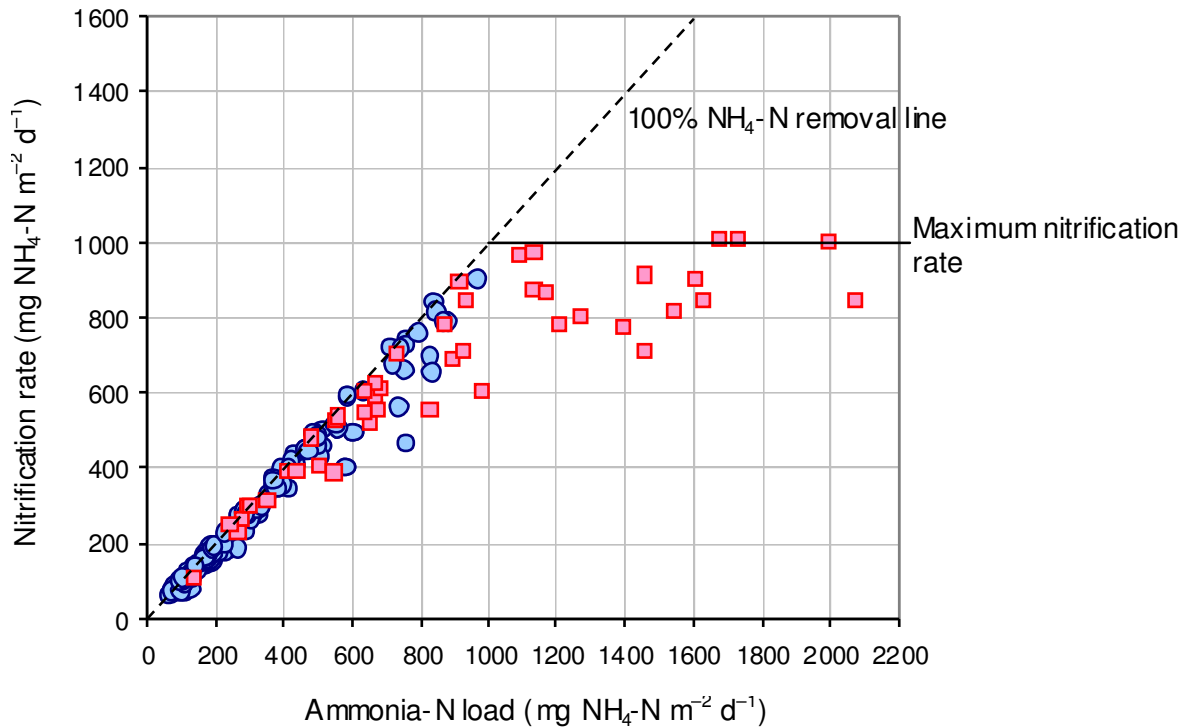
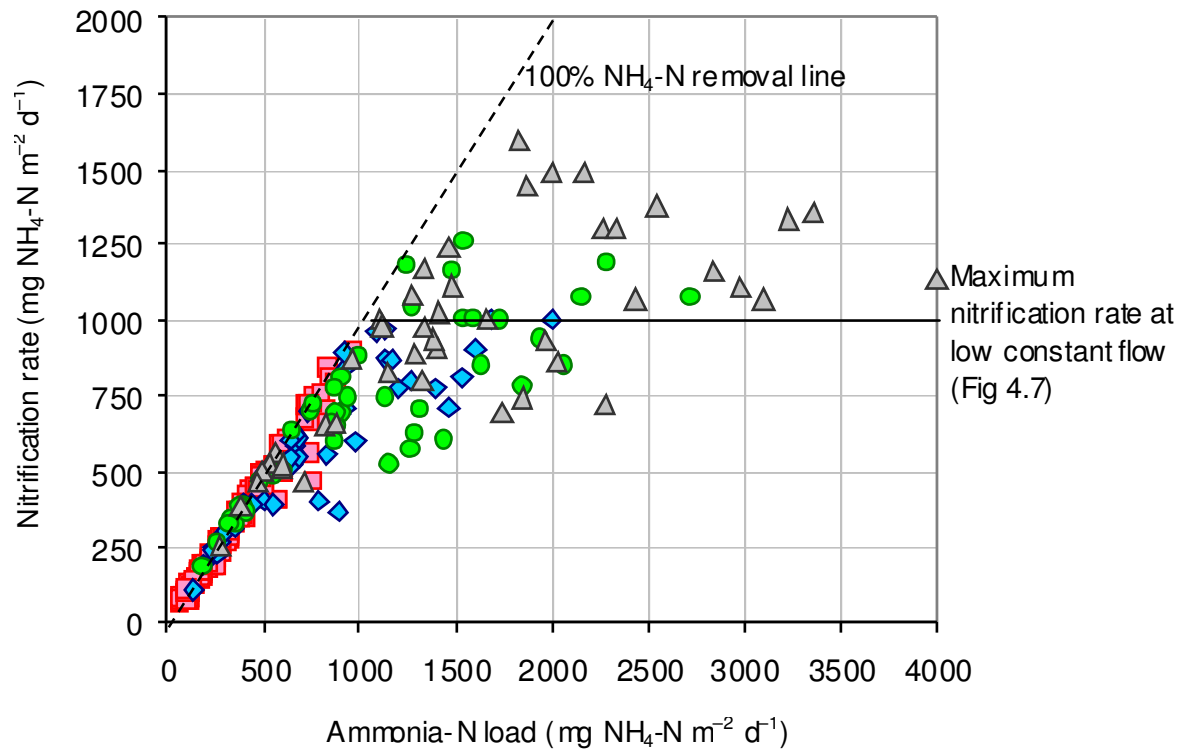


**Figure 4.7.** Relationship between ammonia-N surface load and apparent nitrification rate for: (●) large pilot-scale NTF; and (■) small pilot-scale NTF. Both NTFs were operated under constant hydraulic surface loads of 170–175 L m<sup>-2</sup> d<sup>-1</sup>. Ammonia surface loads were increased by increasing the influent ammonia-N concentration.

#### **4.3.6 Nitrification rate as a function of hydraulic surface load**

Figure 4.8 shows the relationship between ammonia-N surface load and apparent nitrification rate, for four NTFs operated under different surface hydraulic loads. Influent ammonia-N was maintained at  $4.1 \pm 2.2$  mg NH<sub>4</sub>-N/L, with variations in ammonia surface loading based on changes in the hydraulic flow regime. When ammonia-N surface loads were maintained below 966 mg NH<sub>4</sub>-N m<sup>-2</sup> d<sup>-1</sup>, the nitrification performance—as determined by percentage ammonia removal—was independent of hydraulic loading (ANOVA;  $p > 0.05$ ). From Figure 4.8, the superior performance of a NTF operating under higher flow can be seen. In comparison to Figure 4.7, which compared nitrification rate as a function of ammonia loads at a constant hydraulic load, it can be seen that the maximum apparent rate had increased beyond 1000 mg NH<sub>4</sub>-N m<sup>-2</sup> d<sup>-1</sup> to values as high as 1596 mg NH<sub>4</sub>-N m<sup>-2</sup> d<sup>-1</sup>. This data suggest that increasing ammonia-N surface loads by increasing the hydraulic load enhanced apparent nitrification rates. This apparent performance enhancement observed under increased flows may be attributable to a combination of both the promotion of enhanced exposure to higher ammonia concentrations down the NTF, thus producing uniformly higher rates throughout the bed depth, and also through an increased oxygen transfer resulting from operating under higher flows.



Hydraulic load (L m<sup>-2</sup> d<sup>-1</sup>)

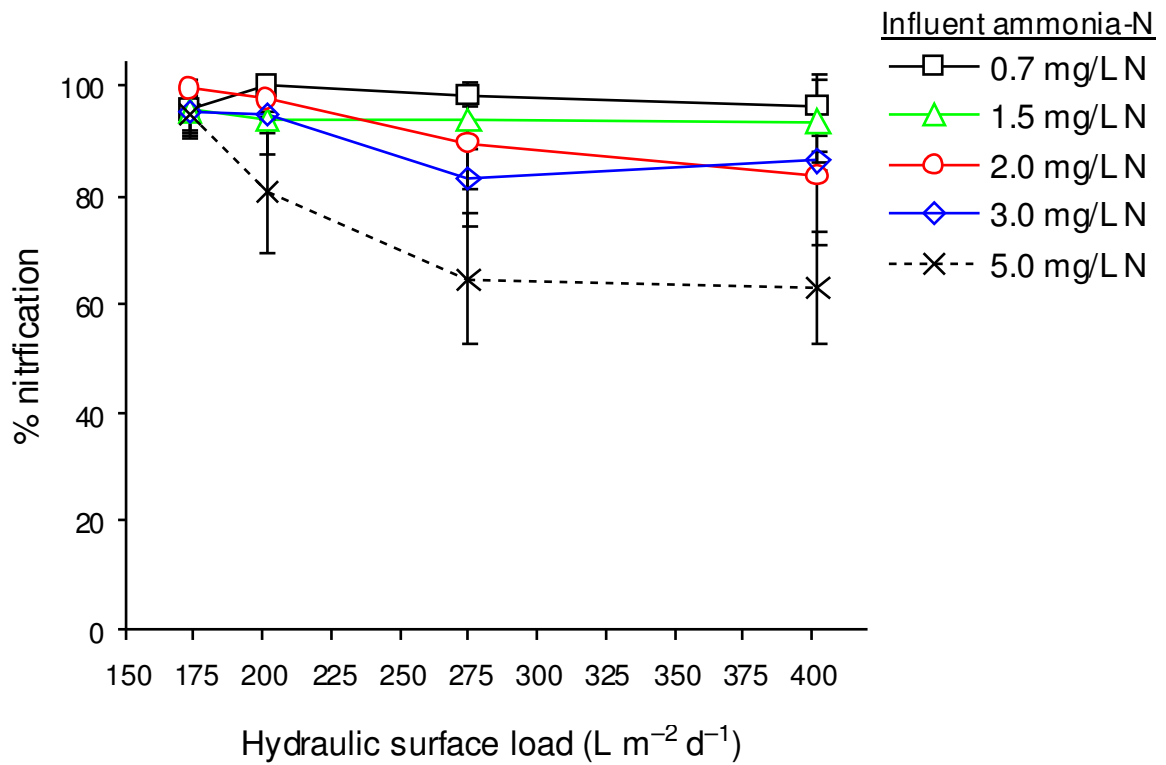
- 173.3 ■ Large-scale NTF
- 201.2 ◆ Small-scale NTF (1)
- 275.0 ● Small-scale NTF (2)
- 402.0 ▲ Small-scale NTF (3)

**Figure 4.8.** Relationship between ammonia-N surface load and apparent nitrification rate when operated under various hydraulic surface loads, at relatively constant ammonia-N concentration loads of  $4.1 \pm 2.2$  mg/L. Variations in ammonia surface loading was achieved by changing the hydraulic flow.

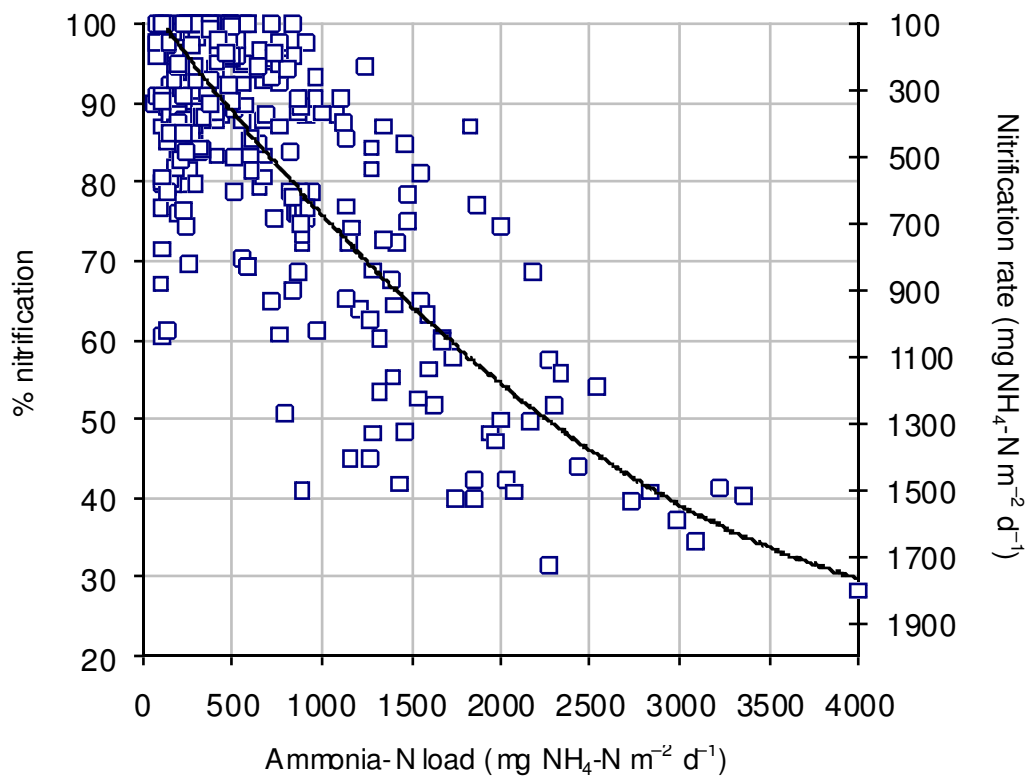
#### **4.3.7 Percentage nitrification as a function of hydraulic surface load and ammonia surface load**

Figure 4.9 compares percentage nitrification across all pilot-NTFs which operated under various hydraulic surface loads ranging between 173.3 and 402.4 L m<sup>-2</sup> d<sup>-1</sup>, and across a range of influent ammonia concentrations. From Figure 4.9, it can be seen that once hydraulic loading was increased above 173.3 L m<sup>-2</sup> d<sup>-1</sup>, a significant decrease in percentage nitrification was evident only once the influent ammonia-N concentration was increased well beyond 3.0 mg/L. When influent ammonia-N concentrations were maintained below 2.0 mg/L, no significant decline in percentage nitrification between each flow rate was identified (ANOVA;  $p > 0.05$ ). Furthermore, above hydraulic surface loads of 275 L m<sup>-2</sup> d<sup>-1</sup>, the effect of flow on peak percentage nitrification was negligible (ANOVA;  $p > 0.05$ ).

Figure 4.10 demonstrates that by increasing the ammonia surface load, either by increasing the flow or the influent ammonia-N concentration, the nitrification rate will increase, however percentage nitrification efficiency is reduced. From this data, it can be seen that nitrification in excess of 80 % can be achieved when ammonia surface loads are maintained below 1000 mg NH<sub>4</sub>-N m<sup>-2</sup> d<sup>-1</sup>. This data could be used to assist an NTF operator to find the best "trade-off" between mass and percentage ammonia-N removal.



**Figure 4.9.** Percentage nitrification as a function of hydraulic load for various ammonia concentration loads. Data points represent the mean of five to eight individual sampling events  $\pm 1$  SD.



**Figure 4.10.** Percentage nitrification and corresponding nitrification rate as a function of the ammonia surface load.

#### **4.3.8 *Distribution of biomass through the large pilot-scale NTF***

In Figure 4.11, profiles of TOC and ammonia-N concentrations measured throughout the depth of the NTF are plotted along side the respective mean biomass concentrations measured as total protein, total carbohydrates and wet weight of media. Total protein and carbohydrate data presented here, represents the mean of eight profiles obtained at steady-state conditions; when ammonia-N and TOC concentration loads were maintained between 1.0–5.0 and 5.9–9.3 mg/L respectively. The TOC data represents the mean of five profiles obtained during the study. The ammonia data is a representation of a typical ammonia profile observed down the NTF. From Figure 4.11, it can be seen that the strong gradient in ammonia-N and TOC concentrations through the NTF was reflected by the biomass densities, where biomass density was highest at the top of the NTF and decreased substantially with an increase in bed depth.

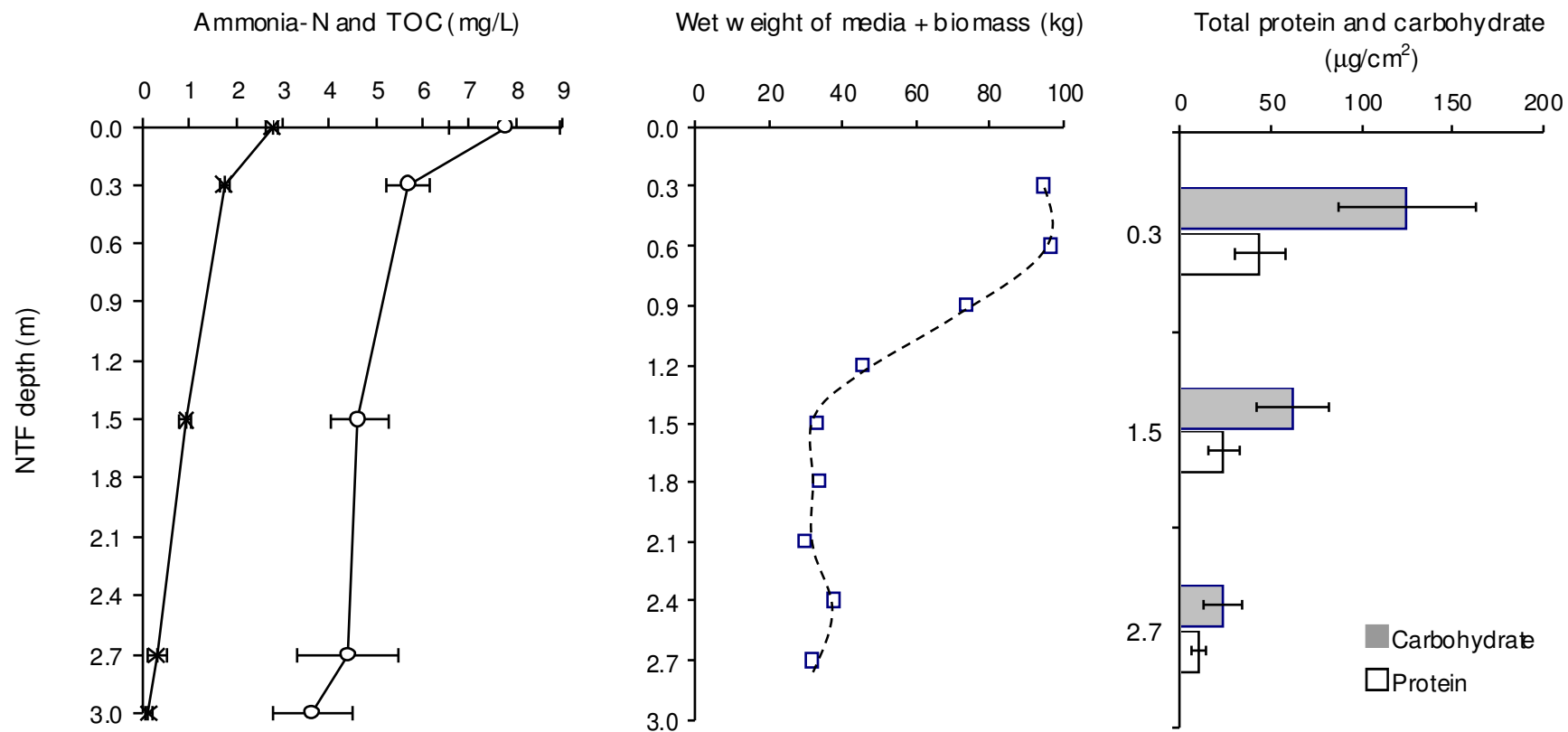


**Figure 4.11.** Distribution of biomass measured down the large pilot-scale NTF and corresponding ammonia-N (\*) and TOC (○) concentration profiles. (Parameter means shown  $\pm$  1 SD).

#### **4.3.9 Impact of seasonal variation on nitrification performance**

To determine the influence of seasonal changes in feed water quality parameters on nitrification, Spearman's correlation analysis was used to identify relationships between percentage nitrification with: pH; temperature; alkalinity; DO; and organic carbon concentrations. For the duration of the study, influent pH and alkalinity was stable, measuring 7.9 and 108 mg CaCO<sub>3</sub>/L respectively, and did not correlate with percentage nitrification ( $p > 0.05$ ; Table 4.2). Similarly, influent organic carbon, measured as sBOD<sub>5</sub> and TOC, were low, and did not correlate with nitrification performance ( $p > 0.05$ ; Table 4.2). An example of seasonal changes in temperature observed over 11 months of operation during the year 2004 is depicted in Figure 4.12. No relationship between percentage nitrification and influent temperature was identified, despite significant variations in temperature which ranged from 10.7 to 23.9°C ( $p > 0.05$ ; Table 4.2). Statistically, an inverse relationship between nitrification and DO concentration was observed, however, influent DO had remained very stable between 5 and 7.5 mg/L (Table 4.2).

When comparing influent and effluent values, it can be seen that some of these parameters underwent significant changes in response to filtration or nitrification (Table 4.2). DO was typically highest in the NTF's effluent, yielding concentrations commonly around 10 mg/L. Significant removal in organic carbon, measured as sBOD<sub>5</sub> and TOC, was also observed, resulting mean removals of 59 % and 16.5 % respectively. Total alkalinity and pH were consistently lower in the effluent than that measured in the influent, where the magnitude of difference proved to be a function of ammonia removal. Figure 4.13 shows a very good correlation between total alkalinity consumption, and ammonia-N removal. It was calculated that 7.4 mg/L of alkalinity (as CaCO<sub>3</sub>) was consumed for every 1 mg/L of ammonia-N oxidised, which was comparable to the theoretical value of 7.14 mg/L. For the ammonia concentration loads applied, total alkalinity was considered to be in excess, and therefore it was unlikely to have limited nitrification. Similarly, effluent pH values varied depending on the mass of ammonia-N removed. The oxidation of ammonia also resulted in a small decrease in effluent pH.

From Figure 4.14, it can be seen that pH decreased by a value of 0.18 for every 1 mg/L of ammonia-N oxidised.

**Table 4.2.** Summary of the physicochemical analysis of the large pilot-scale NTFs Influent and effluent.

		Temperature (°C)	pH	Total alkalinity (mg/L CaCO <sub>3</sub> )	DO (mg/L)	sBOD <sub>5</sub> (mg/L)	TOC (mg/L)	Turbidity (NTU)
<b>Influent</b>	Spearman correlation v % nitrification- $r_s$	0.02	-0.03	0.29	-0.71**	-0.23	0.01	0.23
	Number of observations ( $n$ )	137	54	39	27	26	25	55
-----								
	mean	17.13	7.97	108.91	6.44	2.09	7.3	7.90
	min	10.74	7.75	102.0	5.0	0.30	5.9	3.6
	max	23.92	8.43	116.0	7.50	5.30	15.2	173.70
	$n$	online	95	55	online	31	26	online
<b>Effluent</b>	mean	N/A	7.80	96.80	8.13	1.20	6.10	6.27
	min	N/A	7.19	76	6.0	0	2.39	1.8
	max	N/A	8.3	107	10.2	3.4	10.8	43.7
<b>Difference</b>	mean ( $\pm 1$ SD)	N/A	↓ 0.3 $\pm$ 0.2	↓ 13.2 $\pm$ 9.0	↑ 2.8 $\pm$ 3.2	↓ 1.1 $\pm$ 1.2	↓ 2.1 $\pm$ 2.0	↓ 1.5 $\pm$ 5.9
	Spearman correlation v NH <sub>4</sub> -N removal- $r_s$	N/A	0.73***	0.96***	N/A	0.20	0.36	N/A
	Number of observations ( $n$ )	N/A	64	66	N/A	23	26	N/A

\*\*Correlation is significant at  $p < 0.01$  level (2-tailed); \*\*\*Correlation is significant at  $p < 0.001$  level (2-tailed). Arrows refer to change relative to the influent: ↑ increase, ↓ decrease.

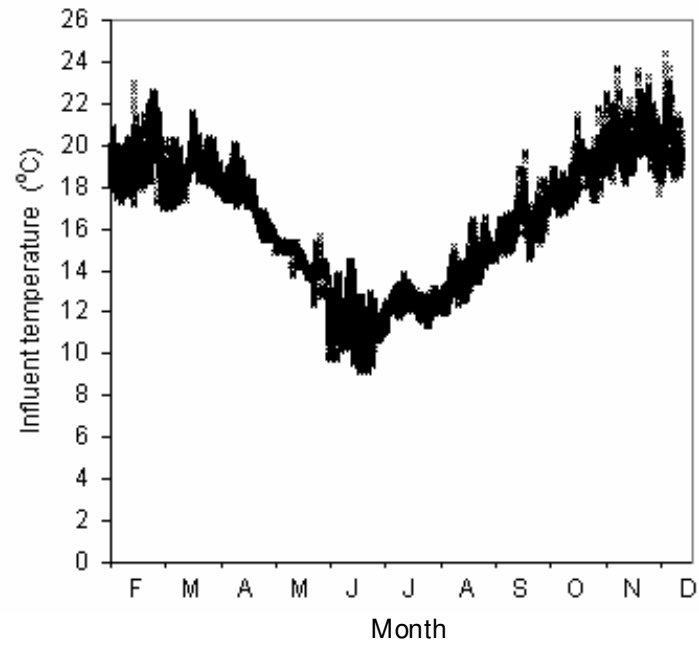


**Figure 4.12.** Seasonal variation of influent temperature during the year 2004.

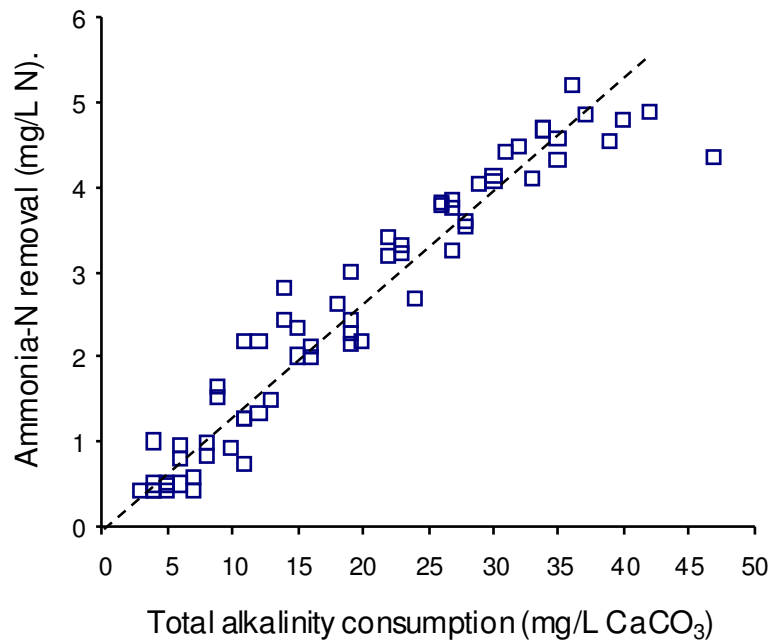


**Figure 4.13.** Relationship between ammonia-N removal and total alkalinity consumption. Dashed line represents theoretical total alkalinity (CaCO<sub>3</sub>) consumption.

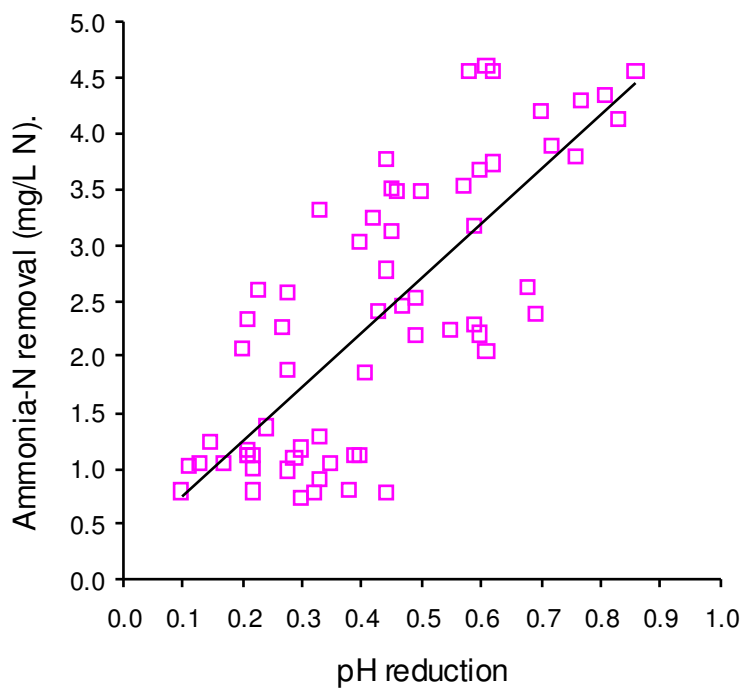


**Figure 4.14.** Relationship between ammonia-N removal and magnitude pH reduction.

#### **4.3.10 Impact of inert solids on NTF performance**

To investigate the impact of high SS on NTF performance, influent turbidity was increased above background concentrations which typically ranged between 2–17 NTU, to  $42 \pm 32$  NTU (equivalent to  $51 \pm 25$  mg SS/L) by dosing a slurry of clay into the inflow of the large pilot-scale NTF. As expected, turbidity correlated well with SS concentrations, where the NTU:SS (mg/L) ratio was approximately 1:1 ( $n = 36$ ); something which was similar to Buaran's raw water data (see Chapter 2, Section 2.3.5). Higher turbidity loads also accompanied an increase in TOC from background concentrations of 7.3 to 15.2 mg/L, however sBOD<sub>5</sub> concentrations remained low, measuring  $2.7 \pm 1.3$  mg/L. The nitrification rates were observed closely during an experimental period of 30 days when operating under high turbidity loads. Figure 4.15 compares apparent nitrification rates between periods of low and high turbidity, and demonstrates that high turbidity and SS had no adverse impact on nitrification. Statistical analysis also confirmed that there was no significant relationship between percentage nitrification and influent turbidity ( $r_s = 0.23$ ;  $p > 0.05$ ; Table 4.2). The impact of high turbidity and SS loads on nitrification behaviour within the NTF was also determined by comparing nitrification rates measured through the depth of the bed, which also confirmed that nitrification rates remained unaffected when operated under high SS or turbidity loads (Figure 4.16).

Influent and effluent turbidity data recorded at 10 minute intervals provided no evidence of biomass sloughing, instead effluent turbidity was typically 1.5 NTU below that of influent concentrations (Table 4.2). From the onset of high turbidity loads, the initial difference between influent and effluent turbidity had increased to 27 NTU, however this subsided back down to 1.9 NTU within 9 d of operation. *In situ* analysis of the biofilm samples using SEM, confirmed the incorporation of clay particles into the biofilm matrix (Plate 4.2.a and 4.2.b). It was possible that the clay particles provided an attractive support medium for bacteria (Plate 4.2.a), whilst other regions of the biofilm appeared to be completely covered by clay particles. Plate 4.2.c shows a dense layer of clay 'smothering' the biofilm with a diatom emerging through the clay crust.

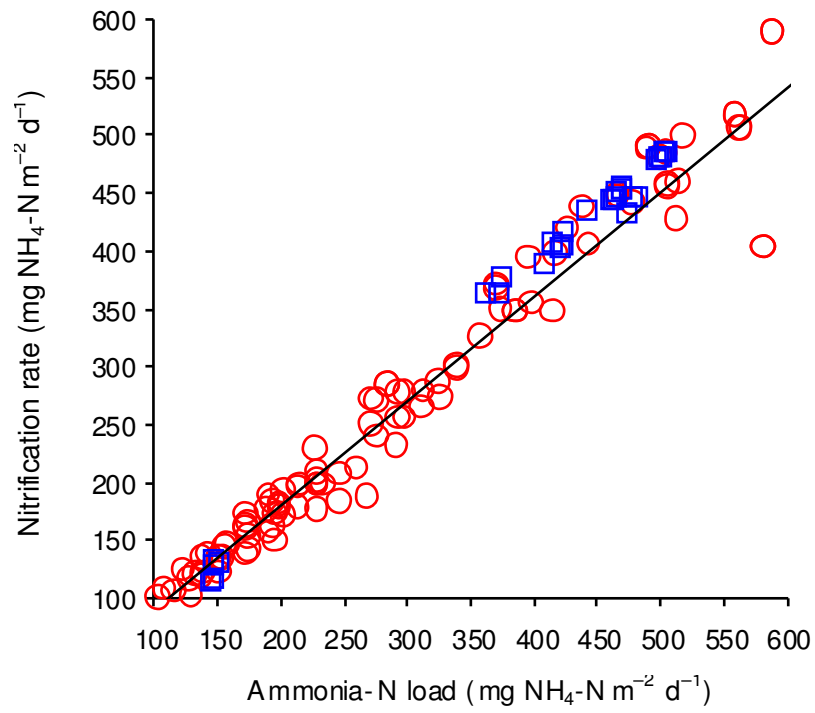


**Figure 4.15.** Impact of high inert solids on the apparent nitrification rate of the large pilot-scale NTF. Data points represent conditions of: (○) low influent turbidity of 3.6–17 NTU; and (□) high influent turbidity of 30–173 NTU.

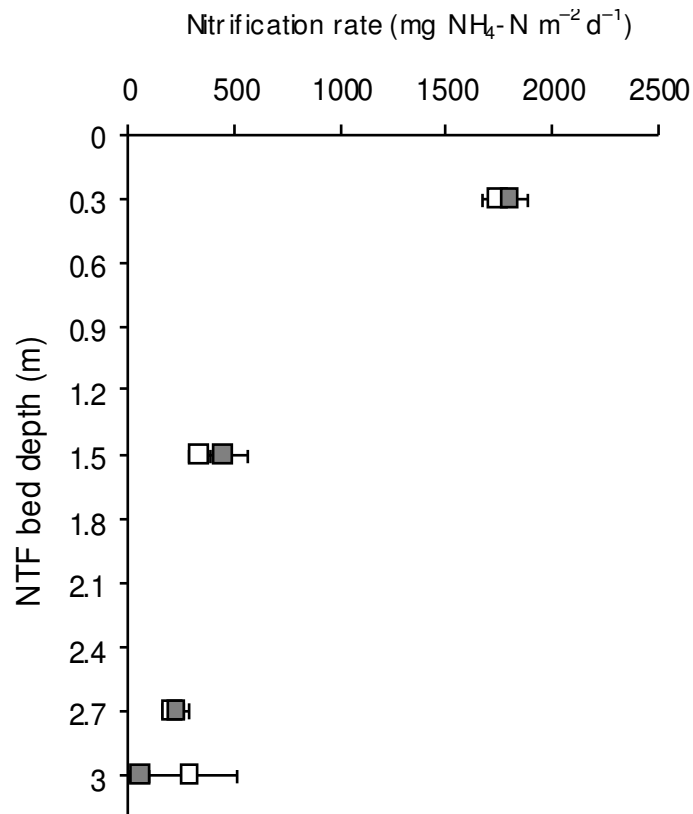


**Figure 4.16.** Impact of high inert solids on nitrification rates measured through the depth of the large pilot-scale NTF. Data points represent conditions of: (■) low influent turbidity of 3.6–17 NTU; and (□) high influent turbidity of 30–173 NTU. (Data points represent parameter means  $\pm$  1 SD).

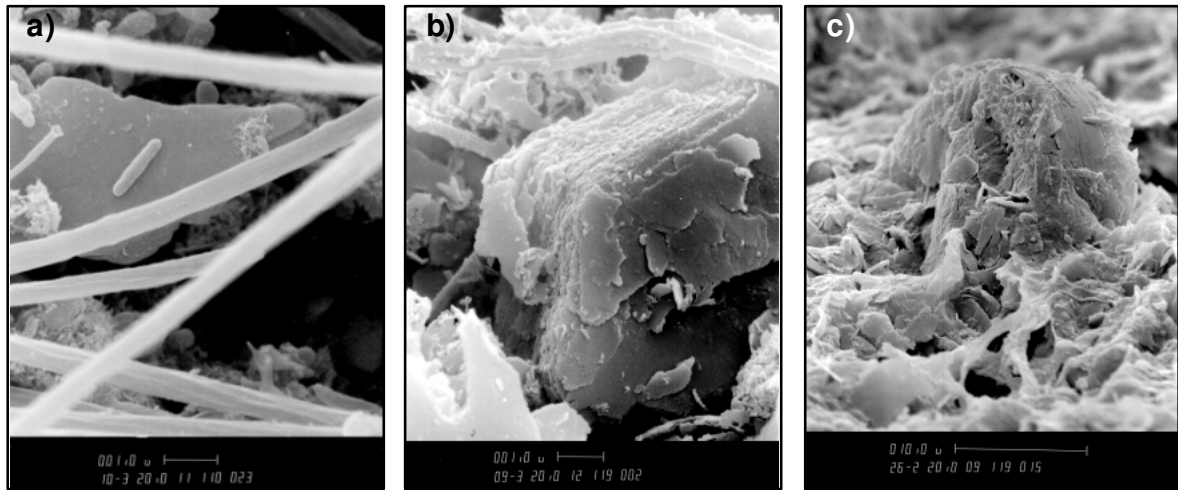


**Plate 4.2.** SEM depicting the *in situ* ultra structure of the NTF biofilm during high inert SS loads: (a) rod shaped bacterial cell attached to a clayparticle; (b) formation of “pack-of-cards” type clay agglomerate within the biofilm; and (c) outer clay crust and an emerging diatom.

#### **4.3.11 Hydraulic characterisation of the large pilot-scale NTF**

Tracer analysis for the large pilot-scale NTF was performed under three different operating conditions: (i) one week into start-up; (ii) on completion of start-up, when operated under low ammonia-N concentration loads of 1.0 mg/L; and (iii) at steady-state, after increasing the ammonia-N concentration load to 5.0 mg/L. Hydraulic flow was maintained at 8 m<sup>3</sup>/h (5.2 m/h). The RTD curve for each scenario is presented in Figure 4.17. Corresponding fluorescent micrographic representation of biomass abundance at the time of individual tracer experiments is also compared. It can be seen that the experimental RTD curves and HRTs obtained at one week and two months after start-up are very similar, with HRTs of 162 and 168 seconds respectively. However, as the media became occupied by more biomass, instigated by higher ammonia-N loads, a 26 % increase in HRT (228 seconds) was observed.

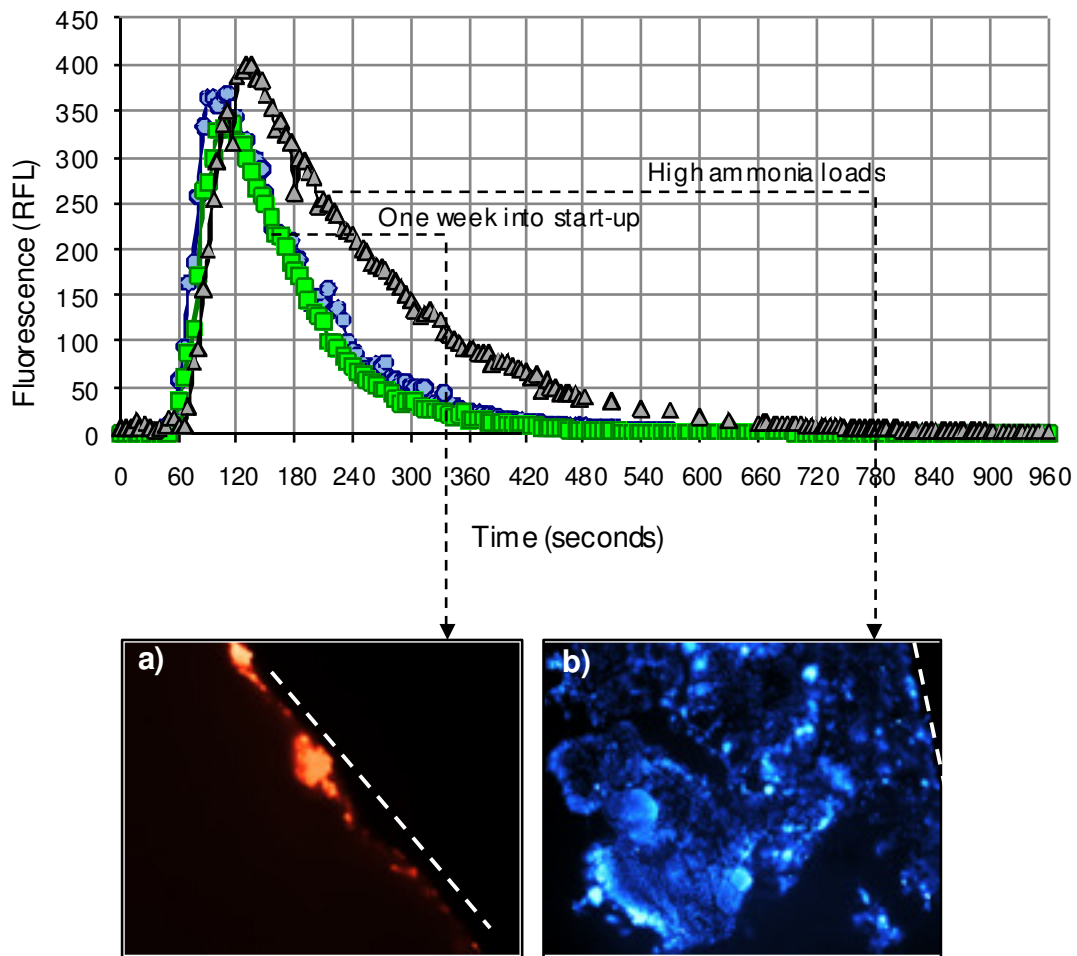


**Figure 4.17.** Residence time distribution curves resulting from a pulse injection of the tracer rhodamine WT, observed: (■) one week into start-up; (●) on completion of start-up; (▲) under steady-state conditions when operating under high ammonia loads; and corresponding fluorescent micrographic representations of biomass abundance: (a) biomass targeted with EUB338 labelled with Cy3 after FISH, one week into start-up; and (b) biomass stained with DAPI at steady-state conditions when operated under high ammonia loads. Dashed line represents filter media. (All images acquired at 400x magnification).

## 4.4 Discussion

This chapter presents the findings from a series of pilot experiments which investigated the application of NTFs for the removal of low concentrations of ammonia as an alternative to pre-chlorination.

Analysis of ammonia-N within Hope Valley raw water revealed only low background concentrations within the range 0 to 0.1 mg/L. Since nitrifiers may therefore be limited by the low availability of inorganic nitrogenous substrates, it was postulated that native nitrifying bacterial populations might be present in such low numbers, that there would be insufficient seed population to support initial biofilm development. However, pilot trials confirmed that a nitrifying biofilm could be established quickly, with the onset of nitrification observed within 14 d at 15.5–22.3°C once influent flows were supplemented with low concentrations of ammonia-N ( $1.1 \pm 0.3$  mg NH<sub>4</sub>-N/L). Fluorescence micrographs of biofilm sections stained with DAPI and also observed with SEM confirmed biofilm development, where a significant increase in biofilm thickness with time was clearly evident. Based on effluent inorganic nitrogen concentrations, there was a well recognised pattern of nitrification which occurred during biofilm maturity. The chronological order of ammonia, nitrite and nitrate profiles observed over a period of time can indicate the magnitude of AOB and NOB development. Characteristic consumption of ammonia-N was observed within 14 d, which coincided with production of nitrite and nitrate. The early production of nitrate, when coupled with an increase in nitrite, signified the early and equal development of NOB in association with AOB. The use of FISH for probing the microbial biofilm structure confirmed that both AOB and NOB development was rapid. Small colonies of AOB and NOB, equal in abundance, were clearly seen attached to the support media within 8 d of supplementing influent with low concentrations of ammonia. Effluent nitrite peaked within 18 d of operation, and gradually subsided to low concentrations two weeks later. The decrease in nitrite coupled with a further increase in effluent nitrate, signified the maturation of NOB populations. Complete nitrification was observed within two months of filter start-up, indicating that the nitrifying biofilm had fully matured. This was characterised by low nitrite-N (<0.02 mg/L) and high nitrate-N concentrations within the NTF effluent.

Although high ammonia conversion to nitrate was observed by day 40, profiles of inorganic nitrogen species within the depth of the NTF confirmed that complete steady-state nitrification performance throughout the entire NTF required an additional 15 to 25 d to be achieved. Results obtained from this pilot study confirmed that a mature nitrifying biofilm was established under ammonia-limiting conditions. It also showed that the biofilm was capable of achieving complete nitrification and suggests that there were sufficient nitrifying population present in Hope Valley water to seed the NTF without the addition of an external nitrifying inoculum. The nitrification start-up time was comparable to times required by wastewater BNR processes, which operate under higher ammonia concentrations. Boller *et al.* (1990) reported that a start-up time of 50 d was required for a pilot RBC treating wastewater in order to reach steady-state nitrification.

The basic principle which governs microbial reactions in attached-growth biofilm reactor, is the rate of substrate diffusion from the bulk liquid phase into the biofilm—a process which is governed by the magnitude of the concentration gradient (Harremoës 1982). Based on this phenomenon, the impact of low ammonia-N concentrations on NTF performance was investigated.

Once a mature nitrifying biofilm was established, the ability of the large pilot-scale NTF to remove ammonia for a range of low feed ammonia-N concentration was investigated under a steady influent hydraulic surface load of  $173 \text{ L m}^{-2} \text{ d}^{-1}$  (5.2 m/h). This was achieved by increasing influent ammonia-N concentrations incrementally from 0.5 to 5.0 mg/L. Since the hydraulic load applied to the NTF remained constant, variations in ammonia surface load ( $40\text{--}966 \text{ mg NH}_4\text{-N m}^{-2} \text{ d}^{-1}$ ) were achieved by varying the influent ammonia-N concentration. Both the influent ammonia-N concentrations and surface loads applied to the NTF were below the loading range for typical wastewater NTF applications. Within this range, results from this study showed that apparent nitrification rates increased linearly with an increased ammonia surface load, and complete nitrification was consistently observed (Figure 4.7). The first-order relationship between ammonia surface load and nitrification rates suggests that the NTF had additional or 'spare' nitrifying capacity. Nitrification rates appeared low, however this

data suggests that the low rates were merely an artifact of the low ammonia surface load, where rates were likely to be limited by the mass of the ammonia, and not by the rate of ammonia flux (i.e. diffusion) into the biofilm. The impact of ammonia diffusion limitations on the apparent NTF performance was therefore not as significant as first hypothesised; where nitrification in excess of 90 % was consistently achieved when operated under these markedly reduce ammonia concentrations and mass loads. It was possible that diffusion limitations may have been overcome by additional convective forces acting on the biofilm when immobilised on a fixed media.

A smaller pilot-scale NTF (Filter 1) was later employed to determine the maximum achievable nitrification rate, by increasing the influent ammonia-N concentration well beyond 5 mg/L. Similar to the large pilot-scale NTF, the hydraulic surface load was maintained at  $174 \text{ L m}^{-2} \text{ d}^{-1}$ , therefore higher ammonia surface loads were achieved by increasing influent ammonia-N concentration from 1 to 9.9 mg/L. The corresponding ammonia surface loads were 138–2100  $\text{mg NH}_4\text{-N m}^{-2} \text{ d}^{-1}$ . Available data suggest that these higher surface loads ( $>1000 \text{ mg NH}_4\text{-N m}^{-2} \text{ d}^{-1}$ ) represented typical design loading criteria for trickling filters used for wastewater applications (Metcalf and Eddy, 1993; Daigger *et al*, 1994 and Parker *et al*, 1997). Similarly to the large pilot NTF, results obtained from the small pilot NTF showed that apparent nitrification rates increased linearly with an increase in ammonia surface load. The zero-order nitrification rate (maximum rate) of  $1000 \text{ mg NH}_4\text{-N m}^{-2} \text{ d}^{-1}$  was achieved once the ammonia surface load was increased beyond  $1100 \text{ mg NH}_4\text{-N m}^{-2} \text{ d}^{-1}$  (Figure 4.7). Similar to the large pilot-scale NTF, when the ammonia surface load was maintained at below  $1000 \text{ mg NH}_4\text{-N m}^{-2} \text{ d}^{-1}$ , percentage nitrification in excess of 90 % was consistently observed. Furthermore, results showed that the apparent nitrification rates between the small-scale and large-scale pilot NTFs agreed well, where identical performance was achieved when operated under similar ammonia surface- and concentration loads. It is therefore reasonable to suggest that if the large pilot-scale NTF was able to operate under higher ammonia loads beyond  $1000 \text{ mg NH}_4\text{-N m}^{-2} \text{ d}^{-1}$ , then similar nitrification rates as seen with the smaller-scale NTF would be expected. However, it was also acknowledged that some variability in results obtained from the small pilot-scale NTF

may be attributed to short-circuiting of influent ammonia down the inside face of the NTF into the effluent, in which case higher nitrification rates could be expected from the large pilot-scale NTF.

When the NTF was operated under hydraulic surface loads of  $173 \text{ L m}^{-2} \text{ d}^{-1}$ , long-term monitoring of inorganic nitrogen species (ammonia-N, nitrite-N and nitrate-N) and nitrification rates through the depth of the large pilot-scale NTF showed that most of the nitrification activity was occurring within the top bed depth of 0.3 m and reduced significantly with increasing depth. Nitrite did not accumulate appreciably through the depth of the NTF, indicating that the NOB population was competent. Profiles of nitrate generation rates complemented well the ammonia removal rates (nitrification rate). The good mass-balance between ammonia-N removal and nitrate-N production waived any concerns that turbulent aeration and periods of high pH contributed to ammonia removal via ammonia volatilisation. Furthermore, nitrification rates and nitrate generation rates measured throughout both the old and newly reconstructed NTFs were very similar when operated under the same ammonia loads, indicating excellent reproducibility of nitrification performance between both NTFs.

Due to high rates of ammonia removal within the upper bed, depth profiles of ammonia revealed that the lower depths of the NTF were exposed to low ammonia-N concentrations, which limited nitrification potential within the lower regions of the NTF. Results from this study showed that ammonia limitation was responsible for low nitrification activity over a substantial portion of the NTF, and in comparison, Boller *et al.* (1994), Boller *et al.* (1997), Parker *et al.* (1997) and Biesterfeld *et al.* (2003) reported that such limitation had occurred at concentrations below 4 to 5 mg  $\text{NH}_4\text{-N/L}$  (similar to that reported in Figure 4.6). The maximum nitrification rate of  $\approx 2000 \text{ mg NH}_4\text{-N m}^{-2} \text{ d}^{-1}$  was reached at the top bed depth of 0.3 m when influent ammonia-N concentrations were maintained above 4.0 mg/L; conditions which represented non-ammonia-limited nitrification (Figure 4.6). A previous investigation by Boller *et al.* (1994) interpreted this plateau in nitrification rate or the zero-order region to be caused by oxygen limitations. In contrast, the linear increase in nitrification rate with an increase ammonia

concentrations (first-order region) seen at lower filter depths, confirmed that the limiting effects imposed on nitrification potential was as a direct consequence of low substrate ammonia concentrations. When ammonia loading was increased to improve non-ammonia-limited conditions throughout the entire NTF, a significant improvement in nitrification rates per unit of surface area through the entire NTF depth occurred, due to the higher concentrations of ammonia reaching the lower depths. Parker *et al.* (1989) also confirmed that deeper penetration of higher ammonia concentrations (> 5.0 mg/L) down a NTF produced both more uniform and higher nitrification rates at the lower filter bed depths. These findings are in agreement with previous investigations that attribute the increase in nitrification rates to a higher concentration gradient between the liquid and biofilm phase, which increases the mass flux of ammonia (Gullicks and Cleasby 1986). These findings also suggest that the lower bed depths had residual nitrification capacity, which could then accommodate the increase in ammonia load; evidenced by the increase in ammonia-N concentration loading from 0.5 to 5.0 mg/L producing no significant breakthrough of ammonia-N into the effluent. Having this additional reserve of nitrifying capacity is advantageous in maintaining consistent effluent ammonia-N concentrations under conditions of variable influent ammonia loading or during possible ammonia spike events, something which can also aid in preventing disinfection problems from occurring when chlorine is used (Parker *et al.* 1989). Current research shows that pre-treatment using a NTF offers a process which can “peak-lop” ammonia concentration, which in turn will decrease the ammonia-related chlorine demand and improve overall control of the disinfection process.

When nitrification activity was normalised to the mass of attached biomass, a clear decrease in nitrification activity per weight of biomass with depth was also observed. Consequently, the nitrifying community at the lower depths of the NTF appeared to exhibit a lower rate of activity than nitrifiers which occupied the top of the NTF, which was most likely due to the large difference in ammonia concentrations between the depths. These findings support the hypothesis that nitrification at the lower depths of the NTF was first-order-limited; where low ammonia-N concentrations presented mass transfer limitations. In contrast, Persson *et al.* (2002) found no significant difference in

nitrification activity throughout the depths of a NTF treating municipal wastewater, when nitrification activity was normalised per unit dry weight of biofilm. This observation was explained by possible diffusion limitations encountered in the upper bed depths. The discrepancy between results could also be attributed to the fact that the lower half of the pilot NTF operated in this current study were exposed to lower ammonia concentrations (0.2–2.0 mg/L) than that experienced by most conventional wastewater NTFs.

The strong gradient in nitrification activity observed down the NTF had also been reported to some extent in studies by Duddles and Richardson (1973), Boller *et al.* (1994) and Biesterfeld *et al.* (2003). Andersson *et al.* (1994) and Boller *et al.* (1994) found that a homogeneous distribution in nitrification activity along a NTF could be achieved by operating two NTFs in alternating series filtration mode, which involved alternating flow directions at one week intervals. Furthermore, predation of the biofilm by filter flies, worms and snails has been reported to decrease nitrification rates in the lower depths of NTFs (Gujer 1984; Wanner and Gujer 1985; Parker *et al.* 1989; Biesterfeld *et al.* 2003), however similar to Biesterfeld *et al.* (2003), *in situ* analysis of the biofilm ultra structure did not support predation as an explanation for the decline in nitrification rates throughout the lower depths. Similar to the findings of Biesterfeld *et al.* (2003), only a few stalked ciliates were observed for the duration of this study (See Chapter 1, Plate 1.1). In order to overcome non-homogeneous nitrification activity through the NTF bed, this study investigated increasing the hydraulic bading as another alternative to utilising the remainder of the NTF volume in an attempt to increase overall nitrification rates.

Experiments conducted on the small pilot-scale NTFs showed that an increase in hydraulic surface loading increased apparent nitrification rates. When the NTF operated under steady hydraulic surface flow of  $173 \text{ L m}^{-2} \text{ d}^{-1}$ , and variable ammonia-N load, the maximum nitrification rate recorded was  $1000 \text{ mg NH}_4\text{-N m}^{-2} \text{ d}^{-1}$ . The Increase in hydraulic surface load from 173 to 201, 275 and  $402 \text{ L m}^{-2} \text{ d}^{-1}$  enhanced the nitrification rate well beyond 1000, to rates as high as  $1600 \text{ mg NH}_4\text{-N m}^{-2} \text{ d}^{-1}$ , however percentage nitrification was reduced, whereby doubling the hydraulic surface load decreased mean

percentage nitrification by 22 % of the maximum. This decline in percentage nitrification was most apparent once influent ammonia-N concentration loads were increased beyond 3.0 mg/L, or surface load of 1000 mg NH<sub>4</sub>-N m<sup>-2</sup> d<sup>-1</sup>. At concentrations below 2.0 mg NH<sub>4</sub>-N/L, the effect of hydraulic loading on peak percentage nitrification was minimal. Since Buaran WTP raw feed ammonia-N concentrations were typically below 2.5 mg/L, results suggest that near complete nitrification can be expected at high hydraulic surface loads of 402 L m<sup>-2</sup> d<sup>-1</sup>.

Although the pilot-scale NTFs were operated under low ammonia concentration, some 10- to 50-fold lower than wastewater, results suggest when operated under mass surface loads equivalent to the loading criteria for wastewater NTF applications (i.e. by increasing hydraulic load), comparable rate removals can be expected; where the maximum nitrification rate obtained in this study was comparable to rates observed from NTFs treating wastewater by Andersson *et al.* (1994), Boller *et al.* (1994), Boller *et al.* (1997), Parker *et al.* (1997) and Persson *et al.* (2002). In comparison to these studies, and based on apparent nitrification rates, the impact of ammonia diffusion limitations on overall filter performance was insignificant. Similar to wastewater applications, these data suggest that mass loading based on media surface area is the most important NTF design and operational parameter in relation to treatment efficiency.

The increase in nitrification rate (35 %) observed at higher flows may be attributed to higher ammonia concentrations reaching the lower depths of the NTF. It was expected that HRT of the filtrate would differ considerably when varying the hydraulic flow rate, and therefore would expect to have had strong influence on the contact time in which the filtrate was exposed to the biofilm. In accordance with Tekerlekopoulou and Vayenas (2007), it was probable that the increase in flow reduced the retention time, which may have caused a better exploration of the entire filter depth, by exposing a greater surface area of support media to higher ammonia concentrations and hence a higher concentration gradient. During high flows, more of the support media may have been utilised, which caused the noticeable increase in nitrification capacity, however tracer experiments used to ascertain the HRT, and profiling of nitrification behaviour

throughout the small pilot-scale NTFs in response to varying flow rates, were not conducted to confirm this hypothesis.

The increase in nitrification rates in response to higher flow rates are in agreement with research conducted by Parker *et al.* (1989), Andersson *et al.* (1994), Boller *et al.* (1994) and Parker *et al.* (1997). In addition to improving greater exploration of the NTF's bed, based on the wider literature, it was acknowledged that the increase in hydraulic surface load may have assisted nitrification in other ways. Andersson *et al.* (1994) attributed better nitrification rates during higher flow rates to enhanced aeration, which facilitated better oxygen transfer. In addition, high flow rates may have induced greater biomass sloughing, resulting in a thinner biofilm which can then maximise oxygen transfer to the target nitrifying population, which is generally located deep within the biofilm. Similar observations have been reported by Boller *et al.* (1997) when regularly backwashing biofilters to maintain a thin biofilm in order to improve oxygen transfer and nitrification. It should also be acknowledged that varying the flow rate past a biofilm can also influence the mass transport of solutes into a biofilm, whereby an increase in flow velocity between the biofilm and bulk liquid phase can enhance convection and hydrodynamic dispersion of solutes. In turn, this can improve then the rate of microbial transformations (Wuertz *et al.* 2003).

Results showed that the gradient in nitrification activity per surface area along the NTF was pronounced, and also reflected biomass concentrations down the filter bed; something which was confirmed by quantifying the attached biomass measured as total protein and total carbohydrate. Weighing of the support media established similar observations. Ammonia depletion at the lower filter bed depths was the probable cause of the pronounced gradient in biomass concentration, which was confirmed by profiling nitrification behaviour down the NTF. Results confirmed that nitrification activity was highest at the top of the filter, which then left only small concentrations of ammonia-N to sustain a smaller quantity of nitrifying biomass in the lower depths of the NTF. A distinct gradient in biomass concentration along NTFs and RBCs was also observed in studies by Boller *et al.* (1990), Boller *et al.* (1994), Persson *et al.* (2002) and Lydmark *et al.*

(2006), which for most cases was also the result of nutrient depletion at the lower or later sections. Employing the technique of FISH, Persson *et al.* (2002) also showed that AOB numbers correlated with substrate concentration profiles down a NTF, where AOB were most abundant at the top of a NTF where considerable ammonia oxidation was taking place, after which they reduced significantly with increasing depth. Persson *et al.* (2002) also confirmed that times of high ammonium concentrations throughout an entire NTF bed produced a more evenly distributed biofilm through the NTF. For the current study, it was hypothesised that increasing the flow rate—in an attempt to provide both a homogenous distribution of ammonia substrate concentrations and removal rate—may have also encouraged a more even coverage of biomass throughout the entire depth of the NTF; something which may in turn be responsible for the improved nitrification capacity observed at higher flow rates. Profiling the distribution of biomass density throughout the NTF when operating under different flow rates, would be required to confirm this hypothesis.

Influent organic carbon, measured as TOC and sBOD<sub>5</sub>, was typically low, therefore competition by heterotrophs for oxygen within the NTF was considered to be negligible. Regardless of the native sBOD<sub>5</sub> and TOC concentration in the raw feed water, no significant relationship between organic load and percentage nitrification was identified. In addition to high ammonia removal, results from this pilot study confirmed significant TOC and sBOD<sub>5</sub> removal within the range of 0–68%. For the low carbon and ammonia concentration loads exercised in this study, results suggest that DO was sufficient to sustain simultaneous nitrogen and carbon oxidation. It was anticipated that higher organic loads would be required in order to exert a tangible negative impact on nitrification. Where ammonia-N limitations have been shown to decrease nitrifying activity in the lower depths of the NTF, high organic loads are expected to suppress nitrification activity at the top due to heterotrophic competition for oxygen; something which has been documented by Wanner and Gujer (1985), Parker and Richards (1986) and Daigger *et al.* (1994). According to the nitrification profiles and nitrification rate obtained from the current study, results demonstrated a potential for additional nitrifying capacity at the lower bed depths of the NTF, which may guard against high pulses of

ammonia when operated under higher organic loads. The impact of increased organic carbon loads on nitrification performance and bed depth nitrification profile is discussed further in Chapter 5.

Nitrification performance of BNR processes can be influenced by many environmental factors including temperature (Parker *et al.* 1989; Metcalf and Eddy 2003), pH (Painter and Loveless 1983; Ishikawa *et al.* 2003), alkalinity (Persson *et al.* 2002), and DO (Boller *et al.* 1990; Boller *et al.* 1997; Rusten *et al.* 2000). These factors were closely monitored because they are considered integral to the stability of NTF performance. Pilot results confirmed that variations in influent pH, temperature, alkalinity and DO had no detrimental impact on nitrification stability. Clearly the NTF had some spare capacity to accommodate for small seasonal and stochastic changes in these parameters.

In contrast to the literature, data obtained from the current pilot trials indicate little correlation of nitrification efficiency with influent temperature, despite significant seasonal variation, which ranged from 10.7 to 23.9°C. These findings are consistent with those of Daigger *et al.* (1994) who reported similar findings for wastewater NTFs. For a NTF operating under low ammonia-N concentrations, results from the current study suggest that there was some additional spare nitrification capacity within the NTF, thereby enabling it to maintain a high level of nitrification efficiency during the winter months.

Results showed that DO concentrations were sufficient to allow for maintenance of complete nitrification, even during highest ammonia loads. The ability of the filter to maintain saturated effluent oxygen concentrations during high ammonia loads highlighted the efficient passive aeration of infiltrating water, which resulted in significant oxygenation of the inflowing water during the filtration process. Due to the high void volume and uniform configuration of the media, results suggest that excellent oxygen transfer from the atmosphere into the bulk liquid occurred, which consistently yielded effluent DO concentrations above influent concentrations. For the range of conditions

the NTF operated under during the present study, it was concluded that natural draft provided sufficient aeration without the need for forced ventilation.

This study correlated alkalinity consumption with ammonia removal. It was calculated that 7.4 mg/L of total alkalinity (as  $\text{CaCO}_3$ ) was consumed for every 1 mg/L of ammonia-N oxidised. This was consistent with wider literature who reported that 7 to 8 mg/L of alkalinity were consumed for every 1 mg/L of ammonia-N oxidised to nitrate-N, and was close to the theoretical value of 7.14 mg of  $\text{CaCO}_3$ /L (Liu and Liptak 1997). For the range of ammonia loads assessed during the current research, regular monitoring showed that influent alkalinity consistently exceeded nitrification-rate-limiting concentrations, therefore was considered to have had no negative impact on nitrification performance. Similarly, for the narrow influent pH range of 7.7–8.4 observed during this study, no significant relationship with nitrification was established. In order to observe some degree of impact, the literature shows that pH values must be well below 6.5 or exceed 8.5 to influence nitrification (Painter and Loveless 1983; Ishikawa *et al.* 2003). Similar to alkalinity, ammonia removal also correlated well with a decline in pH due to the production of  $\text{H}^+$  ions during the oxidation of ammonia (Heard *et al.* 2002), where pH had decreased by approximately 0.18 units for every 1 mg/L ammonia-N oxidised. The reduction in total alkalinity and pH provided evidence of normal nitrification function inside the NTF. Furthermore, these results suggest that measuring the decline in alkalinity and pH may be used as a tool to accurately predict nitrification performance. In addition, earlier work conducted by Portolesi (2004) who investigated the impact of the large pilot-scale NTF on the downstream coagulation and clarification process using flocculation jar tests, found that the decrease in effluent pH had enhanced coagulation when using aluminium sulphate. In comparison to the NTF's clarified influent, Portolesi (2004) found that the clarified effluent had superior water quality characteristics as determined by turbidity, colour and natural organic matter.

In addition to ammonia and organic carbon, the raw water at Buaran WTP was typically high in turbidity and SS, especially during rainstorms, due to run off into a network of rivers and canals that feed the water treatment plant. For this reason the influence of

high inert solids loading was investigated. Background turbidity of Hope Valley reservoir typically ranged between  $\approx 2$  to 17 NTU, therefore a slurry of pottery clay was dosed to increase the turbidity of the influent to a mean value of 42 NTU (51 mg SS/L). Under these conditions, results confirmed that high turbidity and SS loads had no impact on nitrification performance, where percentage nitrification remained in excess of 95 %.

During times of operating under additional SS loads, steady-state SS removal within the filter ranged between 0 and 8 mg/L (1.9 NTU), indicating that only a small fraction of solids was retained within the filter matrix. Results obtained from SEM and turbidity data confirmed that clay particles did not have scouring effects on the biofilm, instead some clay became incorporated into the biofilm matrix; something which can then have both beneficial or negative effects on nitrification (Wuertz *et al.* 2003). It is possible that clay particles increase the specific surface area and provide attractive attachment sites and microhabitats for bacteria, whereby positively charged clay particles have been reported to promote the attachment of negatively charged bacteria (Wuertz *et al.* 2003). Other nitrification enhancing mechanisms of clay have been associated with the nutritional effects caused by kaolin particles, because of the release of ions by the clay (Perez-Rodriguez *et al.* 1992; Wuertz *et al.* 2003). It has been documented that clays have the ability to absorb cations (for example  $\text{NH}_4^+$ ) and exchange them to the surrounding medium during times of ammonia deficiency (Perez-Rodriguez *et al.* 1992). For example,  $\text{H}^+$  produced during nitrification can be exchanged with cations retained by the clay (Wuertz *et al.* 2003). Furthermore, clay may also have a negative impact on biofilms. Magdaliniuk *et al.* (1995) found that small clay particles covered the cell surface, hindering the exchange of substrates and metabolites. The use of SEM also confirmed that some areas of the biofilm were completely smothered by a clay crust. The extent of SS impact on nitrification capacity of the NTF needs further investigation, however results from this study confirmed that influent SS within the order of  $51 \pm 25$  mg/L ( $42 \pm 32$  NTU) had neither a negative nor beneficial impact on nitrification performance. In contrast, research by Boller *et al.* (1990), Andersson *et al.* (1994) and Rusten *et al.* (2000) has shown that high SS can suppresses nitrification. Anderson *et al.* (1994) reported a decrease in nitrification rate from  $2.6$  to  $1.8 \text{ g N m}^{-2} \text{ d}^{-1}$ , when

influent SS exceeded 15 mg/L. The decline in nitrification capacity observed by Anderson *et al.* (1994) may have been attributed to particulate organic matter constitutes of the solids, which promoted heterotrophic competition for oxygen—as reported in studies by Parker *et al.* (1995), Rusten *et al.* (2000) and Biesterfeld *et al.* (2003). For the current study, the addition of SS also accompanied higher influent TOC concentrations of 15.2 mg/L, which was approximately 8 mg/L above background native concentrations. Despite the significant increase in TOC, influent sBOD<sub>5</sub> concentration remained low, at  $2.7 \pm 1.3$  mg/L, suggesting that the organic constituent of the SS was recalcitrant and was therefore likely to have had no impact on nitrification through competitive heterotrophic interactions. Similar observations were identified at Buaran WTP, where high SS and organic matter concentrations did not coincide with high BOD<sub>5</sub> concentrations. Unfortunately, the impact of higher SS or turbidity applications, which may have arguably been more representative of Buaran's peak loads, were not investigated here due to difficulties associated with reliably dosing large quantities of the clay slurry. However, results suggest that for influent SS concentrations within the order of  $51 \pm 25$  mg/L, pre-treatment for SS removal prior to biological filtration would not be required. It should also be noted that a strategy report prepared by Holmes (2001) recommended that a peak lopping SS process and improved screens should be considered upstream of the proposed NTFs.

Investigations by Parker *et al.* (1989) and Lutz *et al.* (1990) have shown NTFs to release higher SS into the nitrified effluent than in the original influent, due to biomass sloughing. In contrast, for the entire duration of the current study, effluent NTU was consistently lower than that measured in the influent by an average of 1.5 NTU. In agreement with Parker *et al.* (1997), online turbidity data obtained every 10 minutes indicated that sloughing associated with conventional trickling filters was not observed; something which may eliminate the need for downstream clarifiers or humus tanks. The absence of sloughing may be attributed to the low substrate loads and subsequent low sludge yield of nitrifying bacteria. Sloughing has been more commonly associated with filters operating under higher nutrient loads (Characklis and Marshall 1990).

Tracer experiments were performed to determine and compare the hydraulic characteristics of the NTF during early and late stages of start-up, and at steady-state conditions once the ammonia-N concentration loading was increased beyond 1 mg/L to a maximum of 5 mg/L. Results from the tracer test conducted after two months of commissioning on a mature nitrifying biofilm exposed to low ammonia concentrations, showed no alteration to the NTF's initial hydraulic characteristics or HRT. The HRT was a rapid 2.8 minutes, and in such time, complete nitrification was consistently achieved. A noticeable increase in HRT from 2.8 to 3.8 minutes was noticed only once influent ammonia-N concentrations were increased from 1 to 5 mg/L. The increase in HRT coincided with a significant increase in biomass abundance, which was a function of higher nutrient loads at the time. Similar observations have also been reported by Tandukar *et al.* (2006). The impact of biomass on HRT and RTD of biological filters has been widely documented, and will be discussed in greater detail in Chapter 6.

# 5 INFLUENCE OF ORGANIC CARBON LOADING ON NITRIFYING TRICKLING FILTER PERFORMANCE

## 5.1 Introduction

Mathematical models have become increasingly important to improve operational strategies and design of NTFs, which have been largely derived from research at the pilot- or full-scale level for wastewater treatment. Empirical models developed by Pearce (1999) and Pearce and Williams (1999), have improved the design and operation of plastic-packed and mineral media trickling filters for nitrification, and have been shown to give accurate predictions of effluent quality. The models were derived from several pilot- and full-scale stone- and plastic-packed trickling filters treating municipal wastewater. Both models propose that the effluent ammonia-N concentration increases with an increase in ammonia and BOD<sub>5</sub> loading. Many studies on wastewater BNR processes, including activated sludge and trickling filters, have attributed high C:N ratios with the suppression of nitrification. These biofilm systems showed that high organic carbon concentrations promoted faster growing heterotrophs which can out-compete the slow growing nitrifiers for aerobic space and oxygen, resulting in suppressed nitrification (Zhang *et al.* 1994; Okabe *et al.* 1996).

Whilst trickling filter design and performance for wastewater treatment has been widely reported, little is known about their application for potable water treatment; where NTFs are expected to operate under lower organic and nutrient concentrations, some 10- to 50-fold lower than that of typical wastewater applications. The total inorganic nitrogen concentrations of Buaran raw water fluctuated daily from 0.8 to 6.0 mg/L (during the period from 2002–2005). Weekly BOD<sub>5</sub> concentrations varied between 7 to 10 mg/L, with occasional short lived peaks up to 15 mg/L. The sBOD<sub>5</sub> represented 62 to 85 % of total BOD<sub>5</sub>, suggesting a large fraction was immediately available to heterotrophic

microorganisms. Successful maintenance of a stable ammonia removal process may be influenced by heterotrophic domination, such that it is an important factor to consider when designing a trickling filter.

In order to maintain complete nitrification, biological processes responsible for carbon removal and nitrification are usually conducted in separate unit operations. For wastewater BNR processes, high nitrification rates usually occur when most of the degradable organic carbon has been removed prior to nitrification. Harremoes (1982) concluded that  $sBOD_5$  needed to be less than 20 mg/L to initiate nitrification. For a NTF operated under low carbon and nitrogen loads, one possible outcome might be the active selection of both heterotrophic and nitrifying microbial populations within specific regions of the NTF as a consequence of relative substrate availabilities. The effect would be to minimise the competition between heterotrophs and nitrifiers for DO via the vertical separation of heterotrophic populations from nitrifying populations. For NTFs, separating the filter bed into vertical zones of carbon removal (predominantly heterotrophic) and nitrification (predominantly autotrophic) may be a function of bed depth and relative substrate availability, since ammonia and organic carbon concentrations are expected to change with depth. As water percolates through a biological filter, each depth-wise increment of the bed is exposed to a gradient of changing conditions where different microorganisms can develop (Wik 2000). For this study, it was hypothesised that during periods of increased organic carbon loads, heterotrophic bacteria are likely to dominate the top filter depths where the greatest concentration of organic substrate is introduced. The lower depths of the filter would therefore be expected to receive filtrate lower in organic content than above, and would favour the growth of nitrifiers (Metcalf and Eddy 2003).

Findings from Chapter 4 showed that under low organic loads, highest ammonia removal occurred at the filter top and reduced with depth, suggesting the NTF had spare nitrifying capacity at the lower depths. During times of higher organic loads, it was hypothesised that the lower filter depths may accommodate higher pulses in ammonia concentrations brought on by an increase in heterotrophic activity at the top, activity

which has the capacity to suppress nitrification. The filter depth at which most of the ammonia is removed will depend on influent carbon concentrations, making bed depth and surface area crucial design parameters for NTFs. Stratification of heterotrophs and autotrophs down NTFs and along RBCs treating wastewater has been reported by Wanner and Gujer (1985), Parker and Richards (1986), Daigger *et al.* (1994), Gupta and Gupta (1999) and Wik (2000). However, the influence of increased organic carbon loads on the nitrification depth profile of a NTF treating potable water is not well understood, and hence was investigated during this study. Furthermore, the biodegradability of organic carbon varies widely among aquatic systems, and, in accordance with Strauss and Lamberti (2002), would be expected to have a variable influence on nitrification. Therefore, additional research was conducted in order to investigate the effects of carbon availability on the nitrification capacity of a NTF.

During the present study, the pilot-plant operated under various C:N ratios (defined as  $sBOD_5$ /ammonia-N) to simulate the raw water quality of Buaran WTP. The first aim was to observe the influence of increased organic carbon loads on the filter's nitrifying capacity, and the subsequent impact on nitrification throughout the depths of the filter. This was achieved by dosing an external carbon source either intermittently or continuously, to mimic variations in organic carbon delivery identified at Buaran WTP. The second aim was to evaluate the nitrification model of Pearce (1999), originally developed for plastic-packed wastewater NTFs, when used for potable water treatment. Model outputs were compared with observed NTF performance values obtained during operation under variable nitrogen and organic carbon loads within, and below the range from which the model was derived. The third aim was to investigate the influence of carbon biodegradability on nitrification performance. This was achieved by comparing a surrogate carbon source (sucrose) with a less readily biodegradable organic carbon source (soluble organic fertiliser) on NTF nitrifying capacity.

## 5.2 Methods

### 5.2.1 *Experimental design*

Pilot plant NTFs were operated under conditions that simulated the raw water quality of Buaran WTP, namely variations in C:N ratio and sBOD<sub>5</sub> concentrations. Ammonium sulphate and organic carbon was dosed into the NTF influent in order to mimic such variations in C:N ratio, ammonia-N, and sBOD<sub>5</sub> concentrations. Long-term experiments were conducted on the large pilot-scale NTF, unless otherwise stated. A detailed description of the large pilot-scale NTF can be found in Chapter 3.

A summary of influent ammonia-N and sBOD<sub>5</sub> concentrations and corresponding C:N ratios and loading rates for each experiment are displayed in Table 5.1. The influent C:N ratio was adjusted by varying the dose of organic carbon and/or ammonium sulphate. For Experiments B through E, the influent ammonia-N was maintained at low concentrations of  $\approx 0.5$  mg NH<sub>4</sub>-N/L, where the C:N ratio (range 3 to 10) was adjusted by varying the dose of sucrose ( $\approx 1.5$  to 5.0 mg sBOD<sub>5</sub>/L; Experiments B, C and E) or methanol ( $\approx 5.0$  mg sBOD<sub>5</sub>/L; Experiment D). For Experiments F, G and H, the C:N ratio was decreased within the range of 1 to 2 by increasing the influent ammonia-N concentration to  $\approx 5.0$  mg NH<sub>4</sub>-N/L. Influent sBOD<sub>5</sub> concentrations were maintained at high concentrations (5–9 mg sBOD<sub>5</sub>/L) via the addition of sucrose. For Experiment G, sucrose was dosed intermittently (48-h on, 48-h off) to mimic fluctuations in organic carbon often observed at Buaran WTP. Experiments A through to H were performed on the large pilot-scale NTF. Experiment I was performed using a small pilot-scale NTF, where sucrose dosing was substituted with organic fertiliser (trade name 'Rooster Booster') to mimic a less biodegradable sBOD<sub>5</sub> source. A detailed description of the small pilot-scale NTF can be found in Chapter 3. The NTFs operated under each organic load until steady-state nitrification performance was reached. Steady-state nitrification was assumed to have been reached once the daily coefficient of variation for percentage nitrification or nitrification rate was  $\leq 5\%$ .

### **5.2.2 Large pilot-scale NTF—sampling and chemical analysis**

Influent, effluent and depth profile 0.5 L grab sampling was performed, on average between two to three times per week, with samples taken at 10:00 am ( $\pm 2$  h). Samples were stored on ice during transport, and were analysed within 2 h of sampling for: ammonia-N; nitrite-N; nitrate-N; total TOC; and sBOD<sub>5</sub>; using procedures described in Chapter 3, Section 3.5. Profile samples were taken from the large pilot NTF at bed depths of 0.3, 1.5 and 2.7 m from the surface, in accordance with the procedure described in Chapter 3 Section 3.2.11. Ammonia-N profile data were used to calculate nitrification rates throughout the NTF at the time of sampling. Nitrification rates were calculated for bed depths of 0.3, 1.5, 2.7 and 3 m by using the difference in ammonia-N concentrations between the adjacent sample depths, and were determined as a function of media surface area. Influent and effluent samples were analysed regularly for: total alkalinity; pH; DO; and turbidity; using methods described in Chapter 3, Sections 3.5 and 3.6. Influent temperature was recorded online at 30 minute intervals. Long-term monitoring of influent temperature, total alkalinity, pH, DO, turbidity, TOC and sBOD<sub>5</sub> from the large pilot NTF was performed in order to evaluate the impact of seasonal variation of these parameters on nitrification performance.

### **5.2.3 Small pilot-scale NTF—sampling and chemical analysis**

Influent and effluent 0.5 L grab sampling was performed, on average between two to three times per week, with sampling conducted at 10:00 am ( $\pm 2$  h). Samples were stored on ice during transport, and were analysed within 2 h of sampling for: ammonia-N; nitrite-N; and nitrate-N. TOC and sBOD<sub>5</sub> were also measured within the influent on average twice per week.

### **5.2.4 Organic carbon biodegradability test**

To measure the biodegradability of a carbon substrate, oxygen consumption was measured at 24-h intervals over 5 d using the BOD method described in Chapter 3, Section 3.5.5. The carbon substrates compared were: (i) 6.25 mg/L of sucrose in Hope Valley raw water; (ii) 200 mg/L of organic fertiliser in Hope Valley raw water; (iii) 200

mg/L organic fertiliser in Hope Valley raw water, containing 1000 µl of a seeded culture; and (iv) Buaran raw water sample. The bacterial seed represented a culture that had been previously acclimated to the carbon source (organic fertiliser) in an aerated beaker for a duration of one week. Analysis of Buaran's raw water samples were conducted on-site at Buaran WTP by technical laboratory staff.

### 5.2.5 *Pearce's nitrification model*

The Pearce (1999) nitrification model is an empirical model derived from plastic-packed wastewater NTF applications, which is used to predict effluent ammonia-N concentration in response to variations in hydraulic loading, temperature, and ammonia-N and BOD<sub>5</sub> surface loads (Equation 5.1). For this study, operational data was grouped according to ammonia loads of  $815 \pm 130 \text{ mg m}^{-2} \text{ d}^{-1}$  (simulation 1) and between 96 to  $220 \text{ mg NH}_4\text{-N m}^{-2} \text{ d}^{-1}$  (simulation 2), which represented values within and below the range respectively from which the wastewater model was derived. For each simulation, model outputs were compared with observed NTF performance values obtained when operating under variable organic carbon loads. Simulations were computed at an influent temperature of 16°C, and a hydraulic surface load of  $173.3 \text{ L m}^{-2} \text{ d}^{-1}$  (5.2 m/h), which represented the mean temperature and flow rate the NTF operate under during the this study.

**Equation 5.1.** Pearce (1999) NTF nitrification model.

$$\text{amm.N}_{\text{out}} = 20.8 \times \text{amm.N}_{\text{in}}^{1.53} \times \text{BOD}_{\text{in}}^{1.03} \times IV^{-0.36} \times \text{temp}_{\text{in}}^{-0.12}$$

Where  $\text{amm.N}_{\text{out}}$  = 24 h composite effluent ammonia-N concentration (mg/L)  
 $\text{amm.N}_{\text{in}}$  = ammonia-N load ( $\text{g m}^{-2} \text{ d}^{-1}$ )  
 $\text{BOD}_{\text{in}}$  = BOD<sub>5</sub> load ( $\text{g m}^{-2} \text{ d}^{-1}$ )  
 $IV$  =  $\text{L/m}^2/\text{d}$   
 $\text{temp}_{\text{in}}$  = influent temperature (°C)

**Table 5.1.** Experimental conditions used to determine the effect of carbon loadings on the performance of the nitrifying trickling filters: influent ammonia-N and sBOD<sub>5</sub> concentrations and corresponding C/N ratio and loading rates (mean ± 1 SD).

Experiment	Influent ammonia-N		Influent sBOD <sub>5</sub>		C:N ratio	External organic carbon source	Duration of carbon dosing (days)
	mg/L	mg m <sup>-2</sup> d <sup>-1</sup>	mg/L	mg m <sup>-2</sup> d <sup>-1</sup>			
A <sup>1</sup>	0.56 – 5.57	97.0 – 966.1	1.3 ± 0.5	225.2 ± 87.9	-	None	0
B*	0.71 ± 0.2	122.9 ± 41.4	6.1 ± 3.36	1066.9 ± 577.2	8.5/1	Sucrose	64
C	0.56 ± 0.1	97.8 ± 19.7	5.4 ± 0.15	931.4 ± 26.0	10/1	Sucrose	18
D	0.6 ± 0.01	104.8 ± 1.0	5.0 ± 0.0	866.4	8/1	Methanol	11
E	0.52 ± 0.02	90.1 ± 2.6	1.5 ± 0.4	259.9 ± 60	3/1	Sucrose	8
F	4.7 ± 1.1	826.1 ± 1639	8.8 ± 2.9	1533.5 ± 510.6	2/1	Sucrose	12
G <sup>†</sup>	4.8 ± 0.5	840.1 ± 86.2	9.4 ± 0.9	1625.4 ± 162.7	2/1	Sucrose	three 48 h spikes
H	4.8 ± 0.3	822.4 ± 61.4	5.3 ± 1.0	910.9 ± 169.1	1/1	Sucrose	10
I <sup>a</sup>	1.3 ± 0.3	220.8 ± 48.3	11.5 ± 3.4	1992.8 ± 589.3	8.8/1	Organic fertiliser	16

<sup>1</sup> Data obtained from NTF when operated under low sBOD<sub>5</sub> loads (Chapter 4). sBOD<sub>5</sub> represents native organic carbon present in Hope Valley reservoir water.

\* Experiment conducted on old pilot NTF plant.

† Intermittent carbon spikes (48-h on / 48-h off).

<sup>a</sup> Experiment conducted on small pilot-scale NTF.

## 5.3 Results

### 5.3.1 *Comparing organic carbon biodegradability of Buaran raw water with selected carbon sources*

Figure 5.1 compares daily soluble carbonaceous biological oxygen demand for: (i) different carbon sources (sucrose and organic fertiliser); (ii) Buaran raw water; and (iii) organic fertiliser seeded with a bacterial culture that had been previously acclimatised. Despite exerting a similar final sBOD<sub>5</sub> concentration on day 5, the magnitude of oxygen uptake varied over time for different carbon sources. Oxygen consumption curves for sucrose and Buaran raw water showed similar first-order-like characteristics, where 43 % and 66 % respectively of overall oxygen consumption occurred within the first 24 h of incubation. Surprisingly these results show that Buaran's raw water contained readily available organic carbon, similar to that of sucrose. This observation may be a result of nearby pollutant sources (i.e., municipal sewage and food industries) which are in close proximity to the WTP (see Chapter 2). Based on these findings, sucrose was chosen as the surrogate carbon source for this study.

In contrast to sucrose and Buaran's raw water, a lag phase between 0 and 24 h was observed for the organic fertiliser (un-seeded) test, where only 3.8 % of DO had been consumed within this time period. The lag was followed by a steady increase in oxygen consumption. However, when a competent bacterial seed was added to the organic fertiliser carbon source, the oxygen consumption curve behaved very similarly to that of Buaran's raw water, and was also not dissimilar to that of sucrose. These results suggest that the organic fertiliser may not be as recalcitrant as first observed, and suggests that there would have been a carbonaceous oxygen demand exerted on the filter when dosed. Employing this respiration technique for determining the degree of organic carbon biodegradability in Buaran's raw water was inconclusive; since the biodegradation curve of organic carbon from Buaran's raw water behaved similarly to both the seeded organic fertiliser and the sucrose biodegradation curve.

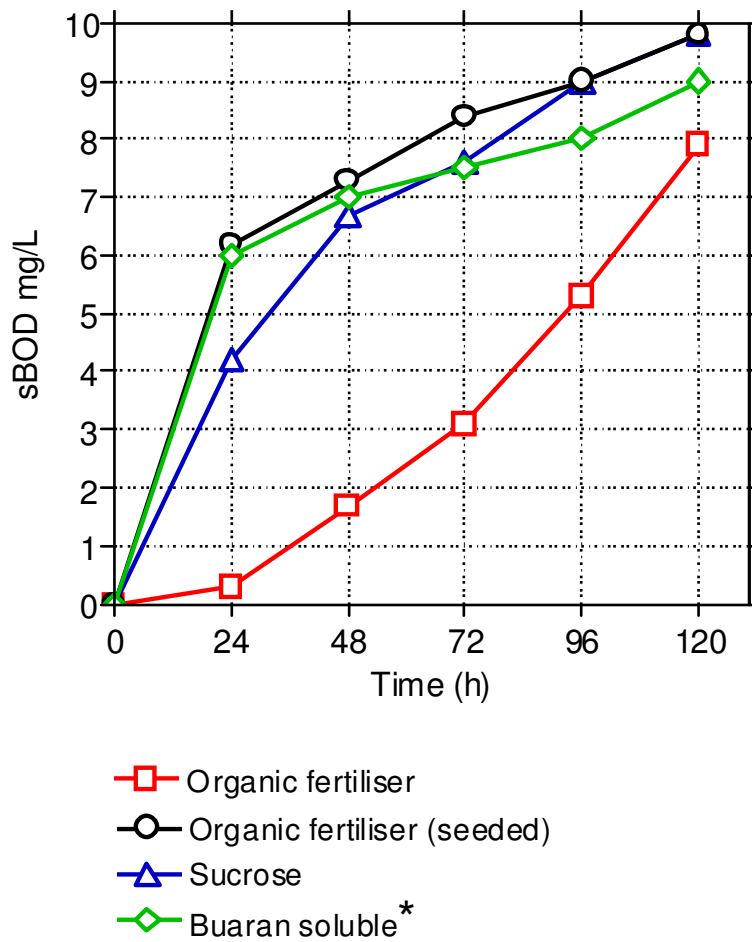


**Figure 5.1.** Comparison of BOD<sub>1</sub> to BOD<sub>5</sub> of selected carbon sources and of Buaran raw water.

\*Data provided by staff from Thames Pam Jaya, Buaran WTP, Jakarta, Indonesia.

### **5.3.2 Comparison of nitrification performance between experiments**

Figure 5.2 compares steady-state percentage nitrification between all experiments that operated under various ammonia-N and sBOD<sub>5</sub> surface loads. Given that the NTF during Experiment A operated in absence of an external carbon source, and a high percentage nitrification was consistently achieved (mean  $90 \pm 8 \%$ ;  $n=136$ ; Chapter 4), Experiment A was used as the comparator for all experiments (B, C, D, E, F, G, H, I). Comparisons made with Experiment A were achieved using data of similar influent ammonia-N concentration. Analysis by ANOVA showed that Experiment E (low sucrose augmented carbon loads) and Experiment I (high native-like carbon loads) achieved equal nitrification performance to that of Experiment A ( $p>0.05$ ), where no difference in nitrification performance was observed. The greatest decline in nitrification was observed for experiments where influent sBOD<sub>5</sub> was increased and maintained  $\geq 5.0$  mg/L ( $\approx 870$  mg sBOD<sub>5</sub> m<sup>-2</sup> d<sup>-1</sup>) via the addition of sucrose or methanol.

Statistically, percentage nitrification for Experiments B, C, D, F, G and H were significantly lower than Experiment A. Significance values are displayed in Figure 5.2. For experiments where the NTF was operated under similar ammonia-N and carbon loads (Experiments B, C and D), similar nitrification performance was observed ( $p>0.05$ ). There was also good reproducibility between both the old and newly reconstructed pilot NTFs (Experiments B and C), with similar filter performance observed. There was no significant difference ( $p>0.05$ ) in percentage nitrification between experiments that operated under similar ammonia-N and sBOD<sub>5</sub> loads, whether operated at a continuous sucrose carbon loading (Experiment F) or fed intermittent sucrose carbon spikes lasting 48 h (Experiment G).

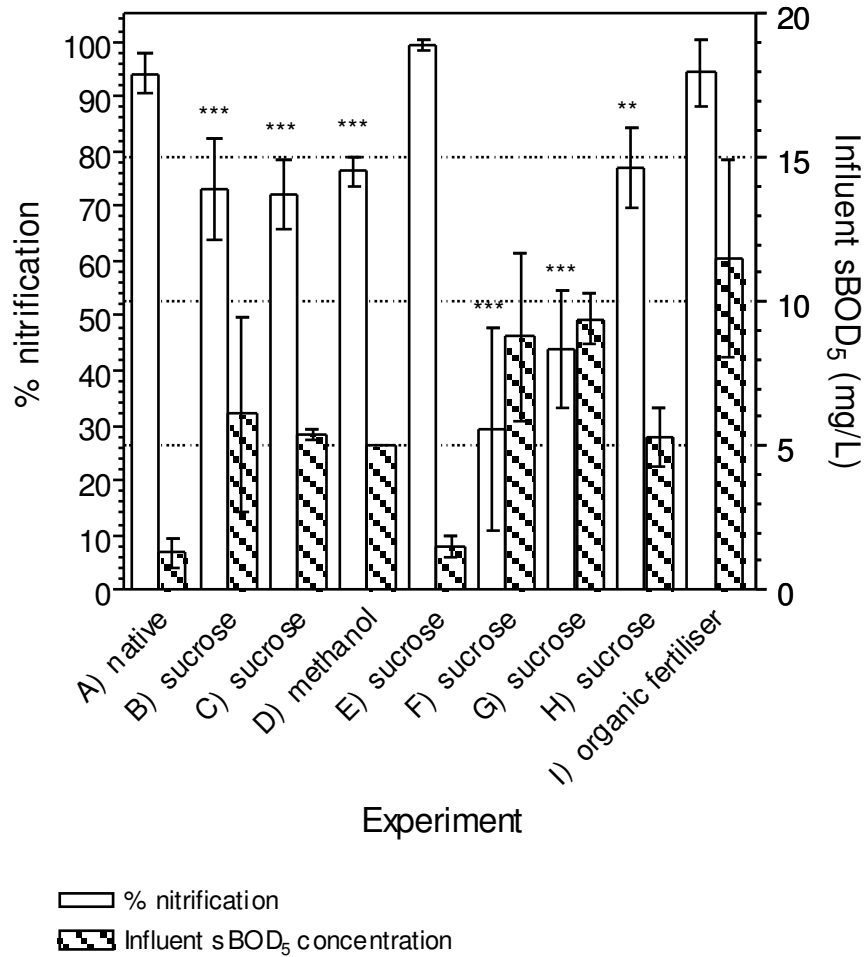


**Figure 5.2.** Effect of influent sBOD<sub>5</sub> concentration and external carbon source on NTF performance. Asterisks denote a statistically significant difference between pairwise experimental comparisons, in comparison with Experiment A which operated without the addition of an external carbon source, with significance level shown as follows: \*\*  $p < 0.01$ ; \*\*\*  $p < 0.001$ . (Individual column means shown  $\pm$  1 SD).

### **5.3.3 Percentage nitrification as a function of organic load**

Figure 5.3 shows percentage nitrification as a function of sBOD<sub>5</sub> surface load (mg sBOD<sub>5</sub> m<sup>-2</sup> d<sup>-1</sup>). A negative correlation was observed between sBOD<sub>5</sub> surface load and percentage nitrification once influent sBOD<sub>5</sub> was increased from background native concentrations via the addition of sucrose or methanol ( $r_s = -0.85$ ;  $p < 0.01$ ; Table 5.2). These results indicate that 90 to 100 % of nitrification was achieved only when the organic surface load was less than 700 mg sBOD<sub>5</sub> m<sup>-2</sup> d<sup>-1</sup> ( $\approx 4$  mg sBOD<sub>5</sub>/L). A rapid decline in nitrification occurred once the organic surface load was increased beyond 750 to 2100 mg sBOD<sub>5</sub> m<sup>-2</sup> d<sup>-1</sup>. A negative relationship between organic loading and percentage nitrification was not observed for Experiment I where the organic loading was maintained high at  $1993 \pm 589$  mg sBOD<sub>5</sub> m<sup>-2</sup> d<sup>-1</sup> ( $11.5 \pm 3.4$  mg sBOD<sub>5</sub>/L) for 16 d, via the addition of a native-like carbon source (soluble organic fertiliser). These findings suggest that sucrose and methanol adversely affect the nitrification performance, however the organic fertiliser did not—something which may reflect differences in carbon biodegradability.

### **5.3.4 Nitrification rate as a function of organic load**

Figure 5.4 shows the apparent nitrification rate (mg NH<sub>4</sub>-N m<sup>-2</sup> d<sup>-1</sup>) as a function of organic surface load (mg sBOD<sub>5</sub> m<sup>-2</sup> d<sup>-1</sup>). Statistically, a significant negative relationship (Pearson's;  $p < 0.0001$ ) between nitrification rate and sBOD<sub>5</sub> surface load was observed when ammonia-N surface loads were maintained at both high ( $815 \pm 130$  mg NH<sub>4</sub>-N m<sup>-2</sup> d<sup>-1</sup>;  $r = -0.94$ ) and low fixed loads ( $94 \pm 10$  mg NH<sub>4</sub>-N m<sup>-2</sup> d<sup>-1</sup>;  $r = -0.74$ ). For the organic loading range of 50 to 900 mg sBOD<sub>5</sub> m<sup>-2</sup> d<sup>-1</sup>, regression analysis of log-transformed data confirmed that differences between the two slopes were not significant (ANCOVA;  $p > 0.05$ ), which suggested that the magnitude of decline in nitrification rate in response to organic carbon load for a low- and high-ammonia-loaded NTF was similar, despite differences between their C:N ratios. This data suggests that the sBOD<sub>5</sub> surface load rather than the C:N ratio was the most important factor influencing nitrification.

### **5.3.5 Nitrification as a function of C:N ratio**

Analysis by ANOVA found no relationship between C:N ratio and percentage nitrification. When influent ammonia-N was increased to lower the C:N ratio, no significant improvement or indeed change in nitrification was observed. This can be seen when comparing percentage nitrification between Experiments B, C, and D, which operated under a C:N ratio of 8–10, with Experiment H, where ammonia-N was increased to reduce the C:N ratio to 1 ( $p>0.05$ ; Figure 5.2). In addition, when comparing nitrification performance between experiments which operated under a similar C:N ratio, for example Experiments E and F which measured 3:1 and 2:1 respectively, differences between percentage nitrification were significant ( $p<0.001$ ; Figure 5.2). Furthermore, when the NTF operated under stable ammonia loads, an increase in C:N ratio (i.e. increase in organic load) appeared to impacted negatively on percentage nitrification. However, when grouping the data obtained from operation under both variable ammonia and organic loads, analysis by Spearman's correlation identified no relationship between percentage nitrification and C:N ratio ( $r_s = -0.17$ ;  $p>0.05$ ; Table 5.2).

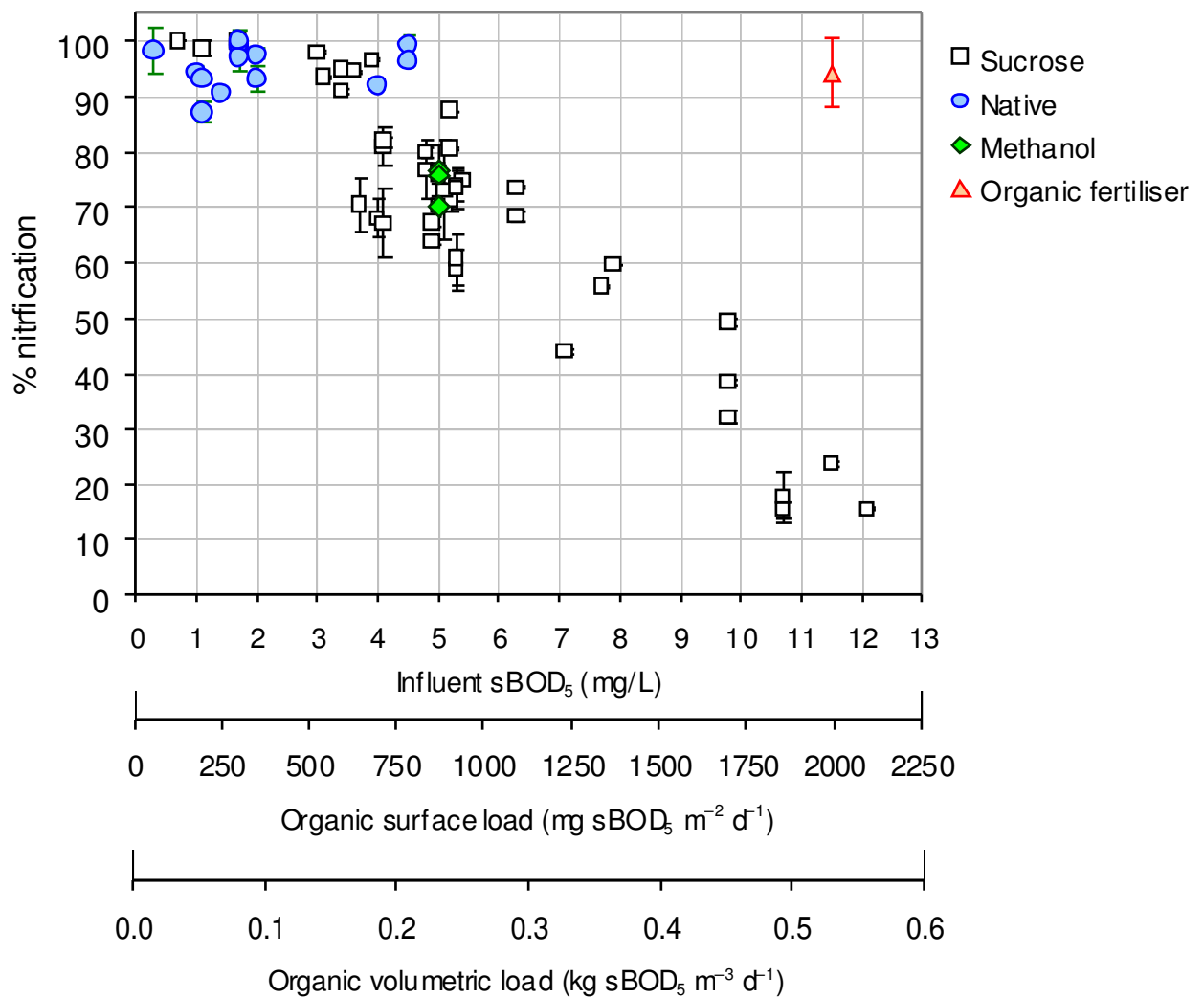


**Figure 5.3.** Steady-state relationship between percentage nitrification and organic load, obtained from experimental data where ammonia-N was loaded between  $94 \pm 10$  to  $815 \pm 130$  mg NH<sub>4</sub>-N m<sup>-2</sup> d<sup>-1</sup>. (Parameter means shown  $\pm 1$  SD).

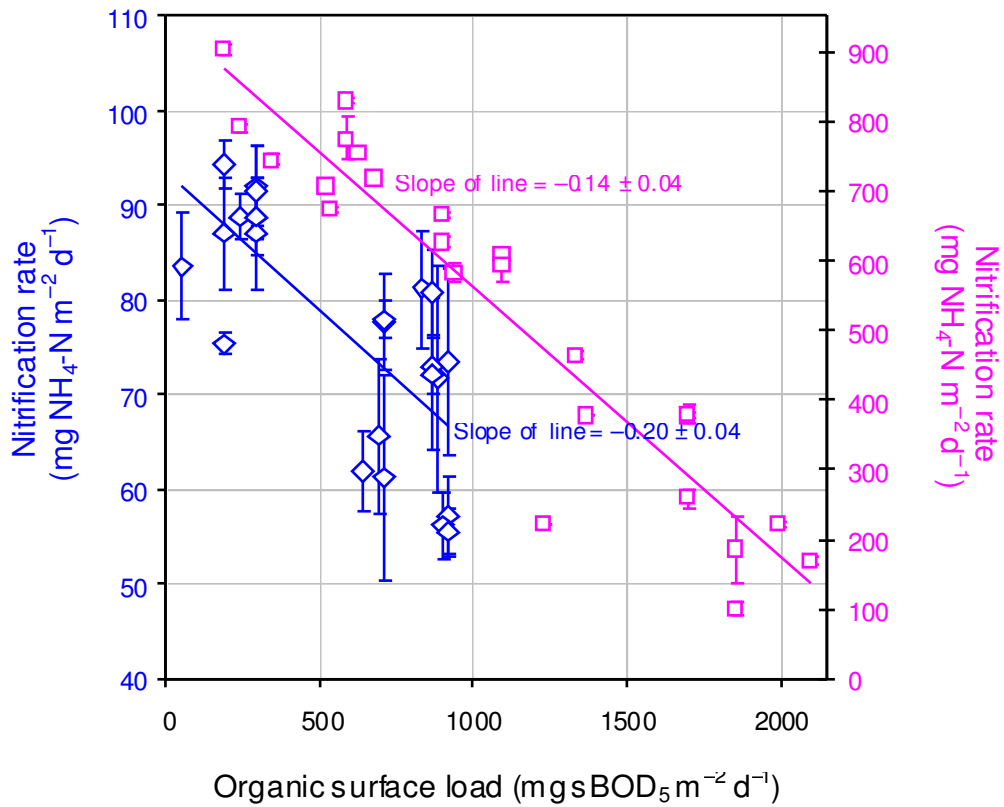


**Figure 5.4.** Apparent nitrification rate as a function sBOD<sub>5</sub> surface load, observed under: (i) low ammonia-N loads of  $94 \pm 10 \text{ mg NH}_4\text{-N m}^{-2} \text{ d}^{-1}$  ( $\diamond$ ); and (ii) high ammonia-N loads  $815 \pm 130 \text{ mg NH}_4\text{-N m}^{-2} \text{ d}^{-1}$  ( $\square$ ). (Data points represent parameter means  $\pm 1$  SD).

**Table 5.2.** Spearman's correlation coefficient highlighting relationships between NTF performance and physiochemical water quality parameters.

Parameter	Influent sBOD <sub>5</sub> (mg/L)	Influent C:N ratio	% nitrification	sBOD <sub>5</sub> removal (mg m <sup>-2</sup> d <sup>-1</sup> )	Influent temp. (°C)	Influent Tot. Alkalinity (mg CaCO <sub>3</sub> /L)	Influent pH	Influent DO (mg/L)
Influent C:N ratio	0.287*							
<i>n</i>	56							
% nitrification	-0.854**	-0.17						
<i>n</i>	56	56						
sBOD <sub>5</sub> removal (mg m <sup>-2</sup> d <sup>-1</sup> )	0.757**	0.667**	-0.820**					
<i>n</i>	59	51	39					
Influent temp.(°C)	0.358**	-0.201	-0.198	-0.545				
<i>n</i>	54	54	54	17				
Influent Tot. Alkalinity (mg CaCO <sub>3</sub> /L)	0.447	-0.351	-0.194	-0.221	0.646*			
<i>n</i>	19	21	21	13	21			
Influent pH	-0.718	-0.481	0.577*	0.032	-0.602*	-0.144		
<i>n</i>	17	18	18	11	18	16		
Influent DO (mg/L)	-0.379	0.227	0.285	0.298	-0.553*	-0.617*	0.014	
<i>n</i>	14	15	15	13	15	14	11	
Effluent DO (mg/L)	-0.735**	-0.259	-0.793**	-0.786**	0.589	0.407	-0.134	-0.32
<i>n</i>	24	25	26	18	25	21	18	15

\*Correlation is significant at  $p < 0.05$  level (2-tailed); \*\*Correlation is significant at  $p < 0.01$  level (2-tailed).

### **5.3.6 Effect of carbon loading and operation time on nitrification: low ammonia-N loaded NTF**

Figure 5.5 shows the trickling filter's nitrification performance once influent sBOD<sub>5</sub> was increased on day 0 from background concentrations of 1.3 (225 mg sBOD<sub>5</sub> m<sup>-2</sup> d<sup>-1</sup>) to 5.8 ± 2.7 mg/L (1005 mg sBOD<sub>5</sub> m<sup>-2</sup> d<sup>-1</sup>). Influent ammonia-N was maintained at low concentrations of 0.6 ± 0.2 mg/L (≈102 mg NH<sub>4</sub>-N m<sup>-2</sup> d<sup>-1</sup>). Combined data from Experiments B, C and D is displayed (Figure 5.5). Data from Experiment B was divided into Run 1 and Run 2. The duration of carbon dosing for Run 2 was increased from 14 d (Run 1) to 64 d. Short-term observations show that the filter responded rapidly to the increase in sucrose or methanol augmented carbon loads, where a rapid decline in percentage nitrification occurred within 8 to 10 d of carbon dosing. Nitrification declined from 90 ± 5 % (90.1 ± 1.7 mg NH<sub>4</sub>-N m<sup>-2</sup> d<sup>-1</sup>) on day 0 to 69 ± 7 % (64 ± 6 mg NH<sub>4</sub>-N m<sup>-2</sup> d<sup>-1</sup>) between days 8 to 18. Similar results were obtained for all experiments where no significant difference between percentage nitrification for Experiments B, C and D between days 8 to 18 was observed (ANOVA; *p*>0.05). In contrast to short-term observations, the nitrification performance appeared to recover in response to prolonged periods of high organic loads. From Experiment B (Run 2), it can be seen that nitrification increased gradually after day 25, reaching 88.5 % (80 mg NH<sub>4</sub>-N m<sup>-2</sup> d<sup>-1</sup>) on day 45. The increase in ammonia removal observed here, may be attributed to the assimilatory requirements of the developing heterotrophic population for nitrogen, or via simultaneous nitrification–denitrification, since there was only low concentrations of NO<sub>x</sub> detected within the filters effluent (<0.2 mg NO<sub>x</sub>/L; see Figure 5.6.d).

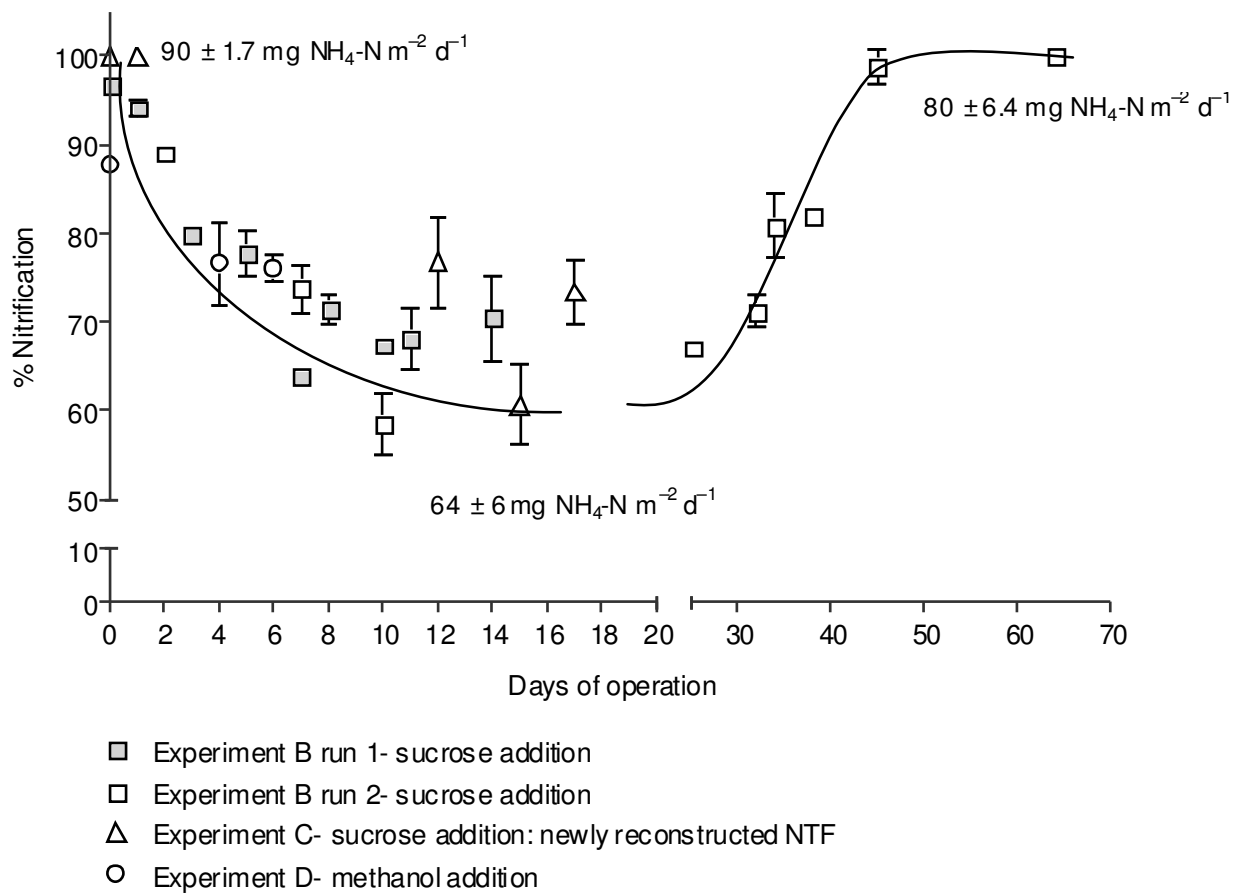


**Figure 5.5.** Nitrification performance of the NTF, as a function of time, following an increase in influent sBOD<sub>5</sub> concentration from 1.3 to  $5.8 \pm 2.7 \text{ mg/L}$  (on day 0). Data obtained from Experiments B, C and D using either sucrose or methanol as the sBOD<sub>5</sub> source. Nitrification rates are also presented in  $\text{mg NH}_4\text{-N m}^{-2} \text{ d}^{-1}$ . (Individual data points show parameter means  $\pm 1 \text{ SD}$ ).

### **5.3.7 Nitrification depth profile and nitrogen budget: low ammonia-N loaded NTF**

To monitor the impact of organic carbon on the nitrification performance within a low ammonia-N loaded NTF ( $\approx 0.5 \text{ mg NH}_4\text{-N/L}$ ), depth profiles of inorganic nitrogen species were measured at regular time intervals following the increase in organic carbon load. Representative steady-state profiles of the NTF taken: (i) before increasing the organic carbon load; (ii) when operated under high organic carbon loads, for Experiments B, C, D and E; and (iii) recovery, once organic carbon dosing was returned to background concentrations; are given in Figure 5.6. The ammonia concentration profile data also provided a basis to calculate and compare nitrification rates through the NTF bed in response to periods of low and high carbon loads (Figure 5.8).

Figure 5.6.a shows a bed depth profile of ammonia-N, nitrite-N, and nitrate-N taken before carbon dosing commenced (day 0). The mean of three combined profiles, obtained from Experiments B, C and D is displayed. Highest ammonia-N removal of  $55.8 \pm 6.1 \%$  was observed at a filter bed depth of 0.3 m from the surface.  $83 \pm 13 \%$  of ammonia-N removal was achieved at the bed depth of 1.5 m. Complete nitrification was consistently observed, and was characterised by the absence of nitrite-N throughout the filter bed, and by the production of nitrate, which complemented the decrease in ammonia. A nitrogen budget demonstrated that 85 to 100 % of ammonia-N was recovered in the form of nitrate-N at all filtrate sample depths. Only 2 % or 0.012 mg/L of nitrogen was not accounted for in the filter's effluent, which could be attributed to assimilation, ammonium volatilisation and/or denitrification (Figure 5.7).

Figure 5.6.b and Figure 5.6.c show a depth profile of ammonia-N, nitrite-N, and nitrate-N observed after 7 and 15 d of additional carbon loading using sucrose. The mean of three combined profiles obtained from Experiments B (Run1, Run2) and C, which operated under similar organic carbon and ammonia-N load is displayed. Ammonia-N profiles observed on day 7 (Figure 5.6.b) and day 15 (Figure 5.6.c) appeared similar. A significant decline in ammonia removal throughout the entire filter bed was observed. Overall ammonia-N removal had declined to  $67 \pm 7.1 \%$ . The greatest decline in

ammonia-N removal was observed at bed depth of 0.3 m, where percentage ammonia-N removal declined from  $55.8 \pm 6.1$  % to  $23.3 \pm 4.4$  % on day 7 (Figure 5.6.b) and  $25.6 \pm 14.7$  % on day 15 (Figure 5.6.c). Nitrite-N was not detected throughout the filter, suggesting any nitrite produced via the oxidation of ammonia was oxidised to nitrate. Small concentrations of nitrate-N were detected, which complemented the decrease in ammonia-N. The narrow error bars were an indication of good reproducibility between experiments. A nitrogen budget demonstrated that 65 to 82 % of ammonia-N removed was recovered in the form of nitrate-N. These results suggest that nitrification was the major process responsible for ammonia removal. Elimination of nitrogen via assimilation or denitrification had increased from 2 % (0.012 mg N/L) when operated under low carbon loads, to a mean value of 25 %, or 0.12 mg N/L (Figure 5.7). Influent pH, temperature and hydraulic flow were largely unchanged between all experiments, therefore nitrogen losses via ammonium volatilisation were expected to be minimal.

Figure 5.6.d shows the profile of ammonia-N, nitrite-N and nitrate-N throughout the filter bed on day 64 (obtained from Experiment B, Run 2). These results are typical of depth profiles of ammonia-N, nitrite-N, and nitrate-N observed between days 40 to 64 after increasing the influent organic carbon concentration to 5 mg sBOD<sub>5</sub>/L using sucrose. Ammonia-N removal had increased to 100 %. Nitrite-N was not detected, and low concentrations of nitrate-N (0.2 mg NO<sub>3</sub>-N/L) were produced only in the lower depths of the filter, presumably where organic carbon concentrations were lower, and the inhibitory effect is consequently reduced. A nitrogen budget demonstrated that only 25.3 to 59.2 % of ammonia-N removed was recovered in the form of nitrate-N at all filter sample depths. In comparison to earlier nitrogen budgets obtained between days 7 and 15 (Figures 5.6.b and 5.6.c), elimination of nitrogen via assimilation or denitrification had increased further to 75 % or 0.37 mg N/L (Figure 5.7). This was also observed on day 9 for Experiment D, when methanol was used as the sole carbon source (Figure 5.6.e). For Experiment D, the filter was capable of removing 73 % ammonia-N, however, nitrite-N and nitrate-N concentrations measured at all filter bed depths remained below 0.02 mg/L. A nitrogen budget found 73 % (0.36 mg N/L) of ammonia removed was

unaccounted for in the NTF's effluent as  $\text{NO}_x$ , therefore nitrogen losses were attributed to assimilation and/or simultaneous nitrification–denitrification (Figure 5.7).

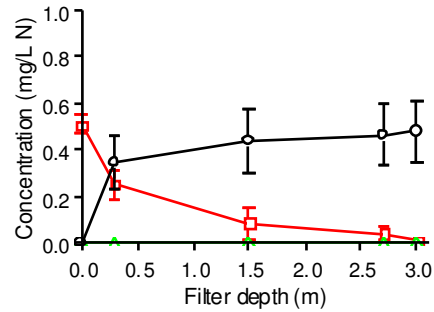
Figure 5.6.f shows the recovery of nitrification throughout the NTF bed 9 d after sucrose dosing was terminated for Experiment B Run 1. When compared to Figure 5.6.a (before carbon dosing), the filter bed profiles of ammonia-N, nitrite-N and nitrate-N appeared remarkably similar, which suggests that the filter had redeemed original steady-state nitrifying capacity.

By the end of Experiment B, Run 2 (Day 64), prolonged dosing of sucrose had caused significant damage to the trickling filter structure and support media. The biofilm appeared thicker and had a "jelly-like" appearance, consistent with the characteristics of EPS. Excessive weight caused by heterotrophic growth and EPS, had squashed the bottom two layers of support media, and had caused the base of the filter to sag. Car jacks were used to elevate the base of the trickling filter level, which further exacerbated the crushing of the bottom two layers of support media. Before and after photographs (Plate 5.1.a and 5.1.b) of biofilm and filtrate samples sites, revealed that the media bed had collapsed by 0.3 m. Clogging of the media by copious quantities of biomass had caused ponding on the bed surface (Plate 5.1.c). It was presumed that excessive heterotrophic growth and EPS production had also caused narrowing of the effluent drains, which in turn caused filtrate to pond at the filter base and overflow out the trickling filter ventilation ports. As outlined in Chapter 3 Section 3.3.5, a new filter was designed and constructed to support the excessive weight of biomass generated by an increase in organic carbon loads. Experiments C and D were conducted on the newly reconstructed filter. Experiment C was terminated after 18 days in order to prevent permanent damage to the trickling filter and support media.

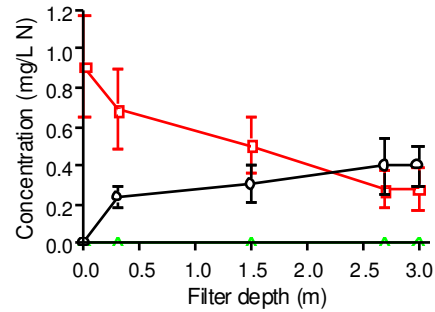
Figure 5.6.g shows a bed depth profile of ammonia-N, nitrite-N, and nitrate-N taken during Experiment E, where in order to improve nitrification, the influent  $\text{sBOD}_5$  was decreased from  $\approx 5.0 \text{ mg/L}$  ( $870 \text{ mg sBOD}_5 \text{ m}^{-2} \text{ d}^{-1}$ ) to  $1.5 \pm 0.4 \text{ mg/L}$  ( $260 \text{ mg sBOD}_5 \text{ m}^{-2} \text{ d}^{-1}$ ). Background  $\text{sBOD}_5$  concentrations of the Hope Valley Reservoir water prior to

sucrose dosing was less than 0.3 mg/L. Influent ammonia-N was maintained at  $0.52 \pm 0.02$  mg/L ( $90.1 \pm 2.6$  mg m<sup>-2</sup> d<sup>-1</sup>). The mean of three steady-state profiles taken during the experiment is displayed. Complete nitrification was achieved at a bed depth of 3.0 m, however in comparison to Experiment A (Figure 5.6.a), a small decline in ammonia-N removal down the filter bed was observed, which was most apparent within the top half of the NTF bed. A nitrogen budget demonstrated that 98 % of ammonia-N removed was recovered in the form of nitrate-N within the effluent (Figure 5.7).

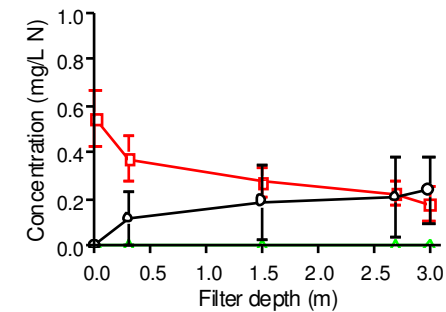
a) Day 0: no carbon addition



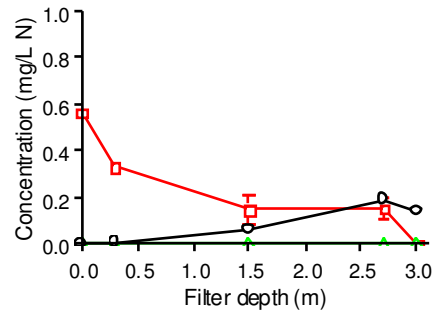
b) Days 7–8: sucrose addition– 5.7 mg sBOD<sub>5</sub>/L



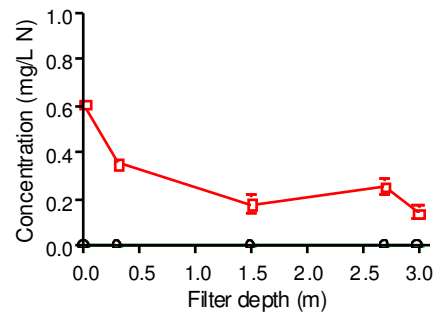
c) Days 12–15: sucrose addition– 5.7 mg sBOD<sub>5</sub>/L



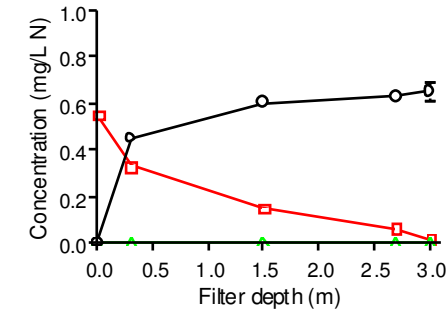
d) Day 64: sucrose addition– 6.1 mg sBOD<sub>5</sub>/L



e) Day 9: methanol addition– 5.0 mg sBOD<sub>5</sub>/L



f) Recovery: carbon dosing terminated



g) Days 7–9: sucrose addition– 1.5 mg sBOD<sub>5</sub>/L

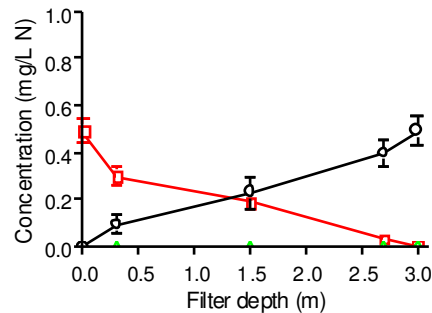
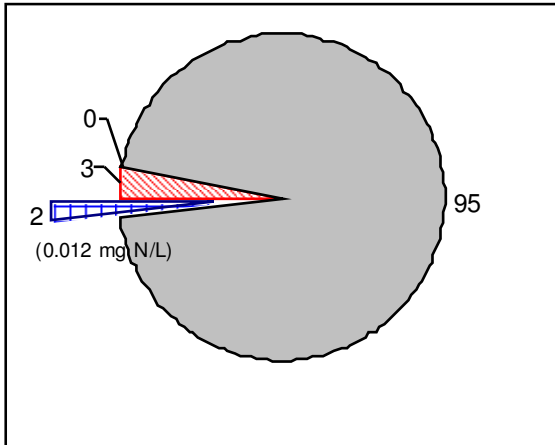


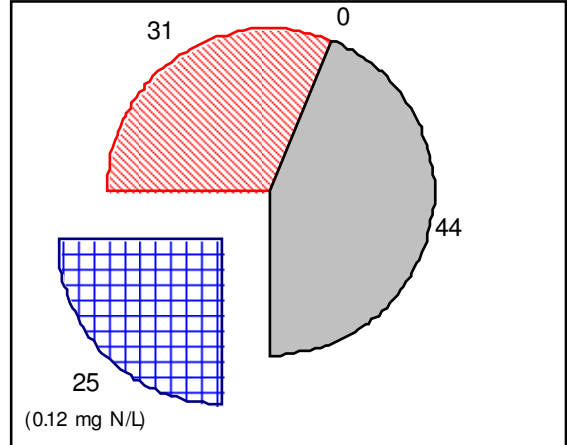
**Figure 5.6.** Concentration profiles of inorganic nitrogen species measured throughout the depth of the NTF: (a) mean of three profiles observe when the NTF operated under low influent organic carbon concentrations of 1.3 mg sBOD<sub>5</sub>/L; (b) mean of 3 profiles obtained from Experiments B and C, 7 to 8 d after increasing the influent organic carbon concentration to 5.7 mg sBOD<sub>5</sub>/L via the addition of sucrose; (c) mean of 3 profiles obtained from Experiments B and C, 12 to 15 d after increasing the influent organic carbon concentration to 5.7 mg

sBOD<sub>5</sub>/L via the addition of sucrose; (d) profile observed during Experiments B, 64 d after increasing the influent organic carbon concentration to 6.1 mg sBOD<sub>5</sub>/L via the addition of sucrose; (e) profile observed during Experiment D, 9 d after increasing the influent organic carbon concentration to 5.0 mg sBOD<sub>5</sub>/L via the addition of methanol; (f) recovery profile, observed once the influent organic carbon concentration was returned to background concentrations of 1.3 mg sBOD<sub>5</sub>/L; and (g) mean of three profiles observed during Experiment E, when operated under influent organic carbon concentrations of 1.5 mg sBOD<sub>5</sub>/L via the addition of sucrose. For all experiments Influent ammonia-N was maintained steady at  $0.5 \pm 0.2$  mg NH<sub>4</sub>/L. Symbols denote: (□) ammonia-N; (△) nitrite-N; and (O) nitrate-N. (Data points represent individual parameter means  $\pm 1$  SD).

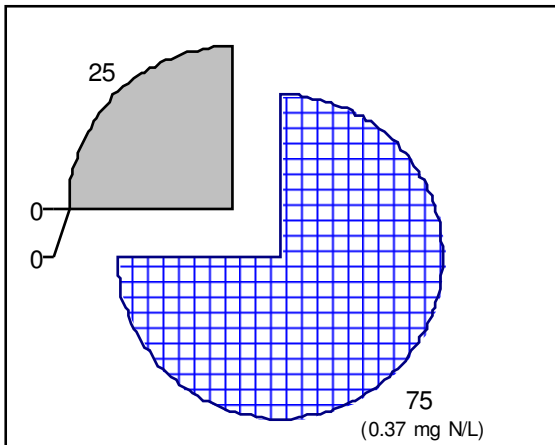
a) No carbon addition–1.3 mg sBOD<sub>5</sub>/L



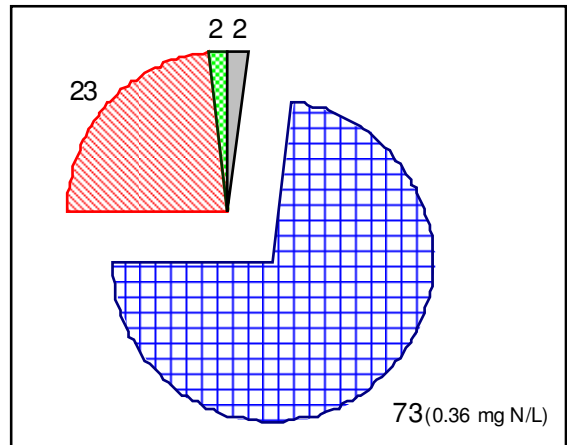
b) Days 7–15: sucrose addition–5.7 mg sBOD<sub>5</sub>/L



c) Day 64: sucrose addition–6.1 mg sBOD<sub>5</sub>/L



d) Day 9: methanol addition–5.0 mg sBOD<sub>5</sub>/L



e) Days 7–9: sucrose addition–1.5 mg sBOD<sub>5</sub>/L

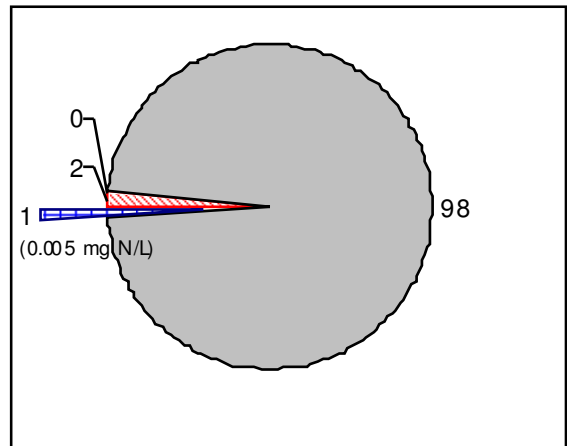


**Figure 5.7.** Nitrogen mass-balance showing effluent nitrogen species composition as percentage of total inorganic nitrogen. Inorganic nitrogen not accounted for is

represented as “assimilated / Denitrified  $N_2$ ”. Influent ammonia-N represented 100 % of total nitrogen present. (a) Experiment A– low influent organic carbon concentrations of 1.3 sBOD<sub>5</sub>/L; (b) mean obtained from Experiments B and C, 7 to 15 d after increasing the influent organic carbon concentration to 5.7 mg sBOD<sub>5</sub>/L via the addition of sucrose; (c) Experiment B– 64 d after increasing the influent organic carbon concentration to 6.1 mg sBOD<sub>5</sub>/L via the addition of sucrose; (d) Experiment D– 9 d after increasing the influent organic carbon concentration to 5.0 mg sBOD<sub>5</sub>/L via the addition of methanol; and (e) mean obtained from Experiment E, 7 to 9 d after increasing the influent organic carbon concentration to 1.5 mg sBOD<sub>5</sub>/L via the addition of sucrose.

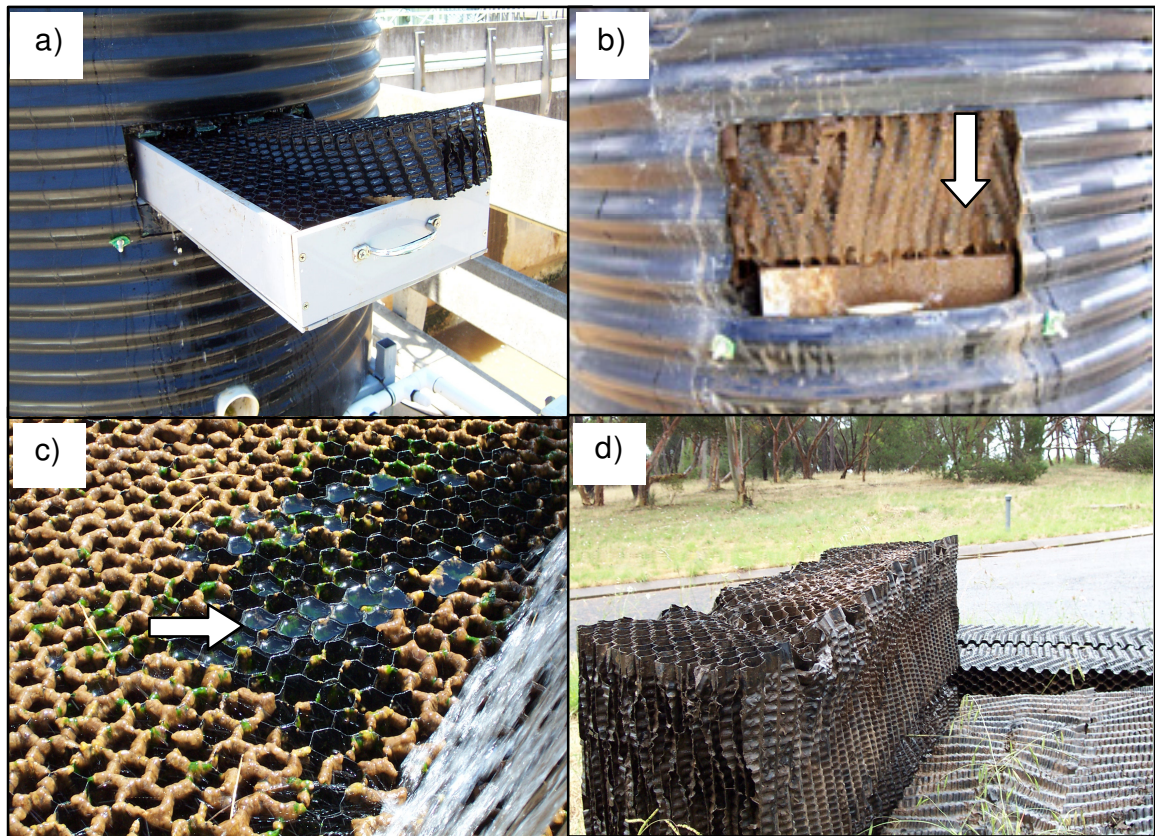


**Plate 5.1.** Impact of high carbon loads on NTF support media: (a) filtrate and biofilm sample site before increasing the organic carbon load; (b) filtrate and biofilm sample site 64 d after operating under high organic carbon loads (Experiment B); (c) ponding of filtrate on media surface observed during Experiment B; and (d) crushed media.

Ammonia profile data collected from the NTF provided a basis for calculating nitrification rates through the NTF (Figure 5.8). The operational data set was divided into periods of uniform influent ammonia-N concentrations ( $0.5 \pm 0.2$  mg/L) and sucrose augmented sBOD<sub>5</sub> concentration loads of 0.5 mg/L,  $1.5 \pm 0.4$  mg/L and  $5.5 \pm 0.5$  mg/L. Differences in nitrification performance were based on comparing nitrification rates measured at depth through the NTF, and were evaluated by non-parametric Kruskal–Wallis ANOVA with Dunn’s multiple comparison testing. The data presented, represents the mean of three or more individual sampling events. From Figure 5.8, it can be seen that once the influent sBOD<sub>5</sub> concentration was increased from background concentration of 0.5 mg/L to 1.5 mg/L and 5.5 mg/L, a significant decrease in nitrification rates at 0.3 m occurred ( $p < 0.05$ ), which was an area of the filter that was exposed to the highest concentrations of organic carbon. In comparison to periods of low influent sBOD<sub>5</sub> concentrations, nitrification rates measured at the lower depths during periods of high influent sBOD<sub>5</sub> concentration appeared to increase slightly, however not significantly ( $p > 0.05$ ). Higher nitrification rates might have been expected at these lower depths, due to lower organic carbon concentrations brought about by carbon respiration and assimilation in the preceding upper regions of the NTF (see Section 5.3.10).

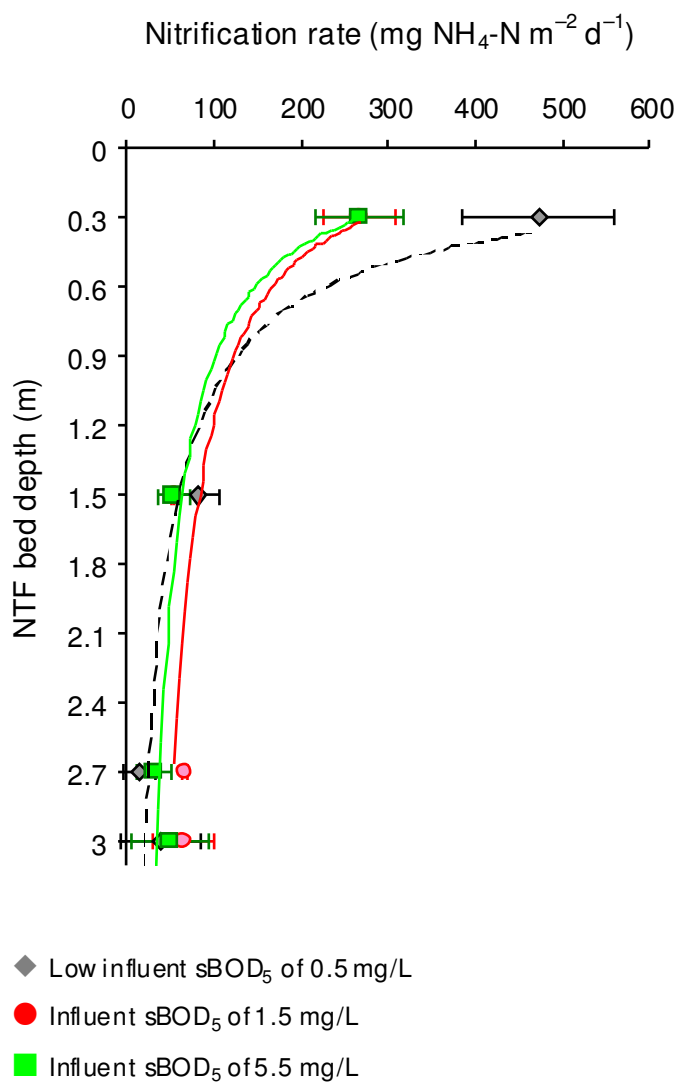


**Figure 5.8.** Comparison of nitrification rates measured through the depth of the large pilot-scale NTF during operational periods of high and low influent  $\text{sBOD}_5$  concentrations. Low influent ammonia-N concentrations fixed at  $0.5 \pm 0.2 \text{ mg NH}_4\text{-N m}^{-2} \text{d}^{-1}$ . (Data points show parameter means  $\pm 1 \text{ SD}$ ).

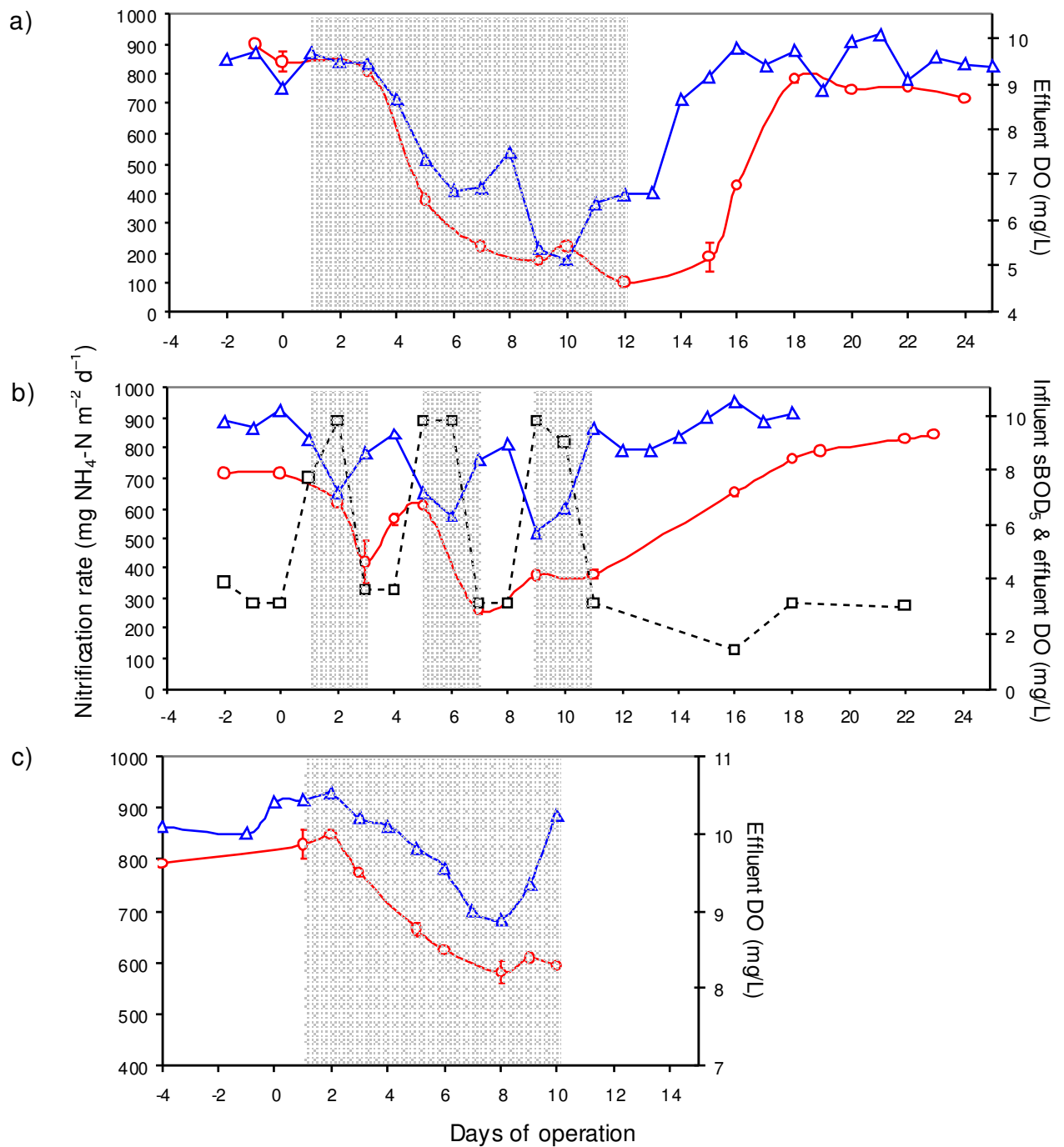
### **5.3.8 Effect of carbon loading and operation time on nitrification: high ammonia-N loaded NTF**

Figure 5.9.a shows the apparent nitrification rate as a function of time during Experiment F, where organic loading was increased to  $1533.5 \pm 510.6 \text{ mg sBOD}_5 \text{ m}^{-2} \text{ d}^{-1}$  ( $8.8 \pm 2.9 \text{ mg sBOD}_5/\text{L}$ ) via the addition of sucrose on day 1. Influent ammonia-N was maintained at  $826.1 \pm 164 \text{ mg NH}_4 \text{ m}^{-2} \text{ d}^{-1}$  ( $4.7 \pm 1.1 \text{ mg/L}$ ). A rapid decline in nitrification rate was observed within 5 d of dosing sucrose. The nitrification rate declined from  $851.0 \pm 46.0 \text{ mg NH}_4\text{-N m}^{-2} \text{ d}^{-1}$  to a steady-state of  $177.18 \pm 58.2 \text{ mg NH}_4\text{-N m}^{-2} \text{ d}^{-1}$  (24.6 % nitrification) between days 7 and 12 of operating under high organic carbon load. Sucrose dosing was terminated on day 12 due to ponding on the media bed surface. The nitrification rate increased thereafter to  $787.0 \pm 10.7 \text{ mg NH}_4\text{-N m}^{-2} \text{ d}^{-1}$  (89 % nitrification) on day 18, 7 d after sucrose dosing ceased. Figure 5.9.a also characterises the NTF's effluent DO concentrations, recorded daily at 12 pm. From the onset of carbon dosing, effluent DO decreased gradually from  $9.4 \pm 0.3 \text{ mg DO/L}$  to steady-state concentrations of  $5.8 \pm 0.7 \text{ mg DO/L}$  on days 7 and 11. Effluent DO responded rapidly to the cessation of carbon dosing on day 12, rapidly increasing to  $8.6 \text{ mg DO/L}$  2 d later. An original steady-state DO concentration of  $9.5 \text{ mg/L}$  was reached 4 d after sucrose dosing had ceased.

Figure 5.9.b shows the apparent nitrification rate as a function of time during Experiment G, where sucrose was spiked intermittently (48-h on / 48-h off) to mimic fluctuations in organic carbon often observed at Buaran WTP. Intermittent carbon spikes were maintained at  $1625.4 \pm 162.7 \text{ mg sBOD}_5 \text{ m}^{-2} \text{ d}^{-1}$  ( $9.4 \pm 0.9 \text{ mg/L}$ ; Figure 5.9.b). Influent ammonia-N was maintained at  $822.4 \pm 61.4 \text{ mg NH}_4\text{-N m}^{-2} \text{ d}^{-1}$  ( $4.8 \pm 0.3 \text{ mg/L}$ ). Results demonstrated that the rate of nitrification progressively worsened with each carbon spike, however small rate increases were observed in between spikes. Nitrification rates had declined from  $717 \pm 0.9 \text{ mg NH}_4\text{-N m}^{-2} \text{ d}^{-1}$  ( $96.4 \pm 0.1 \%$  nitrification) on day 0, to  $258.3 \pm 13.6 \text{ mg NH}_4\text{-N m}^{-2} \text{ d}^{-1}$  ( $32.0 \pm 8.7 \%$ ) by day 9. Sucrose dosing was again terminated after the third spike due to filtrate ponding on the media surface. The nitrification rates increased rapidly thereafter to  $762.0 \pm 8.2 \text{ mg NH}_4\text{-N m}^{-2} \text{ d}^{-1}$  (92.6 % nitrification) on day 12, 3 d after sucrose dosing had ceased.

$\text{N m}^{-2} \text{d}^{-1}$  ( $95 \pm 1.5$  % nitrification), 7 d after sucrose dosing was stopped. Effluent DO fluctuated in response to carbon spiking Figure 5.9.b). During each carbon spike, effluent DO progressively decreased from  $9.8 \pm 0.3$  to  $7.2$  mg/L (1<sup>st</sup> spike), to  $6.3$  mg/L (2<sup>nd</sup> spike), and to  $5.7$  mg/L (3<sup>rd</sup> spike). In between carbon spikes, it can be seen that effluent DO concentrations responded rapidly to the absence of added carbon, increasing immediately to within the range of  $8.3$  to  $9.5$  mg/L.

Figure 5.9.c shows the apparent nitrification rate as a function of time during Experiment H, where organic loading was about half that loaded in Experiments G and F above, and maintained at  $910 \pm 169$  mg sBOD<sub>5</sub>  $\text{m}^{-2} \text{d}^{-1}$  ( $5.3 \pm 1$  mg/L) on day 1. Ammonia-N loading was maintained at  $822 \pm 61$  mg NH<sub>4</sub>-N  $\text{m}^{-2} \text{d}^{-1}$  ( $4.8 \pm 0.3$  mg/L), the same as used for Experiments G and F. Similar to Experiment F, nitrification rates decreased to a steady-state within a similar time period of 8 to 10 d, despite operating under a lower organic load. In comparison to Experiment F, the magnitude of nitrification suppression observed during Experiment H was not as severe, where nitrification rates had decreased from  $821 \pm 29$  to  $601.7 \pm 20$  mg NH<sub>4</sub>-N  $\text{m}^{-2} \text{d}^{-1}$  (74 % nitrification; Figure 5.9.c) within 8 d of increasing the organic load. Similar to Experiments E and G, effluent DO concentrations fluctuated in response to carbon loading. From the onset of carbon dosing, effluent DO decreased gradually from  $10.4$  to  $8.9$  mg/L within 8 d, and increased rapidly back to steady-state concentrations once sucrose dosing was stopped.



**Figure 5.9.** NTF nitrification performance as a function of time, once influent sBOD<sub>5</sub> concentration was increased on day 1 by the addition of sucrose: (a) Experiment F– influent organic carbon concentration was increased to  $8.8 \pm 2.9$  mg sBOD<sub>5</sub>/L; influent ammonia-N was maintained at  $4.7 \pm 1.1$  mg NH<sub>4</sub>-N/L; (b) Experiment G– influent organic carbon was dosed intermittently to concentrations of  $9.4 \pm 0.9$  mg sBOD<sub>5</sub>/L;

influent ammonia-N was maintained at  $4.8 \pm 0.5$  mg  $\text{NH}_4\text{-N/L}$ ; and (c) Experiment H–influent organic carbon concentration was increased to  $5.3 \pm 1.0$  mg  $\text{sBOD}_5\text{/L}$ ; influent ammonia-N was maintained at  $4.8 \pm 0.3$  mg  $\text{NH}_4\text{-N/L}$ . Symbols denote: nitrification rate ( $\circ$ ); effluent DO ( $\triangle$ ); and influent  $\text{sBOD}_5$  ( $\square$ ). Shaded regions represent the duration of carbon dosing. (Daily parameter means shown  $\pm 1$  SD).

### **5.3.9 Nitrification depth profile and nitrogen budget: High ammonia-N loaded NTF**

To monitor the impact of organic carbon on the nitrification performance within a high ammonia-N loaded NTF ( $\approx 5.0$  mg  $\text{NH}_4\text{-N/L}$ ), profiles of inorganic nitrogen species were measured throughout the NTF at time intervals of 2 to 4 d during each experiment. Representative steady-state profiles of the NTF taken: (i) before increasing the organic carbon load (Experiment A); (ii) when operated under high influent organic concentrations above 5.3 mg  $\text{sBOD}_5\text{/L}$  (Experiments F, G and H); and (iii) during filter recovery, once organic carbon dosing was stopped; are given in Figure 5.10. The ammonia concentration profile data also provided a basis with which to calculate and compare nitrification rates through the NTF bed in response to high organic loads (Figure 5.12).

All profiles (Figure 5.10) showed that significant ammonia-N oxidation to nitrate occurred at the upper filter depth of 0.3 m. Although nitrite was detected, nitrite-N accumulation was not observed for any experiment, where concentrations remained below 0.3 mg  $\text{NO}_3\text{-N/L}$  throughout the entire NTF bed depth. Profiles of ammonia-N, nitrite-N, and nitrate-N taken before carbon dosing commenced (day 0), for Experiments F, G and H appeared similar (Figure 5.10.a). Complete nitrification was consistently observed, whereby the final effluent contained only nitrate. In contrast to Figure 5.10.a, inorganic nitrogen profiles taken when operated under higher organic carbon loads (Experiments F and G) showed a significant decline in nitrification throughout the filter bed.

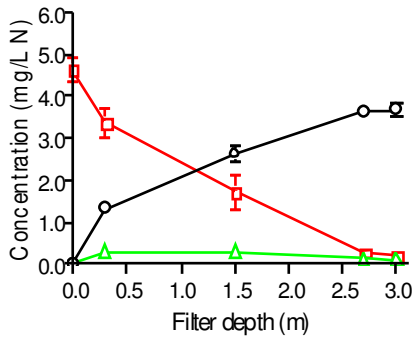
Figure 5.10.b shows the mean of four depth profile of ammonia-N, nitrite-N, and nitrate-N observed during Experiment F, on days 6, 8, 11 and 13, after influent  $\text{sBOD}_5$  was increased from  $1.3 \pm 0.5$  mg/L ( $225.2 \pm 87.9$  mg  $\text{sBOD}_5 \text{ m}^{-2} \text{ d}^{-1}$ ) and maintained at  $8.8 \pm 2.0$  mg/L ( $1533.5 \pm 510.6$  mg  $\text{sBOD}_5 \text{ m}^{-2} \text{ d}^{-1}$ ). Figure 5.10.c shows a profile taken on day 8 of Experiment G, which operated under similar organic and nitrogen loads to that of Experiment F, however sucrose was dosed intermittently to mimic fluctuations in

Buaran's organic carbon regime. Both profiles appeared similar, where a significant decline in ammonia-N removal throughout the entire filter bed was observed. Small concentrations of nitrate-N were detected, which complemented the decrease in ammonia-N. Figure 5.10.d shows an inorganic nitrogen profile of the NTF during Experiment H, when influent sBOD<sub>5</sub> was reduced from 8.8 mg/L ( $1533.5 \pm 510.6 \text{ mg sBOD}_5 \text{ m}^{-2} \text{ d}^{-1}$ ) to  $5.3 \pm 1 \text{ mg/L}$  ( $910.9 \pm 169.1 \text{ mg sBOD}_5 \text{ m}^{-2} \text{ d}^{-1}$ ). Results demonstrated a significant improvement in nitrification throughout the NTF column in response to the decrease in organic loads, however in comparison to periods of lower organic loads (Figure 5.10.a), impeded nitrification through the NTF column was still evident, and was most apparent for the top 1.5 m.

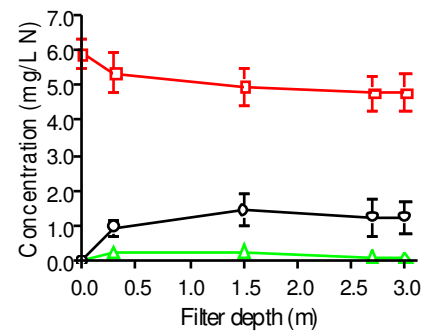
Figure 5.10.e shows the recovery of nitrification through the NTF after termination of sucrose dosing. Each data point represents the mean of several daily average values compiled from all experiments, between days 10 to 12 after sucrose dosing was terminated. When compared with Figure 5.10.a (before carbon dosing), filter bed profiles of ammonia-N, nitrite-N and nitrate-N appeared identical.

For all experiments, a nitrogen budget demonstrated that only 2 to 5 % of ammonia-N removed (0.1–0.25 mg N/L) was not recovered in the form of nitrite-N or nitrate-N within the filters effluent (Figure 5.11), highlighting that a large fraction of ammonia-N removal was accounted for by nitrification. The mass of unreconciled nitrogen appeared to be a function of carbon loading and removal. When grouping all the data together (obtained from both low- and high-ammonia loaded experiments), statistical analysis using Spearman's correlation confirmed that the mass of nitrogen (mg/L) lost from the system increased linearly with an increase in sBOD<sub>5</sub> loading and removal (respectively  $r_s = 0.46, 0.44; p < 0.05$ ), which may be attributed to nitrogen assimilation and/or conversion of nitrate to nitrogen gas via denitrification.

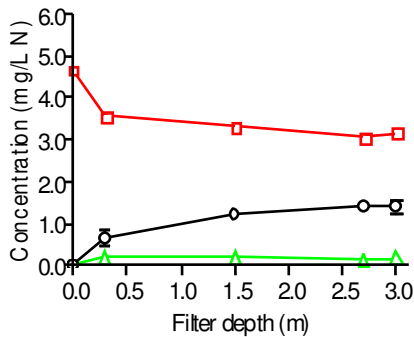
a) Day 0: no carbon addition– 1.3 mg sBOD<sub>5</sub>/L



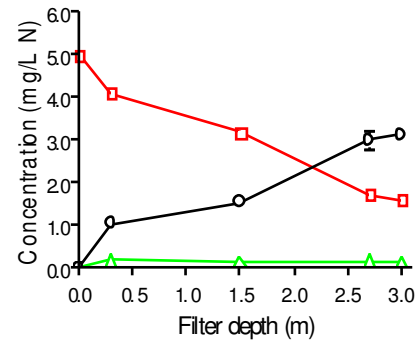
b) Days 6–13: sucrose addition– 8.8 mg sBOD<sub>5</sub>/L



c) 3<sup>rd</sup> sucrose spike– 9.4 mg sBOD<sub>5</sub>/L



d) Day 6: sucrose addition– 5.3 mg sBOD<sub>5</sub>/L



e) Recovery: carbon dosing terminated

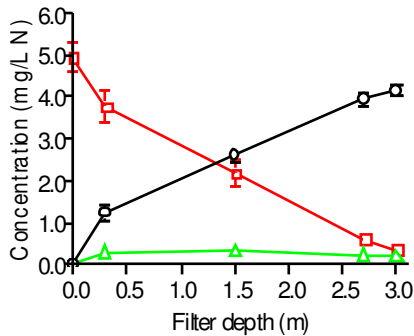
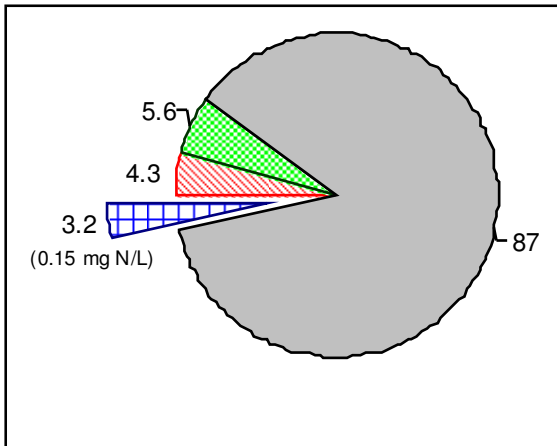


**Figure 5.10.** Concentration profiles of inorganic nitrogen species measured throughout the depth of the NTF: (a) mean of 3 profiles observed when the NTF operated under low influent organic carbon concentrations of 1.3 mg sBOD<sub>5</sub>/L; (b) mean of 4 profiles obtained from Experiment F, 6

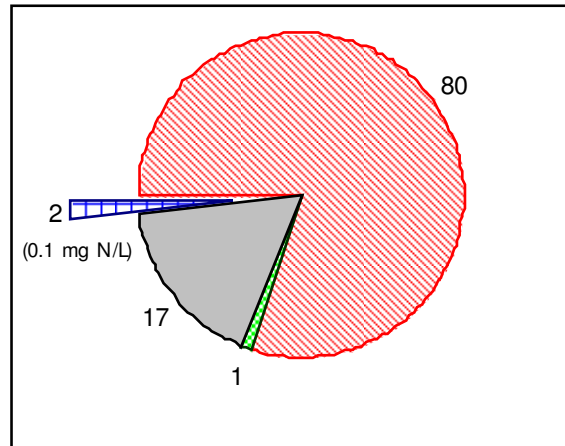
to 13 d after increasing the influent organic carbon concentration to  $8.8 \pm 2.9$  mg sBOD<sub>5</sub>/L via the addition of sucrose; (c) profile observed after the third carbon spike for Experiment G, where the influent organic carbon concentration was increased intermittently to  $9.4 \pm 0.9$  mg sBOD<sub>5</sub>/L via the addition of sucrose; (d) profile obtained from Experiment H, when operated under influent organic carbon concentrations of  $5.3 \pm 1.0$  mg sBOD<sub>5</sub>/L via the addition of sucrose; and (e) recovery profile, observed once

the influent organic carbon concentration was returned to background concentrations of 1.3 mg sBOD<sub>5</sub>/L. For all experiments Influent ammonia-N concentrations were maintained steady at  $4.8 \pm 0.5$  mg NH<sub>4</sub>/L. Symbols denote: (□) ammonia-N; (△) nitrite-N; and (O) nitrate-N. (Data points represent the mean of multiple experimental observations  $\pm$  1 SD).

a) No carbon addition— 1.3 mg sBOD<sub>5</sub>/L



b) Days 6-13: sucrose addition— 8.8 mg BOD<sub>5</sub>/L



c) Day 6: sucrose addition— 5.3 mg sBOD<sub>5</sub>/L

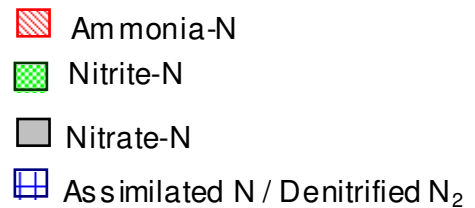
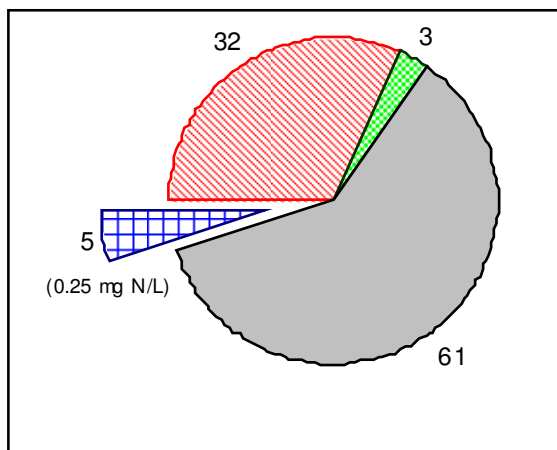


**Figure 5.11.** Inorganic nitrogen mass-balance showing effluent nitrogen species composition as percentage of total inorganic nitrogen. Inorganic nitrogen not accounted for is represented as “assimilated / Denitrified N<sub>2</sub>”. Influent ammonia-N represented 100 % of total nitrogen present. (a) Experiment A— low influent organic carbon concentrations of 1.3 sBOD<sub>5</sub>/L, with no external carbon addition; (b) mean obtained from Experiments F and G, 6 to 13 d after increasing the influent organic carbon concentration to 8.8 mg sBOD<sub>5</sub>/L via the addition of sucrose; and (c) Experiment H— when operated under influent organic carbon concentration of 5.3 ± 1.0 mg sBOD<sub>5</sub>/L via the addition of sucrose.

Ammonia profile data collected from the NTF provided a basis for calculating nitrification rates at depths through the NTF. The operational data set was divided into periods of uniform ammonia concentration loads ( $5.0 \pm 0.7$  mg/L) and sBOD<sub>5</sub> concentration loads of  $1.3 \pm 0.5$  (native background concentration),  $5.3 \pm 1.0$  mg/L (sucrose addition) and  $8.8 \pm 2.9$  mg/L (sucrose addition). Differences in nitrification performance were based on comparing nitrification rates along the NTF, and were evaluated by Kruskal–Wallis ANOVA with Dunn’s multiple comparison testing. Figure 5.12 shows the nitrification rates measured through the NTF for each influent sBOD<sub>5</sub> concentration load. The data presented, represents the mean of 3 to 4 individual sampling events. Results show that a significant decline in nitrification rate throughout the entire filter bed had occurred once the influent sBOD<sub>5</sub> concentration was increased to 5.3 and 8.8 mg/L via the addition of sucrose. The most significant decline in nitrification rate was observed within the upper bed depths of 0.3 ( $p < 0.05$ ) and 1.5 m ( $p < 0.05$ ). Results confirmed that the hypothesised improvement in nitrification throughout the lower depths of the NTF, in response to high organic loads did not occur.

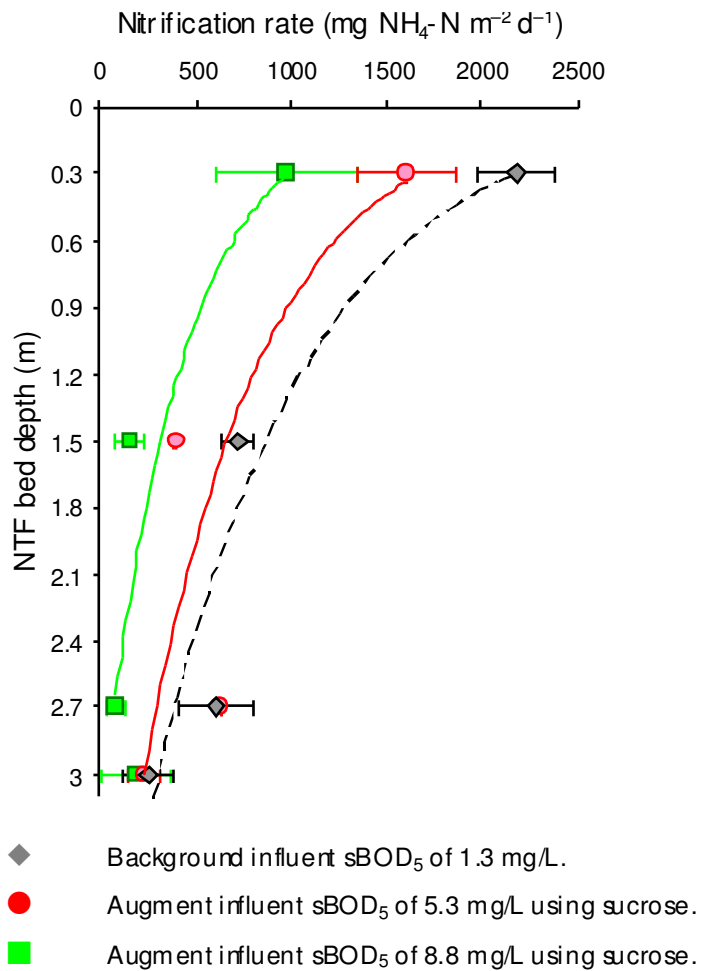
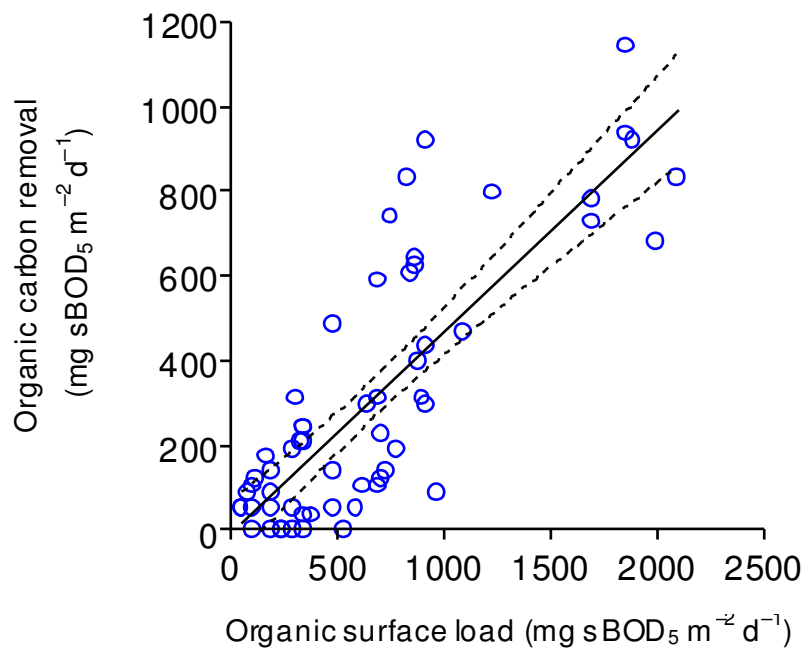


**Figure 5.12.** Comparison of nitrification rates measured down the large pilot-scale NTF during operational periods of high and low influent  $\text{sBOD}_5$  concentrations. High influent ammonia-N concentrations fixed at  $5.0 \pm 0.7 \text{ mg NH}_4\text{-N m}^{-2} \text{d}^{-1}$ . (Data points show the mean of a minimum of 3 separate sampling intervals  $\pm 1 \text{ SD}$ ).

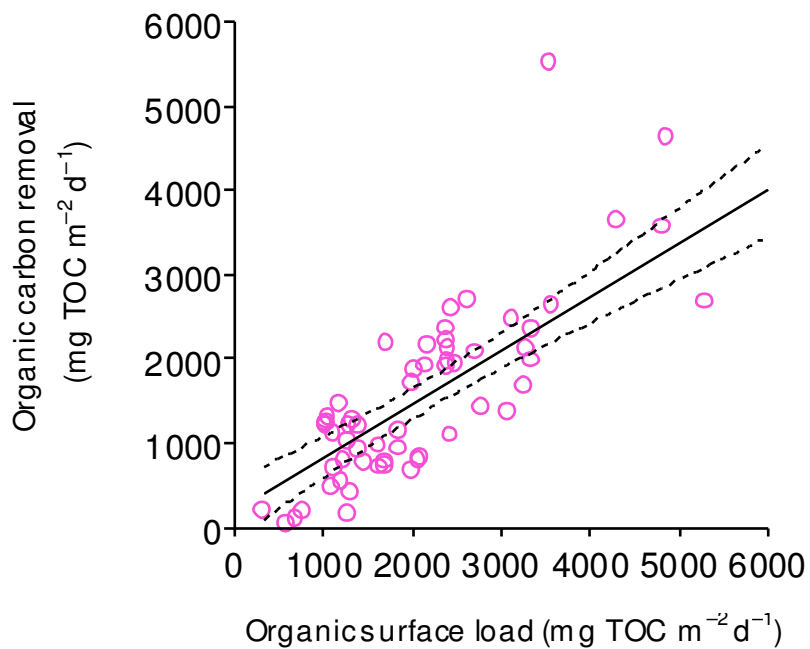
### 5.3.10 Organic carbon removal

Figure 5.13 shows a linear relationship between sBOD<sub>5</sub> loading and sBOD<sub>5</sub> removal, which was obtained for all experiments (Pearson's  $r = 0.82$ ;  $p < 0.0001$ ; Table 5.2). Mean sBOD<sub>5</sub> removal was  $47.6 \pm 34\%$  and had ranged between 8.8 and 100%. A maximum removal of  $1.1 \text{ g sBOD}_5 \text{ m}^{-2} \text{ d}^{-1}$  was observed. An increase in sBOD<sub>5</sub> removal correlated well with a decrease in percentage nitrification, signifying that a shift from a nitrifying system to a predominantly carbon oxidation system had occurred ( $r = -0.82$ ;  $p < 0.01$ ; Table 5.2). A positive correlation between C:N ratio and rate of sBOD<sub>5</sub> removal was also observed ( $r = 0.67$ ;  $p < 0.001$ ; Table 5.2).

Figure 5.14 shows a linear relationship between TOC loading and TOC removal, which was also obtained from all experiments ( $r = 0.73$ ;  $p < 0.0001$ ). Mean TOC removal was  $25.2 \pm 23\%$ , and had ranged between 0 to 88% throughout the course of the study. A maximum removal of  $5.51 \text{ g TOC m}^{-2} \text{ d}^{-1}$  was observed. Representative steady-state profiles of TOC and sBOD<sub>5</sub> measured throughout the NTF for Experiments C, F, G and H, which operated under various influent sBOD<sub>5</sub> concentrations, ranging from 5.4 to 9.4 mg sBOD<sub>5</sub>/L are presented in Figure 5.15. Depth profiles show good agreement between TOC and sBOD<sub>5</sub> concentrations ( $r = 0.67$ ;  $n = 54$ ;  $p < 0.0001$ ). Results show that TOC and sBOD<sub>5</sub> removal were highest at bed depth of 0.3 m from the surface and declined with depth;  $34 \pm 5.5\%$  and  $17.3 \pm 10.3\%$  removal of sBOD<sub>5</sub> and TOC respectively occurred at 0.3 m. The increase in filtrate TOC and sBOD<sub>5</sub> concentrations seen at some filter bed depths may be an artefact of biomass detachment.



**Figure 5.13.** Relationship between sBOD<sub>5</sub> surface load and removal rate. Broken lines represent 95 % confidence bands.



**Figure 5.14.** Relationship between TOC surface load and removal rate. Broken lines represent 95 % confidence bands.

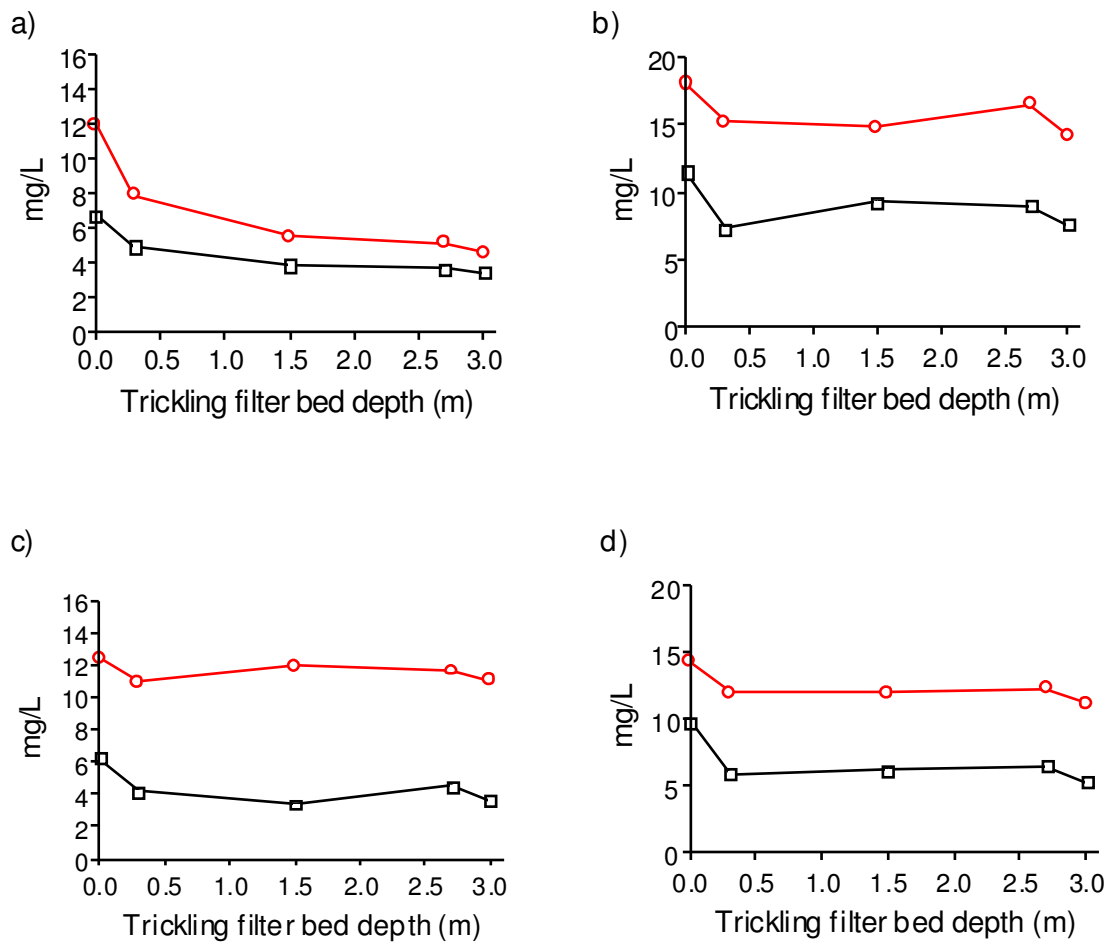


**Figure 5.15.** Concentration profiles of TOC (○) and sBOD<sub>5</sub> (□) measured throughout the NTF. (a) Profile obtained from Experiments C, when operated under influent organic carbon concentrations of  $5.4 \pm 0.5$  mg sBOD<sub>5</sub>/L via the addition of sucrose. Influent ammonia-N was maintained at  $0.56 \pm 0.1$  mg N/L; (b) profile obtained from Experiment F, when operated under influent organic carbon concentrations of  $8.8 \pm 2.9$  mg sBOD<sub>5</sub>/L via the addition of sucrose. Influent ammonia-N was maintained at  $4.7 \pm 1.1$  mg N/L; (c) profile obtained from Experiment G, where the influent organic carbon concentration was increased intermittently to  $9.4 \pm 0.9$  mg sBOD<sub>5</sub>/L via the addition of sucrose. Influent ammonia-N was maintained at  $4.8 \pm 0.5$  mg N/L; and (d) profile obtained from Experiment H, when operated under influent organic carbon concentrations of  $5.3 \pm 1.0$  mg sBOD<sub>5</sub>/L via the addition of sucrose. Influent ammonia-N was maintained at  $4.8 \pm 0.3$  mg N/L.

### **5.3.11 Environmental parameters**

To determine the potential influence of environmental parameters on nitrification, Spearman's correlation analysis was used to identify relationships between percentage nitrification with pH, temperature, alkalinity, and DO. During all experiments, influent DO and alkalinity were stable, measuring  $5.9 \pm 0.4$  mg DO/L and  $113.7 \pm 5.1$  mg CaCO<sub>3</sub>/L respectively, and did not correlate with percentage nitrification ( $p > 0.05$ ; Table 5.2). No relationship between nitrification and influent temperature was identified, despite significant variations in temperature which ranged from 10.4 to 21.8°C ( $p > 0.05$ ; Table 5.2). Influent pH remained very stable at  $7.9 \pm 0.16$ , however correlated well with nitrification ( $r_s = 0.557$ ;  $p < 0.05$ ; Table 5.2). Temperature correlated with pH, DO, and total alkalinity ( $p < 0.05$ ; Table 5.2), a likely indication of sequential seasonal change within the source water.

For the duration of this study, online measurements showed that influent DO concentrations were stable, however effluent DO fluctuated in response to organic loading. When operated under low organic loads below  $870 \text{ mg sBOD}_5 \text{ m}^{-2} \text{ d}^{-1}$  ( $< 5.0$  mg sBOD<sub>5</sub>/L), NTF effluent DO was saturated measuring  $9.6 \pm 0.5$  mg/L. A inverse linear relationship between effluent DO and influent sBOD<sub>5</sub> concentration was observed once influent sBOD<sub>5</sub> was increased beyond 5 mg/L via the addition of sucrose ( $r_s = -0.735$ ;  $p < 0.0001$ ; Figure 5.16; Table 5.2). In addition, effluent DO correlated well with sBOD<sub>5</sub> removal ( $r_s = -0.786$ ;  $p < 0.0001$ ) and percentage nitrification ( $r_s = 0.793$ ;  $p < 0.0001$ ; Figure 5.17; Table 5.2). The decline in effluent DO in response to an increase in influent sBOD<sub>5</sub> concentration and sBOD<sub>5</sub> removal may be attributed to heterotrophic respiration of the organic substrate. From Figure 5.17, it can be seen that maximum nitrification performance was achieved when effluent DO concentrations were greater than 9 mg/L, and decreased within the range of 15 to 40 % when effluent DO concentrations were less than 7.0 mg/L.

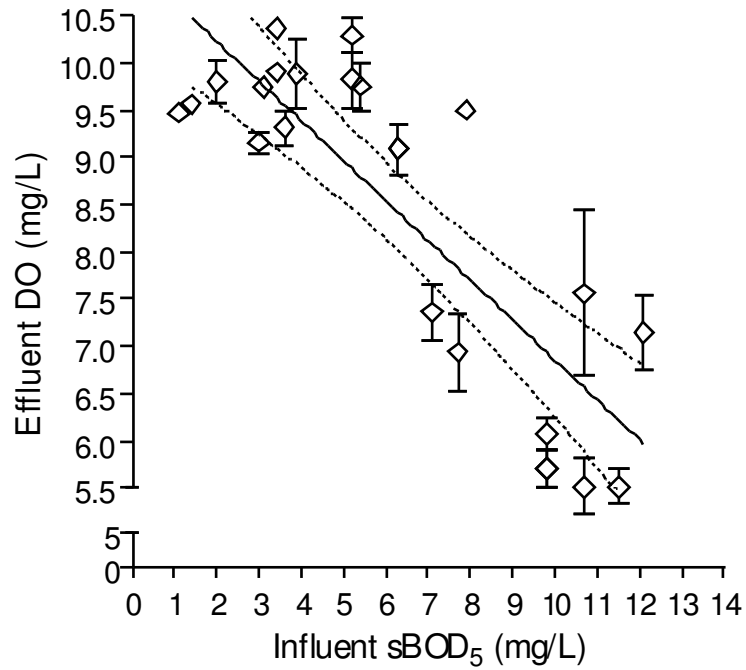


**Figure 5.16.** Steady-state relationship between influent sBOD<sub>5</sub> concentration and effluent DO. Data points represent mean of daily values logged at 10 minute intervals, obtained from Experiments E, F, G and H. Data was obtained at influent temperatures between 17–21°C. (Data points represent mean values  $\pm$  1 SD; broken lines represent 95 % confidence bands for the fitted line).



### **5.3.12 Nitrification model**

The Pearce (1999) nitrification model is used to predict effluent ammonia-N concentration in response to ammonia-N and total BOD<sub>5</sub> surface loading. Two simulations were computed and were compared with observed performance values obtained from the current pilot study (Figure 5.18). It should be noted that the Pearce (1999) model was derived and computed using total BOD<sub>5</sub> values, unlike this study which measured soluble carbonaceous BOD<sub>5</sub>.

#### **Simulation 1**

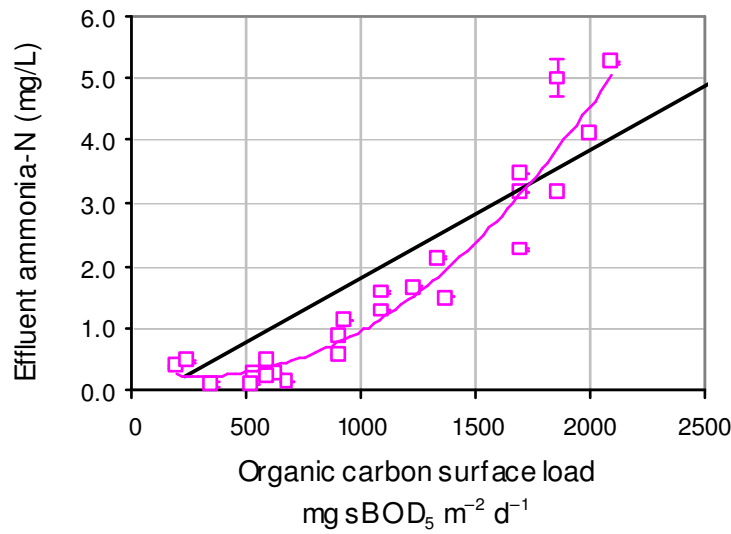
To validate the model, the pilot-plant NTF was firstly operated under fixed ammonia-N load of  $815 \pm 130 \text{ mg m}^{-2} \text{ d}^{-1}$  ( $\approx 5.0 \text{ mg/L}$ ) which represented a value within the range for wastewater from which the model was derived, and also represented the maximum nitrogen load the filter would be expected to operate under at Buaran WTP. Figure 5.18.a shows the predicted and observed effluent ammonia-N breakthrough curve in response to sucrose augmented organic loads. It can be seen that the predicted and observed ammonia-N values were comparable. Both show a significant linear increase in effluent ammonia-N when organic surface loading was increased from 250 to 1500  $\text{mg sBOD}_5 \text{ m}^{-2} \text{ d}^{-1}$ . When organic surface loading was increased beyond 1500  $\text{mg sBOD}_5 \text{ m}^{-2} \text{ d}^{-1}$ , observed values began to deviate from the predicted curve; whereby effluent ammonia-N had increased more rapidly in response to higher organic loads than predicted by the model.

#### **Simulation 2**

For the second simulation the NTF was operated under low ammonia-N loads maintained between 96 to 220  $\text{mgNH}_4\text{-N m}^{-2} \text{ d}^{-1}$  (equivalent to 0.5 – 1.3  $\text{mg/L}$ ) which represented typical operating loads expected for Buaran WTP, and was below the range from which the Pearce (1999) model was derived. From Figure 5.18.b it can be seen that observed effluent ammonia-N concentrations increased more rapidly in response to an increase in sucrose augmented sBOD<sub>5</sub> loads than predicted by the model. When sucrose was substituted with a less readily biodegradable carbon source

(soluble organic fertiliser), observed and predicted effluent ammonia-N values were comparable, where predicted and observed ammonia-N removal measured 93 and 91 % respectively. These findings suggest that the model did not fit the observed data obtained at higher organic loadings imposed by a readily available carbon source like sucrose, however worked well for the more native-like carbon source (organic fertiliser), and therefore suggests that the model was highly dependant on the nature of the influent organic carbon.

a) Simulation 1.



b) Simulation 2.

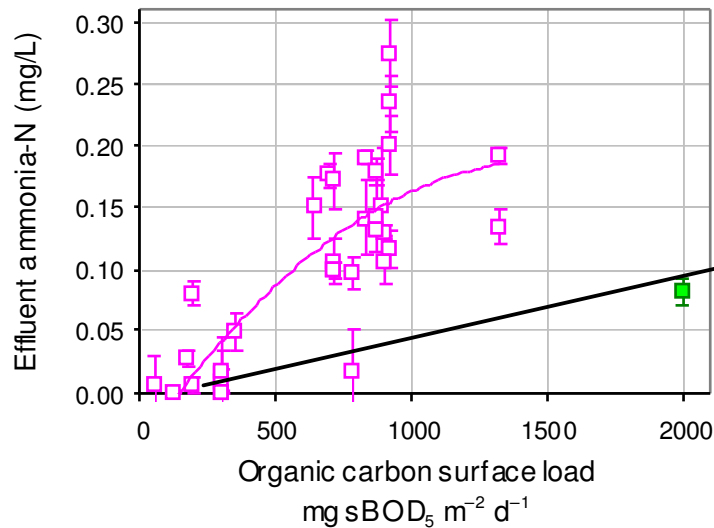


**Figure 5.18.** Observed and predicted effluent ammonia-N concentration as a function of organic surface load. (a) Simulation 1: high influent ammonia-N concentration maintained at 5.0 mg/L ( $815 \text{ mg NH}_4\text{-N m}^{-2} \text{ d}^{-1}$ ) and variable  $\text{sBOD}_5$  surface loading. (b) Simulation 2: low influent ammonia-N concentration maintained at 0.55 mg/L ( $96 \text{ mg NH}_4\text{-N m}^{-2} \text{ d}^{-1}$ ) and variable sucrose induced  $\text{sBOD}_5$  surface loads; and 1.3 mg  $\text{NH}_4\text{-N/L}$  ( $220 \text{ mg NH}_4\text{-N m}^{-2} \text{ d}^{-1}$ ) for soluble organic fertiliser induced  $\text{sBOD}_5$  surface loads. Plotted data represents: predicted model output (—); observed values using sucrose ( $\square$ ); and observed values using soluble organic fertiliser ( $\blacksquare$ ).

## 5.4 Discussion

The effect of organic carbon on nitrification in fixed-film processes treating high-strength wastewater is widely documented, however, little is known about their application for raw source water for potable water treatment where influent ammonia-N and BOD<sub>5</sub> concentrations are 10- to 50-fold lower. Although ammonia and BOD<sub>5</sub> concentrations of Buaran raw water are low, C:N ratios were similar to that of municipal wastewater. Consequently, it was necessary to consider the possibility of nitrification suppression caused by heterotrophs which may interfere with the ammonia removal processes. The experimental component of this chapter investigated the impact of organic carbon on the nitrifying capacity of a pilot-scale NTF designed to remove low concentrations of ammonia-N. A series of experiments were conducted which simulated variations in inorganic nitrogen and organic carbon at concentrations observed in Buaran's WTP raw source water. Variations in carbon loads were achieved by dosing mostly sucrose, either for prolonged periods, or intermittently, to mimic fluctuations in organic carbon delivery observed at Buaran WTP. The influence of a more native organic carbon source on NTF performance was also investigated. In addition, performance data was compared with the Pearce (1999) NTF model, developed from several wastewater NTFs. The influence of carbon loading on nitrification and nitrification profile down the pilot NTF will be discussed.

An external organic carbon source was required to mimic typical BOD<sub>5</sub> concentrations of Buaran WTP raw water. It was hypothesised that the carbonaceous matter within Buaran raw water might be recalcitrant due to the native biomass consuming all of the readily biodegradable substrates before the water reaches the WTP. However, similar to sucrose, the respirometry curve of Buaran raw water shows that the carbonaceous matter was largely available and consequently exerted a high BOD on day 1 (Figure 5.1). Therefore, sucrose was initially selected because, somewhat surprisingly, the BOD respiration curve followed that of the raw water of the Buaran WTP. It was later postulated that organic carbon in Buaran raw water might not be as readily available as sucrose. Due to the polluted nature of Buaran raw water, and subsequent high

bacteriological bad, it was hypothesised that the raw water might contain a native population that was acclimatised to the native carbon present within the catchment. The native population may be responsible for the high oxygen demand observed on day 1 of the biodegradability test. To test this hypothesis, biodegradation curves of what was thought to be representative of a recalcitrant carbon source (soluble organic fertiliser) was compared with Buaran raw water and sucrose. Low oxygen demand exerted by the organic fertiliser at 24 and 48 h was an indicator that organic fertiliser had more of a recalcitrant nature than sucrose or Buaran raw water. However, when the organic fertiliser biodegradability test was repeated using a seed inoculum previously acclimatised, similar biodegradation curve to Buaran raw water and sucrose was observed. Results suggest that the seed inoculum was capable of utilising the carbon immediately, unlike the non-seeded sample, which demonstrated lag-phase-like characteristics. The BOD test was therefore an effective method for identifying distinct differences between sucrose and soluble organic fertiliser biodegradability by measuring the rate of oxygen uptake. However, using this method to ascertain the degree of organic carbon biodegradability of Buaran's raw water was inconclusive; since the biodegradation curve of organic carbon from Buaran's raw water behaved similarly to both the seeded organic fertiliser and the sucrose biodegradation curve.

The outcome of respirometry measurements is dependent upon both the nature of the carbon source, which could not be ascertained for the Buaran water, and the presence of a biota acclimated to, and capable of, degradation of the carbon source. Clearly, the carbon source within the organic fertiliser was both available and suitable for degradation by a competent microbial population. Furthermore, the evidence suggests—from the production of the seed inoculum for the BOD measurements on the organic fertiliser—that this competent population could be developed within 7 d. Consequently, the organic fertiliser may not be as recalcitrant a carbon source as first suggested. The influence of this source of carbon substrate, which would clearly be different from sucrose, on the nitrifying performance of a NTF was investigated.

For this study, nitrification was strongly impacted upon by organic loading rate. Complete nitrification occurred only when influent sBOD<sub>5</sub> was maintained below 4.0 mg/L. A negative relationship between ammonia-N removal and influent sBOD<sub>5</sub> was identified, where a steady decline in ammonia-N removal was observed once influent sBOD<sub>5</sub> was increased from 5.0 to 12.1 mg/L by the addition of sucrose. When sucrose was substituted with methanol, equal decline in nitrification performance occurred, which confirmed that nitrification inhibition was independent of these two carbon sources. Current findings, which were obtained from a NTF operated under low ammonia-N concentrations, are parallel to observations obtained from wastewater fixed-film reactors and NTFs. Harremoes (1982) demonstrated that the nitrification rate of a wastewater fixed-film reactor was highest when the influent sBOD<sub>5</sub> concentration was below 5 mg/L, and was inhibited at concentration above 5 mg/L. Similarly, Huang and Hopson (1974) demonstrated a steady inhibition of nitrification once sBOD<sub>5</sub> concentration was increased from 1.0 to 8.0 mg/L, and Figueroa and Silverstein (1991) reported inhibition of nitrification in wastewater NTFs at sBOD<sub>5</sub> concentrations above 10 mg/L.

Nitrification efficiency was correlated negatively with sucrose and methanol-induced volumetric sBOD<sub>5</sub> loading. Due to the high hydraulic load under which the filter was operated, the BOD<sub>5</sub> loads applied in this study were parallel to those encountered by many low flow rate wastewater NTFs (see Chapter 1, Table 1.1; Metcalf and Eddy 2003). 90 to 100 % of nitrification occurred when the organic loading rate was less than 0.14 kg sBOD<sub>5</sub> m<sup>3</sup> d<sup>-1</sup>, and had reduced to 50 % and 10 % at 0.35 and 0.52 kg sBOD<sub>5</sub> m<sup>3</sup> d<sup>-1</sup> respectively. These findings are in agreement with the design loading criteria for trickling filters described by Metcalf and Eddy (2003), who suggested that for a well nitrified effluent, typical organic loads of trickling filters ranged between 0.07 to 0.22 kg sBOD<sub>5</sub> m<sup>3</sup> d<sup>-1</sup>. Previous review data collated by Metcalf and Eddy (2003) on wastewater NTFs, suggested that 90 % of nitrification capacity can be expected at organic loads less than 0.08 kg sBOD<sub>5</sub> m<sup>3</sup> d<sup>-1</sup>, whereas inhibition of nitrification can be expected to occur under organic loads greater than 0.6 kg sBOD<sub>5</sub> m<sup>3</sup> d<sup>-1</sup>.

Results from this study have confirmed that organic surface load, and not C:N ratio, was the crucial factor regulating the nitrification capacity of the pilot NTF. No significant correlation between C:N and percentage nitrification was identified. Furthermore, when the NTF was operated under high carbon loads, increasing the influent ammonia-N concentration, in order to lower influent C:N ratio, did not improve nitrification as determined by both percentage nitrification and nitrification rate. For any given organic carbon load, nitrification rates ( $\text{mg NH}_4\text{-N removed m}^{-2} \text{d}^{-1}$ ) appeared to increase with the increase in ammonia surface loads, however this observation was merely an artefact of higher ammonia concentration loads. In contrast, Strauss and Lamberti (2000) showed that for aquatic systems low in nitrogen, the C:N ratio was a critical factor in the regulation of nitrification, whereby heterotrophic bacteria were subject to nitrogen limitation and competed with nitrifiers for available nitrogen. Strauss and Lamberti (2000) augmented TOC concentrations via the addition of glucose to fresh water stream sediments in order to investigate the effects of C:N ratio (defined as  $\text{TOC/NH}_4\text{-N}$ ) on nitrification rates. Their results confirmed that a high C:N ratio of 40 increased competition and metabolic need for ammonia by the heterotrophic community, and decreased the amount of nitrogen available to the nitrifiers, which in turn, lowered nitrification rates. In contrast to the findings of the current study, Strauss and Lamberti (2000) also reported that when ammonia was increased, so as to lower the C:N ratio, competition for nitrogen diminished, which resulted in increased nitrogen availability for nitrifiers, and improved nitrification rates. Similar observations were also reported by Verhagen and Laanbroek (1991) in a nitrogen-limited environment.

For the current study, within the influent  $\text{sBOD}_5$  or C:N ratio ranges used ( $\text{sBOD}_5/\text{NH}_4\text{-N}$ , 1 to 10;  $\text{TOC/NH}_4\text{-N}$ , 4 to 20), nitrogen was not at rate-limiting concentrations, where assimilative demands required only 2 to 25 % of total available nitrogen, which implies that excess nitrogen was available to the heterotrophic community in relation to the amount of available organic carbon. Since nitrogen was in sufficient supply, even during high organic loads, it was probable that nitrification was regulated by the heterotrophic communities' metabolic need and competition for oxygen, rather than competition for nitrogen. It was likely that heterotrophic competition for oxygen increased with carbon

load, as reported by Zhang *et al.* (1994). The de-oxygenation of the filter's effluent in response to higher organic carbon loads may support this hypothesis, however does not necessarily reflect competitive interactions for oxygen; which may be occurring locally within the biofilm. Therefore, for a system where nitrogen was sufficient, this study found that carbon loading, and the subsequent competition for DO that it promotes, rather than C:N ratio, was most likely the primary factor controlling nitrification. However, if oxygen was sufficient, Zhang *et al.* (1994) reported that high concentrations of organic carbon does not inhibit nitrification, rather nitrogen concentration or the C:N ratio becomes the controlling factor, as observed by Strauss and Lamberti (2002) in well oxygenated sediments.

Results obtained during this pilot study confirmed that additional loads of organic carbon, via the addition of sucrose or methanol, reduced the nitrifying capacity of the trickling filter. Regardless of carbon loading and influent C:N ratio, the nitrification capacity for all experiments decreased to steady-state performance within a similar time period of 8 to 10 d after the onset of carbon dosing. For Experiment B, where carbon loading was maintained for 60 consecutive days, ammonia removal increased after 40 d, which could be attributed to (i) simultaneous nitrification-denitrification and/or (ii) heterotrophic uptake (see Section 5.3.7). After 60 d of operating under high carbon loads, the NTF support media collapsed under its own weight due to excessive biomass production. Media clogging, caused by biomass and subsequent preferential channelling and pooling of water, was thought to have contributed to the collapse of the support media. A visual inspection of the media at all biofilm sample sites revealed the presence of a thicker biofilm which exerted a "jelly-like" appearance, consistent with the characteristics of copious EPS production. The extent of heterotrophic development and EPS production in response to organic carbon application is recommended as a subject for further investigation (see Chapter 6). The pilot NTF was decommissioned and a new filter with additional internal media support stands was constructed (see Chapter 3, Section 3.3.5). For the following high carbon loading experiments, the duration of sucrose dosing was kept below 14 d to prevent potential and irreversible damage to NTF support media. It was possible that the increase in ammonia removal observed

during Experiment B after 40 d of carbon dosing may have also occurred in other experiments, if carbon dosing was permitted beyond 40 d.

Results from the current study have also confirmed that intermittent carbon spikes, operating in cycles of 48-h on: 48-h off, had an equal inhibitory effects on the NTF's nitrifying capacity to that observed during times of a continuous carbon dosing regime. Nitrification suppression may have been due to heterotrophs out-competing nitrifiers for oxygen; a phenomenon that has been widely documented (Okabe *et al.* 1996; van Benthum *et al.* 1998; Satoh *et al.* 2000; van Loosdrecht *et al.* 2000). The oxygenation and de-oxygenation of the filter's effluent observed here in response to the absence and presence of carbon, was characteristic of heterotrophic competition for oxygen.

In order to regain nitrification capacity following conditions of increased sBOD<sub>5</sub> loading, carbon dosing (sucrose or methanol) was stopped. As soon as the influent sBOD<sub>5</sub> was decreased to background concentrations, immediate improvements in nitrification occurred within 1 to 2 d. Obviously, a substantial fraction of nitrifiers had survived within the biofilm to allow for a rapid population recovery. In the absence of a carbon substrate, and following the decline in heterotrophic competition for oxygen, it was probable that the nitrifiers which survived had regained access to oxygen, which then permitted the immediate improvement in nitrifying activity. For all experiments, original steady-state nitrification performance was reached within 8 d after carbon dosing had ceased. Within this time period, high ammonia conversion to nitrate was consistently observed, however complete recovery throughout the entire filter bed required an additional 2 to 4 d. For all experiments, nitrite accumulation was not observed, suggesting equilibrium persistence of AOB and NOB during both favourable and unfavourable conditions.

Results from this study have demonstrated that nitrification was reduced to negligible amounts within 8 to 10 d of operating under increased carbon loads, beyond 8 mg/L sBOD<sub>5</sub> (1390 mg sBOD<sub>5</sub> m<sup>-2</sup> d<sup>-1</sup>), via the addition of sucrose. Strauss and Lamberti (2000) showed that the critical C:N ratio for nitrification varied among aquatic systems

depending on the availability of the ambient organic carbon source, therefore, an extension of this work was undertaken in order to determine whether varying degrees of carbon availability affected nitrification. Organic carbon amendments were achieved by dosing solubilised organic fertiliser, which represented a more native and possibly a less biodegradable carbon source. Results confirmed that nitrification performances differed significantly for each carbon source. In contrast to sucrose, when organic fertiliser was dosed, no significant loss in nitrification capacity was observed within the 16 d of operation, during which time complete nitrification was consistently achieved at high influent sBOD<sub>5</sub> concentrations of  $11.5 \pm 3.4$  mg/L ( $1992.8 \pm 589.3$  mg sBOD<sub>5</sub> m<sup>-2</sup> d<sup>-1</sup>).

A variable nitrification response to different carbon sources suggests that the critical carbon load was highly variable depending on the biodegradability of available organic carbon. The ability for the NTF to sustain complete nitrification under increased organic fertiliser induced carbon loads, may suggest that the organic carbon source was of a recalcitrant nature; something which was found *not* to be the case following respirometry measurements. It was thought probable, that the organic fertiliser exerted a lower heterotrophic oxygen demand than that of sucrose. The higher biodegradability of sucrose presumably created conditions that led to stronger interspecies competition for oxygen, which then exerted a superior influence on nitrification performance. This observation questions the validity of the biodegradation study, whereby the respirometry measurements obtained from the organic fertiliser (seeded) and sucrose exerted very similar DO uptake curves, and yet the nitrification performance of the NTFs when operated under each carbon source differed significantly. It was likely then, that sucrose initiated competition between heterotrophic and nitrifying bacteria at concentrations lower than that of native carbon present in more natural systems.

These results suggest that critical carbon loads determined using sucrose, occurred at lower organic carbon loads than those that might be expected for a more native carbon source—which would almost certainly be less bio-available. Therefore, NTFs may operate effectively at higher native carbon loads than those suggested in this study,

which were based mainly on sucrose. However, published data from Metcalf and Eddy (2003), confirmed that the inhibition of nitrification observed under sucrose-induced carbon loads from this study, was within the same order of magnitude as that observed in other wastewater applications. In summary, techniques used here for biodegradation studies on selected carbon sources did not appear to be an adequate surrogate measurement for extrapolation to NTF performance specific for Buaran WTP. However, results do suggest that nitrification performance was carbon-specific, and hence NTF performance is expected to vary between sites of application. Clearly, additional research is needed to test the effects of naturally occurring organic carbon sources at Buaran on NTF nitrifying capacity.

Findings from Chapter 4 showed that when the NTF was operated under low carbon loads, ammonia removal was highest at the top of the filter and reduced with depth. The lower depths received filtrate low in ammonia concentration, and nitrification was first-order-limited. When operated under higher carbon loads, it was expected that heterotrophic activity at the top of the filter would increase, and cause higher pulses of ammonia to reach the lower depths of the filter; where there was previously 'spare' nitrifying capacity. Segregation of carbon oxidation in the upper filter depths and nitrification in the lower depths in NTF's used for wastewater applications, has been previously reported by Wanner and Gujer (1985), Parker and Richards (1986), Daigger *et al.* (1994), Metcalf and Eddy (2003), and Pearce (2004). Published data from wastewater NTFs, indicates that this transition occurs at organic carbon concentrations of 20 mg sBOD<sub>5</sub>/L (Daigger *et al.* 1994). In contrast, steady-state nitrification profiles and rates, measured through the depth of the NTF operated at Hope Valley, showed that influent sBOD<sub>5</sub> concentrations as low as 5.0 mg/L (870 mg sBOD<sub>5</sub> m<sup>-2</sup> d<sup>-1</sup>) caused severe inhibition of nitrification throughout the entire NTF bed. Similar to the findings of earlier studies however, nitrification inhibition was most evident at the top of the NTF. It was hypothesised that the nitrification capacity at the bottom of the NTF would increase during periods of high organic loads to compensate for the decrease in nitrification capacity observed at the top, however nitrification performance at the bottom half remained unchanged in comparison to periods where the NTF operated under low

organic loads. It was probable that the low concentrations of organic carbon reaching the lower depths still imposed inhibitory effects on nitrification; particularly given that the abundance of nitrifiers was most likely low at these depths—as suggested by the observed gradient in nitrification activity and nitrifier biomass down the filter prior to carbon dosing (see Chapter 4). Similarly, intermittent sBOD<sub>5</sub> spikes of 9.4 mg/L lasting 48 h (Experiment G) caused significant suppression of nitrification through the entire NTF bed. For all experiments, nitrite accumulation throughout the entire bed was not observed, suggesting equal performance by AOB and NOB during these unfavourable conditions. For all experiments, complete recovery of nitrification throughout the entire filter bed was observed 12 ± 2 d after carbon dosing was ceased.

When influent sBOD<sub>5</sub> was maintained at 5.0 mg/L beyond 40 consecutive days via the addition of sucrose, ammonia removal increased from 60 to 100 %, however nitrite was not detected, and only low concentrations of nitrate-N of 0.2 mg/L were produced; suggesting that nitrification was not the cause of the ammonia removal. A nitrogen budget demonstrated that only 25.3 to 59.3 % of the ammonia-N removed was accounted for in the form of nitrite-N and nitrate-N throughout the entire filter bed depth. This was observed to a greater extent when sucrose was substituted with methanol as the sole carbon source. Here, the NTF was capable of removing 72.7 % ammonia-N, however depth profiles of nitrite-N and nitrate-N showed that concentrations remained below 0.02 mg/L, again suggesting that nitrification was not the main ammonia removal mechanism. Hydraulic flow and temperature were largely unchanged and the pH values were typically below 8, therefore nitrogen losses via ammonium volatilisation were expected to be minimal. These results suggest either that simultaneous nitrification–denitrification may have occurred, or that nitrogen assimilation increased with increasing organic load.

Simultaneous nitrification–denitrification has been previously reported in trickling filter biofilms by Schramm *et al.* (1996) and Pearce (2004). It was possible that oxygen diffusion limitations, fuelled by an increase in organic substrate, had promoted the development of aerobic and anoxic microenvironments, which allowed for sequential

utilisation of the electron acceptors oxygen and nitrate. The lag period of 40 d until simultaneous ammonia and nitrate removal was observed, may represent the time needed for the biofilm to reach a sufficient thickness to support the formation of anoxic sub-layers. Denitrification performance may have been improved in Experiment D since methanol is a better organic electron donor than sucrose.

For experiments where the concentrations of nitrite-N and nitrate-N did not reconcile with the mass of ammonia-N removed, ammonia removal may also be due to nitrogen assimilation. A study conducted on several full-scale wastewater NTFs by Pearce (2004), showed nitrogen assimilation increased with organic surface loading, and accounted for up to 55 % of total nitrogen removal. When operated under high sucrose-induced carbon loads, a nitrogen budget calculated during the current study showed that on average, 2 to 25 % of the ammonia-N removed was not accounted for as NO<sub>x</sub> within the filter's effluent. These observed losses were similar to the theoretical nitrogen assimilation demand of 3 to 27 %, which was based on biomass composition incorporating 5 % of nitrogen by dryweight and at a net biomass yield of 0.65 g /g BOD<sub>5</sub> (Pearce 2004). Similar to Pearce (2004) assimilative demands for nitrogen appeared to increase with both BOD<sub>5</sub> application and removal. Furthermore, the difference between calculated nitrogen assimilation requirements and the observed mass of nitrogen unaccounted for may indicate extent of the contributory role played by denitrification for total nitrogen removal.

A well operated trickling filter can provide both adequate carbon removal and nitrification (Metcalf and Eddy 2003; Pearce 2004). Combined carbon removal and nitrification in trickling filters occurs when volumetric loading rates are typically between the range of 0.1–0.3 kg sBOD<sub>5</sub> m<sup>-3</sup> d<sup>-1</sup> (Metcalf and Eddy 2003). Results from this study have shown that ammonia-N and sBOD<sub>5</sub> removal in excess of 50 % can be consistently achieved when the NTF is operated within this range. As the volumetric organic loading was increased beyond 0.3 to 0.5 kg sBOD<sub>5</sub> m<sup>-3</sup> d<sup>-1</sup> (surface loading of 1330 to 2096 mg sBOD<sub>5</sub> m<sup>-2</sup> d<sup>-1</sup>), the NTF transformed from a predominantly nitrifying, to a carbon oxidation system, where sBOD<sub>5</sub> and TOC removal had increased up to 1.1 and 3.5 g m<sup>-</sup>

$^2 \text{ d}^{-1}$  respectively. Depth profiles of  $\text{sBOD}_5$  and TOC down the NTF bed showed that carbon removal was highest at the top 0.3 m, and decreased with an increase in bed depth. As expected, heterotrophic numbers (see Chapter 6) reflected the carbon removal profile down the filter bed, where heterotrophs were most abundant at the top and decreased in response to a decline in organic carbon concentration. The unexpected removal of ammonia-N also observed at 0.3 m depths in the biofilter during high carbon loads, may therefore be reasonably attributed to the assimilatory nitrogen requirements of heterotrophic populations.

In addition to carbon loading, DO, temperature, pH and alkalinity all affect nitrification, and therefore needed to be considered when assessing the influence of carbon loading on NTF nitrification performance. Regular monitoring of these parameters showed that influent DO, temperature, pH and alkalinity were stable, and were therefore considered to have had an insignificant impact on NTF nitrification capacity. No significant relationship between nitrification efficiency and influent: DO; temperature; or alkalinity was identified. Statistically, a weak but significant relationship between nitrification and influent pH was observed, however this was thought to be of limited practical relevance, since pH had remained very stable at  $7.9 \pm 0.16$  for the entire study duration.

Results from this study showed that de-oxygenation of the effluent occurred when carbon loading was increased beyond  $5 \text{ mg sBOD}_5/\text{L}$  via the addition of sucrose. The extent of de-oxygenation correlated well with  $\text{sBOD}_5$  loading. From the onset of carbon dosing, effluent DO progressively decreased over  $8 \pm 2 \text{ d}$ , from saturated concentrations of 9 to 10 mg/L, down to values of 5 to 6 mg/L. De-oxygenation of the effluent was coupled with a steady decline in filter nitrification capacity, and may confirm the substantial development of heterotrophs, which were otherwise underestimated using heterotrophic plate counts as reported in Chapter 6. Once carbon dosing was terminated, the effluent DO increased rapidly. Rapid fluctuations in effluent DO in response to the presence and absence of carbon, confirmed the presence of heterotrophic activity, and was best demonstrated during Experiment G where carbon was dosed intermittently. In addition, effluent DO correlated well with  $\text{sBOD}_5$  and

ammonia-N removal, and may be a useful quantitative predictor of NTF nitrification and carbon removal performances. As effluent DO decreased, a transition from a nitrifying to a predominantly carbon oxidation system had occurred. The relationship between oxygen consumption and carbon removal, provided supportive evidence that heterotrophic biochemical oxidation of the carbon substrate was occurring. Energy obtained from this process is used for cell maintenance and synthesis of new cell tissue (Metcalf and Eddy 2003), and therefore it was reasonable to assume a large heterotrophic presence within the filter bed.

Most of our current understanding of trickling filters is limited to wastewater applications, and whilst their performance for wastewater treatment systems is widely reported, little is known about their design for potable water treatment. An empirical model developed by Pearce (1999), showed that nitrification efficiency of NTFs treating wastewater was influenced by organic carbon surface loading. The aim of the current study was to determine whether this model can be transferred to a potable water NTF when operated under ammonia-N loads well below the range from which the model was derived. When the pilot-scale NTF was operated under fixed ammonia loads within the model range, predicted and observed values were comparable. The relatively good agreement between the simulated and measured data showed that this kind of model is capable of quantitatively describing the nitrification behaviour, and can accurately predict effluent ammonia-N concentrations when ammonia-N surface loading is greater than  $830 \text{ mg m}^{-2} \text{ d}^{-1}$ . However, when operated under fixed ammonia-N loads of  $96 \text{ mg m}^{-2} \text{ d}^{-1}$ , which were well below the model's range, effluent ammonia-N increased more rapidly in response to sucrose-induced  $\text{sBOD}_5$  loads than predicted. When sucrose was substituted with soluble organic fertiliser, the observed ammonia-N removal was similar to the model predicted values.

These discrepancies observed between the model and values obtained during sucrose augmented carbon loads could be attributed to: (i) the Pearce (1999) model being derived from total  $\text{BOD}_5$  values, unlike data from this study which measured soluble carbonaceous  $\text{sBOD}_5$ ; and (ii) differences between the biodegradability nature of

organic carbon used in this study (sucrose), and carbon present in municipal wastewater. Furthermore, the Pearce (1999) model was based on the concept that heterotrophic activity was the key mechanism responsible for the breakthrough of effluent ammonia-N during high organic loads. Following this study, other mechanisms such as excessive EPS production were considered to have contributed to the decline in ammonia-N removal performance; something which was not accounted for in the model. The differences between the model prediction and observed values may suggest that EPS had a greater detrimental impact on nitrification than did heterotrophic competition. The extent of EPS production and its impact on nitrification capacity is discussed further in Chapter 6.

## 6 EFFECT OF CARBON TO NITROGEN RATIO ON BIOFILM PROTEIN AND CARBOHYDRATE COMPOSITION

### 6.1 Introduction

Determination of the protein and carbohydrate composition of biofilms serves as a useful analytical parameter, because the relative concentration of each reflects the availability of carbon, nitrogen and the C:N ratio (Ganf *et al.* 1986; Dumaz and Sanin 2001). Extracellular carbohydrates, also referred to as extracellular polysaccharides, are produced by many bacteria, and are a major structural and functional component of biofilms. The protein fraction of biofilms represents cell mass and extracellular proteins which exist in the extracellular medium. The carbohydrate and protein content of biofilms have been widely studied in BNR processes for wastewater treatment; where polysaccharide concentration has been shown to influence the stability and performance of the treatment process (Bura *et al.* 1998; Dumaz and Sanin 2001; Liao *et al.* 2001). Many studies have reported that changes in biofilm polysaccharide concentrations were generally governed by nutrient concentration, C:N ratio, and carbon biodegradability (Stover 1980; Dumaz and Sanin 2001; Sponza 2003). When the C:N ratio is high, carbon utilisation by the microbial population can shift to excessive EPS production (Wuertz *et al.* 2003). This was confirmed by Bengtsson (1991), who reported that high yields of EPS in pure culture systems was most evident when carbon was present in excess, and nitrogen was limited. Wu *et al.* (1982) and Dumaz and Sanin (2001) made similar observations when varying C:N ratio in a lab scale activated sludge reactor. These studies reported that high C:N produced activated sludge flocs high in carbohydrate composition and low in protein content. In addition, Allison and Sutherland (1987) also demonstrated that bacteria cultured under carbon limiting conditions produced only trace amounts of carbohydrate.

Most of the available information regarding the effect of C:N ratio on carbohydrate and protein content of biofilms, has been obtained from studies involving pure bacterial cultures, or from *wastewater* BNR processes. In particular, the author is unaware of studies which characterise biofilm polysaccharides and protein composition within a *potable water* NTF operated under low carbon and nitrogen concentrations. Results from Chapter 5 showed that when the organic carbon loading was increased via the addition of sucrose (Experiment B), a visual inspection of the biofilm had revealed a thick jelly-like appearance, consistent with the characteristics of EPS. This observation coincided with nitrification inhibition, however, most of the available literature on *wastewater* NTFs attribute the loss in nitrifying capacity to heterotrophic competition, not EPS production. These early results clearly identified a need to further investigate the extent of polysaccharide production in response to carbon loading and its influence on nitrification capacity.

The aim of this study was to determine the effect that C:N ratio had on the protein and polysaccharide composition of biofilms at various filter depths, and to correlate biofilm composition with filter nitrification performance. The influence of two different organic carbon sources: (a) readily biodegradable organic carbon sources (sucrose and methanol); and (b) a native-like organic carbon source (soluble organic fertiliser) on biofilm polysaccharide composition was investigated. In addition, heterotrophs were quantified using traditional plate count techniques to confirm the extent of their presence within the biofilm in response to changes in carbon loading. Furthermore, tracer experiments were conducted to determine the influence that C:N and changes in biofilm composition have on NTF hydrodynamics.

## **6.2 Methods**

### **6.2.1 *Experimental design***

Experiments were conducted on two pilot scale NTFs (large and small pilot-scale), which operated under conditions that mimicked the quality of Buaran WTP raw water supply—namely ammonia and sBOD<sub>5</sub> concentrations, and C:N ratio. Variations in carbon and nitrogen were achieved by supplementing the influent of the large and small pilot-scale NTFs with an external carbon source and ammonium sulphate (Table 6.1). A description of each experiment, outlining operational conditions—namely: ammonia load; organic load; and C:N ratio; which was obtained from Chapter 5, Section 5.2.1—is repeated in Table 6.1. Long-term experiments were mostly conducted on the large pilot-scale NTF, therefore the majority of data was obtained from this filter except where otherwise identified. A more detailed description of each pilot NTF can be found in Chapter 3. For each experiment, biomass was harvested from 3 biofilm sample sites (see Chapter 3, Section 3.2.10), which were positioned through the vertical axis of the large pilot-scale NTF and quantified for total protein and total carbohydrates, as well as enumerated for culturable heterotrophic bacteria. Changes in biofilm composition were correlated with apparent NTF nitrification performance and variations in operational conditions.

### **6.2.2 *Total Protein and total Carbohydrate***

The distribution of biomass throughout the large pilot-scale NTF was determined by quantifying total protein and total carbohydrate per cm<sup>2</sup> of support media surface area. Biomass was harvested from biofilm sample sites located along the vertical axis at depths of 0.3, 1.5 and 2.7 m from the filter surface and analysed for total protein and total carbohydrates in accordance with procedures described in Chapter 3, Section 3.7.

### **6.2.3 Heterotrophic plate counts**

Biomass was harvested from biofilm sample sites located along the vertical axis of the large pilot-scale NTF, at bed depths of 0.3, 1.5 and 2.7 m from the surface. Heterotrophic bacteria within the biomass were enumerated per cm<sup>2</sup> of media surface area by spread-plating in accordance with procedures described in Chapter 3, Section 3.7.4. Results were expressed as CFU per cm<sup>2</sup>.

### **6.2.4 Hydraulic tracer analysis**

Tracer experiments were conducted on the large pilot-scale NTF to investigate the impact of C:N ratio, and the subsequent changes in biofilm composition, on the hydraulic characteristics of the NTF—as determined by the corresponding HRT and RTD. Tracer analysis was performed as described in Chapter 3, Section 3.8 under three varying conditions: (i) low organic loads (Experiment A); (ii) high organic loads (Experiment F); and (iii) recovery following cessation of carbon addition. For all experiments, the hydraulic flow was maintained at 8 m<sup>3</sup>/h (5.2 m/h). The HRT of the NTF was then calculated from the recorded tracer time–concentration data as described in Chapter 3, Section 3.8.

**Table 6.1.** Influent ammonia-N and sBOD<sub>5</sub> concentrations and corresponding loading rates that the NTF was operated under (mean ± 1 SD).

Experiment	Influent ammonia-N		Influent sBOD <sub>5</sub>		C:N ratio	External organic carbon source	Duration of carbon dosing (days)
	mg/L	mg m <sup>-2</sup> d <sup>-1</sup>	mg/L	mg m <sup>-2</sup> d <sup>-1</sup>			
<b>A</b> <sup>1</sup>	0.56–5.57	97.03–966.06	1.3 ± 0.5	225.2 ± 87.9	–	None	0
<b>B</b> *	0.71 ± 0.2	122.9 ± 41.4	6.1 ± 3.36	1066.9 ± 577.2	8.5/1	Sucrose	64
<b>C</b>	0.56 ± 0.1	97.8 ± 19.7	5.4 ± 0.15	931.4 ± 26.0	10/1	Sucrose	18
<b>D</b>	0.6 ± 0.01	104.8 ± 1.0	5.0 ± 0.0	866.4	8/1	Methanol	11
<b>E</b>	0.52 ± 0.02	90.1 ± 2.6	1.5 ± 0.4	259.9 ± 60	3/1	Sucrose	8
<b>F</b>	4.7 ± 1.1	826.1 ± 163.9	8.8 ± 2.9	1533.5 ± 510.6	2/1	Sucrose	12
<b>G</b> <sup>†</sup>	4.8 ± 0.5	840.1 ± 86.2	9.4 ± 0.9	1625.4 ± 162.7	2/1	Sucrose	three 48 h spikes
<b>H</b>	4.8 ± 0.3	822.4 ± 61.4	5.3 ± 1.0	910.9 ± 169.1	1/1	Sucrose	10
<b>I</b> <sup>a</sup>	1.3 ± 0.3	220.8 ± 48.3	11.5 ± 3.4	1992.8 ± 589.3	8.8/1	Organic fertiliser	16

<sup>1</sup> Data obtained when operated under low organic loadings (Chapter 4). sBOD<sub>5</sub> represents native organic carbon present in Hbpe Valley reservoir.

\* Experiment conducted on old pilot plant NTF.

<sup>†</sup> Intermittent carbon spikes (48-h on / 48-h off cycles).

<sup>a</sup> Experiment conducted on small pilot-scale NTF.

## 6.3 Results

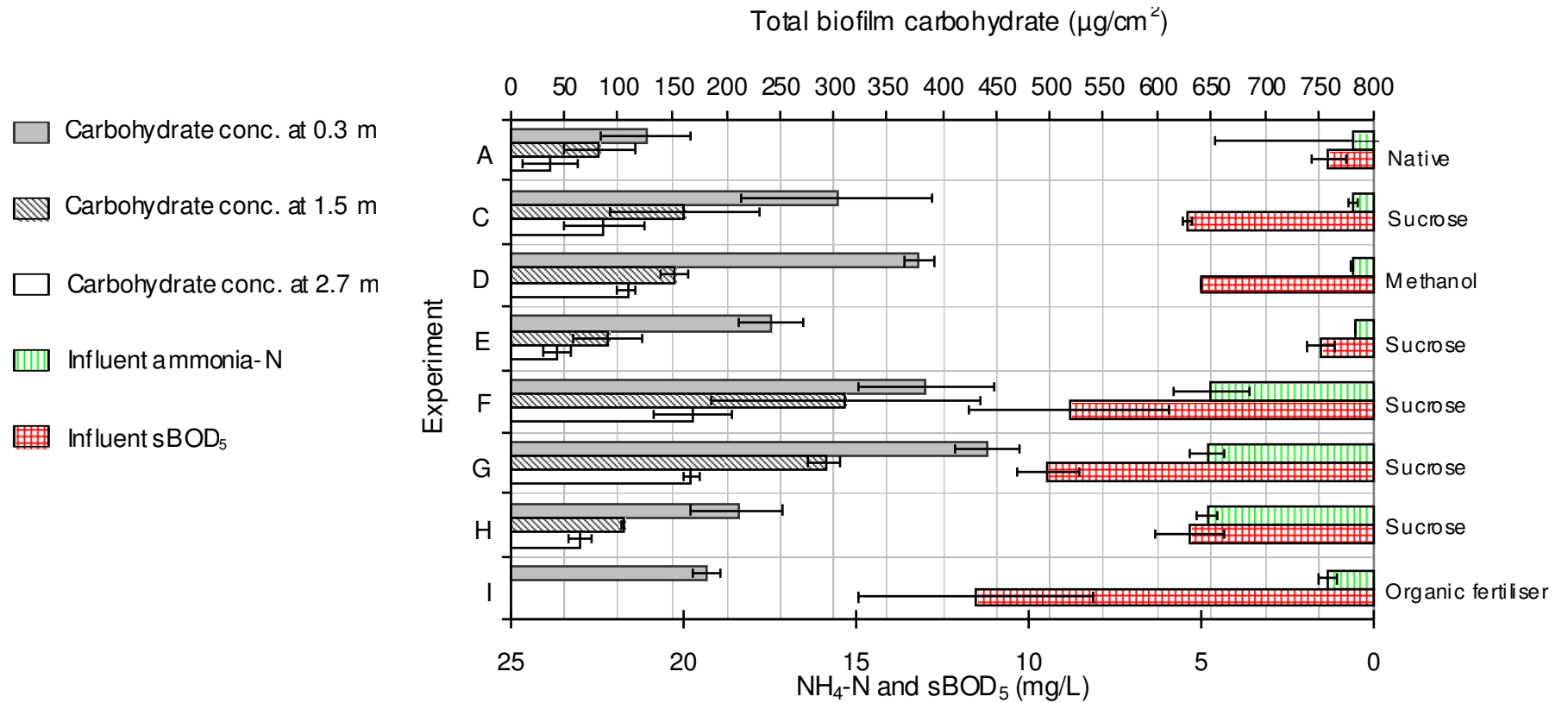
### 6.3.1 *Biofilm carbohydrate composition*

Figure 6.1 compares the mass of carbohydrate measured within the biofilm matrix, sampled from filter depths of 0.3, 1.5, and 2.7 m for Experiments A, C, D, E, F, G, H, and I, which operated under various organic and ammonia surface loads. sBOD<sub>5</sub> was increased from background concentrations ( $1.3 \pm 0.5$  mg/L; Experiment A) to levels shown in Table 6.1 for the respective experiments. Differences in biofilm carbohydrate composition between experiments were evaluated by Kruskal–Wallis ANOVA with Dunn's multiple comparison *post hoc* testing.

For all experiments, biofilm carbohydrate was greatest at the top 0.3 m and declined with increasing bed depth. The most significant difference in mean biofilm carbohydrate composition between experiments was identified at the top filter bed depth of 0.3 m. At this depth, mean mass of carbohydrate observed during Experiment A—operated at background sBOD<sub>5</sub> concentrations—were significantly lower than those measured during Experiments C ( $p < 0.01$ ), D ( $p < 0.05$ ), F ( $p < 0.001$ ), and G ( $p < 0.001$ ), where influent sBOD<sub>5</sub> was maintained  $> 5.3$  mg/L via the addition of sucrose or methanol. No significant difference in mean biofilm carbohydrate mass was identified between Experiment A and experiments where influent sBOD<sub>5</sub> was maintained below 2 mg/L via the addition of sucrose (Experiment E), or was maintained at 11.5 mg/L via the addition of soluble organic fertiliser (Experiment I) ( $p > 0.05$ ). For Experiments C (sucrose induced sBOD<sub>5</sub>) and D (methanol induced sBOD<sub>5</sub>) which operated under identical ammonia-N and sBOD<sub>5</sub> loads, biofilm carbohydrate composition for all biofilm sample sites were similar ( $p > 0.05$ ), which suggested that biofilm polysaccharide composition was independent of these two carbon sources. The biofilm polysaccharide composition also appeared to be independent of C:N ratio.

When the NTF operated under stable organic loads, a decrease in C:N ratio (i.e. increase in ammonia load) did not alter biofilm carbohydrate composition. This can be seen when comparing Experiment C with Experiment H, where no significant difference between mean biofilm carbohydrate mass was found at any of the biofilm sample sites

of 0.3, 1.5 and 2.7 m (Mann–Whitney  $U$  test;  $p>0.05$ ). Similarly, the carbon dosing regime employed in this study (i.e., continuous or intermittent spikes), had no discernable influence on biofilm carbohydrate composition. When comparing Experiments F (continuous high sBOD<sub>5</sub> loading) with Experiment G (intermittent sBOD<sub>5</sub> spikes), no significant difference between mean biofilm carbohydrate mass was identified at 0.3, 1.5 and 2.7 m ( $p>0.05$ ). A positive correlation did exist between influent sBOD<sub>5</sub>, achieved via the addition of sucrose or methanol, and biofilm carbohydrate mass for all biofilm sample sites, at depths 0.3, 1.5 and 2.7 m (respective  $r_s = 0.82, 0.76, 0.80$ ;  $p<0.01$ ; Table 6.2). No correlation was established between C:N ratio and biofilm carbohydrate mass for all biofilm sample sites of 0.3, 1.5 and 2.7 m ( $r_s = 0.28, 0.28, 0.31$ ;  $p>0.05$ ; Table 6.2). These results suggest that influent sBOD<sub>5</sub> concentration, and not the C:N ratio, was the regulating factor of biofilm polysaccharide composition. Significant negative correlations between biofilm carbohydrate mass and percentage nitrification for all biofilm sample depths of 0.3, 1.5 and 2.7 m was also observed ( $r_s = -0.72, -0.61, -0.62$ ;  $p<0.01$ ; Table 6.2).



**Figure 6.1.** NTF depth profile of biofilm carbohydrate ( $\mu\text{g}/\text{cm}^2$ ) and corresponding influent ammonia-N and  $\text{sBOD}_5$  concentrations. (Parameter means shown  $\pm 1$  SD).

**Table 6.2.** Spearman's correlation coefficients highlighting relationships between nitrification, organic (sBOD<sub>5</sub>) loading and C:N ratio with biofilm carbohydrate, protein and heterotrophic composition (HPC).

Parameter †		% Nitrification	Influent sBOD <sub>5</sub> loading (mg m <sup>-2</sup> d <sup>-1</sup> )	C:N ratio	CARBOHYDRATE (µg/cm <sup>2</sup> )			PROTEIN (µg/cm <sup>2</sup> )			HPC (µg/cm <sup>2</sup> )		
					TOP	MIDDLE	BOTTOM	TOP	MIDDLE	BOTTOM	TOP	MIDDLE	BOTTOM
CARBOHYDRATE (µg/cm <sup>2</sup> )	TOP	-0.723**	0.824**	0.279									
	<i>n</i>	21	21	21									
	MIDDLE	-0.612**	0.761**	0.284	0.847**	-							
	<i>n</i>	25	22	25	21								
	BOTTOM	-0.622**	0.807**	0.308	0.790**	0.862**	-						
	<i>n</i>	25	22	25	21	25							
PROTEIN (µg/cm <sup>2</sup> )	TOP	-0.108	0.221	0.167	0.208	0.025	-0.022	-					
	<i>n</i>	25	22	25	21	25	25						
	MIDDLE	-0.438*	0.377	0.131	0.470*	0.397*	0.217	0.615**	-				
	<i>n</i>	25	22	25	21	25	25	25					
	BOTTOM	-0.313	0.313	0.078	0.597**	0.399*	0.218	0.502*	0.644**	-			
	<i>n</i>	25	22	25	21	25	25	25	25				
HPC (µg/cm <sup>2</sup> )	TOP	-0.434	0.471	0.339	0.43	0.453	0.490*	-0.248	-0.117	0.028	-		
	<i>n</i>	17	16	17	15	17	17	17	17	17			
	MIDDLE	-0.465	0.612*	0.538*	0.533*	0.563*	0.547*	0.065	0.238	0.195	0.781**	-	
	<i>n</i>	17	16	17	15	17	17	17	17	17	17		
	BOTTOM	-0.454	0.585*	0.632**	0.465	0.578*	0.616**	-0.266	0.15	-0.009	0.685**	0.818**	-
	<i>n</i>	17	16	17	15	17	17	17	17	17	17	17	

†Top– filter bed depth of 0.3 m; Middle– filter bed depth of 1.5 m; Bottom– filter bed depth of 2.7 m.

\*Correlation is significant at  $p < 0.05$  level (2-tailed); \*\*Correlation is significant at  $p < 0.01$  level (2-tailed).

Figure 6.2 shows the progression of biofilm carbohydrate production and removal in response to the presence and absence of an external carbon source (sucrose) for filter bed depths of 0.3, 1.5 and 2.7 m during Experiment F. An inverse relationship between ammonia-N removal and biofilm carbohydrate was clearly evident. The results show a steady increase in biofilm carbohydrate mass at the upper bed depths of 0.3 and 1.5 m, within 12 d of increasing the organic carbon surface load from  $225.2 \pm 88 \text{ mg sBOD}_5 \text{ m}^{-2} \text{ d}^{-1}$  ( $1.5 \pm 0.5 \text{ mg sBOD}_5/\text{L}$ ) to  $1533.5 \pm 510.6 \text{ mg sBOD}_5 \text{ m}^{-2} \text{ d}^{-1}$  ( $8.8 \pm 2.9 \text{ mg sBOD}_5/\text{L}$ ) on day 0 (Figure 6.2, marked *i*). Biofilm carbohydrate measured at the lowest bed depth of 2.7 m remained constant. The increase in biofilm carbohydrate mass observed at 0.3 and 1.5 m coincided with a tenfold reduction in apparent nitrification rate from  $901.3 \pm 8.1$  to  $98.4 \pm 3.7 \text{ mg NH}_4\text{-N m}^{-2} \text{ d}^{-1}$ . Figure 6.2 shows that mass of biofilm carbohydrate at these depths had returned to normal levels within 9 d of decreasing the organic carbon load to background levels (Figure 6.2, marked *d*). The decline in biofilm carbohydrate may be attributed to degradation via the heterotrophic community. The filter also completely recovered its nitrifying capacity within this time frame (Figure 6.2).

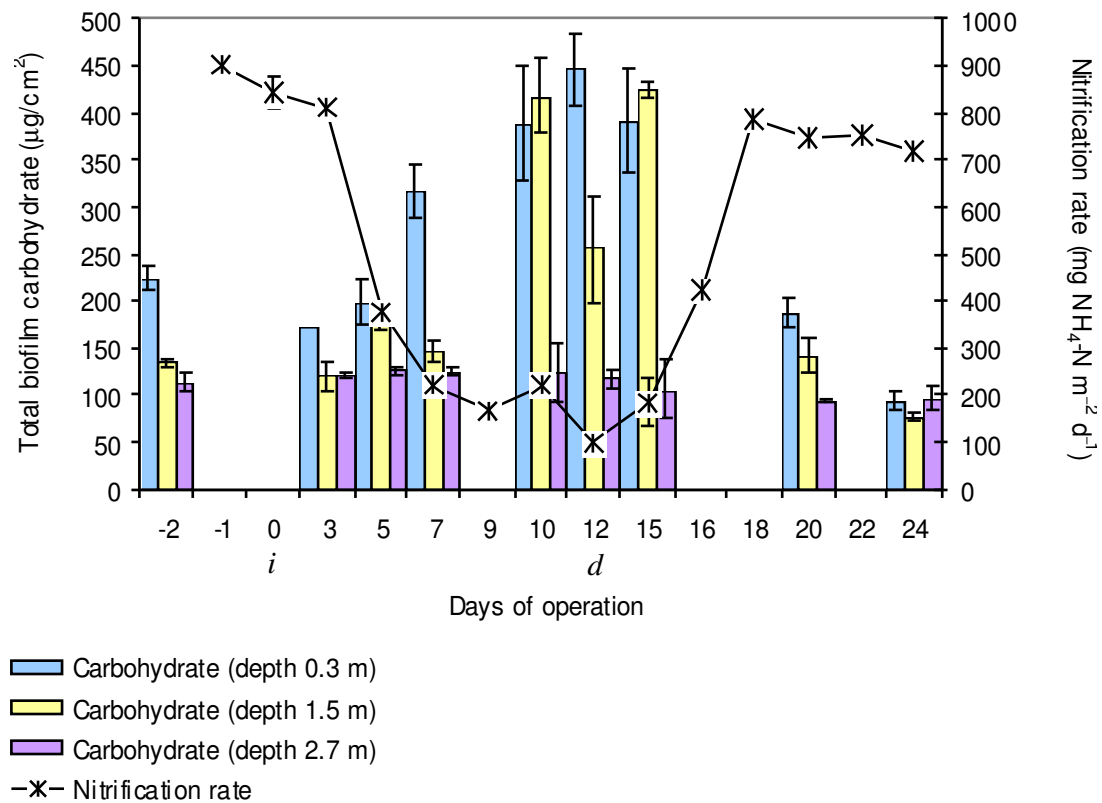


**Figure 6.2.** Relationship between biofilm carbohydrate ( $\mu\text{g}/\text{cm}^2$ ) and apparent nitrification rate in response to an increase in organic carbon loading on day 0 (marked *i*), and a decrease in carbon loading on day 12 (marked *d*) for Experiment F. Between days 0 and 12, the organic surface load was maintained high at  $1533 \pm 510 \text{ mg sBOD}_5 \text{ m}^{-2} \text{ d}^{-1}$  ( $8.8 \pm 2.9 \text{ mg sBOD}_5/\text{L}$ ) via the addition of sucrose. The ammonia-N surface load was maintained steady at  $826 \pm 163 \text{ mg NH}_4\text{-N m}^{-2} \text{ d}^{-1}$  ( $4.7 \pm 1.1 \text{ mg NH}_4\text{-N/L}$ ) for the entire duration of the experiment. (Data points represent parameter means  $\pm 1$  SD of 3 determinations).

### **6.3.2 Biofilm protein composition**

Figure 6.3 compares the mass of biofilm protein sampled from filter depths of 0.3, 1.5, and 2.7 m for Experiments A, C, D, E, F, G, H, and I, which operated under various organic and ammonia surface loads.  $sBOD_5$  was increased from background concentrations (Experiment A) to levels shown in Table 6.1, by the addition of an external carbon source. Differences in biofilm protein composition between experiments were evaluated by Kruskal–Wallis ANOVA with Dunn’s multiple comparison testing.

Greatest biofilm protein mass were identified at the top 0.3 m of the NTF bed, and declined with an increase in bed depth. Only small variations in mean biofilm protein composition were observed across all experiments for all filter bed depths. No significant differences between mean biofilm protein was observed for Experiments D, E, F, G, and H, at all filter bed depths ( $p>0.05$ ). Significant differences in mean biofilm protein were only identified between Experiment A (low  $sBOD_5$  of  $1.3 \pm 0.5$  mg/L) and Experiment C (high  $sBOD_5$  of  $5.4 \pm 0.15$  mg/L) for all biofilm sample sites ( $p<0.01$ ), and between Experiments A and F (high  $sBOD_5$  of  $8.8 \pm 2.9$  mg/L) for filter bed depth of 1.5 m only ( $p<0.01$ ). No significant correlation between biofilm protein and influent  $sBOD_5$  concentration was observed at all biofilm sample depths of 0.3, 1.5, and 2.7 m (respective  $r_s = 0.22, 0.37, 0.31$ ;  $p>0.05$ ; Table 6.2). A negative correlation between percentage nitrification and mass of biofilm protein at filter bed depth of 1.5 m was observed ( $r_s = -0.438$ ;  $p<0.05$ ), however this relationship was not observed at the remaining biofilm sample sites at 0.3 and 2.7 m ( $r_s = -0.10, -0.31$ ;  $p>0.05$ ; Table 6.2).

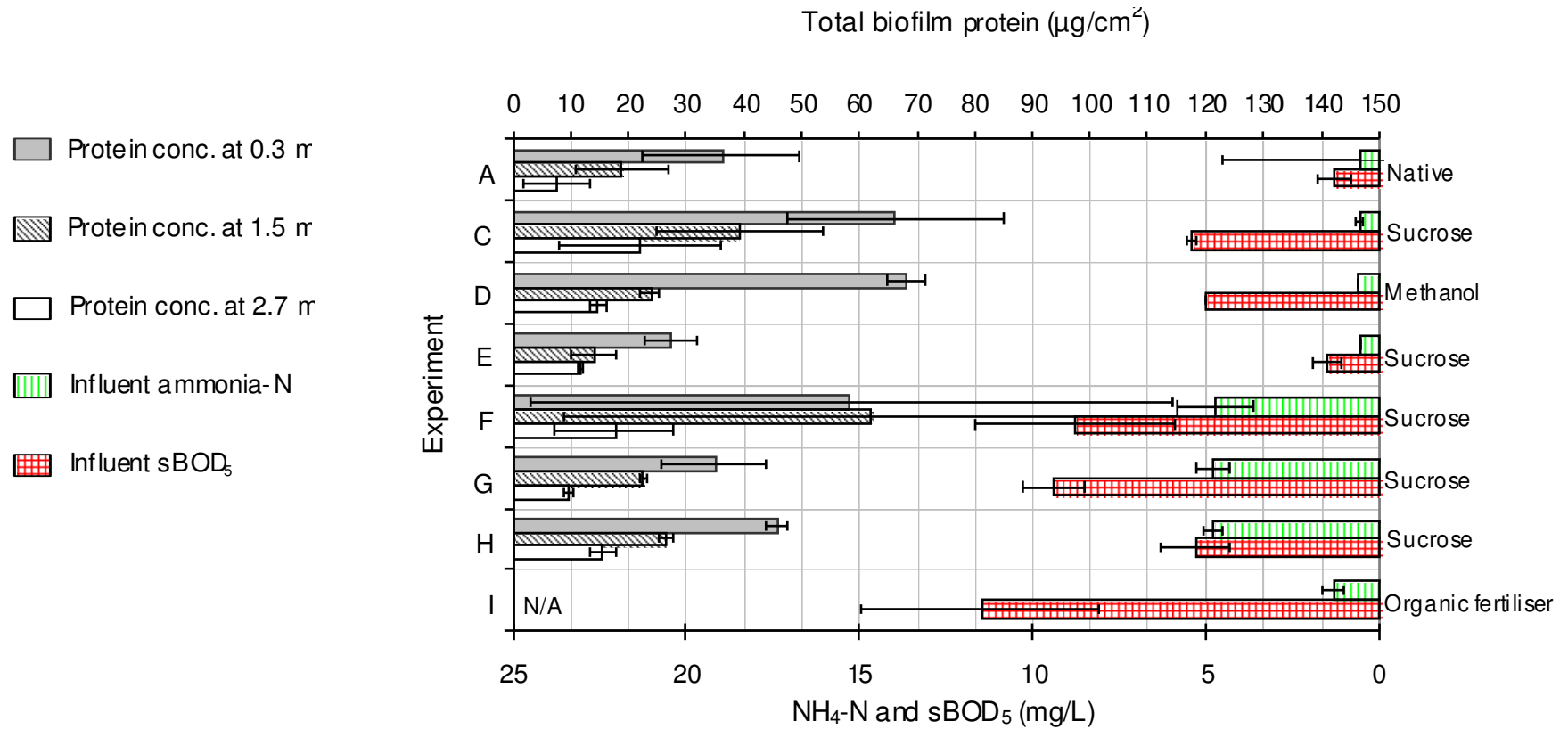


**Figure 6.3.** NTF depth profile of biofilm protein ( $\mu\text{g}/\text{cm}^2$ ) for each experiment and corresponding influent ammonia and sBOD<sub>5</sub> concentrations. (Parameter means shown  $\pm$  1 SD).

### **6.3.3 Protein:carbohydrate ratio**

Analysis shows that the protein:carbohydrate ratio of the biofilm decreased with an increase in carbon loading. A positive correlation between protein:carbohydrate ratio and influent sBOD<sub>5</sub> concentration was identified at all biofilm sample depths of 0.3, 1.5 and 2.7 m (respective  $r_s = 0.46, 0.45, 0.55; p < 0.05$ ).

### 6.3.4 *Biofilm heterotrophic composition*

Figure 6.4 shows the abundance of culturable heterotrophic bacteria throughout the depths of the NTF bed for Experiments A, F, G and H when influent sBOD<sub>5</sub> concentrations were increased from 1.3 mg/L (Experiment A) to 8.8, 9.4, and 5.3 mg/L respectively, via the addition of sucrose. Influent ammonia-N was maintained constant at approximately 5.0 mgN/L. Heterotrophs were typically most abundant at the top filter depth of 0.3 m and declined with an increase in bed depth. A small increase in HPC was evident once influent sBOD<sub>5</sub> concentrations were increased from 1.3 to 5.5, 8.8, and 9.4 mg/L. The greatest increase in HPC ( $\approx 1 - \log_{10}$ ) was observed during Experiment G for all biofilm sample sites at 0.3, 1.5 and 2.7 m. A significant difference in mean HPC was observed between Experiments A and F for all biofilm sample depths of 0.3, 1.5 and 2.5 m (Kruskal–Wallis ANOVA,  $p < 0.05$ ,  $p < 0.01$ ,  $p < 0.05$ ) and between Experiments A and G at all biofilm sample depths of 0.3, 1.5 and 2.5 m ( $p < 0.01$ ,  $p < 0.001$ ,  $p < 0.05$ ). No significant difference in heterotrophic abundance between Experiments F, G, and H was established ( $p > 0.05$ ). A positive correlation between HPC and influent sBOD<sub>5</sub> was confirmed at the lower filter bed depths of 1.5 and 2.7 m ( $r_s = 0.61$ ,  $0.58$ ;  $p < 0.05$ ), but was not observed at 0.3 m ( $r_s = 0.47$ ;  $p > 0.05$ ; Table 6.2). Similarly, a positive correlation between heterotrophs and C:N ratio was confirmed for the lower bed depths of 1.5 and 2.7 m ( $r_s = 0.538$ ;  $p < 0.05$  and  $0.632$ ;  $p < 0.01$ ), however, a similar correlation was not observed at 0.3 m ( $r_s = 0.339$ ;  $p > 0.05$ ; Table 6.2). No consistent pattern of heterotrophs with respect to percentage nitrification was apparent for any of the biofilm sample depths of 0.3, 1.5, and 2.7 m (respective  $r_s = -0.43$ ,  $-0.46$ ,  $-0.45$ ;  $p > 0.05$ ; Table 6.2).

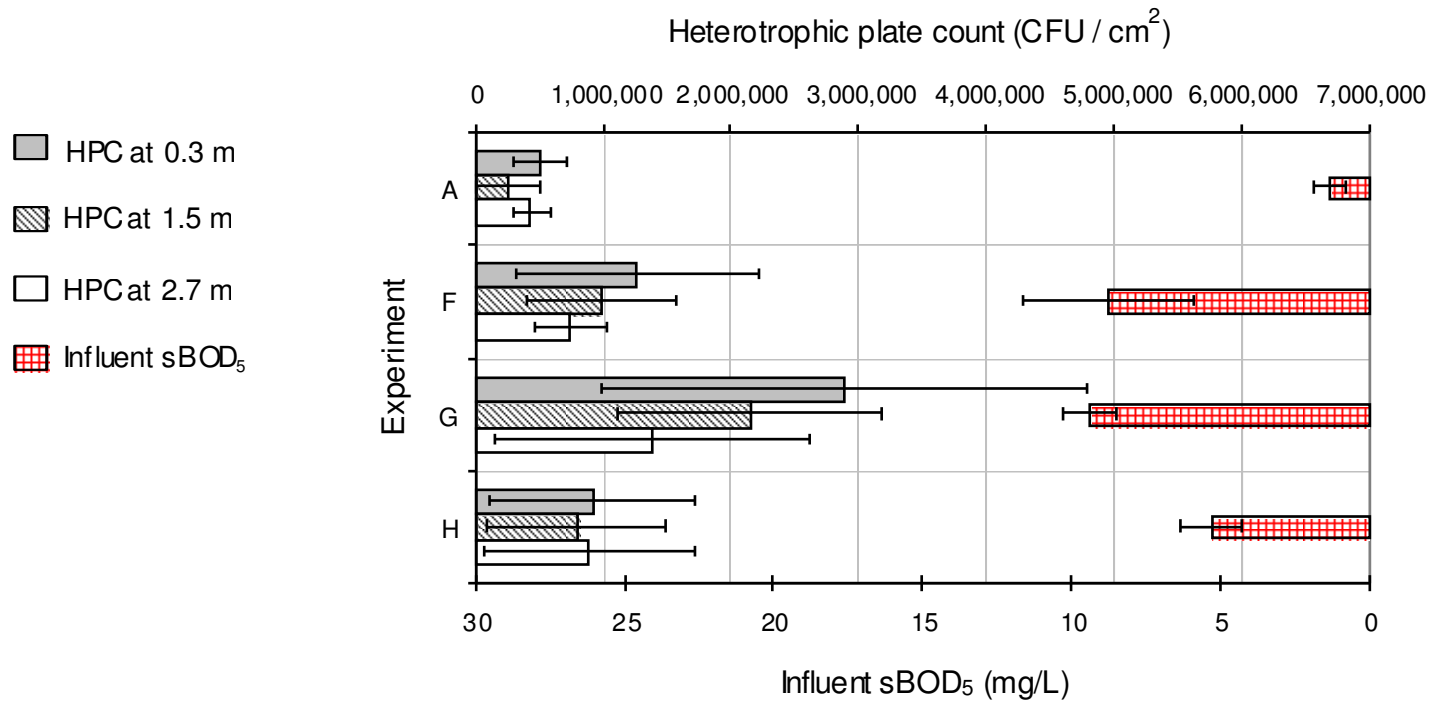
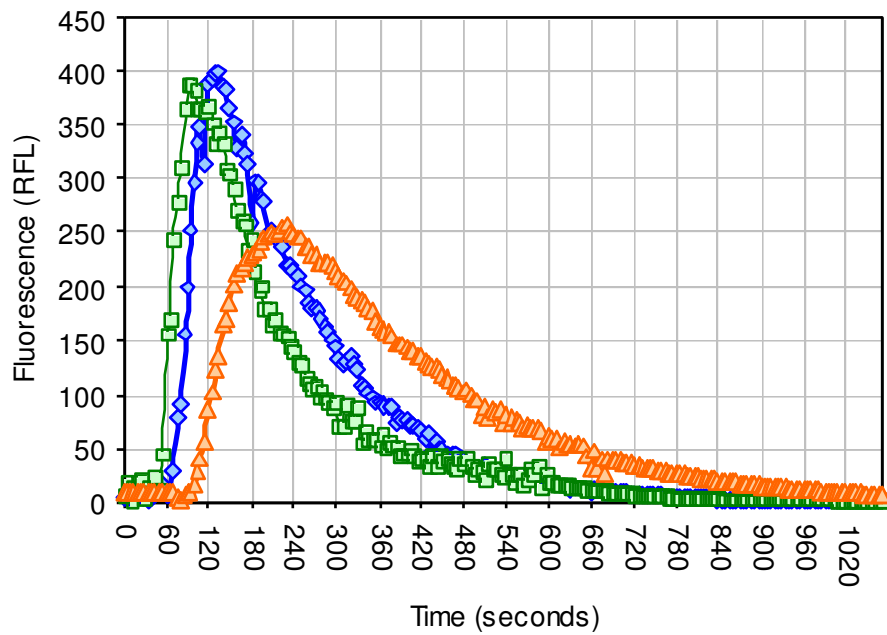


**Figure 6.4.** Large pilot-scale NTF: depth profile of biofilm heterotrophic concentration (CFU/cm<sup>2</sup>) for each experiment and the corresponding sucrose induced influent sBOD<sub>5</sub> concentrations. (Data points represent parameter means ± 1 SD).

### 6.3.5 Hydraulic characterisation

Tracer experiments were performed on the large pilot-scale NTF when operated under low and high organic carbon loads. Figure 6.5 compares RTD curves and HRTs for Experiments A, F, and the recovery phase following cessation of carbon addition. A corresponding table of biomass concentrations (represented as total carbohydrate and protein) sampled from 0.3 m, which was measured at the time of tracer analysis, is also presented. The tracer test for Experiment A was conducted prior to an increase in the NTF's organic carbon load. The tracer test for Experiment F was conducted 6 d after increasing the organic carbon load from  $225.2 \pm 87.9 \text{ mg sBOD}_5 \text{ m}^{-2} \text{ d}^{-1}$  ( $1.3 \pm 0.5 \text{ mg sBOD}_5/\text{L}$ ) to  $1533.5 \pm 510.6 \text{ mg sBOD}_5 \text{ m}^{-2} \text{ d}^{-1}$  ( $8.8 \pm 2.9 \text{ mg sBOD}_5/\text{L}$ ). The recovery RTD curve was obtained after Experiment F, when the NTF returned to operating under low organic carbon loads of  $225.2 \pm 87.9 \text{ mg sBOD}_5 \text{ m}^{-2} \text{ d}^{-1}$  ( $0.5 \text{ mg sBOD}_5/\text{L}$ ), and once the nitrification capacity of the NTF had recovered. It can be seen that the experimental RTD curves and HRT for Experiment A and the recovery phase (operated under low organic loads) were similar, however they differed from Experiment F (high organic carbon loading). The RTD for Experiment F had a more pronounced and longer tail, signifying greater dispersion and mixing, in comparison with that of Experiment A and the recovery phase, which displayed more plug-flow like characteristics. Calculated HRTs for Experiment A, recovery phase, and Experiment F were 228, 222 and 384 seconds respectively. The longer HRT and RTD tailing noted during Experiment F appeared to result from an increase in biofilm carbohydrate and protein mass, which was indicative of high organic loads.

In addition, the HRT data from Chapter 4 was compiled with HRT values from this Chapter to determine the influence of nutrient load on filter HRT. From Figure 6.6 it can be seen that the filter HRT correlated well with nutrient loading, measured as the sum of ammonia and sBOD<sub>5</sub> surface loading ( $r_s = 0.963$ ;  $p < 0.05$ ).



	Biofilm carbohydrate concentration at 0.3 m ( $\mu\text{g}/\text{cm}^2$ )	Biofilm protein concentration at 0.3 m ( $\mu\text{g}/\text{cm}^2$ )	HRT (sec.)
Experiment A (◆)	$122.9 \pm 46.9$	$51.85 \pm 11.5$	228
Experiment F (▲)	$446.0 \pm 38.8$	$148.5 \pm 60$	384
Recovery (■)	$107.0 \pm 7.6$	$42.2 \pm 4.7$	222

**Figure 6.5.** RTD curves after a trace pulse injection of rhodamine WT and corresponding table of biomass concentrations represented as total carbohydrate and total protein for: (◆) Experiments A (low organic loads  $1.3 \pm 0.5$  mg sBOD<sub>5</sub>/L); (▲) Experiment F (high sucrose induced organic loads of  $8.8 \pm 2.9$  mg sBOD<sub>5</sub>/L); and (■) recovery post high organic load (low organic loads). (Parameter means given  $\pm 1$  SD).

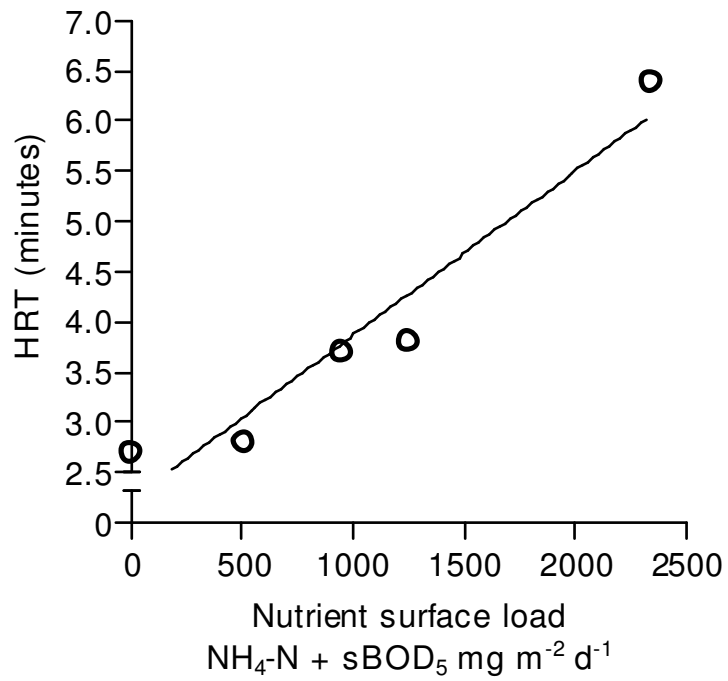


**Figure 6.6.** Steady-state relationship between HRT and NTF nutrient surface load measured as the sum of ammonia-N + sBOD<sub>5</sub> mg m<sup>-2</sup> d<sup>-1</sup>.

## 6.4 Discussion

The experimental component of this chapter investigated the influence that C:N ratio had on the polysaccharide, protein and heterotrophic composition of biofilms sampled from a potable water NTF. The relationship between biofilm composition and filter performance will be discussed.

Results from Chapter 5 showed that the augmentation of NTF organic carbon loading, via the addition of sucrose or methanol, suppressed nitrification, and confirmed for potable water biological treatment what has been widely documented for wastewater BNR processes (Boller *et al.* 1994; Zhang *et al.* 1994; Okabe *et al.* 1996; van Loosdrecht *et al.* 2000; Villaverde *et al.* 2000; Satoh *et al.* 2000). These studies have attributed the loss in nitrification to heterotrophs out-competing nitrifiers for space and oxygen. However, from results reported here, the HPC of the biofilm at various filter bed depths showed only small variations in heterotrophic numbers between experiments, and did not correlate statistically with the decline in percentage nitrification. The most notable increase in heterotrophs was of the magnitude of  $1\text{-log}_{10}$ , when influent carbon was increased from 1.3 to 8.8 mg sBOD<sub>5</sub>/L. A significant relationship between influent sBOD<sub>5</sub> and HPC was identified only at biofilm sample depths of 1.5 m and 2.7 m, and was not observed at the top bed depth of 0.3 m, which received the highest concentrations of carbon substrates. It was possible that HPC method underestimated heterotrophic numbers within the biofilm. It has been documented that this technique may not permit the growth of all viable bacteria present in environmental samples, and is limited to bacteria that are able to grow and form colonies (Mbrikawa and Tonoziuka, 1998; Bhupathiraju *et al.* 1999; Mezzanotte *et al.* 2004). Wagner *et al.* (1993) reported that only 5 to 15 % of total bacteria in activated sludge samples were detected using traditional plate count techniques. In addition, methods that require dilution of cells from biofilm aggregates particles are plagued by low cell recovery (Bhupathiraju *et al.* 1999).

Biofilm protein composition was measured in order to provide additional information regarding biomass growth in response to carbon loading. Similar to the HPC, no consistent pattern of protein content ( $\mu\text{g}/\text{cm}^2$ ) with respect to presence or absence of an external carbon source was identified. Biofilm protein was generally stable across all experiments. Microbial biomass, measured as total protein, did not increase in response to an increase in carbon substrate as observed by Magesan *et al.* (2000). Frolund *et al.* (1996) and Dumaz and Sanin (2001) have previously shown the Bradford protein assay to underestimate actual protein concentrations; something that may have contributed to the lack of detectable changes in biofilm protein between experiments. It was also possible that this method did not have the resolution required to detect the small fluctuations in protein, which may have occurred in response to the small variations in nutrient substrate. More likely, however, is that the stable protein may be an indicator that nitrogen or other nutrients may have been insufficient and limited cell synthesis and growth. The increase in bacterial polysaccharide concentration, measured as total carbohydrate, is a characteristic sign of nutrient limitation. When operated under high carbon loads, the NTF transformed from a nitrification to a predominantly carbon removal system (Chapter 5). This observation, coupled with stable biofilm protein mass, could have indicated that the numbers of heterotrophs did not increase, or more likely, that a shift in community structure had occurred, from nitrifiers to heterotrophs, which was then underestimated by the HPC assay.

An alternative procedure to HPC using FISH and DNA markers, coupled with fluorescence microscopy, may yield additional information. The FISH technique has an advantage over traditional spread plate methods, whereby it uses phylogenetic markers to identify non-culturable bacteria and quantitatively determine the composition of complex biofilm communities (Wuertz *et al.* 2003). *In situ* analysis of the biofilm using FISH should be employed to identify whether this hypothesised shift in community structure had occurred, and to confirm the extent of heterotrophic presence within the NTF biofilm, in response to high organic loads.

Excessive EPS production results from nutrient deficiency, or more accurately nitrogen limitation, and has been identified to be a significant problem in wastewater containing high concentrations of available carbon (Stover 1980; Punal *et al.* 2000; Dumaz and Sanin 2001; Metcalf and Eddy 2003). To date, most of the research related to biofilm polysaccharide concentration in relation to C:N ratio has been obtained from studies on the activated sludge process for wastewater treatment. Particularly, the author is unaware of studies which characterise biofilm polysaccharides concentration within a potable water NTF that was designed to operate under low carbon and nitrogen loads.

This study confirmed for a potable NTF what has previously been identified in wastewater BNR process. Relative to ammonia concentrations, high carbon loads via the addition of sucrose or methanol, significantly increased the mass of biofilm polysaccharide—measured as total carbohydrate. A linear relationship between the mass of biofilm carbohydrate and influent sBOD<sub>5</sub> concentration existed at all biofilm sample sites, and was most evident once influent organic carbon was increased beyond 5 mg/L of sBOD<sub>5</sub> or a surface loading rate of 866.4 mg sBOD<sub>5</sub> m<sup>-2</sup> d<sup>-1</sup>. These findings support those of Stover (1980), Bengtsson (1991), Veiga *et al.* (1997), Punal *et al.* (2000), and Liao *et al.* (2001); who reported that bacterial carbon utilisation shifted towards EPS production when readily available carbon was in excess or nitrogen was limited. Similarly, Wu *et al.* (1982), and Dumaz and Sanin (2001) reported for activated sludge, that C:N ratio influenced the relative distribution of carbohydrate and protein. They reported that a shift from low to high C:N ratio caused a significant increase in carbohydrate, and a decrease in protein concentration. In contrast, results from the present study indicated that protein mass was independent of both carbon loading and C:N ratio for all biofilm sample sites. A linear relationship between the protein:carbohydrate ratio and influent sBOD<sub>5</sub> was evident at all biofilm sample sites, however, since protein remained stable, shifts in protein:carbohydrate ratio was a direct result of the carbohydrate fraction increasing in response to carbon loading.

Dumaz and Sanin (2001) demonstrated that carbohydrate concentrations increased in activated sludge with increased C:N ratio. C:N ratio was increased by varying sucrose

only, where nitrogen remained constant. For the current study, C:N ratio was varied by adjusting both sucrose and ammonia concentrations. Results confirmed that an increase in biofilm polysaccharide production was a function of carbon loading only, and not C:N ratio. No significant relationship between C:N ratio and mass of biofilm carbohydrate was identified for any of the biofilm sample sites. Similarly, no significant difference between mean biofilm carbohydrate mass, between experiments which operated under identical carbon but different ammonia-N loads, was identified. Since the mass of carbohydrate was a function of carbon loading not C:N ratio, it was possible the filter was nitrogen limited, even at highest ammonia-N loads. However, calculation of theoretical stoichiometric yield for heterotrophic biomass (Metcalf and Eddy 1994), suggested that nitrogen was sufficient in all experiments, and therefore was not likely to have been limiting. In addition, theoretical and observed nitrogen assimilation requirements identified in Chapter 5, also showed that under high carbon loads, nitrogen was sufficient, where only 2 to 25 % of influent ammonia-N was required for biomass growth. Given that nitrogen was sufficient, the increase in biofilm polysaccharide may be attributed to the readily biodegradable nature of the carbon substrate (sucrose), or occurred in response to limitations in available phosphorous.

Phosphorous is also essential for bacterial growth, and therefore excessive biofilm polysaccharide production observed in this study may have occurred in response to limited phosphorous substrate availability. Studies conducted by Veiga *et al.*, (1997), Bura *et al.*, (1998), and Mohamed *et al.* (1998) all confirmed a significant increase in biofilm polysaccharide production in phosphorous-depleted environments. For the duration of the current study, data obtained from United Water International records, showed that total phosphorous in the feed water was low, and varied between 0.05 to 0.08 mg/L. Working on mean phosphorous values of 0.042 mg/L, C:P defined in terms of BOD:total phosphorous, ranged between 119 and 238. According to recommended values (Metcalf and Eddy 2003) of 1 gram of phosphorous per 100 grams of BOD<sub>5</sub> (ratio of 100) for the activated sludge process, phosphorous may be considered to be insufficient in the NTF. However, it has been emphasised elsewhere that these requirements are not fixed, because the percentage distribution of phosphorous and

nitrogen in cell tissue varies between systems and with environmental conditions (Metcalf and Eddy 2003). The impact of phosphorous on biofilm polysaccharide composition requires further investigation.

The mass of biofilm carbohydrate was monitored more frequently during Experiment F in order to observe polysaccharide production after the onset of sucrose dosing. A steady increase in biofilm polysaccharide was coupled with a decline in NTF nitrification capacity. Once sucrose dosing was terminated, the mass of biofilm polysaccharide returned to background concentrations within 13 d, and this coincided with complete recovery in nitrification. These results are comparable with Stover (1980) who demonstrated that EPS in activated sludge flocs had degraded within 2 weeks once nitrogen and phosphorous was sufficient. Under controlled laboratory conditions, Obayashi and Gaudy (1972) showed lag periods of 2 to 10 d before the degradation of EPS had commenced. Both studies concluded that EPS could serve as a usable source of organic carbon. Furthermore, Zhang and Bishop (2003) showed that the carbohydrate fraction of activated sludge flocs could be used as a carbon source by its own producers as well as other microorganisms.

The study reported here also investigated the influence of intermittent high carbon loads on biofilm composition. Carbon was dosed intermittently in cycles of 48-h on – 48-h off to mimic fluctuations in organic carbon often observed at Buaran WTP. The results showed that there was no significant difference between biofilm composition in terms of carbohydrate, protein and heterotrophic plate count, when compared with the NTF continuously dosed with carbon (Experiment F). The magnitude of nitrification inhibition, which was discussed in Chapter 5, was also similar for the two systems continuously or intermittently dosed with carbon. The NTF fed carbon intermittently or continuously, showed a progressive increase in biofilm carbohydrate. The increase in biofilm carbohydrate was coupled with a decline in nitrification capacity. Furthermore, the results from the intermittently fed NTF, suggest that the rate of polysaccharide production during each carbon spike event had exceeded the rate of degradation between spikes. The elevated biofilm carbohydrate mass seen during elevated organic

spikes may also be attributed to an induced 'feast-famine' type scenario, which has also been shown to stimulate bacteria to produce EPS (Liu and Herbert 2003). Results from the current study suggest that intervals of at least 6–8 d between carbon spikes, which should ideally last no longer than 2–5 d, is essential for maintaining adequate nitrification capacity.

This study has also confirmed that the type of carbon source dosed, determined the quantity of polysaccharide produced within the NTF, which in turn then influenced overall nitrification capacity. When sucrose or methanol was dosed as the sole carbon source, a significant increase in biofilm carbohydrate was identified at all biofilm sample depths. The quantity of polysaccharide produced when operated under methanol- or sucrose-induced sBOD<sub>5</sub> loads was similar throughout the filter bed, and coincided with a decline in nitrification. In contrast, when a more native-like carbon source (organic fertiliser) was dosed to provide the high influent sBOD<sub>5</sub> concentrations, biofilm carbohydrate remained low, and nitrification remained unaffected—whereby nitrification performance was comparable with a low-organic-loaded NTF. These observations may be due to differences in availability between the carbon sources, and the types of organisms for which they selectively enrich. These results are in agreement with Sponza (2003), who reported that the type and biodegradability of carbon substrate in wastewater had a strong influence on biofilm carbohydrate concentration.

Findings from Chapter 5 have demonstrated that the filter could be compartmentalised, where each depth encountered variations in carbon and nitrogen concentrations, which then directly affect the biofilm composition. Carbohydrate, protein and heterotrophic concentrations were all greatest at the top of the filter, which also received highest nutrient concentrations, and reduced with depth in response to carbon and nitrogen gradients. The most significant difference in biofilm carbohydrate between experiments was identified at the top filter bed depth of 0.3 m, which was exposed to greatest fluctuations in nitrogen and carbon concentrations. Due to the high removal of carbon and nitrogen observed at the top, the lower depths experienced more stable conditions, therefore changes in biofilm composition between experiments were not as great.

Statistically, nitrification performance was found to be a function of biofilm carbohydrate mass, and reflected nitrogen removal profiles down the filter column. The impediment of ammonia-N removal down the filter bed correlated well with an increase in biofilm carbohydrate at all biofilm sample depths. A similar relationship was not identified with biofilm HPC or protein composition.

EPS strongly influences the mass transfer properties of biofilms (Wuertz *et al.* 2003), where external layers of polysaccharides can influence physicochemical processes such as diffusion by acting as diffusion barriers, molecular sieves, and adsorbents (Charackis and Marshall 1990). It was therefore reasonable to suggest that high biofilm polysaccharide concentrations observed during this study, may have caused mass transfer limitations for oxygen and ammonia through the biofilm depth, which subsequently impeded the filter's ability to maintain nitrification. To the author's knowledge, the relationship between the mass of biofilm polysaccharide and nitrification performance has not been widely reported for NTFs treating wastewater, and may reflect differences between water composition which included nutrient availability and carbon biodegradability.

Tracer experiments were performed to determine and compare the hydraulic characteristics of the NTF when operated under various nitrogen and organic carbon loads. This study identified a strong relationship between HRT and nutrient loading. Many studies have shown that RTD and HRT vary according to the type of support media, hydraulic loading, and the amount of biomass present (Seguret *et al.* 2000). Here, the media used and the hydraulic loading were consistent between all experiments, therefore it was reasonable to suggest that changes in HRT and RTD were a function biomass quantity, which in turn, was influenced by nutrient loading. The most significant change in filter HRT and RTD was identified when the NTF was operated under high organic carbon loads, where the HRT had almost doubled, and the RTD curve showed signs of greater tailing. This observation coincided with an increase in biofilm carbohydrate and protein mass, and a decline in nitrification capacity. Visual inspection of the filter media also revealed a thicker biofilm. The diffusion of the tracer in

and out of the biofilm is influenced by biomass volume and according to Riemer *et al.* (1980) and Stevens *et al.* (1986), and could explain the longer tail observed on the RTD curve. For this study, the increased RTD tail observed during high organic carbon loads may also be attributed to a thicker biofilm and a higher mass of carbohydrate, because EPS has the ability to retain many times its weight in water (Chenu and Roberson 1996). The longer HRT and drawn-out RTD curve may also be attributed to media 'clogging', or 'ponding', which was most evident at the top of the filter. This was observed at the end of Experiments B, F and G where organic loading was increased, and was probably due to excessive biofilm polysaccharide accumulation.

These results suggest that changes in filter RTD curves and HRT can be a useful parameter for monitoring general filter 'health', and could also indicate when preventative measures should be taken to avoid filter clogging or even collapse. One measure to maintain favourable hydraulic characteristics may include increasing the hydraulic loading which can induce biomass sloughing. The recovery RTD and HRT was determined several weeks after the organic loading had been reduced to background levels. Results showed that the filter had recovered and regained normal hydraulic characteristics without the need to induce sloughing. The recovery in HRT and RTD was coupled with a decline in biofilm EPS and complete recovery in nitrification throughout the entire filter bed.

Results from this chapter have shown that nitrification performance was strongly associated with biofilm carbohydrate composition. Most studies have attributed the decline in NTF nitrification capacity to heterotrophic competition for resources with the nitrifying population, however, this study found no significant relationship between HPC and nitrification capacity. Due to the complex structure of biofilms, it was possible that HPC might have underestimated the true heterotrophic presence. An alternative procedure using FISH coupled with SEM was later employed to identify the spatial relationship between AOB, NOB and heterotrophs within biofilms sampled from the NTF. Results from these investigations are presented in Chapter 7.

# 7 MICROBIAL ECOLOGY OF A NITRIFYING TRICKLING FILTER TREATING POTABLE WATER

## 7.1 Introduction

Nitrifying biofilms used in wastewater treatment are heterogeneous, both in structure and in microbial composition (Lydmark *et al.* 2006). Therefore characterisation of microbial populations and understanding the complex ecology of biofilms is crucial for improving design and operation of biological treatment processes.

In the past, most of our understanding of biofilm community structure has been reliant on a few species of readily culturable bacteria. Due to difficulties associated with culturing nitrifying bacteria, partly owing to lengthy culture incubation periods, traditional cultivation-dependant methods such as most probable number (MPN) and viable plate counts for the enumeration of AOB and NOB, have proven to be unsuccessful, and have been limited to few species of culturable nitrifiers (Jang *et al.* 2003; Lydmark *et al.* 2006). With the development of molecular techniques, phylogenetic compositions of AOB and NOB have been determined. In wastewater environments, AOB consist of the genera *Nitrosomonas*, *Nitrospira* and *Nitrosococcus*. NOB includes the genera *Nitrobacter*, *Nitrospira*, *Nitrococcus* and *Nitrospina* (Coskuner and Curtis 2002).

The ability to identify phylogenetic composition for AOB and NOB has lead to the design and synthesis of 16S rRNA-targeted oligonucleotide probes capable of detecting microorganisms at different taxonomic levels (Noda *et al.* 2003). The development of *in situ* techniques such as FISH has provided a better understanding of the microbial diversity and ecology of nitrifying biofilms within biological wastewater reactors. In particular, competitive interactions between heterotrophs, AOB and NOB, for space, oxygen and nutrients have been widely investigated (Zhang *et al.* 1994; Okabe *et al.*

1996; Satoh *et al.* 2000; van Loosdrecht *et al.* 2000). Several studies have reported that high levels of organic substrates will cause slow growing AOB and NOB bacteria to become out-competed and overgrown by faster growing heterotrophs (Okabe *et al.* 1996; van Loosdrecht *et al.* 2000). The differences in growth rates may also cause depth-wise stratification of nitrifiers and heterotrophs within the biofilm (Okabe *et al.* 1996). In most cases, the outer heterotrophic layer limits the diffusion of oxygen to nitrifiers that are restricted to the lower depths of the biofilm, to a point where nitrification is inhibited (Okabe *et al.* 1996; vanBenthum *et al.* 1997; Satoh *et al.* 2000).

Research conducted by Mobarry *et al.* (1996), Araki *et al.* (1999), Daims *et al.* (2001), Han *et al.* (2002), and Okabe *et al.* (2002)—using *in situ* techniques such as FISH—has enhanced our overall understanding of biofilm structure and function in wastewater treatment processes; something which has led to improvements in process design and control. However, further research is needed in order to better understand the community structure of biofilm reactors treating potable water, which operate under lower or sometimes nutrient-limited conditions.

This study investigated the application of NTFs as a means of ammonia removal from Buaran WTP. The feed water was characterised by rapid fluctuations in ammonia-N (0.5 to 2.5 mg/L) and turbidity. Organic carbon, measured as BOD<sub>5</sub> varied between 5 to 10 mg/L. Findings from Chapter 6 have suggested that when operated under these conditions, heterotrophic competition may be a smaller contributing factor toward the observed decline in nitrification than previously suggested. Alternatively, biofilm polysaccharide concentration (measured as total carbohydrate) was found to have a greater detrimental impact on nitrification than heterotroph density (quantified using standard HPCs). Due to the complex structure of biofilms, it was hypothesised that culture-dependant methods for enumerating heterotrophs, such as spread plates, might be unrepresentative of true numbers. Therefore, *in situ* techniques such as FISH and SEM need to be employed to identify whether the same stratification of nitrifiers and heterotrophs existed (within the current NTF) during high sBOD<sub>5</sub> loads as has been

previously discovered in *wastewater* biological treatment processes by Zhang *et al.* (1994), Okabe *et al.* (1996), Satoh *et al.* (2000), and van Loosdrecht *et al.* (2000).

Following this, the aim of this part of the research was to survey the microbial ecology of a pilot NTF used for *potable* water treatment. For this study, the pilot NTF was operated under conditions that simulated the raw water quality of Buran water WTP. FISH and SEM were used to identify the spatial relationship between AOB, NOB and heterotrophs in biofilms sampled from the trickling filter, when operated under various ammonia and organic carbon loads.

## **7.2 Methods**

### **7.2.1 *Experimental design***

The pilot plant operated under conditions that simulated the raw water quality at Buaran WTP. Influent was augmented with ammonium sulphate and sucrose to simulate variations in BOD<sub>5</sub>:ammonia-N ratio. A summary of influent ammonia-N and sBOD<sub>5</sub> concentrations and corresponding loading rates for each experiment are displayed in Table 7.1. For Experiment G, sucrose was dosed intermittently (48-h on, 48-h off), to mimic fluctuations in organic carbon often observed at Buaran WTP. Experiments A, C, F, and G were performed using the large pilot-scale NTF described in Chapter 3, Section 3.2. Experiment I was performed using a small pilot-scale NTF, where sucrose dosing was substituted with organic fertiliser (trade name: Rooster Booster) to mimic a native-like sBOD<sub>5</sub> source.

### **7.2.2 *Biofilm sampling***

Biomass was harvested along the vertical axis of the large pilot-scale NTF from biofilm sample sites, positioned at bed depths of 0.3, 1.5 and 2.7 m from the surface. Sampling, and preservation was achieved in accordance with procedures describe in Chapter 3, Section 3.7.5.

### **7.2.3 *FISH and SEM***

FISH and SEM was performed in accordance with procedures described in Chapter 3, Section 3.7.

### **7.2.4 *Large pilot-scale NTF—sampling and chemical analysis***

Profile sampling consisted of collecting filtrate grab samples (0.5 L) throughout the NTF, at the time of biofilm harvest. Profile samples were taken from bed depths of 0.3, 1.5 and 2.7 m from the surface, in accordance with the procedure described in Chapter 3

Section 3.2.11. Samples were analysed on the same day of sampling for ammonia-N, nitrite-N, nitrate-N, TOC and sBOD<sub>5</sub> using procedures described in Chapter 3, Section 3.5

#### **7.2.5      *Small pilot-scale NTFs—sampling and chemical analysis***

Influent and effluent 0.5 L grab sampling was performed at the time of biofilm harvest. Samples were analysed on the same day of sampling for ammonia-N, nitrite-N and nitrate-N. TOC and sBOD<sub>5</sub> was measured within the influent on average once a week.

**Table 7.1.** Trickling filter influent ammonia-N and sBOD<sub>5</sub> concentrations and corresponding loadings rate (mean ± 1 SD).

Experiment	Influent ammonia-N		Influent sBOD <sub>5</sub>		External carbon source	Duration of carbon dosing (Days)
	mg/L	mg m <sup>-2</sup> d <sup>-1</sup>	mg/L	mg m <sup>-2</sup> d <sup>-1</sup>		
<b>A</b> <sup>1</sup>	4.9 ± 0.6	846.6 ± 113.4	1.3 ± 0.5	225.2 ± 87.9	none	0
<b>C</b>	0.56 ± 0.1	97.8 ± 19.7	5.4 ± 0.15	931.4 ± 26.0	Sucrose	18
<b>F</b>	4.7 ± 1.1	826.1 ± 163.9	8.8 ± 2.9	1533.5 ± 510.6	Sucrose	12
<b>G</b> <sup>†</sup>	4.8 ± 0.5	840.1 ± 86.2	9.4 ± 0.9	1625.4 ± 162.7	Sucrose	three 48 h spikes
<b>I</b> <sup>2</sup>	1.3 ± 0.3	220.8 ± 48.3	11.5 ± 3.4	1992.8 ± 589.3	Organic fertiliser	16

<sup>1</sup>Data obtained from Chapter 4 when the NTF was operated under low sBOD<sub>5</sub> loads. sBOD<sub>5</sub> represents background native organic carbon present in Hape Valley reservoir.

<sup>†</sup>Intermittent sBOD<sub>5</sub> spikes (48-h on / 48-h off).

<sup>2</sup> Experiment conducted using the small pilot-scale NTF

## 7.3 Results

### 7.3.1 Nitrification performance

Figure 7.1 shows the depth profile of ammonia-N, nitrite-N, and nitrate-N throughout the filter bed for Experiments A, C, F and G. Figures 7.1.b, 7.1.c and 7.1.d shows that an increase in organic carbon load via the addition of sucrose impeded nitrification throughout the entire NTF bed. When comparing Figures 7.1.b, 7.1.c and 7.1.d (increased sBOD<sub>5</sub> loads) with Figure 7.1.a (low sBOD<sub>5</sub> load), a significant decline in ammonia-N removal down the filter bed can be seen. The overall percentage nitrification declined from  $96.0 \pm 4.0$  % (Experiment A) to  $70.4 \pm 7.0$  % (Experiment C),  $31.5 \pm 17.7$  % (Experiment F) and  $50.5 \pm 13.6$  % (Experiment G; Figure 7.2). When sucrose was substituted with organic fertiliser (Experiment I), no statistical difference in percentage nitrification between Experiments A and I was observed (Mann Whitney *U* test;  $p=0.518$ ). The percentage nitrification remained relatively similar at  $94.3 \pm 6.3$  % (Figure 7.2).

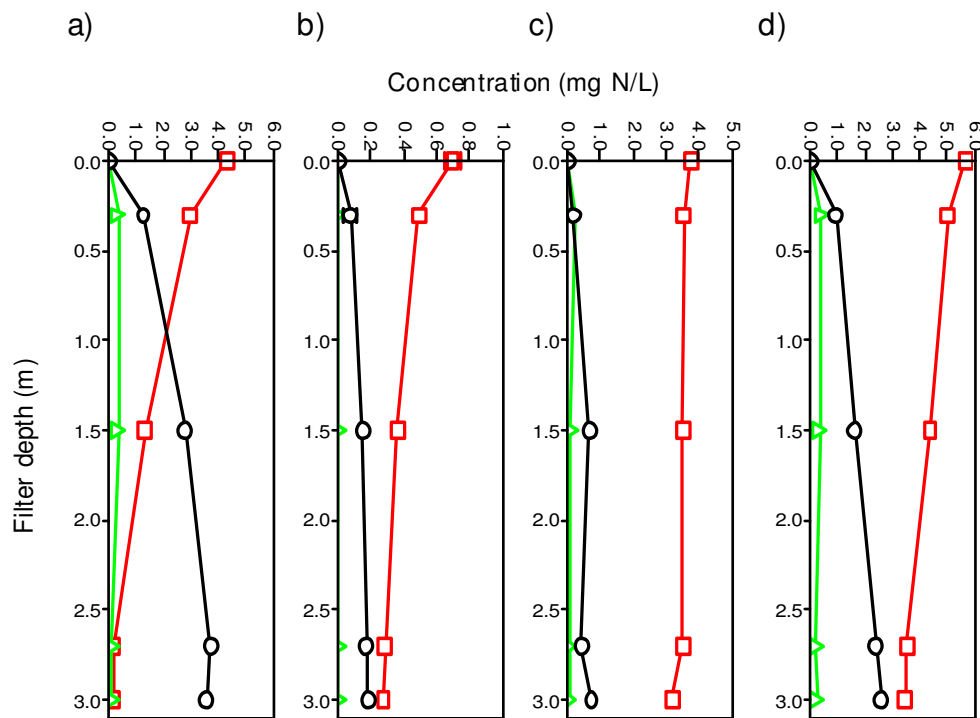


**Figure 7.1.** Concentration profile of: (□) ammonia-N; (△) nitrite-N; and (○) nitrate-N observed through the depth of the large pilot-scale NTF during time of biofilm harvest. (a) Experiment A – profile obtained when operated under low influent sBOD<sub>5</sub> concentrations of  $1.3 \pm 0.5$  mg/L; (b) Experiment C – profile obtained when operated under high influent sBOD<sub>5</sub> concentrations of  $5.4 \pm 0.15$  mg/L via the addition of sucrose; (c) Experiment F – profile obtained when operated under high influent sBOD<sub>5</sub> concentrations of  $8.8 \pm 2.9$  mg/L via the addition of sucrose; and (d) Experiment G – profile obtained when operated under high intermittent influent sBOD<sub>5</sub> concentrations of  $9.4 \pm 0.9$  mg/L. (Data points represent parameter means  $\pm 1$  SD).

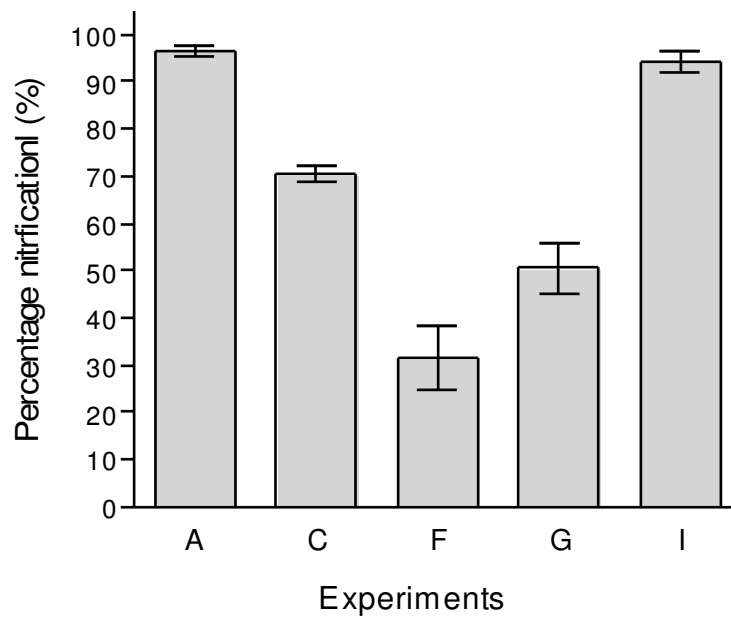


**Figure 7.2.** Mean percentage nitrification values measured for all experiments: Experiment A – NTF operated under low influent sBOD<sub>5</sub> concentrations of  $1.3 \pm 0.5$  mg/L; Experiment C – NTF operated under high influent sBOD<sub>5</sub> concentrations of  $5.4 \pm 0.15$  mg/L via the addition of sucrose; Experiment F – NTF operated under high influent sBOD<sub>5</sub> concentrations of  $8.8 \pm 2.9$  mg/L via the addition of sucrose; Experiment G – NTF operated under high intermittent influent sBOD<sub>5</sub> concentrations of  $9.4 \pm 0.9$  mg/L via the addition of sucrose; and Experiment I – NTF operated under high influent sBOD<sub>5</sub> concentrations of  $11.5 \pm 3.4$  mg/L via the addition of organic fertiliser (individual column means given  $\pm 1$  SD).

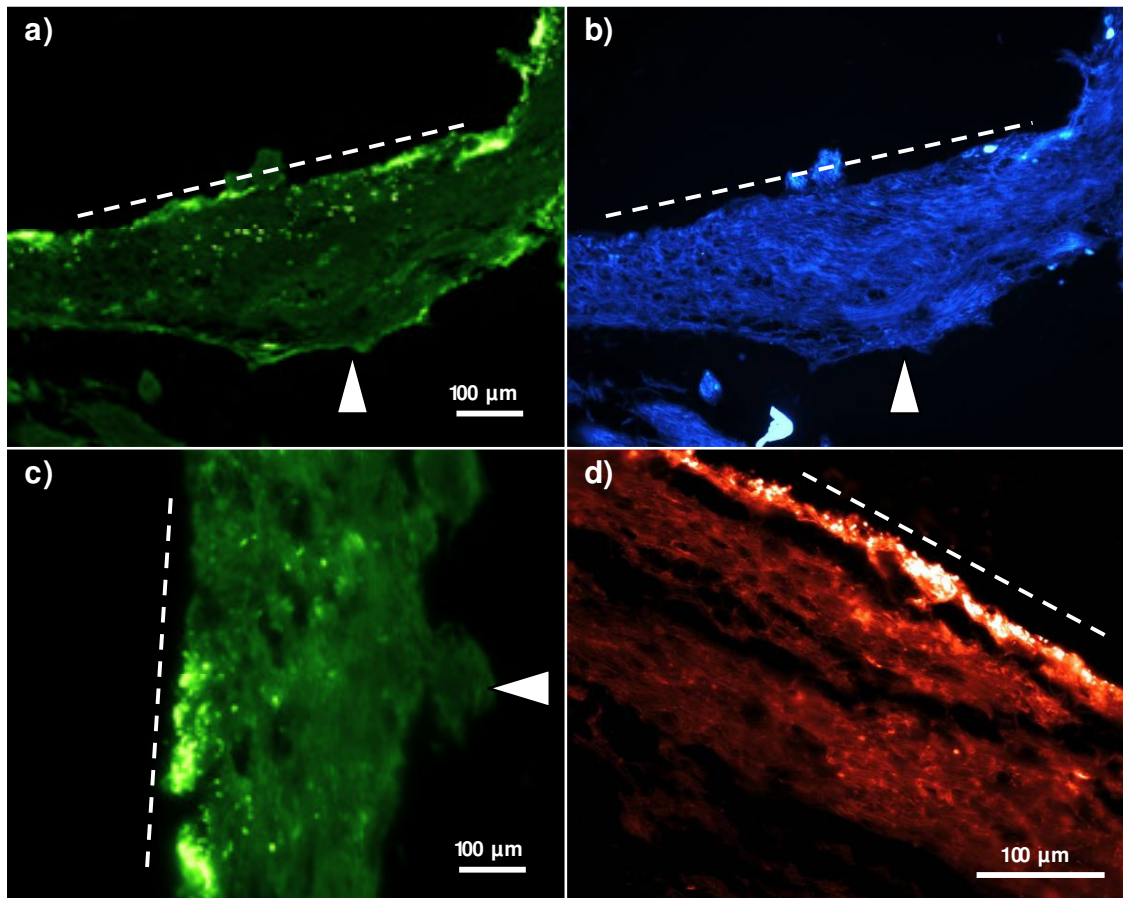
### **7.3.2 Distribution of AOB and NOB during low organic carbon loads: Experiment A**

Plate 7.1 shows the *in situ* structure of a nitrifying biofilm sampled from the surface of the trickling filter when operated under low organic carbon loads (Table 1; Experiment A). The fluorescent micrographs show that NOB (Plate 7.1.a and 7.1.c) and AOB (Plate 7.1.d) targeted with oligonucleotide probes NIT3 and NSO1225 respectively, were limited to the lower depths of the biofilm, closest to the filter support media. Plate 7.1.b shows strong autofluorescence caused by cyanobacteria which appeared dominant within the biofilm. Based on tentative morphological characteristics, they were most likely to be filamentous cyanobacteria, possibly belonging to genera *Anabaena* or *Nodularia*.

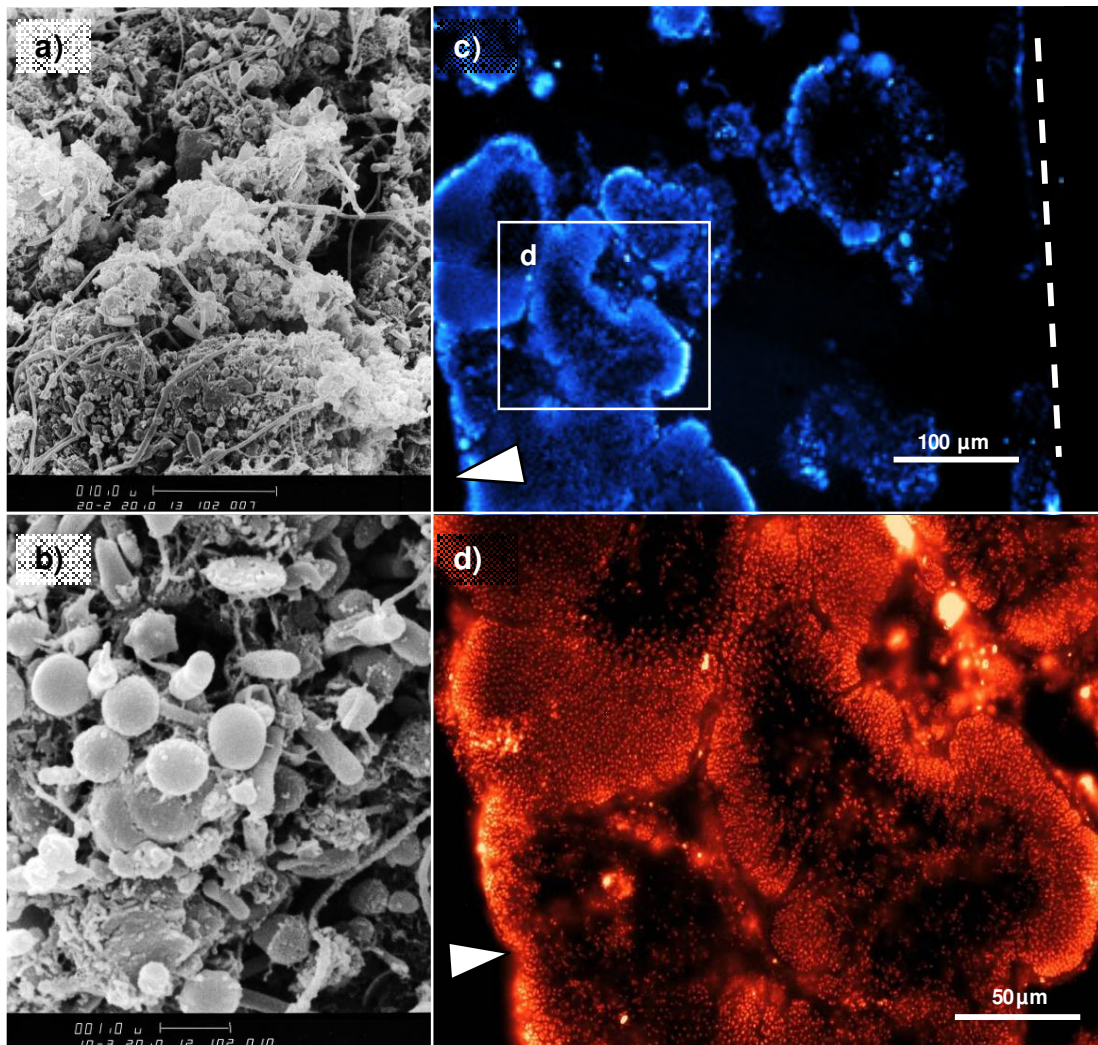
Plate 7.2 shows the *in situ* structure of the biofilm sampled from the trickling filter at the bed depth of 0.3 m during Experiment A (Table 1). Scanning electron micrographs reveal the *in situ* ultra structure of the biofilm's outer surface (Plates 7.2.a and 7.2.b), which shows an abundance of bacterial cells. Plate 7.2.c is a fluorescent micrograph showing the *in situ* structure of a biofilm cross section stained with DAPI. The biofilm structure appeared to be homogenous consisting of many large bacteria colonies scattered throughout the entire biofilm depth. FISH using oligonucleotide probes NSO1225 and NIT3 identified many colonies to be AOB (Plate 7.2.d) and NOB. Colonies ranged in size from approximately 10 to 130  $\mu\text{m}$  in diameter. Mean biofilm thickness was  $496.4 \pm 109 \mu\text{m}$  ( $n = 12$  cross-sections).

Plate 7.3 shows the *in situ* structure of the biofilm at various filter bed depths (0.3, 1.5 and 2.7 m) during Experiment A (Table 1). For all bed depths, AOB and NOB were abundant, and represented the majority of total bacteria identified with DAPI. Clusters of AOB and NOB could be detected throughout the inner- and outer-depths of the biofilm and were generally found in close proximity to each other. Plates 7.3.a and 7.3.b shows clusters of *Nitrobacter* located within the outer depth of the biofilm after FISH, hybridised with oligonucleotide probe NIT3. A positive signal for oligonucleotide probes NIT3 and

NTSPA662, was observed at all filter bed depths, which suggested that the NOB belonged to the genera *Nitrobacter* (Plate 7.3.b), which have been rarely identified in wastewater BNR studies and *Nitrospira* (Plate 7.3.d), which are considered to be the most prevalent genera of NOB in aquatic nitrifying processes. Due to the thin coverage of biomass on the support media at filter bed depths of 1.5 and 2.7 m, preservation of the biofilm structure was difficult to maintain during biofilm sample preparation. As a result, measuring and visualising the entire biofilm cross-section as a whole was difficult. Despite these difficulties, AOB and NOB were clearly visible within all biofilm fragments (Plates 7.3.c, 7.3.d and 7.3.f).



**Plate 7.1.** Fluorescent micrographs showing *in situ* structure of the nitrifying biofilm sampled from the surface (0 m) of the trickling filter, at low organic carbon loads ( $1.3 \pm 0.5$  mg sBOD<sub>5</sub>/L) during Experiment A: (a and c) *in situ* identification of *Nitrobacter* spp after FISH using 16S rRNA oligonucleotide probe NIT3 (x200); (b) auto-fluorescence of filamentous algæ (x200); and (d) *in situ* identification of *Nitrosomonas* spp after FISH using 16S rRNA oligonucleotide probe NSO1225 (x200). Dashed line represents the media–biofilm interface. White arrows point towards the water–biofilm interface.



**Plate 7.2.** *In situ* structure of the nitrifying biofilm sampled from trickling filter bed depth of 0.3 meters during Experiment A, at low organic loads ( $1.3 \pm 0.5$  mg sBOD<sub>5</sub>/L): (a) SEM of the nitrifying biofilm showing bacteria cells located on the outer biofilm surface; (b) higher magnification of image (x10000); (c) corresponding fluorescent micrograph of image (a) showing biofilm cross-section stained with DAPI depicting total cell count (x200); and (d) higher magnification (x400) of image (c), showing AOB after FISH using 16S rRNA oligonucleotide probe NSO1225 specific for *Nitrosomonas* spp. Dashed line represents the media-biofilm interface. White arrows point towards the water-biofilm interface.

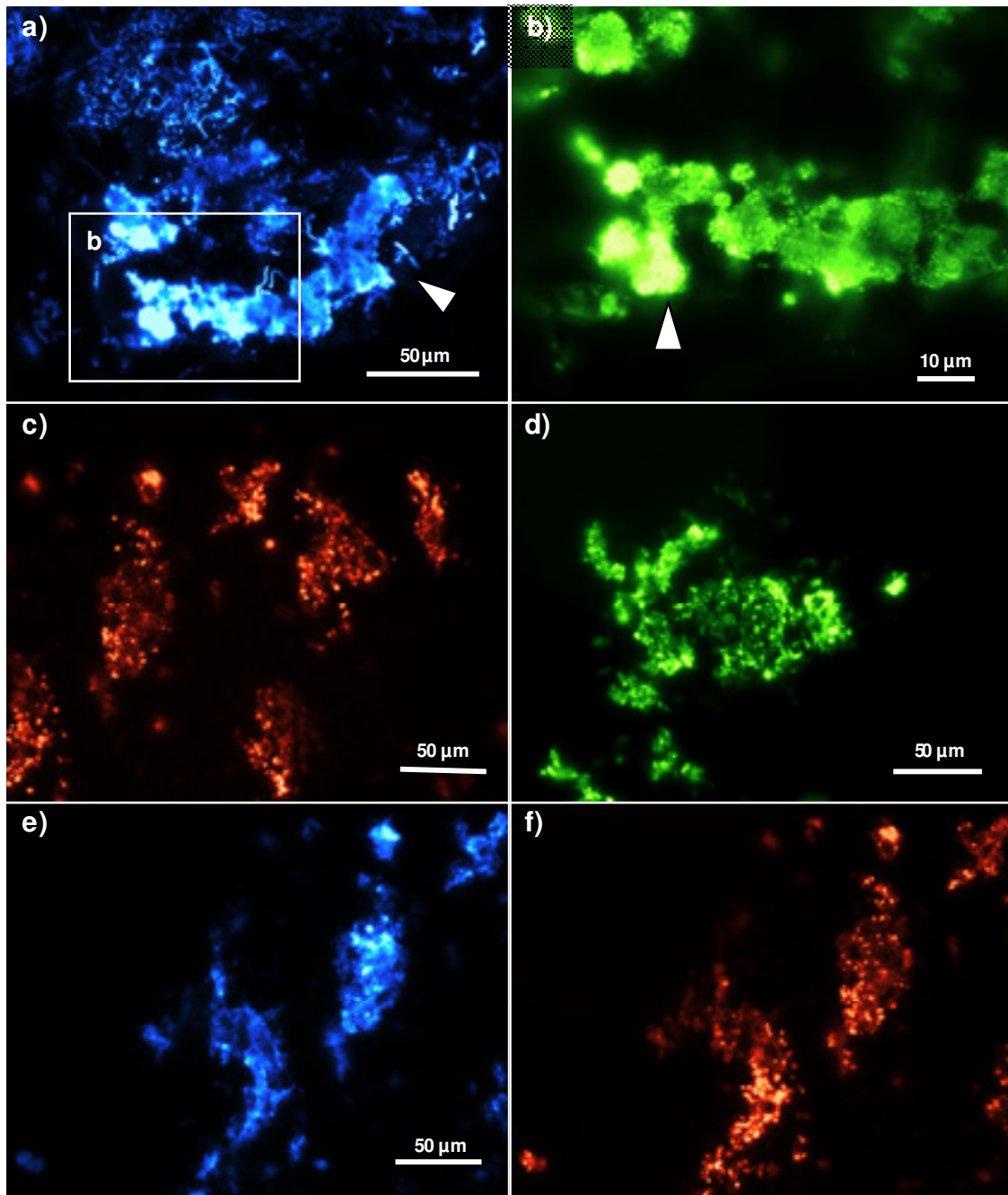


**Plate 7.3.** *In situ* structure of the biofilm *fragments* sampled from various filter bed depths during Experiment A, at low organic loads ( $1.3 \pm 0.5$  mg sBOD<sub>5</sub>/L): (a) total cell count using DAPI of biofilm sampled from bed depth of 0.3 m (x400); (b) *in situ* identification of *Nitrobacter* spp within the outer depths of the biofilm after FISH using

16S rRNA oligonucleotide probe NIT3 (x1000); *in situ* identification of *Nitrosomonas* spp (c) and *Nitrospira* spp (d) within the biofilm sampled from filter bed depth of 1.5 m, after FISH using 16S rRNA oligonucleotide probe NSO1225 and NTSPA662 respectively (x400); (e) total cell count using DAPI of biofilm sampled from filter bed depth of 2.7 m (x400); and (f) corresponding fluorescent micrograph of image (e), showing *Nitrosomonas* spp after FISH using 16S rRNA oligonucleotide probe NSO1225 (x400). White arrows point towards the water–biofilm interface.

### **7.3.3 Vertical distribution of AOB, NOB and heterotrophs during high organic carbon loads**

#### **Experiment C**

Plate 7.4 shows the *in situ* structure of the biofilm at various filter bed depths during Experiment C following an increase in influent sBOD<sub>5</sub> concentration from 1.3 to  $5.4 \pm 0.15$  mg/L. The background concentration (1.3 mg/L) represents the native sBOD<sub>5</sub> of Hope Valley reservoir raw water, prior to dosing with sucrose. Influent ammonia-N concentration was maintained at  $0.56 \pm 0.1$  mg NH<sub>4</sub>-N/L. Plate 7.4.a is an electron micrograph of the biofilm sampled from a filter bed depth of 0.3 m. In contrast to periods when the filter operated under low organic loads (Plate 7.2), a thick woven mat of filamentous-like bacteria appeared to dominate the outer depths of biofilm. Plate 7.4.b shows the structure of the filamentous-like bacteria in greater detail. Similarly, the electron micrographs of Plates 7.4.a and 7.4.b, of biofilm sampled from the middle of the trickling filter (bed depth of 1.5 m), show filamentous-like bacteria to be dominant. Plate 7.4.d is a FISH micrograph, using the generic oligonucleotide probe EUB338 which is specific for most bacteria, of the same biofilm sample used for the SEM image of Plate 7.4.c. This confirmed that the outer filamentous growth was in fact bacterial, not fungal mycelium.

Plate 7.4.e is a scanning electron micrograph of the biofilm sampled from the bottom of the trickling filter. Some filamentous-like bacteria can be seen embedded within a thick layer of EPS. Plate 7.4.f shows the EPS layer in greater detail (green arrow). Large crevasses have formed within the EPS crust, possibly a drying artefact during the dewatering procedure required for SEM. This crevasse revealed a cluster of bacterial cells attached to the media surface, located beneath the EPS layer. Plate 7.4.g is a fluorescent micrograph of a biofilm cross section stained with DAPI. The spatial distribution of microorganisms, covered by a thick EPS crust and filamentous-like bacteria complements the electron micrographs seen in Plates 7.4.e and 7.4.f. A strong fluorescent signal was detected close to the media, indicating many of the microorganisms were located deep within the biofilm or attached to the media surface. Auto-fluorescence was observed, presumably caused by EPS within the mid depths of

the biofilm. In comparison with the lower depths of the biofilm, the mid depths were low in cell density. Similar to Plates 7.4.e and 7.4.f, some filamentous-like bacteria can be seen within the outer layer of the biofilm (red arrow).

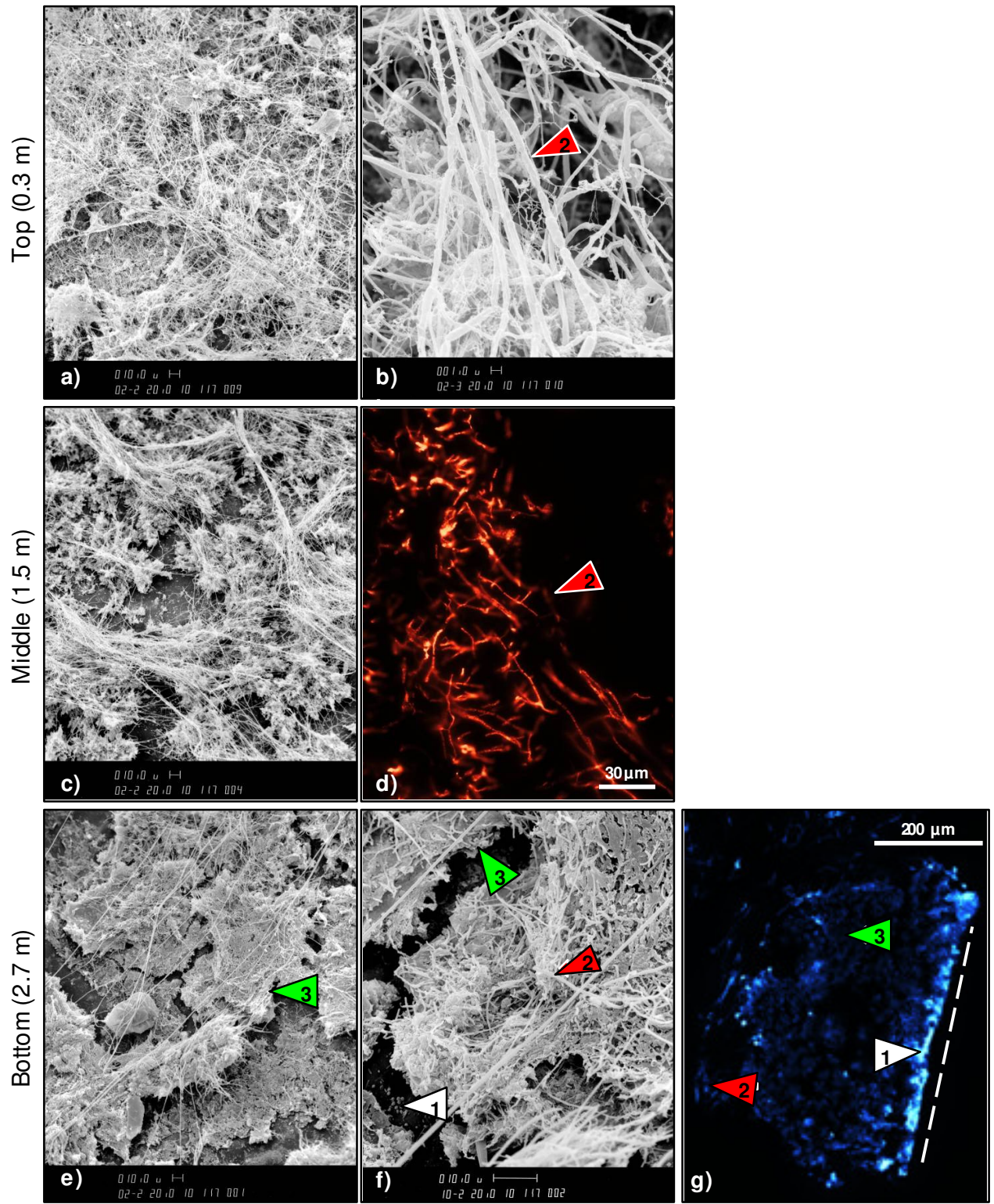


**Plate 7.4.** *In situ* structure of the biofilm at various filter bed depths during: Experiment C– high sBOD<sub>5</sub> ( $5.4 \pm 0.15$  mg/L) loading using sucrose; (a) SEM of the biofilm sampled from the top of the trickling filter; (b) increased magnification (x10000) of image (a) showing the structure of filamentous-like bacteria; (c) SEM of the biofilm sampled from the mid bed depth of the trickling filter; (d) *in situ* identification of filamentous heterotrophs within the outer depths of the biofilm after FISH with Cy3-labeled EUB338 oligonucleotide probe specific for most bacteria (x400); (e) SEM of the biofilm sampled from the bottom of the trickling filter; (f) increased magnification (x10000) of image (e) showing microorganisms embedded in a thick EPS layer; and (g) biofilm cross-section stained with DAPI (x100). White arrows (1) show bacteria cells attached to the media surface. Red arrows (2) show outward growth of heterotrophic filamentous-like bacteria, located at the water–biofilm interface. Green arrows (3) highlight the thick layer of EPS. Dashed line represents the media–biofilm interface.

## Experiment F

Plate 7.5 shows the *in situ* structure of the biofilm sampled from the top of the filter (0.3 m) during Experiment F, where influent sBOD<sub>5</sub> and ammonia-N concentrations were increased and maintained at around  $8.8 \pm 2.9$  mg/L and  $4.7 \pm 1.1$  mg/L respectively (Table 7.1). Plate 7.5.a shows a biofilm cross-section stained with DAPI. In comparison to periods when the NTF operated under lower organic loads, fewer numbers of bacteria labelled with oligonucleotide probe NSO190, NSO1225 and NIT3 could be identified, which was possibly caused by a decline in AOB and *Nitrobacter* species. Stronger signals for NOB were obtained using probe NTSPA662, which suggested that *Nitrospira*-like bacteria were more prevalent than *Nitrobacter* under these conditions. The majority of AOB clusters that were targeted with probe NSO1225, were detected within the mid to lower depths of the biofilm (Plate 7.5.b). AOB clusters ranged in diameter from 7 to 46  $\mu\text{m}$ . Some *Nitrospira*-like bacteria were identified within the mid depths of the biofilm (Plate 7.5.f).

Auto-fluorescence, possibly caused by EPS, was most evident within the mid depths of the biofilm (Plate 7.5.c). A thick outer layer comprised mostly of heterotrophic, filamentous-like bacteria was detected using probe EUB338 (Plate 7.5.d). Bacterial chains up to 48  $\mu\text{m}$  long could be seen. Bacteria filaments ranged in size from 2.2–5.0  $\mu\text{m}$  long and 1.0–1.3  $\mu\text{m}$  wide. None of the oligonucleotide probes (NSO190, NSO1225, NIT3 and NTSPA662) used to target AOB and NOB bound to the outer filamentous layer. Plate 7.5.e is an electron micrograph of the same biofilm sample shown in Plate 7.5.d showing the outer heterotrophic layer in more detail; a thick woven matrix of branched filaments can be seen. The depth-wise stratification of nitrifiers and heterotrophs observed here can be attributed to differences in biomass yields, where in the presence of sucrose, faster growing heterotrophs appeared to out-compete slower growing nitrifiers for aerobic space, and subsequently dominated the outer biofilm depths.

Plate 7.6 shows the *in situ* structure of the biofilm sampled from the middle of the filter (1.5 m) during Experiment F (fed  $8.8 \pm 2.9$  mg sBOD<sub>5</sub>/L and  $4.7 \pm 1.1$  mg NH<sub>4</sub>-N/L). The

majority of bacteria targeted using probe EUB338 were filamentous-like bacteria, and were most abundant in the outer depths of the biofilm (Plate 7.6.a). Biofilm sections hybridised with probe EUB338 confirmed that the mid depths of the biofilm were low in bacterial density (Plate 7.6.b). The mid section shows individual bacterial cells targeted with EUB338 scattered within a dense EPS matrix (Plate 7.6.b). A few clusters of AOB were identified using probe NSO1225. AOB were limited to the lower depths of the biofilm, close to the support media (Plate 7.6.c). Few NOB could be detected with NIT3 within the biofilm cross section (Plate 7.6.e). Instead strong background fluorescence caused by EPS can be seen. Plate 7.6.f, shows total cells stained with DAPI. Most of the microorganisms identified with DAPI were located deep within the biofilm, closest to the filter support media surface. Similar to Plate 7.6.b, few cells stained with DAPI can be seen scattered throughout the mid depths of the biofilm.

Plates 7.7.a, 7.7.b and 7.7.c are fluorescent micrographs showing the *in situ* structure of a biofilm cross-section stained with DAPI, which was sampled from the bottom of the trickling filter (2.7 m) during Experiment F (fed  $8.8 \pm 2.9$  mg sBOD<sub>5</sub>/L and  $4.7 \pm 1.1$  mg NH<sub>4</sub>-N/L). Similar to the top (Plate 7.5; 0.3 m) and mid (Plate 7.6; 1.5 m) filter bed depths, fluorescent micrographs show a thick outer layer comprised mostly of filamentous-like bacteria. Plate 7.7.e is a higher magnification image (x400) of Plate 7.7.c after FISH, using oligonucleotide probe EUB338. This confirmed that the outer filamentous layer was bacterial, and not fungal mycelium. A biofilm cross-section stained with DAPI showed that greater numbers of bacteria were located deep within the biofilm close to the media surface, than at the mid depths (Plate 7.7.b). A fraction of these bacteria identified by DAPI were confirmed, using FISH, to be AOB and NOB. These results show AOB targeted with probe NSO1225 were limited to the lower depths of the biofilm, close to the media surface (Plates 7.7.d and 7.7.f). AOB were more abundant than NOB populations identified using probe NIT3, however, the few clusters of NOB identified with probe NIT3, were in close proximity to AOB, deep within the biofilm.

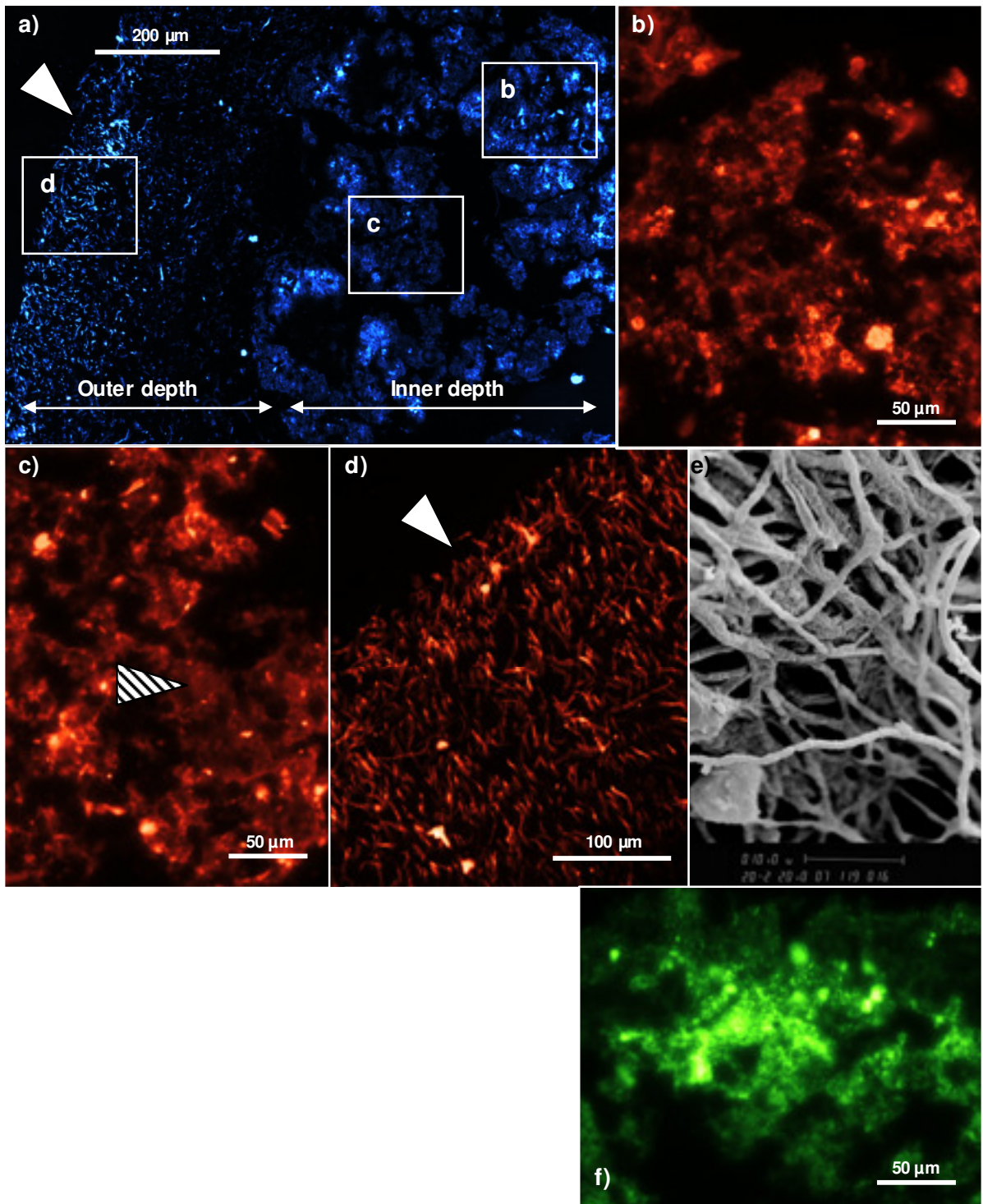


**Plate 7.5.** *In situ* structure of the biofilm sampled from the top (0.3 m) of the trickling filter during Experiment F – high sBOD<sub>5</sub> ( $8.8 \pm 2.9$  mg/L) loading using sucrose: (a) biofilm cross-sections stained with DAPI (x100); (b and c) *in situ* identification of AOB

within the mid and lower depths of the biofilm after FISH using a Cy3-labeled NSO1225 oligonucleotide probe (x400); (d) *in situ* identification of heterotrophs within the outer depths of the biofilm after FISH with Cy3-labeled EUB338 oligonucleotide probe specific for most bacteria (x200); (e) SEM of the same biofilm sample from image (d) showing a woven matrix of filamentous-like bacteria; and (f) identification of *Nitrospira* genus with in mid depths of the biofilm using FISH with target specific 16S rRNA oligonucleotide probe NTSPA662 (x400). Hatched arrow shows the auto-fluorescence caused by EPS. White arrows point towards the water–biofilm interface.

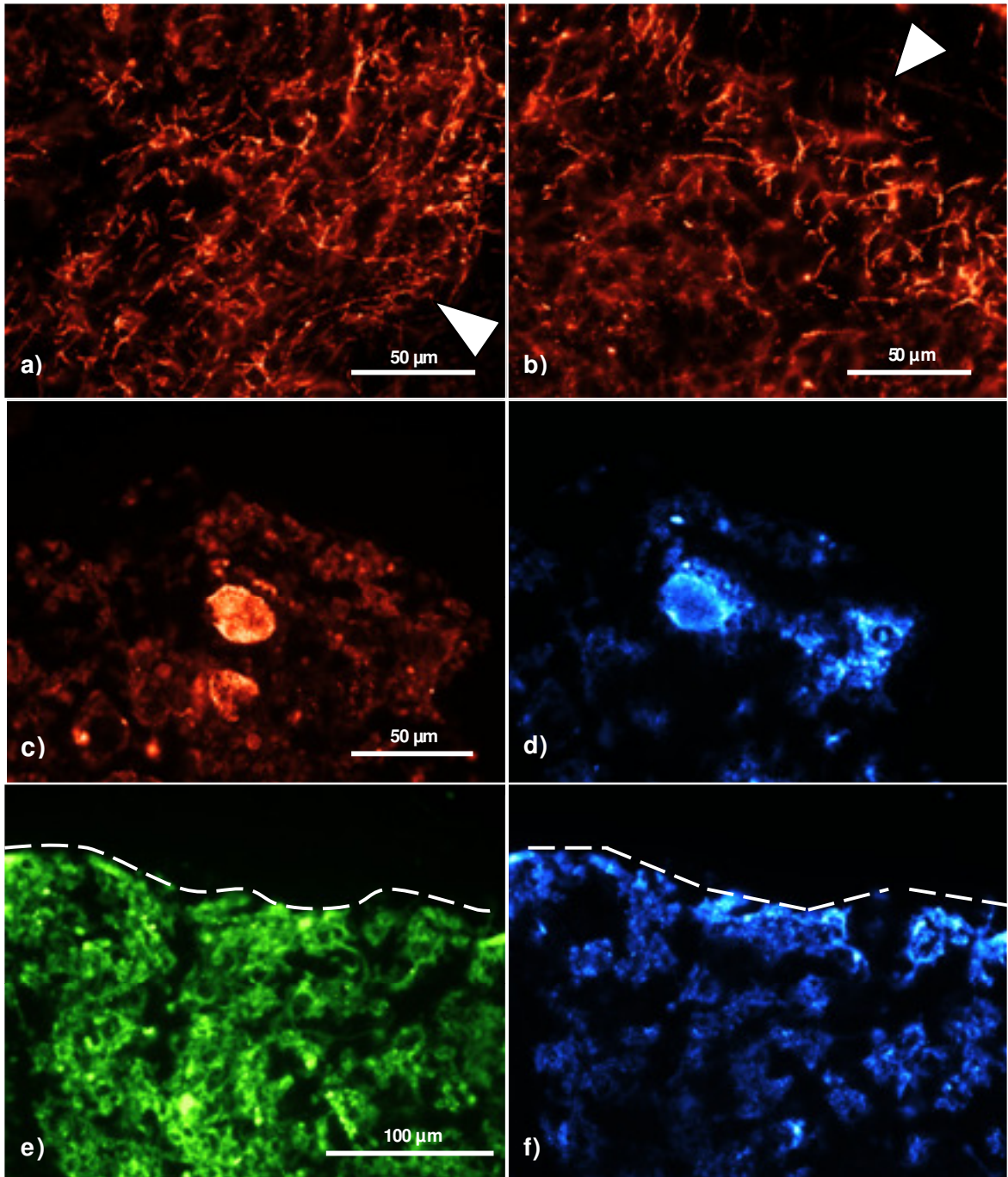


**Plate 7.6.** *In situ* structure of the biofilm sampled from the middle (1.5 m) of the trickling filter during Experiment F– high sBOD<sub>5</sub> ( $8.8 \pm 2.9$  mg/L) loading using sucrose: (a) identification of heterotrophs within the outer depths of the biofilm after FISH with Cy3-

labeled EUB338 oligonucleotide probe specific for most bacteria (x400); (b) identification of heterotrophs within the middle to outer depths of the biofilm after FISH with Cy3-labeled EUB338 oligonucleotide probe specific for most bacteria (x400); (c) identification of AOB within the lower depths of the biofilm after FISH using a Cy3-labeled NSO1225 oligonucleotide probe (x400); (d) total DAPI stained cells (x400); (e) identification of NOB within the lower depths of the biofilm after FISH using a Cy3-labeled NIT3 oligonucleotide probe (x200); and (f) total DAPI stained cells (x200). Dashed line indicates the media–biofilm interface. White arrows point towards the water–biofilm interface.

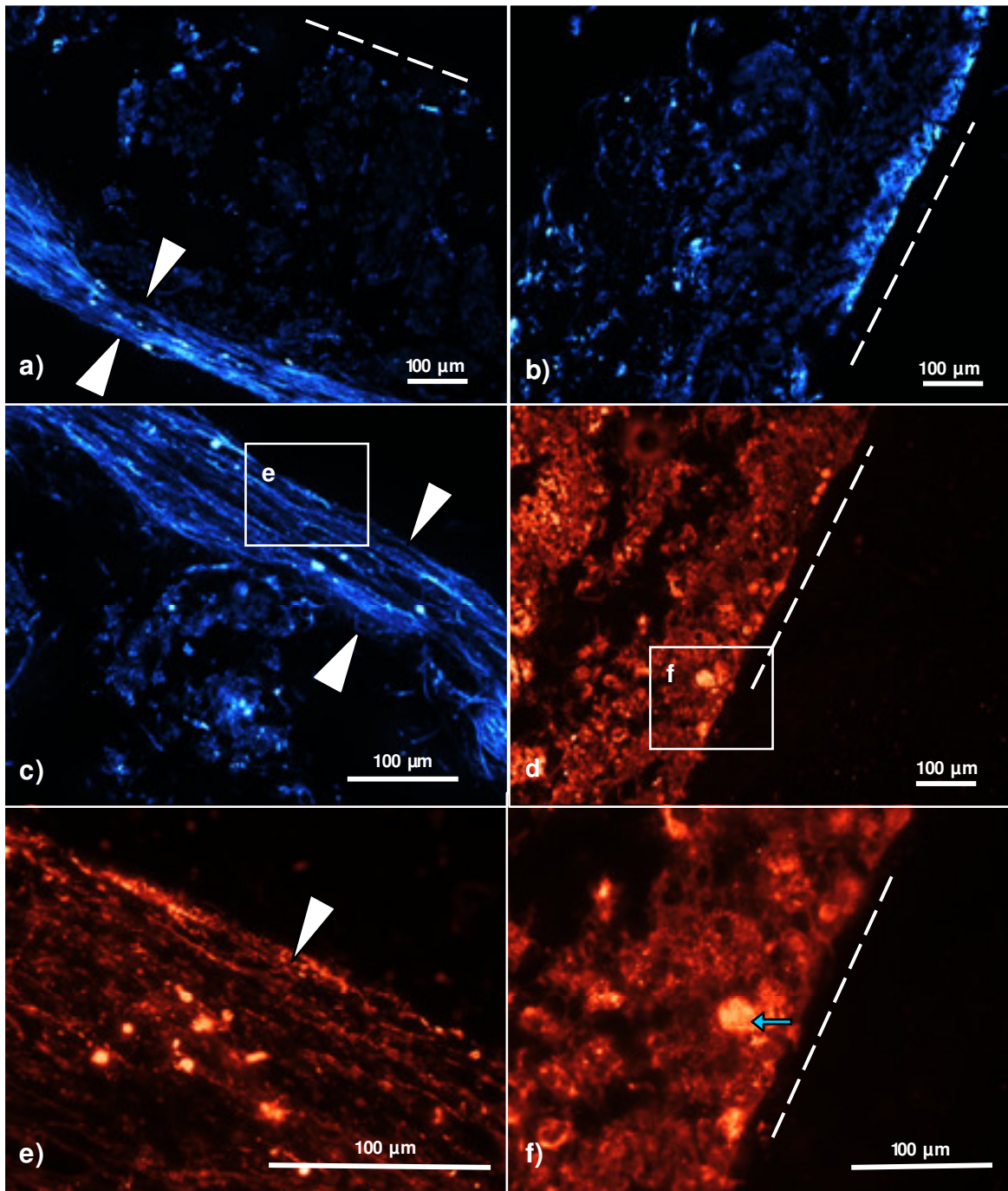


**Plate 7.7.** *In situ* structure of the biofilm sampled from the bottom (2.7 m) of the trickling filter obtained during Experiment F – high sBOD<sub>5</sub> ( $8.8 \pm 2.9$  mg/L) loading using sucrose: (a, b and c) total cell count using DAPI. (d) identification of AOB within the inner depths of the biofilm after FISH with Cy3-labeled NSO1225 oligonucleotide probe

specific for *Nitrosomonas* spp (x200); (e) identification of heterotrophs within the outer depths of the biofilm after FISH with Cy3-labeled EUB338 oligonucleotide probe specific for most bacteria (x400); and (f) higher magnification of image (d) showing a colony of AOB (x400). Dashed line represents the media–biofilm interface. White arrows point towards the outer heterotrophic growth, situated within the water–biofilm interface.

## Experiment G

Plate 7.8 shows the *in situ* structure of the biofilm sampled from the top of the trickling filter (0.3m) 7 d into Experiment D, where sucrose ( $9.4 \pm 0.9$  mg sBOD<sub>5</sub>/L) was dosed intermittently to mimic fluctuations in organic carbon observed at Buaran WTP and at ammonia-N concentration of  $4.8 \pm 0.5$  mg/L. The biofilm characteristics resembled those of the biofilm cross-sections observed from Experiment F (continuously fed high influent ammonia-N and sBOD<sub>5</sub>). A very thick outer heterotrophic layer consisting of filamentous bacteria was identified (Plate 7.8.a). Similarly, AOB and NOB targeted with probes NSO1225 and NIT3 were limited to the sub-depths of the biofilm. Few AOB and NOB could be detected within the mid- and outer-biofilm depths. Large quantities of EPS identified by auto-fluorescence can be seen within the mid depths of the biofilm. A large number of bacteria cells stained with DAPI can be seen scattered within this EPS matrix (Plate 7.8.b).

For all experiments, stronger signals and hence more AOB could be detected within biofilm cross-sections using oligonucleotide probe NSO1225 than when using NSO190, and therefore suggests that NSO1225 was the better probe for detecting AOB during the study.

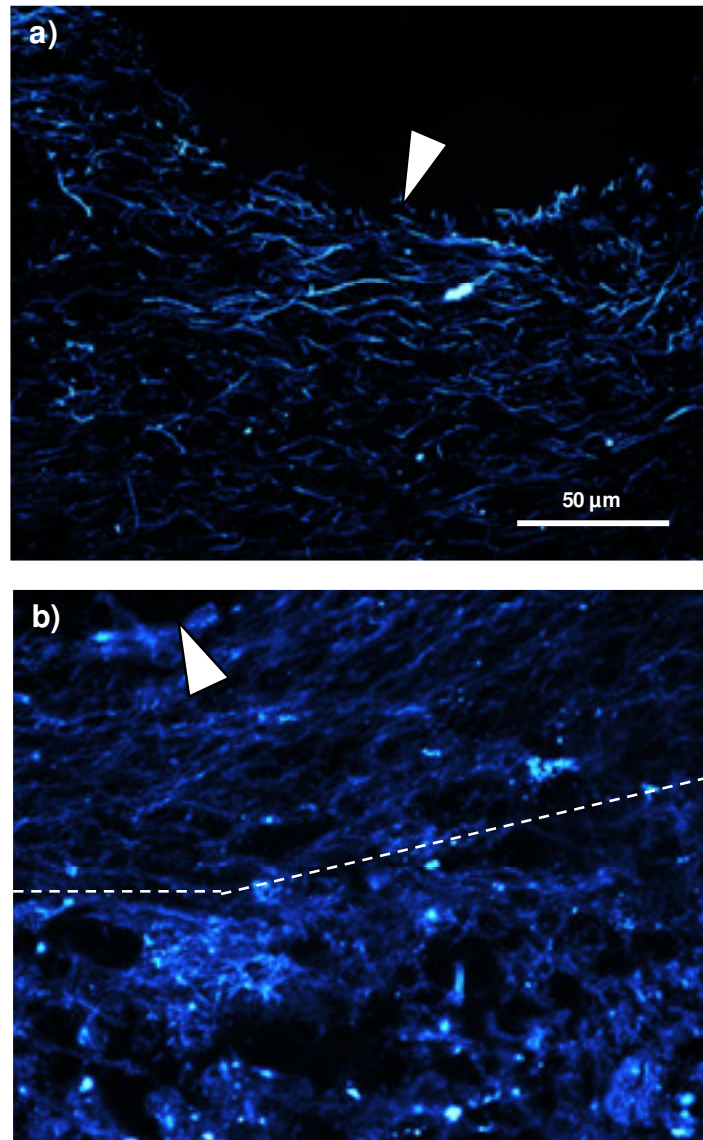


**Plate 7.8.** *In situ* structure of the biofilm sampled from the top of the trickling filter (0.3 m) during Experiment G – Fed intermittent organic spikes ( $9.4 \pm 0.9$  mg sBOD<sub>5</sub>/L) using sucrose: (a) biofilm cross-sections stained with DAPI, showing outer heterotrophic filamentous growth (x400); and (b) biofilm cross-section stained with DAPI, showing the middle to outer depths of the biofilm, separated by the dashed line. White arrows point to the outer heterotrophic growth situated within the water–biofilm interface.

#### **7.3.4 Experiment I: comparing the *in situ* structure of organic fertiliser-fed and sucrose-fed biofilms**

Plate 7.9 compares the *in situ* ultra structure of the biofilms sampled from a filter bed depth of 0.3 m for Experiments F and I, when influent sBOD<sub>5</sub> was increased to  $8.8 \pm 2.9$  and  $11.5 \pm 3.4$  mg/L by dosing sucrose and organic fertiliser respectively (Table 7.1). A difference in the biofilm population structure of the trickling filter when operated under organic fertiliser-induced sBOD<sub>5</sub> (Plates 7.9.a and 7.9.b) compared to that of sucrose (Plate 7.9.c), was clearly identified using SEM. Many rod-shaped bacteria (existing as either short bacterial chains of 4–6; triads or tetrads), dominated the outer surface of the biofilm when organic fertiliser was used as the sole carbon source. This is in contrast to a dense woven matrix of filamentous-like bacteria and thick EPS crust, which was observed when operated under sucrose induced sBOD<sub>5</sub> (Plate 7.9.c).

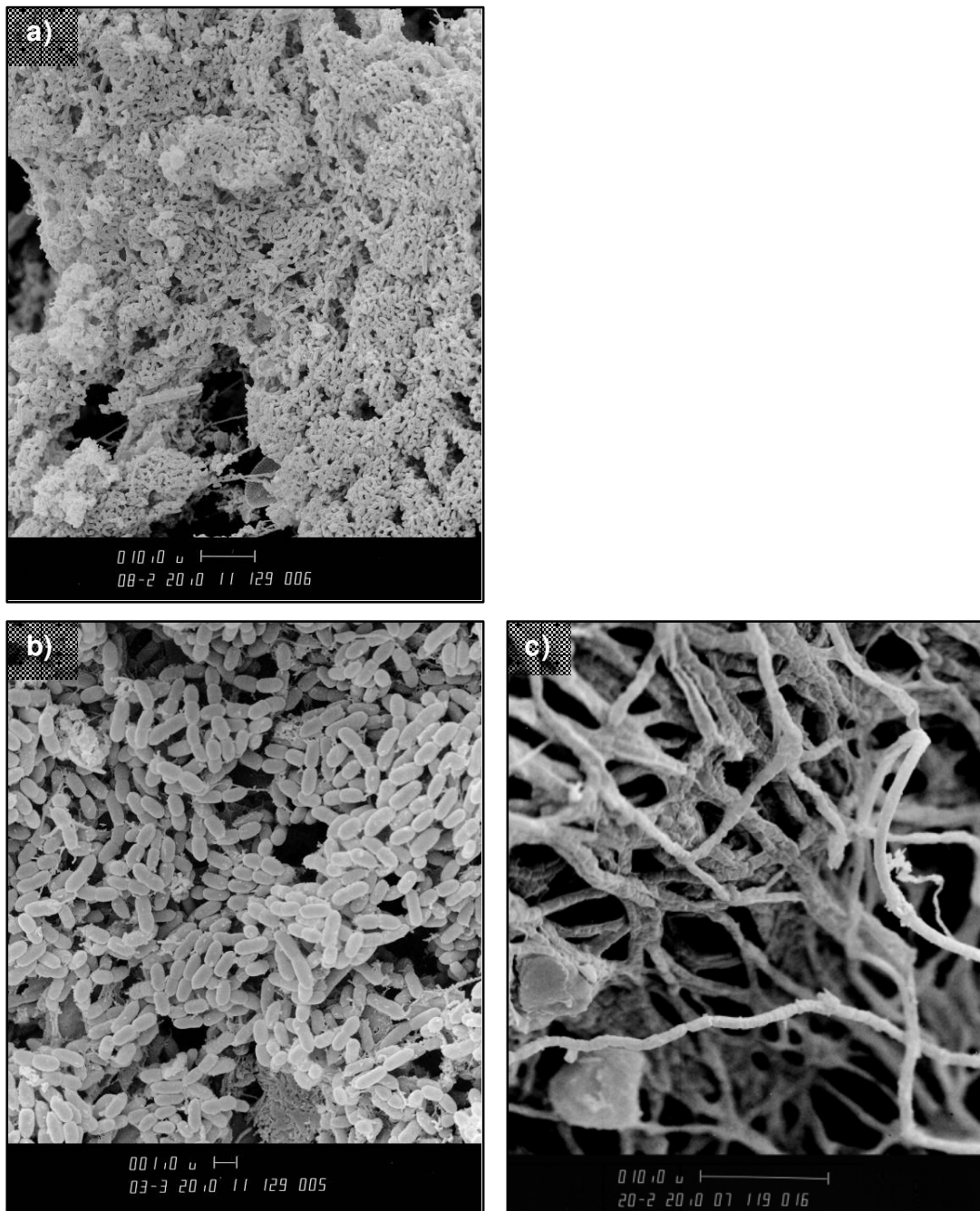


**Plate 7.9.** *In situ* structure of the biofilm samples from the trickling filter bed depth of 0.3 m during Experiment F (fed sucrose equivalent to  $8.8 \pm 2.9$  mg sBOD<sub>5</sub>/L) and Experiment I (fed organic fertiliser equivalent to  $11.5 \pm 3.4$  mg sBOD<sub>5</sub>/L): (a) scanning electron micrograph of the outer biofilm surface from Experiment I when operated under organic fertiliser-induced sBOD<sub>5</sub>; (b) higher magnification (x10000) of image (a); and (c) SEM of Experiment F (sucrose-induced sBOD<sub>5</sub>).

### **7.3.5 Biofilm thickness**

Microscopic examination of biofilm samples conducted during Experiment F, revealed that the presence of an organic substrate (sucrose;  $8.8 \pm 2.9$  mg sBOD<sub>5</sub>/L) promoted strong stratification between nitrifiers and heterotrophic bacteria, which were separated by a thick EPS layer. The thickness of these visible zones: (1) inner biofilm growth attached to media surface; (2) middle EPS layer, low in microbial density; and (3) outer filamentous heterotrophic layer; at filter bed depths of 0.3, 1.5 and 2.7 meters, are presented in Figure 7.3. The thickest zone was the EPS layer (Zone 2), which varied between 215 to 626  $\mu\text{m}$  thick, and represented 40 to 59 % of the total biofilm depth for all filter bed depths. The inner biofilm growth (Zone 1) represented 5.5 to 6.7 % of the total biofilm thickness. Mean thickness of Zone 1 for all filter bed depths ranged from 15 to 125  $\mu\text{m}$ . The outer heterotrophic layer (Zone 3) was thickest at the filter bed depth of 0.3 m ( $323.4 \mu\text{m} \pm 79.8$ ), representing 32.8 % of total biofilm depth. The thickness of the outer heterotrophic layer was similar for filter bed depths of 1.5 m and 2.7 m, ranging from  $124.6 \pm 43.9$   $\mu\text{m}$  at 2.7m to  $143.3 \pm 31.4$   $\mu\text{m}$  at 1.5 m, representing 17.4 % and 18.9 % of the total biofilm depth respectively.

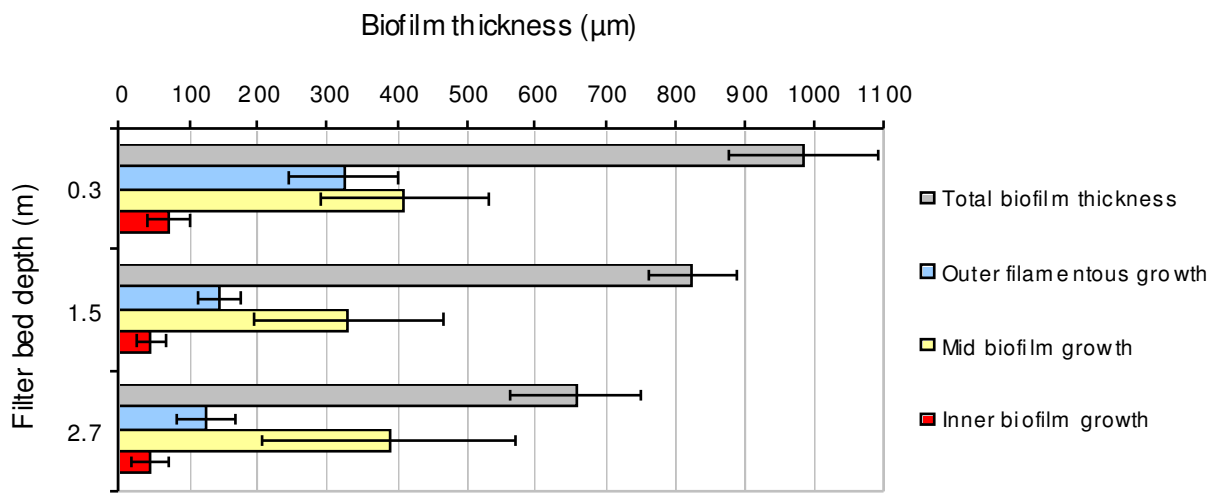


**Figure 7.3.** Profile of biofilm thickness throughout the depths of the trickling filter during high sBOD<sub>5</sub> loads (8.8 mg/L) at a ammonia-N load of 4.7 mg/L (Experiment F). Mean measurements taken from 8–17 random fields of view ± 1 SD.

## 7.4 Discussion

This chapter has investigated the spatial distribution of AOB, NOB and heterotrophs within biofilms sampled from a pilot scale NTF, designed to remove ammonia from polluted drinking watersupplies. The combination of FISH and SEM employed for the *in situ* analysis of biofilms, successfully identified the spatial distribution of AOB, NOB and heterotrophic bacteria in biofilm cross-sections. Oligonucleotide probes NSO190 and NSO1225 were successful in identifying the beta sub-group of AOB Proteobacteria, which included species from the genera *Nitrosomonas* and *Nitrosopira*. NOB identified in this study belonged to the genera *Nitrobacter* and *Nitrospira*, and were identified using oligonucleotide probes NIT3 and NTSPA662 respectively. This is in contrast to many other studies, which have reported that *Nitrobacter* were either not detected, or rarely identified in full-scale wastewater treatment plants, including NTFs and in laboratory-scale reactors (Mobarry *et al.* 1996; Wagner *et al.* 1996; Schramm *et al.* 1998; Okabe *et al.* 1999; Daims *et al.* 2001; Persson *et al.* 2002; Wuertz *et al.* 2003; Lydmark *et al.* 2006).

In contrast, *Nitrospira* species have been identified to be the dominant NOB in nitrifying systems (Schramm *et al.* 1998; Daims *et al.* 2001; Wuertz *et al.* 2003). However, Schramm *et al.* (1996) identified *Nitrobacter* in biofilm cross-sections sampled from a NTF of an aquaculture water recirculation system. Similarly Coskuner and Curtis (2002) identified both *Nitrobacter* and *Nitrospira* from a typical activated sludge system using FISH. These conflicting findings suggest that *Nitrobacter*, although not widely detected, can be dominant in some nitrifying systems. The persistence of *Nitrobacter* and *Nitrospira* may be determined by concentrations of nitrite and DO in their environment. *Nitrospira*-like oxidisers can adapt to low oxygen and low nitrite concentrations, unlike *Nitrobacter*, which favour oxygen and nitrite rich environments (Schramm *et al.* 1998; Daims *et al.* 2001; Kim and Kim 2006).

When the trickling filter was operated under low organic carbon loads, FISH revealed AOB and NOB clusters were abundant at all filter bed depths and represented the

majority of total bacteria identified using DAPI. Colonies of AOB and NOB were detected throughout the inner- and outer-depths of the biofilm. AOB and NOB were generally found in close proximity to one another; supporting the findings of Okabe *et al.* (1996), Schramm *et al.* (1996), Okabe *et al.* (1999), Wijeyekoon *et al.* (2000), and Lydmark *et al.* (2006). These studies suggest that the close proximity of AOB and NOB reduces the diffusion path of the intermediate nitrite, thereby facilitating the sequential oxidation of nitrite to nitrate. This was also characterised in Figure 7.1 which shows filter depth profiles of ammonia-N, nitrite-N, and nitrate-N. No accumulation of nitrite-N down the trickling filter bed was observed for all experiments, implying sequential and immediate oxidation to nitrate. Biofilms sampled from the surface of the filter were dominated by filamentous cyanobacteria. Here, AOB and NOB were located deep within the sub-layers of the biofilm overgrown by *Anabaena*- or *Nodularia*-like cyanobacteria. The depth-wise stratification of nitrifiers and cyanobacteria may have resulted from the cyanobacteria's requirement for sunlight.

The increase in organic substrate via the addition of sucrose caused a rapid decline in the trickling filters nitrifying capacity, impeding ammonia removal at all filter bed depths as previously discussed in Chapter 5. In comparison to heterotrophic plate counts, biofilm EPS concentration (measured as total carbohydrates) was found to have a greater association with nitrification capacity. A strong negative correlation between biofilm carbohydrate concentration and percentage nitrification was observed at all filter bed depths of 0.3, 1.5 and 2.7 m (Chapter 6). *In situ* examination of the biofilm using FISH and SEM showed that an increase in influent sBOD<sub>5</sub> as low as 5.4 mg/L or 931.4 mg m<sup>-2</sup> d<sup>-1</sup> not only increased biofilm EPS concentration, but promoted a rapid change in biofilm population structure—otherwise underestimated using HPC. During periods of low sBOD<sub>5</sub> loads (Experiment A), the biofilm was thin and densely packed with nitrifiers. Biofilm thickness at the filter bed depth of 0.3 m was 496 ± 109 µm, however, because of the thin coverage of biomass at the two deeper levels (1.5 and 2.7 m), measurements were difficult to obtain.

Biofilms appeared to be homogenous in structure, and dominated by many large bacterial colonies of AOB and NOB distributed throughout the sub- and outer-depths of the biofilm. During periods of high organic carbon loads (for example Experiment F), biofilm thickness increased significantly, measuring  $986 \pm 106$ ,  $823 \pm 63$ , and  $657 \pm 95$   $\mu\text{m}$  at filter bed depths of 0.3, 1.5, 2.7 m respectively. *In situ* analysis of the biofilm using SEM and FISH revealed a more complex heterogenous population structure. Depth-wise stratification of nitrifiers and heterotrophs was evident at all filter bed depths and for all experiments when sucrose was used as the sole sBOD<sub>5</sub> source (Experiments C, F and G). Fewer AOB and even less NOB clusters were identified using FISH—those detected were restricted within the sub-layers of the biofilm, at depths of 650 to 980  $\mu\text{m}$  below the biofilm surface. AOB and NOB were covered by an outer layer of heterotrophic bacteria ranging from 93 to 423  $\mu\text{m}$  thick. The outer heterotrophic layer, previously not identified using HPC, was comprised mostly of filamentous-like bacteria, possibly from the genus *Actinomyces*. These observations coincided with the impediment of nitrification at all filter bed depths (Figures 7.1.b, 7.1.c and 7.1.d). The abundance of filamentous bacteria may be attributed to the tendency of filaments to form in environmental niches that are oxygen transfer-limited (McCoy and Costerton 1982), which for this study was indicative of filter conditions during high organic loads.

DO has been shown to be able to penetrate up to 600  $\mu\text{m}$  below the biofilm surface in a heterotrophic–autotrophic mixed biofilm (Zhang *et al.* 1994). Other studies have shown DO to penetrate 50 to 250  $\mu\text{m}$  below the surface in various nitrifying biofilms (Schramm *et al.* 1996; Okabe *et al.* 2002; Kindaichi *et al.* 2004). Based on these findings, it was possible that during high organic loads, AOB and NOB were restricted to biofilm depths where oxygen was depleted. Oxygen is the limiting factor for nitrification and nitrifier abundance (Zhang *et al.* 1994; Schramm *et al.* 1996). In addition to the high biofilm polysaccharide concentrations outlined in Chapter 6, the decline in nitrification during Experiments C, F, and G was also attributed to fast growing heterotrophs out-competing slow growing AOB and NOB for oxygen. In turn the competition for oxygen promoted depth wise stratification of heterotrophs and nitrifiers, a phenomena also observed by Zhang *et al.* (1994). Schramm *et al.* (1996) and Jang *et al.* (2002) also identified

clusters of AOB and NOB deep within biofilms where oxygen was depleted. It was possible that AOB and NOB in the sub-layers of the biofilm entered a stationary growth phase. In these sub-layers, FISH revealed more *Nitrospira*-like bacteria than *Nitrobacter*. The shift in NOB populations may be attributed to the ability of *Nitrospira*-like bacteria to tolerate low nitrite and oxygen concentrations caused by the decline in nitrification, and heterotrophic competition (Schramm *et al.* 1998; Daims *et al.* 2001; Kim and Kim 2006).

*In situ* analysis of the biofilm community structure using FISH and SEM, confirmed for biological potable water treatment, what has previously been observed in wastewater nitrogen removal processes by Boller *et al.* (1994), Zhang *et al.* (1994), Okabe *et al.* (1996), Satoh *et al.* (2000), and van Loosdrecht *et al.* (2000). All studies attribute the loss of nitrification to an increase in organic substrate, which promoted stratification between nitrifiers and heterotrophs, thereby inducing interspecies competition for space and oxygen. However, none have identified high biofilm polysaccharide concentrations nor attributed it to a decline in nitrification performance. High biofilm polysaccharide concentrations (measured as total carbohydrate) identified in Chapter 5 were also visible under SEM and fluorescence microscopy. Plate 7.4.f depicts a thick layer of EPS, which was essentially 'smothering' the biofilm. When comparing these results with Plate 7.2.a (SEM of biofilm during low sBOD<sub>5</sub> loading), the EPS layer was absent. Instead many bacterial cells could be seen. When comparing fluorescent micrographs of biofilm cross-sections sampled during low and increased sBOD<sub>5</sub> loads (e.g. Plates 7.2.c, 7.5.c and 7.6.e), more auto-fluorescence, presumably caused by extracellular polysaccharides, can be seen. Schramm *et al.* (1998) also noted strong auto-fluorescence caused by extracellular material when biofilm sections were excited with blue light. Microscopic examination of biofilm cross-sections during Experiment F showed that background fluorescence caused by extracellular polysaccharides was most evident in the mid depths of the biofilm, separating the thick outer heterotrophic growth from AOB and NOB. The mid depths of the biofilm appeared to be lower in microbial content, with few microcolonies loosely scattered in contrast to the more tightly packed morphological appearance observed during periods of low organic loads

(Plate 7.2). These findings are similar to those of Lydmark *et al.* (2006), who attributed similar observations to higher concentrations of extracellular polysaccharides, which for the current study was produced in response to high organic loads. Therefore, the decline in nitrification may also be attributed to the thick EPS layer, because of its capacity to act as an external diffusive barrier, and therefore influence the mass transfer properties of biofilms (Characklis and Marshall 1990; Wuertz *et al.* 2003). It was possible also that the thick EPS layer limited the diffusion of oxygen and nutrients to AOB and NOB located deep within the biofilm.

For this study, the choice of organic carbon source influenced the type of biofilm ultrastructure that developed, and this in turn impacted on filter performance. The influence of a readily available organic carbon source (sucrose) and a more native-like organic carbon source (organic fertiliser) on biofilm population structure was investigated. Differences in carbon biodegradability between the two carbon sources were previously discussed in Chapter 5. *In situ* analysis of the biofilm using SEM and FISH showed that sucrose-fed biofilms sampled from the trickling filter had a loose and “fluffy” morphology dominated by a thick mat of filamentous-like bacteria. Moy *et al.* (2002) reported similar morphological observations with glucose-fed aerobic sludge granules. Energy-rich organic substrates including glucose and sucrose, have been known to promote filamentous growth in activated sludge (Chudoba *et al.* 1985; Moy *et al.* 2002). In contrast, the morphology of organic fertiliser-fed biofilms, which operated under similar sBOD<sub>5</sub> loadings and were sampled from the same filter bed depth, had a more uniform and dense structure, dominated by many rod shaped bacteria which existed in short chains. Unlike the sucrose-fed biofilms, the organic fertiliser-fed biofilm was able to sustain complete nitrification, which may suggest that the organic fertiliser was of a more recalcitrant nature than sucrose. It was possible that the organic fertiliser exerted a lower heterotrophic oxygen demand than sucrose, therefore reduced interspecies competition for oxygen within the biofilm. Future investigations employing ion-selective microelectrodes to spatially measure the microbial activity within the biofilm would help to test this hypothesis.

## 8 GENERAL DISCUSSION

Pollution of water supplies in developing countries requires the application of cost effective technologies to supply safe municipal drinking water. The absence of water catchment protection often results in contamination of drinking water supplies, which adversely affects water treatment processes and increases capital and operational costs. Buran WTP in Jakarta is one of many examples and was selected as a case study due to the availability of water quality data, and WTP operations data. Parallel with many other unprotected and polluted drinking water catchments in South East Asia, analysis of Buaran's raw water highlighted ammonia, turbidity, organic carbon, manganese and iron to be key management issues for the WTP. Conclusions drawn from the study were that Buaran's raw water was of poor quality, resulting in high inorganic chlorine demand arising from ammonia, nitrite, and manganese as well as high chlorine demand related to the organic matter concentration. Statistical analysis confirmed a positive linear relationship between chlorine dose applied at the WTP and raw water ammonia concentration, which showed that 9.75 mg/L of chlorine was dosed for every 1 mg/L of ammonia-N present. The installed treatment barrier for ammonia removal was pre-chlorination and this required high chlorine doses (up to 25 mg  $\text{CL}_2/\text{L}$ ). Pre-chlorination can lead to the formation of disinfection by-products, is incompatible with PAC dosing and the highly variable raw water ammonia concentration makes it difficult and expensive to control (Cammarota 2001). Pre-chlorine overdosing incurs excessive operation cost and causes corrosion of WTP infrastructure (Cammarota 2001). Pre-chlorination underdosing leads to ineffective manganese removal and increased disinfection demand. Control of ammonia at Buaran WTP is critical if water is to be produced that is properly disinfected and aesthetically acceptable.

This study investigated the application of NTFs to remove low concentrations of ammonia from polluted surface water supplies. The concept was to employ NTFs to oxidise ammonia to less chlorine demanding forms of nitrogen (i.e. nitrate) as an alternative to pre-chlorination. The rationale for this study was that NTFs are widely used for the remediation of nitrogen rich wastewater, where general attributes of

nitrification have been extensively explored. However, comparatively little is known about their performance under lower ammonia concentrations. Key challenges identified for applying NTFs to potable water treatment were low ammonia concentrations, which can present mass transfer limitations and suppression of nitrification posed by high organic and SS concentrations. These factors, as well as the impact of hydraulic load, and *in situ* analysis of biofilm community structure were investigated. The impact of seasonal variations in water quality parameters, namely pH, DO, temperature, and total alkalinity on NTF performance were also assessed.

This study was the first to demonstrate that high rate plastic-packed NTFs were able to operate equally successfully, under ammonia-N concentrations, some 10- to 50-fold lower and at hydraulic loading rates 30 to 100 times greater than those of conventional wastewater applications. The potable water NTF developed here operated under a rapid hydraulic retention time of less than 2.8 minutes, where in such time significant biological oxidation of ammonia to nitrate was observed under these markedly reduced concentrations. In excess of 95 % of ammonia was consistently removed via nitrification when influent ammonia-N was maintained between 0.4 and 5.0 mg/L (69 – 870 mg  $\text{NH}_4\text{-N m}^{-2} \text{ d}^{-1}$ ) and was independent of seasonal variations in temperature (10.7 – 24°C), pH (7.5 – 8.4), alkalinity (102 – 116 mg  $\text{CaCO}_3\text{/L}$ ), and DO (5 – 7.5 mg/L). Significant break-through of ammonia into the effluent occurred at surface loads above 1000 mg  $\text{NH}_4\text{-N m}^{-2} \text{ d}^{-1}$ . High inert SS loads showed no adverse affect on filter performance, within the range of SS loads employed in this study (8 – 218 mg/L). The results imply that NTFs could operate successfully as a front-end treatment process, where pre-treatment for SS removal would not be required. Sporadic detachment of large fragments of biofilm (sloughing) was not detected, which is a significant advantage since the NTF could be operated reliably without clarifiers or humus tanks.

The results also showed that when operated under mass surface loads equivalent to typical ammonia loading criteria for wastewater NTFs, by increasing hydraulic flow, comparable apparent nitrification rates (mg  $\text{NH}_4\text{-N m}^{-2} \text{ d}^{-1}$ ) were achieved. Under these conditions, performance appeared to be independent of the influent ammonia

concentration. These results confirmed that the postulated mass transport limitations mediated by low ammonia-N concentrations were insignificant. Furthermore the results were similar to those for wastewater NTFs, confirming that even under low ammonia concentrations mass loading based on media surface area was the most important design criteria which relates to treatment efficiency. Experiments also confirmed that increased hydraulic loads enhanced nitrification rates by up to 35 %, which may be attributed to an increase in aeration and/or enhancement of convective forces caused by higher turbulence. However, for low influent ammonia-N concentrations  $< 2.0 \text{ mg/L}$ , the effect of hydraulic surface load ( $173 - 402 \text{ L m}^{-2} \text{ d}^{-1}$ ) on percentage nitrification was minimal.

This study also provided new insight into the distribution of nitrification activity and biomass within a NTF operated under low ammonia concentrations. Results confirmed that both the distribution of biomass and activity down the filter column differed significantly from research obtained from conventional wastewater applications. Long-term monitoring of inorganic nitrogen profiles throughout the filter depth confirmed that nitrification exhibited non-linear behaviour, where ammonia oxidation was highest at the top ( $>40 \%$  at  $0.3 \text{ m}$ ) and reduced significantly with an increase in filter bed depth. Due to high nitrification activity at the top, the lower bed depths were exposed to very low ammonia concentrations, which in turn was responsible for low nitrification activity throughout the bottom half of the NTF. At these lower depths, nitrification exhibited first-order rate characteristics and therefore was dependant on the ammonia concentration. The pronounced gradient in nitrification activity was also reflected by biomass abundance down the filter, where the decline in biofilm carbohydrate, protein and heterotrophic concentrations, and biofilm thickness down the filter bed were a result of changes in nutritional conditions throughout the system. These results suggest that the high nitrification activity at the top of the filter left only low concentrations of ammonia to sustain a lesser quantity of biomass within the lower filter depths. In contrast, Parker *et al.* (1989) showed that a nitrification rate profile obtained from a wastewater NTF was more uniform (zero-order) with depth, which resulted in a more even coverage of biomass throughout the filter (Figure 8.1). The zero-order rate profile was attributed to

the higher ammonia concentrations, where rates became independent of the ammonia concentration. They were however, considered to be flux-limited by DO availability (Figure 8.1). Similar observations were reported by Gullicks and Cleasby (1986) on wastewater NTFs. Furthermore, results from the study reported here showed that by increasing the ammonia surface load, an improvement in the mass of ammonia oxidised at the lower depths was achieved, however, this was accompanied by a decline in percentage nitrification and hence higher ammonia concentrations can be expected in the effluent.

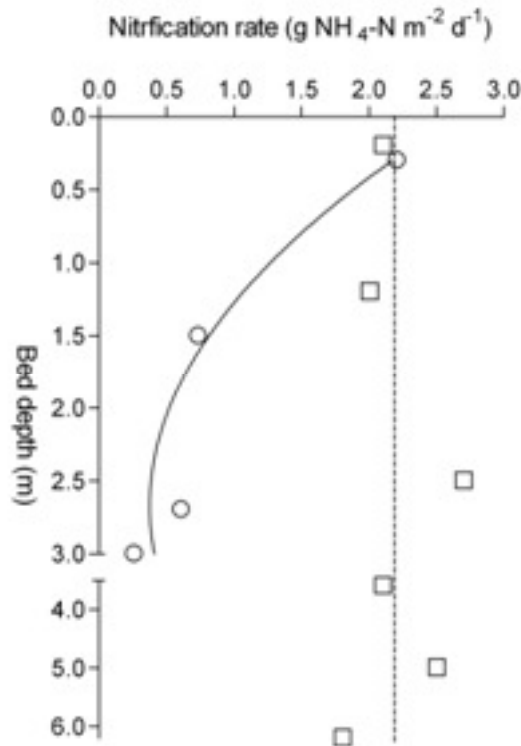


**Figure 8.1.** Comparison of nitrification rate profile obtained in this study (○) when operated under low ammonia-N concentrations ( $<5.0 \text{ mg NH}_4\text{-N/L}$ ), to that obtained from wastewater investigations (□) by Parker *et al.* (1989), when operated under higher influent ammonia concentrations ( $>5.0 \text{ mg NH}_4\text{-N/L}$ ).

This study also investigated the impact of organic carbon quantity and biodegradability on the nitrification behaviour of a pilot NTF designed to remove low concentrations of ammonia-N from polluted potable water supply. The pilot plant NTF was operated under conditions that simulate the raw water quality of Buaran WTP, namely variations in C:N ratio (defined as  $sBOD_5:NH_4-N$ ; range, 3 – 10) and  $sBOD_5$  concentrations (1 – 12 mg/L). The influent C:N ratio was achieved by varying the dose of organic carbon and/or ammonium sulphate. Severe nitrification suppression was noted within 8 d of increasing the carbon load beyond  $870 \text{ mg } sBOD_5 \text{ m}^{-2} \text{ d}^{-1}$  ( $> 5.0 \text{ mg } sBOD_5/L$ ) via the addition of sucrose or methanol. When operated under carbon loads below  $870 \text{ mg } sBOD_5 \text{ m}^{-2} \text{ d}^{-1}$ , simultaneous nitrification and carbon oxidation was observed. This study also confirmed that short intermittent carbon spikes operating in 48-h cycles, which mimicked fluctuations in organic carbon observed at Buaran WTP, had inhibitory effects on filter nitrifying capacity equal to that observed under a continuous carbon dosing regime. Results confirmed that organic carbon loading rather than C:N ratio was an important regulator of filter nitrification capacity, where a linear decline in nitrification performance correlated well with sucrose and methanol augmented carbon loads. These results suggest that nitrification was regulated by the heterotrophic communities' metabolic need and competition for oxygen rather than competition for ammonia. Extensive monitoring of inorganic nitrogen species down the NTF to profile nitrification behaviour showed carbon loads greater than  $870 \text{ mg } sBOD_5 \text{ m}^{-2} \text{ d}^{-1}$  ( $> 5.0 \text{ mg } sBOD_5/L$ ) severely suppressed nitrification throughout the entire filter bed (Figure 8.2). The hypothesized vertical segregation of carbon oxidation in the upper filter depths and nitrification in the lower depths as reported in wastewater investigations by Parker and Richards (1986), Daigger *et al.* (1994), Wik (2000) and Pearce (2004) was not observed (Figure 8.2). Rather, a transition from a nitrifying to a predominantly carbon oxidising system had occurred, and could be best characterised by monitoring effluent DO. A decline in effluent DO correlated well with an increase in  $sBOD_5$  load and  $sBOD_5$  removal. These relationships give supportive evidence to the heterotrophic metabolism of the carbon substrate and therefore it was reasonable to assume a large heterotrophic presence within the filter bed, which was capable of suppressing nitrification. The principle is that nitrification becomes limited in the presence of an organic substrate, by the rapidly

growing heterotrophs overgrowing the slower growing nitrifiers. Consequently, both oxygen penetration into the biofilm and its availability to the nitrifying population is limited (Boller *et al.* 1994; Zhang *et al.* 1994; Okabe *et al.* 1996). This concept which has widely been reported in wastewater BNR investigations was confirmed qualitatively in this study using *in situ* techniques of FISH and SEM.

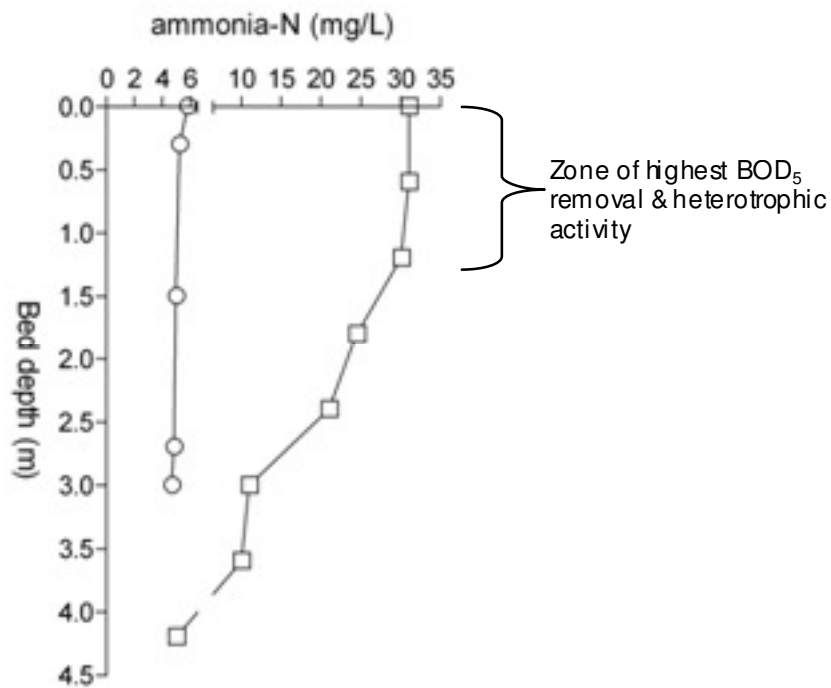


**Figure 8.2.** Comparison of ammonia-N depth profiles obtained from this study (○) to that obtained from wastewater investigations (□) by Pearce (2004), when operated under high organic loads of 0.32 and 0.29 kg BOD<sub>5</sub> m<sup>-3</sup> d<sup>-1</sup> respectively.

This research has provided new insights into the microbial ecology of a nitrifying trickling filter which operates under low ammonia-N concentrations. The combination of FISH and SEM for *in situ* analysis of biofilms was successful in identifying the spatial distribution of AOB, NOB and heterotrophs. When the NTF was operated under low sBOD<sub>5</sub> loads, clusters of AOB and NOB were abundant, and were located in close proximity to each other, which facilitated sequential oxidation of nitrite to nitrate, as evidenced by the absence of nitrite down the filter bed.

Uniquely, this study identified the less common *Nitrobacter* species within the NTF biofilm together with *Nitrospira* species. *In situ* examination of biofilms sampled from the NTF confirmed that an increase in sBOD<sub>5</sub> (> 5.0 mg/L) via the addition of sucrose promoted the rapid growth of heterotrophic bacteria, which dominated the outer depths of the biofilms. During periods of high organic loads, FISH revealed depth stratification within the biofilm between nitrifiers and heterotrophs at all filter bed depths. This coincided with the reduction of nitrification down the entire filter column. It was probable that the outer layer of heterotrophs, which was in the order of 93 to 423 µm thick, reduced DO transfer to the nitrifiers which were located deep within the biofilm. The presence of filamentous heterotrophic bacteria identified *in situ* using FISH and SEM was underestimated when using culture dependant spread plate techniques (HPC), which are limited to bacteria that are able to grow and form colonies (Mezzanotte *et al.* 2004).

*In situ* examination of the biofilm during periods of high sBOD<sub>5</sub> loads also revealed a thick layer of EPS which smothered the biofilm. The abundance of EPS was also confirmed by monitoring biofilm carbohydrate concentrations. A significant relationship between the mass of biofilm carbohydrate and carbon loading was identified at all biofilm sample depths. The mass of biofilm carbohydrate increased within 8 to 10 d after influent carbon was increased beyond 5 mg sBOD<sub>5</sub>/L by the addition of sucrose or methanol. These results suggest that carbon utilisation by the microbial community had shifted from cell growth to EPS production; an indication that carbon was in excess and/or was readily biodegradable, or that essential nutrients (nitrogen and

phosphorous) were limited. Results also demonstrated that NTF performance was strongly influenced by biofilm and carbohydrate composition. Statistically, nitrification performance inversely correlated with biofilm carbohydrate mass. The impediment of nitrification down the filter bed coincided with an increase in biofilm carbohydrate at all biofilm sample sites (0.3, 1.5 and 3.0 m). Given EPS strongly influences the mass transfer properties of biofilms (Wuertz *et al.* 2003), it was reasonable to suggest that the high mass of biofilm polysaccharide observed, may have caused mass transfer limitations for oxygen and ammonia throughout the biofilm, in addition to that caused by heterotrophic microorganisms.

High biofilm polysaccharide production induced by high sucrose augmented sBOD<sub>5</sub> loads, coincided with a significant increase (40 %) in filter HRT, as determined by hydraulic tracer experiments. The longer HRT can be attributed to a thicker biofilm and a higher mass of polysaccharide, because EPS has the ability to retain many times its weight in water (Chenu and Roberson, 1996). In addition to mass transfer limitations, EPS may have promoted more laminar flows, thereby reducing convective forces upon which attached biofilms depend for mass transport. To the author's knowledge, the relationship between biofilm polysaccharide composition and nitrification performance was a unique finding, which has not been reported for NTFs treating wastewater. The high polysaccharide concentrations identified in the current study may reflect differences between the composition of potable and wastewater (e.g. nutrient availability and carbon biodegradability).

This study confirmed that critical carbon loads for nitrification varied between carbon sources, which in turn may be attributed to differences in organic carbon biodegradability. In contrast to sucrose, when a more native-like carbon source (organic fertiliser) was dosed, no significant decline in nitrification capacity was observed. The superior performance seen under the organic fertiliser induced carbon loads may suggest that the carbon was more recalcitrant in nature, which was difficult to ascertain using the BOD respirometry techniques employed in this study. The higher biodegradability of sucrose possibly facilitated greater heterotrophic metabolic activity

and competition for oxygen, which advanced nitrification inhibition. This study also confirmed that sucrose- and organic fertiliser-fed nitrifying biofilms sampled from pilot scale trickling filters operated under similar sBOD<sub>5</sub> loads, showed very different characteristics. Sucrose-fed biofilms exhibited a loose and 'fluffy' morphology dominated by a thick mat of filamentous bacteria and was high in carbohydrate. In contrast, organic fertiliser-fed biofilms had a more uniform and dense ultra-structure dominated by many rod shaped bacteria, and was significantly lower in carbohydrate. Supporting the view of Sponza (2002), the difference between mass of biofilm carbohydrate appeared to reflect carbon biodegradability. The conclusion drawn from this experiment was that the type of carbon source strongly influenced the biofilm characteristics in terms of biomass ecology, morphology, and polysaccharide composition, which in turn influenced the trickling filters nitrifying capacity. Given that the biodegradability of ambient carbon varies amongst aquatic systems (Strauss and Lamberti 2000), additional research is required to test the effects of naturally occurring organic carbon on filter nitrification performance at Buaran WTP, and other potential candidate locations in South East Asia.

Where readily biodegradable carbon is predominant, one approach to improve nitrification performance would be to increase the amount of filter material in the NTF to increase surface area and residence time. As the media volume increases, the organic loading rate decreases and thus treatment efficiency would be expected to improve. Any measures taken to improve the diffusion of oxygen through the biofilm would also improve nitrification. One practice might be to promote detachment of the loosely attached outer heterotrophic layer by enhancing the hydraulic load. Increasing the hydraulic loading rate beyond 300 m<sup>3</sup> m<sup>-2</sup> of cross sectional surface area per day will promote scouring of the biomass (Grady and Lim 1980). Sloughing can also be controlled by varying the rotational speed of the distribution arm (Metcalf and Eddy 2003). Given biofilm thickness is an important controlling factor of nitrification, maintaining a thin biofilm would enhance diffusion of oxygen to the target nitrifying population, which in this study were located deep within the biofilm. Similar observations

were reported by Boller *et al.* (1997) where regularly backwashing biofilters maintained a thin biofilm, which improved the diffusion of oxygen and enhanced nitrification.

Finally, this study evaluated the trickling filter nitrification model developed by Pearce (1999) for wastewater applications. The model predicts effluent ammonia-N concentrations in response to hydraulic loading, temperature and ammonia-N and BOD<sub>5</sub> surface loads. The aim was to determine whether this model can be transferred to a pilot-scale potable water NTF, which operated well below the ammonia loading range from which the model was derived. When the pilot-scale NTF was operated under fixed ammonia-N loads within the model range, predicted and observed values were comparable. However, when operated under fixed ammonia loads below the model range, effluent ammonia-N increased more rapidly in response to sucrose augmented sBOD<sub>5</sub> loading than predicted by the model. This discrepancy could be attributed to differences between the biodegradability nature of the organic carbon used in this study (sucrose), compared with the organic carbon present in domestic wastewater, and the influence posed by the high mass of biofilm polysaccharides encountered in this study, which was not considered in the model.

This study confirmed that a well functioning NTF is a viable, low cost alternative for ammonia removal from source water abstracted from poorly protected catchments found in many developing countries. Results suggest that implementation of a NTF at the front-end of a water treatment train would reduce the ammonia related chlorine demand by 90 %, which for Buaran WTP is currently 5400 kg per day (peak capacity). At a cost of AU\$ 1300 per tonne of chlorine, this process offers significant cost savings. In addition to reducing operational costs, this process has the potential to improve water quality by minimising the formation of disinfection by-products, improving the control of chlorine disinfection and increasing microbiological compliance.

## REFERENCES

- Abell, G. C. J. and Bowman, J. P. (2005). "Ecological and biogeographic relationships of class Flavobacteria in the Southern Ocean." FEMS Microbiology Ecology. **51**(2): 265-277.
- Allison, D. G. and Sutherland, I. W. (1987). "The role of exopolysaccharides in adhesion of freshwater bacteria." General Microbiology. **133**(5): 1319-1327.
- Alpkvist, E. and Klapper, I. (2007). "Description of mechanical response including detachment using a novel particle model of biofilm/flow interaction." Water Science & Technology. **55**(8-9): 265-273.
- Amann, R. I., Krumholz, L. and Stahl, D. A. (1990). "Fluorescent-oligonucleotide probing of whole cells for determinative, phylogenetic, and environmental studies in microbiology." Journal of Bacteriology. **172**(2): 762-70.
- Andersson, B., Aspegren, H., Parker, D. S. and Lutz, M. P. (1994). "High-Rate Nitrifying Trickling Filters." Water Science and Technology. **29**(10-11): 47-52.
- APHA (1992). Standard methods for the examination of water and wastewater. 18th edn. Washington, DC, USA, American Public Health Association / American Waterworks Association / Water Environment Federation.
- Araki, N., Ohashi, A., Machdar, I. and Harada, H. (1999). "Behaviors of nitrifiers in a novel biofilm reactor employing hanging sponge-cubes as attachment site." Water Science & Technology. **39**(7). 23-31.
- Bardolet, R. (1997). Water and wastewater treatment 4th edn, Metra Martech London.
- Bengtsson, G. (1991). "Bacterial exopolymer and PHB production in fluctuating ground-water habitats." FEMS Microbiology Ecology. **86**: 15-24.

- Bhupathiraju, V. K., Hernandez, M., Krauter, P. and Alvarez-Cohen, L. (1999). "A new direct microscopy based method for evaluating in-situ bioremediation." Journal of Hazardous Materials. **67**(3): 299-312.
- Biesterfeld, S., Russell P. and Figueroa, L. (2003). "Linking nitrifying biofilm structure and function through fluorescent in situ hybridization and evaluation of nitrification capacity." Water Environment Research. **75**(3): 205-215.
- Boller, M, Gujer, W. and Nyhuis, G. (1990). "Tertiary rotating biological contractors for nitrification." Water Science & Technology. **22**(1/2): 89-100.
- Boller, M., Tschui, M. and Gujer, W. (1997). "Effects of transient nutrient concentrations in tertiary biofilm reactors." Water Science and Technology. **36**(1): 101-109.
- Boller, M, W. Gujer. and M. Tschui (1994). "Parameters Affecting Nitrifying Biofilm Reactors." Water Science and Technology. **29**(10-11): 1-11.
- Bradford, M. M. (1976). "A rapid and sensitive method for the quantitation of microgram quantities of protein utilizing the principle of protein-dye binding." Analytical Biochemistry. **72**(1-2): 248-254.
- Bukit, N. T. (1995). "Water-Quality Conservation for the Citarum River in West Java." Water Science and Technology. **31**(9): 1-10.
- Bura, R., Cheung, M., Liao, B., Finlayson, J., Lee, B. C., Droppo, I. G., Leppard, G. G. and Liss, S. N. (1998). "Composition of extracellular polymeric substances in the activated sludge floc matrix." Water Science & Technology. **37**(4-5): 325-333.
- Cammarota, F. C. (2001). Ammonia Removal at Buaran Water Treatment Plant, Jakarta. School of Engineering, University of Surrey. Degree of Master of Science.
- Characklis, W. G. and Marshall, K. C. (1990). Biofilms edited by William G. Characklis, Kevin C. New York, Wiley.

- Characklis, W. G. and Wilderer, P. A. (1989). Structure and function of biofilms : report of the Dahlem. Chichester ; New York, Wiley.
- Chenu, C. and Roberson, E. B. (1996). "Diffusion of glucose in microbial extracellular polysaccharide as affected by water potential." Soil Biology & Biochemistry. **28**(7): 877-884.
- Chudoba, J., Cesh, J. S., Frakac, J. and Grau, P. (1985). "Control of activated sludge filamentous bulking VI Formulation of basic principles." Water Research **19**: 1389-1406.
- Coskuner, G. and Curtis, T. P. (2002). "In situ characterization of nitrifiers in an activated sludge plant: Detection of Nitrobacter Spp." Journal of Applied Microbiology. **93**(3) 431-437.
- Daigger, G. T., Heinemann, T. A., Land, G. and Watson, R. S. (1994). "Practical experience with combined oxidation and nitrification in plastic media trickling filters." Water Science & Technology. **29**(10-11). 1994. 189-196.
- Daims, H., Nielsen, J. L., Nielsen, P. H., Schleifer, K. H. and Wagner, M. (2001). "In situ characterization of Nitrospira-like nitrite-oxidizing bacteria active in wastewater treatment plants." Applied & Environmental Microbiology. **67**(11): 5273-84.
- Davis, M. L. and Cornwell, D. A. (1991). Introduction to environmental engineering Mackenzie L. New York, McGraw-Hill.
- Duddles, G. A. and Richardson, S. E. (1973). Application of plastic media trickling filters for biological nitrification systems Springfield VA, Environmental protection agency, technology series report EPA-R2-73-199:111.
- Dumaz, B. and Sanin, F. D. (2001). "Effect of carbon to nitrogen ratio on the composition of microbial extracellular polymers in activated sludge." Water Science & Technology. **44**(10): 221-229.

- Fdz-Polanco, F., Mendez E., Uruena, M. A., Villaverde, S. and Garcia, P. A. (2000). "Spatial distribution of heterotrophs and nitrifiers in a submerged biofilter for nitrification." Water Research. **34**(16): 4081-4089.
- Figueroa, L. A. and Silverstein, J. A. (1991). Pilot-scale Trickling Filter Nitrification at the Longmont WWTP. Environmental Engineering: Proceedings of the specialty conference.
- Frolund, B., Palmgren, R., Keiding, K. and Nielsen, P. H. (1996). "Extraction of extracellular polymers from activated sludge using a cation exchange resin." Water Research. **30**(8): 1749-1758.
- Ganf, G. G., Stone, S. J. L. and Oliver, R. L. (1986). "Use of protein to carbohydrate ratios to analyse for nutrient deficiency in phytoplankton " Australian Journal of Marine and Freshwater Research. **37**(2): 183-197.
- Gebert, W. and Wilderer, P. A. (2000). "Heating up trickling filters to tackle cold weather conditions." Water Science & Technology. **41**(1):163-166.
- Grady, C. P. L. and Lim, H. C. (1980). Biological Wastewater Treatment, Marcel Dekker, Inc., New York, NY.
- Gujer, W. (1984). "Operating experience with plastic media tertiary trickling filters for nitrification." Water Science & Technology. **16**: 201.
- Gullicks, H. A. and Cleasby, J. L. (1986). "Design of Trickling Filter Nitrification Towers." Journal of the Water Pollution Control Federation **58**(1): 60-67.
- Gupta, A. B. and Gupta, S. K. (1999). "Simultaneous carbon and nitrogen removal in a mixed culture aerobic RBC biofilm." Water Research. **33**(2): 555-561.
- Han, D. W., Chang, J. S. and Kim, D. J. (2002). "Nitrifying microbial community analysis of nitrite accumulating biofilm reactor by fluorescence in situ hybridization." Water Science & Technology. **47**(1):97-104.

- Hanson, R. S. and Phillips. J. A. (1981). Chemical composition. In Manual of Methods from General Bacteriology. P. Gerhardt, R. Murray, R. Costlow, E. Nester, W. Wa, N. Kneg and G. Briggs-Phillips (Eds). Academic Press, London, United Kingdom: 333.
- Hamsen, H. J. M., Kengen, H. M. P., Akkermans, A. D. L., Stams, A. J. M. and De Vos W. M. (1996). "Detection and localization of syntrophic propionate-oxidizing bacteria in granular sludge by in situ hybridization using 16S rRNA-based oligonucleotide probes." Applied & Environmental Microbiology. **62**(5): 1656-1663.
- Harremoës, P. (1982). "Criteria for Nitrification in Fixed Film Reactors " Water Science and Technology. **14**(1/2): 167-187.
- Hart, B. T., van Dok, W. and Djuangsih, N. (2002). "Nutrient budget for Saguling Reservoir, West Java, Indonesia." Water Research. **36**(8): 2152-2160.
- Heard, R., Hoyle, B. G. and Heatt, M. J. (2002). "Aerated biological filtration for the removal of ammonia and manganese in a major new water treatment works under construction in Hong Kong." Water Science & Technology: Water Supply. **2**(1): 47-56.
- Henry, J. G. and Heinke, G. W. (1996). Environmental science and engineering 2nd edn by J. Glynn Henry. Englewood Cliffs, N.J., Prentice Hall.
- Holmes, M. (1999). Proposed New Operating Strategy For Improved Water Quality At Buaran Water Treatment Plant. Jakarta, Internal Report Thames Water PLC: 40.
- Holmes, M., Pearce, P. and Cammorata, F. (2001) A Strategy to Improve Water Quality at Buaran WTP: upgrading processes for removal of screenings, turbidity and ammonia. , Internal Report Thames Water PLC, Reading.
- Huang, C. and Hopson, N. E. (1974). "Nitrification Rate in Biological Processes." Journal of the Environmental Engineering Division. **100**(2): 409-422.

- Ishikawa, S., Suzuki, T., Nikata, T., Kakii, K. and Shirakashi, T. (2003). "Tertiary nitrification in a new dual-medium aerated filter." Water Science & Technology. **47**(1). 2003. 219-227.
- Jang, A., Bishop, P. L., Okabe, S., Lee, S. G. and Kim, I. S. (2003). "Effect of dissolved oxygen concentration on the biofilm and in situ analysis by fluorescence in situ hybridization (FISH) and microelectrodes." Water Science & Technology. **47**(1). 49-57.
- Jefferson, K. K. (2004). "What drives bacteria to produce a biofilm?" FEMS Microbiology Letters. **236**(2): 163-173.
- Jetten, M. S. M. *et al.* (2002). Improved nitrogen removal by application of new nitrogen-cycle bacteria. *Reviews in Environmental Science and Biotechnology*. 1, 51–63.
- Kilpatrick, F. A. (1970). Dosage requirements for slug injections of rhodamine BA and WT dyes. Geological Survey Research **700-B**: B250-B253.
- Kim, D. J. and Kim, S. H. (2006). "Effect of nitrite concentration on the distribution and competition of nitrite-oxidizing bacteria in nitrification reactor systems and their kinetic characteristics." Water Research. **40**(5). 887-894.
- Kindaichi, T., Ito, T. and Okabe, S. (2004). "Ecophysiological interaction between nitrifying bacteria and heterotrophic bacteria in autotrophic nitrifying biofilms as determined by microautoradiography-fluorescence in situ hybridization." Applied and Environmental Microbiology. **70**(3): 1641-1650.
- Lanthier, M., Tartakovsky, B., Villemur, R., DeLuca, G. and Guiot, S. R. (2002). "Microstructure of anaerobic granules bioaugmented with *Desulfitobacterium frappieri* PCP-1." Applied & Environmental Microbiology. **68**(8): 4035-4043.
- Levenspiel, O. (1999). Chemical Reaction Engineering, 3rd Edition USA, John Wiley and Sons Inc.

- Liao, B., D. Allen, I. Droppo, G. Leppard. and S. Liss (2001). "Surface properties of sludge and their role in bioflocculation and settleability." Water Research. **35**(2): 339-350.
- Liu, D. H. F. and B. G. Liptak (1997). Environmental engineers' handbook David H.F. Liu, second. Boca Raton, Fla., Lewis Publishers.
- Liu, Y. F. and Herbert, H. P. (2003). "Influences of extracellular polymeric substances (EPS) on flocculation, settling, and dewatering of activated sludge." Critical Reviews in Environmental Science and Technology. **33**(3): 237-258.
- Loy, A., Horn, M. and Wagner, M. (2003). "ProbeBase: An online resource for rRNA-targeted oligonucleotide probes." Nucleic Acids Research. **31**(1): 514-516.
- Lutz, M. P., Pratt, A. M., Parker, D. S. and Brischke, K. V. (1990). "Full-scale performance of nitrifying trickling filters." Proceedings of the of 63rd WPFC Conference, Washington, DC.
- Lydmark, P., Lind, M., Sorensson, F. and Hemansson, M. (2006). "Vertical distribution of nitrifying populations in bacterial biofilms from a full-scale nitrifying trickling filter." Environmental Microbiology. **8**(11): 2036-2049.
- Magdaliniuk, S., Block, J. C., Leyval, C., Bottero, J. Y., Villemin, G. and Babut, M. (1995). "Biodegradation of naphthalene in montmorillonite/polyacrylamide suspensions." Water Science & Technology. **31**(1). 1995. 85-94.
- Magesan, G. N., Williamson, J. C., Yeates, G. W. and Lloyd-Jones, A. R. (2000). "Wastewater C:N ratio effects on soil hydraulic conductivity and potential mechanisms for recovery." Bioresource Technology. **71**(1): 21-27.
- McCoy, W. F. and Costerton, J. W. (1982). "Fouling biofilm development in tubular flow systems." Developments in Industrial Microbiology. **23**: 551-558.
- McIntosh, A. C. (2003). Asian water supplies : reaching the urban poor. Manilla, Asian Development Bank and International Water Association,.

- Metcalf and Eddy (2003). Wastewater engineering : treatment and reuse Metcalf & Boston ; Sydney, McGraw-Hill.
- Mezzanotte, V., Prato, N., Sgorbati, S. and Citterio, S. (2004). "Analysis of microbiological characteristics of wastewater along the polishing sequence of a treatment plant." Water Environment Research. **76**(5): 463-467.
- Mobarry, B. K., Wagner, M., Urbain, V., Rittmann, B. E. and Stahl, D. A. (1996). "Phylogenetic probes for analyzing abundance and spatial organization of nitrifying bacteria." Applied & Environmental Microbiology. **62**(6): 2156-2162.
- Mohamed, M. N., Lawrence, J. R. and Robarts, R. D. (1998). "Phosphorous Limitation of Heterotrophic Biofilms from the Fraser River, British Columbia, and the Effect of Pulp Mill Effluent." Microbial Ecology. **36**: 121-130.
- Morikawa, K. and Tonozuka, T. (1998). "Differences in the characteristics of the bacterial community in the epilithon and river water as demonstrated by plate count and staining methods." Verh. Internat. Verein. Limnol. **26**: 1641–1644.
- Moy, B. Y. P., Tay, J. H., Toh, S. K., Liu, Y. and Tay, S. T. L. (2002). "High organic loading influences the physical characteristics of aerobic sludge granules." Letters in Applied Microbiology. **34**(6). 2002. 407-412.
- Mustika Sari, A. (2004). Potential optimisation of chlorination at Buaran WTP, Jakarta Water and Environmental Engineering, University of Surrey. Degree of Master of Science
- Noda, N., Kaneko, N., Mikami, M., Kimochi, Y., Tsuneda, S., Hirata, A., Mizuochi, M. and Inamori, Y. (2003). "Effects of SRT and DO on N<sub>2</sub>O reductase activity in an anoxic-oxic activated sludge system." Water Science & Technology. **48**(11-12): 363-370.
- Obayashi, A. W. and Gaudy, A. F. (1972). Aerobic digestion of extracellular microbial polysaccarides, 27th industrial waste conference, Purdue university.

- Odegaard, H., Rusten, B. and Westrum, T. (1994). "A new moving bed biofilm reactor: Applications and results." Water Science & Technology. **29**(10-11):157-165.
- Okabe, S., Hirata K. and Watanabe, Y. (1995). "Dynamic changes in spatial microbial distribution in mixed-population biofilms: Experimental results and model simulation." Water Science and Technology. **32**(8): 67-74.
- Okabe, S., Hirata K. and Watanabe, Y. (1997). "Significance of the spatial distribution of microbial species in mixed-population biofilms." Biofouling. **11**(2): 119-136.
- Okabe, S., Hiratia, K., Ozawa, Y. and Watanabe, Y. (1996). "Spatial microbial distributions of nitrifiers and heterotrophs in mixed-population biofilms." Biotechnology and Bioengineering. **50**(1): 24-35.
- Okabe, S., Naitoh, H., Satoh, H. and Watanabe, Y. (2002). "Structure and function of nitrifying biofilms as determined by molecular techniques and the use of microelectrodes." Water Science and Technology. **46**(1-2): 233-241.
- Okabe, S., Satoh, H. and Watanabe, Y. (1999). "In situ analysis of nitrifying biofilms as determined by in situ hybridization and the use of microelectrodes." Applied and Environmental Microbiology. **65**(7): 3182-3191.
- Painter, H. A. and Loveless, J. E. (1983). "Effect of Temperature and pH Value on the Growth-Rate Constants of Nitrifying Bacteria in the Activated Sludge Process " Water Research. **17**(3): 237-248.
- Palupi, K., Sumengen, S., Insuasri, S., Agustina, L., Nunik, S. A., Sunarya, W. and Quraisyn A. (1995). "River Water-Quality Study in the Vicinity of Jakarta." Water Science and Technology. **31**(9): 17-25.
- Parker, D. S., Jacobs, T., Bower, E., Stowe, D. W. and Farmer G. (1997). "Maximizing trickling filter nitrification rates through biofilm control: Research review and full scale application." Water Science and Technology. **36**(1): 255-262.

- Parker, D., Lutz, M., Andersson, B. and Aspegren, H. (1995). "Effect of operating variables on nitrification rates in trickling filters." Water Environment Research. **67**(7): 1111-1118.
- Parker, D., Lutz, M., Dahl, R. and Bernkopf, S. (1989). "Enhancing Reaction-Rates in Nitrifying Trickling Filters through Biofilm Control." Journal Water Pollution Control Federation. **61**(5): 618-631.
- Parker, D., S. and Richards, T. (1986). "Nitrification in Trickling Filters." Water Pollution Control Federation. **58**(9): 896-902.
- Pearce, P. (1999). Design Models for Percolating Filter Plants. Internal Report U.K, Thames Water Plc. Research and Technology.
- Pearce, P. (2004). "Trickling filters for upgrading low technology wastewater plants for nitrogen removal." Water Science & Technology. **49**(11-12): 47-52.
- Pearce, P. and Foster, D. (1999). "Optimizing nitrification on biological filters" Water and environmental management: Journal of the Chartered Institution of Water and Environmental Management. **13**(6): 406-412.
- Pearce, P. and Williams, S. (1999). "A nitrification model for mineral-media trickling filters." Journal of the Chartered Institution of Water and Environmental Management. **13**(2): 84-92.
- Pearce, P., van den Akker, B., Holmes, M. and Fallowfield H. (2003). Initial Findings From A Pilot Scale Study of High Rate Trickling Filters For Ammonia Removal Prior to Water Treatment from a Polluted Lowland Source. Water: The key to sustainable development in Africa. 1st IWA Regional Conference. Capetown IWA.
- Perez-Rodriguez, J. L., Maqueda, C., Lebrato, J. and Carretero, M. I. (1992). "Influence of Clay Minerals Used as Supports in Anaerobic Digesters in the Precipitation of Struvite." Water Research. **26**(4). 1992. 497-506.

- Persson, F., Wik, T., Sorensson, F. and Hemansson, M. (2002). "Distribution and activity of ammonia oxidizing bacteria in a large full-scale trickling filter." Water Research. **36**(6): 1439-1448.
- Portolesi, P. (2004). Impact of a nitrifying biofilter on the coagulation, clarification process using flocculation jar tests as the simulated clarifier. Final year report, Department of Environmental Health, School of Medicine Flinders University of South Australia, South Australia, November 2004.
- Punal, A., Trevisan, M., Rozzi, A. and Lema, J. M. (2000). "Influence of C:N ratio on the start-up of upflow anaerobic filter reactors." Water Research. **34**(9): 2614-2619.
- Riemer, M., Holm Kristensen, G. and Harremoës, P. (1980). "Residence time distribution in submerged biofilters." Water Research. **14**:949-958.
- Rusten, B., Hellstrom, B. G., Hellstrom, F., Sehested, O., Skjelfoss, E. and Svendsen, B. (2000). "Pilot testing and preliminary design of moving bed biofilm reactors for nitrogen removal at the FREVAR wastewater treatment plant." Water Science & Technology. **41**(4-5). 13-20.
- Satoh, H., Okabe, S., Norimatsu, N. and Watanabe, Y. (2000). "Significance of substrate C/N ratio on structure and activity of nitrifying biofilms determined by in situ hybridization and the use of microelectrodes." Water Science & Technology. **41**(4-5). 317-321.
- Schramm, A., De Beer, D., Wagner, M. and Amann, R. (1998). "Identification and activities in situ of Nitrosospira and Nitrospira spp. as dominant populations in a nitrifying fluidized bed reactor." Applied & Environmental Microbiology. **64**(9). 3480-3485.
- Schramm, A., Larsen, L. H., Revsbech, N. P., Ramsing, N. B., Amann, R. and Schleifer, K. H. (1996). "Structure and function of a nitrifying biofilm as determined by in situ hybridization and the use of microelectrodes." Applied and Environmental Microbiology. **62**(12): 4641-4647.

- Seguret, F., Racault, Y. and Sardin, M. (2000). "Hydrodynamic behaviour of full scale trickling filters." Water Research. **34**(5):1551-1558.
- Smart, P. L. and Laidlaw, I. M. S. (1977). An evaluation of some fluorescent dyes for water tracing. Water Resources Research **3**(1): 15-33.
- Sponza, D. T. (2003). "Investigation of extracellular polymer substances (EPS) and physicochemical properties of different activated sludge flocs under steady-state conditions." Enzyme & Microbial Technology. **32**(3-4): 375-385.
- Stevens, D. K., Berthouex, P. M. and Chapman, T. W. (1986). "The effect of tracer diffusion in biofilm on residence time distribution." Water Research. **20**(369-375).
- Stover, E. L. (1980). "Start-up problems at a plant treating food-processing wastewater." Water Pollution and Control Federation. **52**(2): 249-256.
- Strauss, E. A. and Lamberti, G. A. (2002). "Effect of dissolved organic carbon quality on microbial decomposition and nitrification rates in stream sediments." Freshwater Biology. **47**: 65-74.
- Tandukar, M., Uemura, S., Ohashi, A. and Harada, H. (2006). "Combining UASB and the "fourth generation" down-flow hanging sponge reactor for municipal wastewater treatment." Water Science & Technology. **53**(3). 2006. 209-218.
- Tekerlekopoulou, A. G. and Vayenas, D. V. (2007). "Ammonia, iron and manganese removal from potable water using trickling filters." Desalination. **210**(1-3): 225-235.
- TPJ. (2003). Analysis of raw water quality data: Buaran and Pulo Gadung intake. Internal Report, Thames Pam Jaya. Technical support, Jakarta, Indonesia: 46.
- van Benthum, W. A. J., Derissen, B. P., van Loosdrecht, M. C. M. and Heijnen, J. J. (1998). "Nitrogen removal using nitrifying biofilm growth and denitrifying suspended growth in a biofilm airlift suspension reactor coupled with a chemostat." Water Research. **32**(7):2009-2018.

- van Benthum, W. A. J., van Loosdrecht, M. D. M. and Heijnen, J. J. (1997). "Control of heterotrophic layer formation on nitrifying biofilms in a biofilm airlift suspension reactor." Biotechnology and Bioengineering. **53**(4): 397-405.
- van den Akker, B. (2003). A pilot study to investigate ammonia removal from drinking water using a nitrifying trickling filter. Environmental Health. Adelaide, Flinders University. Bachelor of Science (Honours): 102.
- van Loosdrecht, M. C. M., van Benthum, W. A. J. and Heijnen, J. J. (2000). "Integration of nitrification and denitrification in biofilm airlift suspension reactors." Water Science & Technology. **41**(4-5). 2000. 97-103.
- Veiga, M. C., Jain, M. K., Wu, W. M., Hollingsworth, R. I. and Zeikus, J. G. (1997). "Composition and role of extracellular polymers in methanogenic granules." Applied and Environmental Microbiology. **63**(403-407).
- Verhagen, F. J. and Laanbroek, H. J. (1991). "Competition for Ammonium between Nitrifying and Heterotrophic Bacteria in Dual Energy-Limited Chemostats." Applied Environmental Microbiology. **57**(11): 3255-3263.
- Villaverde, S., Fdz-Polanco, F., Lacalle, M. L. and Garcia, P. A. (2000). "Influence of the suspended and attached biomass on the nitrification in a two submerged biofilters in series system." Water Science & Technology. **41**(4-5): 169-176.
- Wagner, M., Amann, R., Lemmer, H. and Schleifer, K. H. (1993). "Probing activated sludge with oligonucleotides specific for proteobacteria: Inadequacy of culture-dependent methods for describing microbial community structure." Applied & Environmental Microbiology. **59**(5): 1520-1525.
- Wagner, M., Rath, G., Koops, H. P., Flood, J. and Amann, R. (1996). "In situ analysis of nitrifying bacteria in sewage treatment plants." Water Science & Technology. **34**(1-2): 237-244.

- Waki, M., Tokutomi, T., Yokoyama, H. and Tanaka, Y. (2007). "Nitrogen removal from animal waste treatment water by anammox enrichment." Bioresource Technology. **98**:2775-2780.
- Wanner, O. and Gujer, W. (1985). "Competition in biofilms " Water Science & Technology. **17**(2/3): 27-39.
- White, G. C. (1999). The handbook of chlorination and alternative disinfectants. New York, J. Wiley.
- Wiesmann, U. (1994). "Biological nitrogen removal from wastewater." Advances in biochemical engineering and biotechnology. **51**: 113-154.
- Wijeyekoon, S., Mino, T., Satoh, H. and Matsuo, T. (2000). "Fixed bed biological aerated filtration for secondary effluent polishing: Effect of filtration rate on nitrifying biological activity distribution." Water Science & Technology. **41**(1). 2000. 187-195.
- Wik, T. (2000). "Strategies to improve the efficiency of tertiary nitrifying trickling filters." Water Science & Technology. **41**(4-5). 2000. 477-485.
- Wimpenny, J., Manz, W. and Szewzyk, U. (2000). "Heterogeneity in biofilms." FEMS Microbiology Reviews. **24**(5):661-71.
- Wu, Y. C., Smith, E. D. and Novak, R. (1982). "Filterability of activated sludge in response to growth." Journal of Water Pollution and Control Federation **54**(5): 444-456.
- Wuertz, S., Bishop P. and Wilderer, P. Eds. (2003). Biofilms in wastewater treatment : an interdisciplinary. London, IWA Publishing.
- Yoo, H., Ahn, K. H., Lee, H. J., Lee, K. H., Kwak, Y. J. and Song, K. G. (1999). "Nitrogen removal from synthetic wastewater by simultaneous nitrification and denitrification (SND) via nitrite in an intermittently-aerated reactor." Water Research. **33**(1): 145-154.

Zhang, T. C., Fu, Y. C. and Bishop, P. L. (1994). "Competition in biofilms." Water Science & Technology. **29**(10-11). 1994. 263-270.

Zhang, X and Bishop, P. L. (2003). "Biodegradability of biofilm extracellular polymeric substances." Chemosphere. **50**(1):63-69.

# APPENDIX

## Publications relevant to this thesis

- van den Akker, B., Holmes, M., Cromar, H., and Fallowfield, H (2008). Application of high rate nitrifying trickling filters for potable water treatment. *Water Research*. **42**(17): 4514–4524.
- van den Akker, B., Holmes, M., Cromar, H., and Fallowfield, H (2009). The impact of organic carbon on the performance of a high rate nitrifying trickling filter designed to pre-treat potable water. *Water Science and Technology*. In press: Accepted 1.06.2009.
- van den Akker, B., Holmes, M., Pearce, P. and Fallowfield, HJ. (2003). A pilot study to investigate ammonia removal from drinking water using a nitrifying trickling filter. **New Zealand Water and Wastes Association** 45th Annual Conference and Expo, pages 1-10, Auckland, NZ, Sept 17-19 2003. NZWWA CD ROM.
- Pearce, P., van den Akker, B., Holmes, M., and Fallowfield, HJ. (2003). Initial Findings From A Pilot Scale Study of High Rate Trickling Filters For Ammonia Removal Prior to Water Treatment from a Polluted Lowland Source. "**Water : The key to sustainable development in Africa**". **1st International Water Association Regional Conference**, Capetown, South Africa, September 2003.
- van den Akker, B., Holmes, M., Pearce, P., Cromar, NJ. and Fallowfield, HJ. (2004). Progress in the development of a biological ammonia removal process for potable water treatment in developing countries. **New Zealand Water and Wastes Association** 46th Annual Conference and Expo, NZ, September, 2004
- van den Akker, B., Holmes, M., Pearce, P., Cromar, NJ. and Fallowfield, HJ. (2005). Progress in the development of a biological filter for potable water treatment in South East Asia. **International Water Association's** 1st ASPIRE Conference and Exhibition, Singapore, July 10-15 2005. IWA CD ROM.
- van den Akker, B., Holmes, M., Cromar, NJ. and Fallowfield, HJ. (2006). Influence of ammonia, carbon and suspended solid loadings on the performance and microbial ecology of a biological filter treating drinking water. **International Water Association's** Biofilm Systems VI Conference, Amsterdam, September 24-27 2006. IWACD ROM.